

**SERVICEABILITY OF CONCRETE BEAMS PRESTRESSED
BY FIBRE REINFORCED PLASTIC TENDONS**

by

AMR A. ABDELRAHMAN

A Dissertation
Submitted to the Faculty of Graduate Studies
in Partial Fulfilment of the
Requirements for the Degree of

DOCTOR OF PHILOSOPHY

Structural Engineering Division
Department of Civil and Geological Engineering
University of Manitoba
Winnipeg, Manitoba

© October 1995



National Library
of Canada

Acquisitions and
Bibliographic Services Branch

395 Wellington Street
Ottawa, Ontario
K1A 0N4

Bibliothèque nationale
du Canada

Direction des acquisitions et
des services bibliographiques

395, rue Wellington
Ottawa (Ontario)
K1A 0N4

Your file *Votre référence*

Our file *Notre référence*

The author has granted an irrevocable non-exclusive licence allowing the National Library of Canada to reproduce, loan, distribute or sell copies of his/her thesis by any means and in any form or format, making this thesis available to interested persons.

L'auteur a accordé une licence irrévocable et non exclusive permettant à la Bibliothèque nationale du Canada de reproduire, prêter, distribuer ou vendre des copies de sa thèse de quelque manière et sous quelque forme que ce soit pour mettre des exemplaires de cette thèse à la disposition des personnes intéressées.

The author retains ownership of the copyright in his/her thesis. Neither the thesis nor substantial extracts from it may be printed or otherwise reproduced without his/her permission.

L'auteur conserve la propriété du droit d'auteur qui protège sa thèse. Ni la thèse ni des extraits substantiels de celle-ci ne doivent être imprimés ou autrement reproduits sans son autorisation.

ISBN 0-612-12944-6

Canada

Name _____

Dissertation Abstracts International is arranged by broad, general subject categories. Please select the one subject which most nearly describes the content of your dissertation. Enter the corresponding four-digit code in the spaces provided.

civil Engineering
SUBJECT TERM

0543

U·M·I

SUBJECT CODE

Subject Categories

THE HUMANITIES AND SOCIAL SCIENCES

COMMUNICATIONS AND THE ARTS

Architecture 0729
Art History 0377
Cinema 0900
Dance 0378
Fine Arts 0357
Information Science 0723
Journalism 0391
Library Science 0399
Mass Communications 0708
Music 0413
Speech Communication 0459
Theater 0465

EDUCATION

General 0515
Administration 0514
Adult and Continuing 0516
Agricultural 0517
Art 0273
Bilingual and Multicultural 0282
Business 0688
Community College 0275
Curriculum and Instruction 0727
Early Childhood 0518
Elementary 0524
Finance 0277
Guidance and Counseling 0519
Health 0680
Higher 0745
History of 0520
Home Economics 0278
Industrial 0521
Language and Literature 0279
Mathematics 0280
Music 0522
Philosophy of 0998
Physical 0523

Psychology 0525
Reading 0535
Religious 0527
Sciences 0714
Secondary 0533
Social Sciences 0534
Sociology of 0340
Special 0529
Teacher Training 0530
Technology 0710
Tests and Measurements 0288
Vocational 0747

LANGUAGE, LITERATURE AND LINGUISTICS

Language
General 0679
Ancient 0289
Linguistics 0290
Modern 0291
Literature
General 0401
Classical 0294
Comparative 0295
Medieval 0297
Modern 0298
African 0316
American 0591
Asian 0305
Canadian (English) 0352
Canadian (French) 0355
English 0593
Germanic 0311
Latin American 0312
Middle Eastern 0315
Romance 0313
Slavic and East European 0314

PHILOSOPHY, RELIGION AND THEOLOGY

Philosophy 0422
Religion
General 0318
Biblical Studies 0321
Clergy 0319
History of 0320
Philosophy of 0322
Theology 0469

SOCIAL SCIENCES

American Studies 0323
Anthropology
Archaeology 0324
Cultural 0326
Physical 0327
Business Administration
General 0310
Accounting 0272
Banking 0770
Management 0454
Marketing 0338
Canadian Studies 0385
Economics
General 0501
Agricultural 0503
Commerce-Business 0505
Finance 0508
History 0509
Labor 0510
Theory 0511
Folklore 0358
Geography 0366
Gerontology 0351
History
General 0578

Ancient 0579
Medieval 0581
Modern 0582
Black 0328
African 0331
Asia, Australia and Oceania 0332
Canadian 0334
European 0335
Latin American 0336
Middle Eastern 0333
United States 0337
History of Science 0585
Law 0398
Political Science
General 0615
International Law and Relations 0616
Public Administration 0617
Recreation 0814
Social Work 0452
Sociology
General 0626
Criminology and Penology 0627
Demography 0938
Ethnic and Racial Studies 0631
Individual and Family Studies 0628
Industrial and Labor Relations 0629
Public and Social Welfare 0630
Social Structure and Development 0700
Theory and Methods 0344
Transportation 0709
Urban and Regional Planning 0999
Women's Studies 0453

THE SCIENCES AND ENGINEERING

BIOLOGICAL SCIENCES

Agriculture
General 0473
Agronomy 0285
Animal Culture and Nutrition 0475
Animal Pathology 0476
Food Science and Technology 0359
Forestry and Wildlife 0478
Plant Culture 0479
Plant Pathology 0480
Plant Physiology 0817
Range Management 0777
Wood Technology 0746
Biology
General 0306
Anatomy 0287
Biostatistics 0308
Botany 0309
Cell 0379
Ecology 0329
Entomology 0353
Genetics 0369
Limnology 0793
Microbiology 0410
Molecular 0307
Neuroscience 0317
Oceanography 0416
Physiology 0433
Radiation 0821
Veterinary Science 0778
Zoology 0472
Biophysics
General 0786
Medical 0760
EARTH SCIENCES
Biogeochemistry 0425
Geochemistry 0996

Geodesy 0370
Geology 0372
Geophysics 0373
Hydrology 0388
Mineralogy 0411
Paleobotany 0345
Paleoecology 0426
Paleontology 0418
Paleozoology 0985
Palynology 0427
Physical Geography 0368
Physical Oceanography 0415

HEALTH AND ENVIRONMENTAL SCIENCES

Environmental Sciences 0768
Health Sciences
General 0566
Audiology 0300
Chemotherapy 0992
Dentistry 0567
Education 0350
Hospital Management 0769
Human Development 0758
Immunology 0982
Medicine and Surgery 0564
Mental Health 0347
Nursing 0569
Nutrition 0570
Obstetrics and Gynecology 0380
Occupational Health and Therapy 0354
Ophthalmology 0381
Pathology 0571
Pharmacology 0419
Pharmacy 0572
Physical Therapy 0382
Public Health 0573
Radiology 0574
Recreation 0575

Speech Pathology 0460
Toxicology 0383
Home Economics 0386

PHYSICAL SCIENCES

Pure Sciences
Chemistry
General 0485
Agricultural 0749
Analytical 0486
Biochemistry 0487
Inorganic 0488
Nuclear 0738
Organic 0490
Pharmaceutical 0491
Physical 0494
Polymer 0495
Radiation 0754
Mathematics 0405
Physics
General 0605
Acoustics 0986
Astronomy and Astrophysics 0606
Atmospheric Science 0608
Atomic 0748
Electronics and Electricity 0607
Elementary Particles and High Energy 0798
Fluid and Plasma 0759
Molecular 0609
Nuclear 0610
Optics 0752
Radiation 0756
Solid State 0611
Statistics 0463
Applied Sciences
Applied Mechanics 0346
Computer Science 0984

Engineering
General 0537
Aerospace 0538
Agricultural 0539
Automotive 0540
Biomedical 0541
Chemical 0542
Civil 0543
Electronics and Electrical 0544
Heat and Thermodynamics 0348
Hydraulic 0545
Industrial 0546
Marine 0547
Materials Science 0794
Mechanical 0548
Metallurgy 0743
Mining 0551
Nuclear 0552
Packaging 0549
Petroleum 0765
Sanitary and Municipal 0554
System Science 0790
Geotechnology 0428
Operations Research 0796
Plastics Technology 0795
Textile Technology 0994

PSYCHOLOGY

General 0621
Behavioral 0384
Clinical 0622
Developmental 0620
Experimental 0623
Industrial 0624
Personality 0625
Physiological 0989
Psychobiology 0349
Psychometrics 0632
Social 0451



SERVICEABILITY OF CONCRETE BEAMS PRESTRESSED

BY FIBRE REINFORCED PLASTIC TENDONS

BY

AMR A. ABDELRAHMAN

A Thesis submitted to the Faculty of Graduate Studies of the University of Manitoba
in partial fulfillment of the requirements of the degree of

DOCTOR OF PHILOSOPHY

© 1996

Permission has been granted to the LIBRARY OF THE UNIVERSITY OF MANITOBA to lend or sell copies of this thesis, to the NATIONAL LIBRARY OF CANADA to microfilm this thesis and to lend or sell copies of the film, and LIBRARY MICROFILMS to publish an abstract of this thesis.

The author reserves other publication rights, and neither the thesis nor extensive extracts from it may be printed or otherwise reproduced without the author's written permission.

ACKNOWLEDGMENT

The author would like to express his sincere appreciation to Dr. Sami Rizkalla for his guidance and continuous encouragement throughout this research work. His valuable suggestions and contagious enthusiasm are gratefully acknowledged.

The author would like to thank Dr. B. Pinkney and Dr. M.L. Ayari for serving on his Ph.D. committee. Thanks are extended to Dr. A. Nanni from Pennsylvania State University for reviewing the thesis as the external examiner. The support provided by Mitsubishi Kasei, Japan, is also gratefully acknowledged for providing the materials used in the test program.

The author wishes to express his thanks to Mssr. M. McVey, E. Lemke, R. Graham, P.Eng. and S. Sparrow, of the Structural Engineering Construction and Research Development Facility for their assistance during fabrication and testing of the specimens. Special thanks are also extended to Mr. H. Louka for his assistance during the experimental phase of this study.

The patience and love of my family Amel, Amira and Ahmed and the support of my father and my mother can not be praised enough; to them this thesis is dedicated.

ABSTRACT

Use of carbon fibre reinforced plastic, *CFRP*, as prestressing reinforcement for concrete structures, has increased rapidly for the last ten years. The non-corrosive characteristics, high strength-to-weight ratio and good fatigue properties of *CFRP* reinforcement significantly increase the service life of structures. However, the high cost and low ductility of *CFRP* reinforcement due to its limited strain at failure are problems yet to be solved for widespread use of this new material. Use of partially prestressed concrete members has the advantages of reducing cost and improving deformability. However, the deflection and cracking of concrete beams partially prestressed by *CFRP* reinforcement should be investigated.

An experimental program undertaken at the University of Manitoba to study the serviceability of concrete beams prestressed by *CFRP* reinforcements is reported. Tests are described of eight concrete beams prestressed by Leadline *CFRP* bars, produced by Mitsubishi Kasei, Japan, and two beams prestressed by conventional steel strands. The beams are 6.2 meters long and 330 mm in depth. The various parameters considered are the prestressing ratio, degree of prestressing, and distribution of *CFRP* rods in the tension zone. The thesis examines the various limit states and flexural behaviour of concrete

beams prestressed by *CFRP* bars, including different modes of failure. The behaviour of beams prestressed by *CFRP* bars is compared to similar beams prestressed by conventional steel strands.

Theoretical models are proposed to predict the deflection prior and after cracking and the crack width of concrete beams prestressed by Leadline *CFRP* bars under service loading conditions. Crack width is predicted using appropriate bond factors for this type of reinforcement. A procedure is formulated for predicting the location of the centroidal axis of the cracked sections prestressed by *CFRP* bars. In addition, a method is proposed to calculate the deflection and the crack width of beams partially prestressed by *CFRP* bars under repeated load cycles within the service loading range. The deformability of concrete beams prestressed by *CFRP* reinforcement is also discussed. A model is proposed to quantify the deformability of beams prestressed by fibre reinforced plastic reinforcements.

The reliability of the proposed methods and the other methods used from the literature to predict the deflection and the crack width is examined by comparing the measured and the computed values of the tested beams and beams tested by others. An excellent agreement is found for the methods predicting the deflection and a good agreement is found for the crack width prediction. Design guidelines for prestressed concrete beams with *CFRP* reinforcement are also presented.

TABLE OF CONTENTS

ACKNOWLEDGMENT	i
ABSTRACT	ii
TABLE OF CONTENTS	iv
LIST OF SYMBOLS	x
LIST OF TABLES	xv
LIST OF FIGURES	xvi
1. INTRODUCTION	
1.1 GENERAL	1
1.2 OBJECTIVES	3
1.3 SCOPE AND CONTENTS	5
2. FIBRE-REINFORCED-PLASTIC REINFORCEMENT	
2.1 BACKGROUND	10
2.2 DEFINITION OF <i>FRP</i>	11
2.3 APPLICATIONS OF <i>FRP</i>	12
2.4 MATERIAL PROPERTIES	18
2.4.1 Fibre Properties	19

2.4.1.1	Glass	20
2.4.1.2	Carbon	21
2.4.1.3	Kevlar 49	21
2.4.2	Matrix Properties	22
2.5	CHARACTERISTICS OF <i>FRP</i> REINFORCEMENT	23
2.5.1	Glass-Based <i>FRP</i> Prestressing Reinforcement	25
2.5.2	Carbon-Based <i>FRP</i> Prestressing Reinforcement	26
2.5.3	Aramid-Based <i>FRP</i> Prestressing Reinforcement	28
2.6	ANCHORAGES OF <i>FRP</i> PRESTRESSING REINFORCEMENT	31
3	BEHAVIOUR OF CONCRETE BEAMS PRESTRESSED BY <i>FRP</i> REINFORCEMENT	
3.1	GENERAL	44
3.2	FLEXURAL BEHAVIOUR	45
3.2.1	Aramid <i>FRP</i>	46
3.2.2	Carbon <i>FRP</i>	48
3.2.3	Glass <i>FRP</i>	51
3.3	BOND AND DEVELOPMENT LENGTH	52
3.3.1	Aramid <i>FRP</i>	55
3.3.2	Glass <i>FRP</i>	58
3.3.3	Carbon <i>FRP</i>	60
3.4	FATIGUE BEHAVIOUR	61
3.4.1	Aramid <i>FRP</i>	62
3.4.2	Glass <i>FRP</i>	65
3.4.3	Carbon <i>FRP</i>	66
3.5	LONG-TERM BEHAVIOUR	68
3.6	DESIGN CONSIDERATIONS	71

3.6.1	Flexural Analysis	72
3.7	DUCTILITY	74
3.8	CASE STUDY: THE FIRST SMART HIGHWAY BRIDGE BUILT IN CANADA	76
4.	SERVICEABILITY OF PRESTRESSED AND PARTIALLY PRESTRESSED CONCRETE BEAMS	
4.1	GENERAL	79
4.2	PARTIAL PRESTRESSING	80
4.2.1	Definition of Partial Prestressing	84
4.2.2	Behaviour in Flexure	88
4.3	SERVICEABILITY LIMIT STATES	90
4.3.1	Short-Term Deflection	91
4.3.1.1	Tension Stiffening Effect	93
4.3.2	Crack Control	104
4.3.2.1	Crack Width Evaluation	106
4.4	SERVICEABILITY OF BEAMS PARTIALLY PRESTRESSED BY <i>FRP</i> 115	
4.4.1	Deflection Prediction	116
4.4.2	Crack Width Prediction	118
5.	THE EXPERIMENTAL PROGRAM	
5.1	GENERAL	129
5.2	TEST SPECIMENS	130
5.3	JACKING SET-UP	131

5.4	TESTING SCHEME	133
5.5	INSTRUMENTATION	134
5.6	MATERIALS	136
5.6.1	Leadline	136
5.6.1.1	Tensile Properties	137
5.6.1.2	Transfer Length	140
5.6.1.3	Flexural Bond Strength	142
5.6.2	Concrete	143
5.6.2.1	Tensile Strength	144
5.6.3	Steel	144
5.7	PRESTRESSING LOSSES	145
6.	RESULTS OF THE EXPERIMENTAL WORK	
6.1	GENERAL	159
6.2	FLEXURAL BEHAVIOUR	160
6.3	FAILURE MODES	168
6.4	STRAIN DISTRIBUTION	170
6.5	CRACKING BEHAVIOUR	172
6.6	COMPARISON OF BEAMS PRESTRESSED BY LEADLINE AND STEEL	174
6.6.1	Load-Deflection	175
6.6.2	Strain Distribution	177
6.6.3	Cracking Behaviour	179
6.6.3.1	Crack Spacing	182

6.6.3.2	Crack Width	183
6.7	EFFECT OF FLANGE WIDTH	185
6.8	EFFECT OF DEGREE OF PRESTRESSING	186
6.9	EFFECT OF DISTRIBUTION OF THE PRESTRESSING BARS IN THE TENSION ZONE	188
7.	FLEXURAL ANALYSIS	
7.1	ANALYSIS PROCEDURE	218
7.1.1	Cracking Moment Calculation	220
7.1.2	Failure Criteria	221
7.2	MATERIAL MODELLING	222
7.2.1	Concrete	223
7.2.2	Leadline	225
7.2.3	Steel	226
7.3	COMPARISON BETWEEN ANALYTICAL AND EXPERIMENTAL RESULTS	226
7.4	DEFLECTION PREDICTION	229
7.4.1	Integration of Curvature	230
7.4.1.1	Ignoring Tension Stiffening	231
7.4.1.2	Accounting for Tension Stiffening	231
7.4.1.2.1	Method #1: Effective Moment of Inertia " I_e "	232
7.4.1.2.2	Method #2: CEB-FIP Code	234
7.4.1.2.3	Method #3: Strain Compatibility Accounting for Concrete in Tension	237
7.4.2	Simplified Method	238
7.4.2.1	Centroidal Distance of Cracked Prestressed Beams	240

7.4.3	Design Recommendations	242
7.5	CRACK WIDTH	244
7.5.1	Influence of Major Parameters	245
7.5.2	Calculation of The Stress in The Reinforcement	248
7.5.3	Crack Width Calculation	249
7.5.3.1	Method #1: Suri and Dilger (1986)	249
7.5.3.2	Method #2: The CEB-FIP Code (1978)	250
7.5.3.3	Method #3: Gergely and Lutz (1966)	251
7.5.4	Design Recommendations	252
7.6	STRAIN DISTRIBUTION	252
7.7	FREQUENT LOADING AND UNLOADING	254
7.7.1	Deflection Prediction	255
7.7.1.1	Proposed Model	256
7.7.2	Crack Width Prediction	260
7.7.2.1	Proposed Model	261
7.8	DEFORMABILITY OF BEAMS PRESTRESSED BY <i>CFRP</i>	262
7.8.1	Proposed Deformability Ratio	266
8.	SUMMARY AND CONCLUSIONS	
8.1	SUMMARY	302
8.2	CONCLUSIONS	304
	REFERENCES	310
	APPENDIX A	323

LIST OF SYMBOLS

a	=	depth of the equivalent rectangular stress block in the compression zone of concrete section.
A	=	average effective area around one reinforcing bar.
A_{cef}	=	effective area of concrete, where reinforcement influences the crack width.
A_{cr}	=	cross-sectional area of transformed cracked section.
A_g	=	gross cross-sectional area of concrete.
A_f	=	area of <i>FRP</i> in the tension zone.
A_{ns}	=	area of non-prestressing reinforcement.
A_{ps}	=	area of prestressing reinforcement.
A_s	=	total area of prestressed and non-prestressed steel in the tension zone.
A_s'	=	area of non-prestressing compression reinforcement.
A_t	=	area of concrete below the neutral axis.
b	=	web width.
c	=	neutral axis depth from the extreme compression fibre in concrete.
c	=	concrete cover measured from the surface of the reinforcement.
d	=	depth of non-prestressing reinforcement from extreme compression fibre.
d_b	=	bar diameter.
d_c	=	concrete cover measured from centre of reinforcement.
d_p	=	depth of prestressing reinforcement from extreme compression fibre.
e	=	eccentricity of prestressing reinforcement, based on gross section properties.
e	=	percentage of error.
e_{cr}	=	eccentricity of prestressing force with respect to the centroid of the transformed cracked section.

E_{el}	=	elastic energy of the beam at failure.
E_{ns}	=	modulus of elasticity of non-prestressed reinforcement.
E_{ps}	=	modulus of elasticity of prestressing reinforcement.
E_s	=	average modulus of elasticity of prestressed and non-prestressed reinforcement.
E_{tot}	=	total energy of the beam at failure.
f_c	=	concrete stress in compression.
f_{cr}	=	tensile strength of concrete.
f_{ct}	=	average tensile stress after cracking.
f_f	=	stress in <i>FRP</i> reinforcement after decompression.
f_g	=	guaranteed ultimate tensile strength.
f_{ps}	=	stress in prestressing reinforcement at ultimate.
f_{pu}	=	ultimate stress of the prestressing reinforcement.
f_{py}	=	yield stress of prestressing reinforcement.
f_r	=	rupture strength of concrete.
f_s	=	stress in steel reinforcement after decompression.
f_y	=	yield stress in non-prestressing reinforcement.
h_1	=	distance from centroid of tensile reinforcement to neutral axis.
h_2	=	distance from extreme tensile fibre to neutral axis.
I_{cr}	=	moment of inertia of the cracked section ignoring concrete in tension.
I_e	=	effective moment of inertia.
$(I_e)_{L2}$	=	effective moment of inertia compared to a downward net positive deflection.
I_g	=	gross moment of inertia.
K	=	coefficient depending on the support and loading condition.
k	=	factor depends on bond properties of reinforcements (Suri and Dilger 1986).

k_1	=	coefficient depending on bond quality of reinforcement (CEB-FIP 1978).
k_2	=	coefficient depending on the shape of the strain diagram.
l	=	strain loss which is equal to the loss of the prestressing force.
L	=	effective length of the member.
l_{av}	=	average spacing between cracks.
m	=	number of reinforcing bars.
m	=	coefficient to determine the tension stiffening in Branson's equation.
M	=	bending moment.
M_{cr}	=	cracking moment.
M'_{cr}	=	net positive moment required to crack the section.
M_D	=	moment due to dead load.
M_{dec}	=	decompression moment.
M_L	=	moment due to live load.
M_{L1}	=	part of the live load moment corresponding to zero deflection.
M_{L2}	=	part of the live load moment that corresponds to a downward deflection of a prestressed member.
M_{LCr}	=	equivalent live load cracking moment.
M_n	=	nominal moment resistance of the section.
M_{np}	=	nominal moment resistance of the section based on prestressing reinforcement only.
M_s	=	applied moment at service load.
n	=	modular ratio E_s / E_c .
P_{cr}	=	cracking load.
P_e	=	effective prestressing force.
P_i	=	initial prestressing force.
P_L	=	applied concentrated load.
P_{rep}	=	load at which the beam is unloaded.
P_u	=	ultimate load.

R	=	coefficient for crack width calculation (Gergely and Lutz 1966).
s	=	spacing between longitudinal reinforcement.
S_b	=	cross-sectional modulus at the tension side.
S_{rm}	=	average spacing between cracks.
w_k	=	characteristic crack width.
w_m	=	mean value for the crack width.
w_{max}	=	maximum crack width at the beam soffit.
w_{rep}	=	maximum crack width due to repeated loading.
y	=	distance measured from the neutral axis.
y_{cr}	=	distance to the centroid of the cracked section, measured from the extreme compression fibre.
y'_e	=	effective centroidal distance from the extreme compression fibre.
y_g	=	gross centroidal distance from the extreme compression fibre.
α_1	=	factor accounting for bond characteristics of reinforcement.
α_2	=	factor accounting for sustained or repeated loading.
β_1	=	bond factor for calculation of the deflection using the CEB-FIP Code.
β_2	=	factor depending on type of loading for calculation of the deflection using the CEB-FIP Code.
δ_{BC}	=	deflection at point C relative to the deflection at point B.
Δ_1	=	equivalent deflection of the uncracked section at a load equal to the ultimate load.
Δ_2	=	deflection at ultimate.
ΔP_c	=	total loss of compression in concrete due to the combined effect of creep, shrinkage of concrete and relaxation of prestressing reinforcement.
ΔP_p	=	increment of force in the prestressing reinforcement.
ΔP_s	=	increment of force in the non-prestressed reinforcement.
ϵ_c	=	concrete strain at the extreme compression fibre.
ϵ'_c	=	concrete strain corresponding to the maximum stress.

ϵ_{ce}	=	concrete strain at the level of the prestressing reinforcement, due to prestressing force.
ϵ_{ct}	=	average tensile strain.
ϵ_{cr}	=	tensile strain at cracking.
ϵ_{cu}	=	ultimate strain of the concrete in compression.
ϵ_e	=	effective strain of the prestressing reinforcement after losses.
ϵ_i	=	initial strain of the prestressing reinforcement.
ϵ_p	=	total strain of the prestressing reinforcement.
ϵ_{s2}	=	strain of the prestressing reinforcement after decompression.
ϵ_{sh}	=	concrete shrinkage.
ϵ_{sr2}	=	strain of reinforcement at cracking load, based on cracked section properties.
ϵ_{tf}	=	maximum tensile strain in the concrete (Bažant and Oh 1984).
ϕ	=	curvature at the given strain increment.
ϕ	=	curvature of the section.
ϕ_1	=	equivalent curvature of the uncracked section at a load equal to the ultimate load.
ϕ_2	=	curvature at ultimate.
ϕ_{cr}	=	curvature of the section based on cracked section properties.
ϕ_g	=	curvature of the section based on uncracked section properties.
ϕ_e	=	effective curvature of the section accounting for tension stiffening.
μ	=	ductility index.
σ_1	=	tensile stress in concrete due to applied loads, based on uncracked section.
ρ	=	ratio of non-prestressing tension reinforcement A_{ns}/bd .
ρ'	=	ratio of non-prestressing compression reinforcement A'_s/bd .
ρ_p	=	ratio of prestressing reinforcement A_{ps}/bd_p .
θ_{BC}	=	slope at point C relative to the slope at point B.

LIST OF TABLES

Table

2-1	Examples of concrete bridges prestressed by <i>FRP</i> reinforcement	32
2-2	Characteristics of <i>FRP</i> prestressing reinforcement	33
4-1	Maximum allowable computed deflection recommended by ACI and CSA Codes	121
4-2	Maximum recommended crack width (CPCI Metric Design Manual)	122
4-3	Recommended limits of crack width given by the CEB-FIP Code 1978 . .	122
4-4	Crack width calculations based on fictitious tensile stress approach	123
4-5	Crack width calculations based on reinforcement stress approach	124
5-1	Test program	147
5-2	Tensile properties of the Leadline	147
5-3	Concrete properties	148
5-4	Prestressing forces in the tested beams	148
6-1	Experimental results of the tested beams	189
6-2	Measured response at stabilization of cracks	189
6-3	Cracking behaviour of the beams at maximum crack width of 0.4 mm . .	190
7-1	Comparison between the predicted and the experimental results	269
7-2	Error of the predicted deflection within service load	270
7-3	Error of the predicted deflection up to the ultimate load	270
7-4	Statistical data of the error of crack width prediction	271
7-5	Member deformability of the tested beams	271

LIST OF FIGURES

Figure

2-1	Specific design load vs. main span for classical form of suspension bridges	34
2-2	Retrofitting of chimney	34
2-3	Strengthening of existing bridges with steel plates and unidirectional carbon fibre reinforced epoxy tapes	34
2-4	Structural floor of bridge enclosure	35
2-5	Tunnel lining by <i>FRP</i> grids	35
2-6	Cross-section of Marie d'Ivry metro station	36
2-7	One of the four turrets constructed to house communications equipments	36
2-8	Tensile stress-strain diagrams for various reinforcing fibres	37
2-9	Tensile stress-strain diagrams of a thermosetting polymer (epoxy) and a thermoplastic polymer (polysulfone)	37
2-10	Tensile stress-strain diagrams of several <i>FRP</i> and prestressing wire	37
2-11	Creep strength of <i>GFRP</i> bars (Polystal)	38
2-12	Fatigue behaviour of <i>GFRP</i> bars (Polystal)	38
2-13	Stress relaxation of <i>GFRP</i> (Polystal), <i>AFRP</i> (Arapree) and prestressing steel (low relaxation)	38
2-14	Stress relaxation of <i>CFCC</i> in normal temperature	39
2-15	Fatigue strength of <i>CFCC</i>	39
2-16	Stress relaxation of Leadline	40
2-17	Stress relaxation of <i>CFRP</i> (Leadline), <i>AFRP</i> rod in alkaline solution	40
2-18	Fatigue behaviour of Leadline	40
2-19	Relaxation of Technora	41
2-20	Fatigue behaviour of Technora	41

Figure		
2-21	Relaxation of Fibra	41
2-22	Stress relaxation of Arapree	42
2-23	Stress-rupture behaviour of Arapree	42
2-24	Anchor for Polystal prestressing tendon, Strabag Bau-AG, "grout type" . . .	43
2-25	Anchorage for <i>CFRP</i> ropes using die-cast wedge by Tokyo Rope	43
3-1	Strain and stress distribution for beams prestressed by <i>FRP</i> with different modes of failure	78
4-1	Idealized load-deflection curves for beams with varying amounts of prestress force (Nilson 1987)	125
4-2	Calculating deflection from the curvature (Collins and Mitchell 1991) . . .	126
4-3	Centroidal distances for uncracked, partially cracked and fully cracked sections	126
4-4	Assumed uniaxial stress-strain relations for concrete in tension and compression (Bažant and Oh 1984)	127
4-5	Average stress vs. average strain relationship for concrete in tension (Collins and Mitchell 1991)	127
4-6	Effective embedment zone defined by the CEB-FIP Code 1978	128
4-7	Equivalent uniform stress distribution (Collins and Mitchell 1991)	128
5-1	Cross-sections of the tested beams	149
5-2	Details of the end zone of the beam	149
5-3	Schematic of the jacking setup	150
5-4	Details of 2-D-8 Leadline anchorage	150
5-5	Details of the hinge system	151
5-6	jacking setup	151
5-7	Load history	152
5-8	Schematic of the test setup	152
5-9	Test setup	153

Figure		
5-10	Location of the demec point stations	153
5-11	Microscope for measuring the crack width	154
5-12	Schematic of the tension test of the Leadline using concrete anchorage (configuration #1)	154
5-13	Tension test of Leadline bar using concrete anchorage (configuration #1) .	155
5-14	Stress-strain relationship of the Leadline bar	155
5-15	Schematic of the tension test of the Leadline using concrete anchorage (configuration #2)	156
5-16	Tension test of Leadline bar using concrete anchorage (configuration #2) .	156
5-17	Transfer length of Leadline	157
5-18	Failure mode of two beams with 800 mm span reinforced by Leadline and steel	157
5-19	Bond stress for Leadline bars and steel strands	158
6-1	Typical load-deflection of beam prestressed by Leadline	190
6-2	Cracking of beam T-4-.5-H	191
6-3	Cracking of beam R-4-.5-H	191
6-4	Cracking of beam T-4-.5-V	192
6-5	Cracking of beam R-4-.5-V	192
6-6	Cracking of beam T-4-.7-V	193
6-7	Cracking of beam R-4-.7-V	193
6-8	Cracking of beam T-2-.5-V	194
6-9	Cracking of beam R-2-.5-V	194
6-10	Cracking of beam S-T-2-.5	195
6-11	Typical Load-deflection of beam prestressed by steel	195
6-12	Cracking of beam S-R-2-.5	196
6-13	Failure due to rupture of Leadline bars	196
6-14	Failure due to crushing of the concrete (beam prestressed by Leadline) . .	197

Figure		
6-15	Beam R-4-.5-V at failure	197
6-16	Failure of beam S-T-2-.5 prestressed by steel	198
6-17	Failure of beam S-R-2-.5 prestressed by steel	198
6-18	Typical load-strain relationship of beam prestressed by Leadline	199
6-19	Concrete strain at the top surface for typical beam prestressed by Leadline	199
6-20	Concrete strain at reinforcement level for typical beam prestressed by Leadline	200
6-21	Neutral axis of beams with 600- and 200-mm flange width	200
6-22	Beam T-4-.7-V at failure	201
6-23	Average crack width for typical beam prestressed by Leadline	201
6-24	Maximum crack width for typical beam prestressed by Leadline	202
6-25	Average crack width measured at two levels below the neutral axis	202
6-26	Crack distribution at service load for beams with 600 mm flange width . .	203
6-27	Crack distribution at service load for beams with 200 mm flange width . .	204
6-28a	Load-deflection of beams prestressed by Leadline & steel (flange width = 600 mm)	205
6-28b	Load-deflection of beams prestressed by Leadline & steel (flange width = 200 mm)	205
6-29	Concrete strain at the top surface of beams prestressed by Leadline & steel	206
6-30	Concrete tensile strain of beams prestressed by Leadline & steel	206
6-31	Strain distribution at the critical section of beams prestressed by Leadline & steel	207
6-32a	Neutral axis of beams with 600 mm flange width and prestressed by Leadline & steel	208
6-32b	Neutral axis of beams with 200 mm flange width and prestressed by Leadline & steel	208

Figure		
6-33	Number of cracks of beams prestressed by Leadline and steel	209
6-34	Spacing between cracks for beams prestressed by Leadline and steel	209
6-35	Variation of the crack spacing at service load limit	210
6-36	Variation of the crack spacing at ultimate load	210
6-37a	Variation of the crack width of beams prestressed by Leadline	211
6-37b	Variation of the crack width of beams prestressed by steel	211
6-38	Maximum crack width vs. the measured strain of beams prestressed by Leadline & steel	212
6-39	Load-deflection of beams with 600 and 200 mm flange width	212
6-40a	Concrete strain at the top surface of beams with 600- and 200-mm flange width	213
6-40b	Concrete strain at reinforcement level of beams with 600- and 200-mm flange width	213
6-41	Maximum crack width of beams with 600- and 200-mm flange width . . .	214
6-42	Neutral axis of beams with 600- and 200-mm flange width	214
6-43	Load-deflection of beams with different jacking stress	215
6-44	Concrete strain at reinforcement level of beams with different jacking stresses	215
6-45	Neutral axis of beams with different jacking stresses	216
6-46	Load-deflection of beams with different number of Leadline bars	216
6-47	Load-deflection of beams with different distribution of the Leadline bars in the tension zone	217
6-48	Maximum crack width of beams with different distribution of the Leadline bars in the tension zone	217
7-1	Strain compatibility of concrete section prestressed by <i>FRP</i>	272
7-2	Stress-strain of the concrete in compression	272
7-3	Calculated rupture strength of concrete	273

Figure	
7-4	Numerical integration of the curvature for deflection calculation 274
7-5	Integration of the curvature at key sections 275
7-6	Error distribution of the predicted deflection ignoring the tension stiffening 275
7-7	Load-deflection using I_e method (Tadros et al.) 276
7-8	Error distribution of the predicted deflection using I_e method (Tadros et al.) 276
7-9	Predicted deflection using the CEB-FIP Code for beam with a small flange width 277
7-10	Predicted deflection using the CEB-FIP Code for beam with a large flange width 277
7-11	Error distribution of the predicted deflection using the CEB-FIP Code . . . 278
7-12	Predicted deflection using integration at key sections 278
7-13	Curvature along the beam span using the CEB-FIP Code'90 279
7-14	Error distribution of the predicted deflection using integration at key sections 279
7-15	Strain compatibility of prestressed concrete section accounting for concrete in tension 280
7-16	Prediction of α_1 for beams prestressed by Leadline 280
7-17	Predicted deflection using strain compatibility with and without accounting for tension stiffening 281
7-18	Error distribution of the predicted deflection using strain compatibility . . 281
7-19	Predicted deflection using method 3 for a beam prestressed by Leadline tested by (Fam and Rizkalla 1995) 282
7-20	Predicted vs. measured effective centroidal distance, y'_e 282
7-21	Predicted deflection using I_e methods (Tadros et al. 1985 and simplified method) 283

Figure	
7-22	Error distribution of the predicted deflection using the simplified method . 283
7-23	predicted versus measured deflection for a typical beam 284
7-24	Error distribution of the predicted deflection for a typical beam 284
7-25	Accuracy of the deflection calculation within service load range 285
7-26	Accuracy of the deflection calculation up to the ultimate load 285
7-27	Non-linear relationship of the stress in the prestressing reinforcement after decompression versus crack width 286
7-28	Linear relationship of the stress in the prestressing reinforcement after decompression versus crack width 286
7-29	Correlation between concrete area in tension A_t and crack width 287
7-30	Strain versus maximum crack width for beams prestressed by Leadline and steel 287
7-31	Calculation of the bond factor, k , using Suri and Dilger (1986) method . . 288
7-32	Crack width prediction using Suri and Dilger (1986) 288
7-33	Predicted crack width using Suri and Dilger method for a beam tested by (Fam and Rizkalla 1995) 289
7-34	Calculation of the bond factor, k_f , using the CEB-FIP Code (1978) 289
7-35	Crack width prediction using the CEB-FIP Code (1978) 290
7-36	Calculation of the bond factor using Gergely and Lutz method (1966) . . . 290
7-37	Crack width prediction using Gergely and Lutz method (1966) 291
7-38	Accuracy of the three methods used for calculating the crack width 291
7-39	Predicted vs. measured strain at the extreme compression fibre 292
7-40	Predicted vs. measured strain at the level of the bottom <i>CFRP</i> bars 292
7-41	Predicted vs. measured strain profiles at service load and before failure . . 293
7-42	Load-deflection of beams prestressed by <i>CFRP</i> bars and steel under repeated load 296
7-43	Proposed model to calculate the deflection of beams prestressed by <i>CFRP</i>

Figure		
	bars under repeated load	296
7-44	Comparison between centroidal distance at repeated loading and at first loading	297
Figure		
7-45	Predicted vs. measured deflection for a beam prestressed by <i>CFRP</i> bars under repeated loading	297
7-46	Proposed model to calculate the crack width of beams prestressed by <i>CFRP</i> bars under repeated load	298
7-47	Predicted crack width for one of the tested beams under repeated loading	298
7-48	Predicted capacity and maximum tensile stress of reinforcement for beams prestressed by Leadline	299
7-49	Capacity and deformability of beams prestressed by Leadline and steel . .	299
7-50	Proposed deformability of concrete beams prestressed by <i>FRP</i>	300
7-51	Deformability of beams prestressed by Leadline and steel	300
7-52	Deformability of beams prestressed by Leadline with different jacking stresses	301

1. _____ INTRODUCTION

1.1 GENERAL

Use of fibre-reinforced-plastic, *FRP*, as prestressing reinforcement for concrete structures, has increased rapidly for the last ten years. *FRP* reinforcement is made from high-tensile-strength fibres such as carbon, glass, aramid and others embedded in polymeric matrices and produced in the form of bars, strands, ropes, tendons and grids, with a wide variety of shapes and characteristics. *FRP* reinforcement is used as prestressing, non-prestressing and shear reinforcement for concrete structures. *FRP* grids also provide an excellent alternative for reinforcing bridge decks and parking structure slabs.

FRP has an outstanding characteristic as a non-corrosive reinforcement, which can increase significantly the service life of structures by reducing concrete deterioration due to corrosion. Other advantages of *FRP* reinforcement of particular interest in the field of structural applications are its high strength-to-weight ratio, good fatigue behaviour, low relaxation, electromagnetic neutrality, and easy handling and installation. The drawbacks

of *FRP* reinforcement are limited to its high cost, susceptibility to the stress-rupture effect (especially for glass *FRP* reinforcement), low shear strength, lack of ductility due its linear stress-strain behaviour up to failure, and low tensile strain at ultimate. Several prestressed concrete bridges have already been built in Japan, Germany, the USA, and Canada using this new material. *FRP* has also been used in other structural applications such as repair of structures, repair of bridges, bridge enclosures, tunnel lining, and marine structures. Special applications include radar stations, structures for magnetic levitation trains, antenna towers, and many non-structural elements.

Application of *FRP* reinforcement in prestressed concrete structures is relatively new. Therefore design engineers are dealing with this new material with extreme caution, especially due to the lack of knowledge of its long-term characteristics. Consequently, it is currently common practice to keep the jacking stress lower than that permitted by the codes for prestressing steel. Partial prestressing, which can be achieved either by lowering the jacking stress of reinforcement or by adding non-prestressed reinforcement in the cross-section, could be ideal for concrete beams prestressed by *FRP* due to the low jacking stresses typically specified for these materials. In fact, use of partial prestressing for concrete members has several advantages over full prestressing since members have less camber, more deformation at ultimate load, and are less costly due to the possibility of increasing the eccentricity of the prestressing reinforcement, thereby reducing the required area of reinforcement. Reduction of the required area of *FRP* reinforcement in

a given cross-section is important due to its relatively high cost.

Since the elastic modulus of *FRP* prestressing reinforcement is lower than that of steel, the expected deformations after cracking and consequently the crack width of members prestressed by *FRP* reinforcement will be greater than those for members prestressed by steel reinforcement. Despite the fact that *FRP* reinforcement is non-corroding, large cracks are not aesthetically desirable. Excessive deformations degrade the appearance of a structure. An appropriate crack width and maximum deflection should be selected according to the type of structure to maintain a good appearance. In conclusion, serviceability of concrete beams partially prestressed by *FRP* reinforcement, in terms of deflection after cracking and cracking behaviour, should be well investigated.

1.2 OBJECTIVES

The main objective of this investigation is to examine the serviceability of concrete members partially prestressed by carbon fibre-reinforced-plastic (*CFRP*) reinforcement.

The various specific objectives are:

1. to study the various flexural limit-states behaviour of concrete beams partially prestressed by *CFRP* reinforcement including behaviour after cracking and modes of failure.

2. to examine the deformational behaviour of partially prestressed concrete beams with *CFRP* reinforcement under service loading conditions, in terms of deflection prior and after cracking and strain distribution along the cross-section at different limit states.
3. to study the cracking behaviour of partially prestressed concrete beams with *CFRP* reinforcement, including crack pattern and crack widths, as related to the following variables:
 - a. Stress in the reinforcement.
 - b. Effective concrete area in tension.
 - c. Number of prestressed *CFRP* bars.
 - d. Degree of prestressing.
4. to compare the behaviour of partially prestressed concrete beams with *CFRP* reinforcement to that of similar beams prestressed by conventional steel strands.
5. to introduce analytical models to predict the deflection as well as the crack width of partially prestressed concrete beams with *CFRP* reinforcement due to first and repeated loading conditions within the service load range.
6. to propose a model to calculate the deformability of beams prestressed by *FRP* reinforcement and to compare it with that of similar beams prestressed by steel strands.

1.3 SCOPE AND CONTENTS

This study comprises experimental and analytical investigations. Based on the measured deflection and cracks, the analytical model will be used to introduce equations and design recommendations to predict the deflection and crack width of concrete members partially prestressed by *CFRP* reinforcement. Each phase of this study is discussed briefly in the following subsections.

Phase I: Experimental Investigation: The experimental program consisted of testing ten prestressed concrete beams. Eight beams were prestressed by *CFRP* bars and two by conventional steel strands. The *CFRP* bars used for pretensioning had a nominal diameter of eight millimetres with a brand name of Leadline and were produced by Mitsubishi Kasei, Japan. In this investigation, the jacking stress was varied between 50 and 70 percent of the nominal strength guaranteed by the manufacturer. The cross-section of five beams was a T-section with a 600-mm flange width; the other five beams had a 200-mm flange width. All beams had a total length of 6.2 meters, a clear span of 5.8 meters and a total depth of 330 mm. This configuration provided a span-to-depth ratio similar to that typically used by the industry for bridge girders. The beams were simply supported with 200-mm overhang at each end and were tested using a four-point loading test setup. All beams were designed to fail in the flexural mode without premature failure due to shear or loss of bond.

The beams were tested using quasi-static monotonic concentrated loads which were cycled three times within the service load range. Deflection of the beam as well as the cracking behaviour, including crack width and pattern, were observed during the tests. The strains in the *CFRP* reinforcement and the concrete were also measured. Several Leadline *CFRP* bars and concrete control specimens were tested to examine the properties of the materials.

Phase II: Analytical Study: This phase of the investigation included a rational analysis to predict the behaviour of concrete beams partially prestressed by *CFRP* reinforcement. The analysis was based on a strain compatibility approach in addition to similar approaches to those adopted by the Canadian, American and the European codes for beams prestressed by conventional steel reinforcement. The analysis used the mechanical properties of the Leadline *CFRP* bars to predict the moment-curvature and load-deflection of beams under short-term loading. Crack width in the service load range was also predicted. Measured and predicted deflection and crack width were compared. The deflection and the crack width of the beams under repeated loading were also predicted and compared to the measured values. The study introduced a model for the deformability of concrete beams prestressed by *FRP* and compared its results with the current model typically used for concrete beams prestressed by steel reinforcement.

Phase III: Design Recommendations: Based on the experimental results of the tested

beams and the analytical methods, new parameters were proposed to predict accurately the deflection, prior to and after cracking, and the crack width of concrete beams partially prestressed by *CFRP* prestressing reinforcement. Design recommendations were introduced for flexural design of partially prestressed concrete members with *CFRP* prestressing reinforcement. The study also provided recommendations to control deflection as well as crack width under first and repeated loading of partially prestressed beams with *CFRP* reinforcement. The following is a brief description of the contents of each chapter in the thesis:

Chapter 2: This chapter covers state-of-the art information on the properties of commercially available *FRP* reinforcement and its application to structural engineering.

Chapter 3: The available literature on the behaviour of prestressed and partially prestressed concrete beams by *FRP* reinforcement is reviewed. The behaviour of beams under flexure, fatigue and long-term loading as well as the bond characteristics of *FRP* reinforcement is described. The ductility provisions for concrete beams prestressed by *FRP* reinforcement are also discussed.

Chapter 4: This chapter presents methods currently available for prediction of deflection prior to and after cracking, and of crack width of partially prestressed concrete beams with steel reinforcement. The Canadian, American and European approaches to the

calculation of deflection and crack width of partially prestressed concrete beams are also presented. A survey of the research on serviceability of beams prestressed by *FRP* reinforcement is also presented in this chapter.

Chapter 5: This chapter describes the experimental program conducted at the University of Manitoba to test ten partially prestressed concrete beams pretensioned by Leadline bars and steel strands. Also presented are the mechanical properties of the Leadline bars in terms of tensile strength, bond characteristics, and transfer length based on beam testing and control specimens.

Chapter 6: The flexural behaviour of the tested beams, in terms of deflection, crack width, crack pattern and strain distribution is described. This chapter also describes the overall behaviour of the beams in terms of cracking load, ultimate carrying capacity, and different modes of failure and their associated deformability. The behaviour of beams prestressed by *CFRP* bars is compared to that of the tested beams prestressed by steel. Effects of the degree of prestressing, and the distribution of the tension reinforcement on the behaviour of the beams are discussed.

Chapter 7: The flexural behaviour in terms of cracking and ultimate capacity of the beams as well as the serviceability limit-states are predicted. Accurate and simplified methods are given to predict deflection prior to and after cracking, including tension

stiffening, under short-term loading. The crack width of the beams is also predicted using three different methods. New methods are proposed to calculate the deflection and the crack width of the beams due to repeated loading. An expression is proposed for the effective centroidal distance of a cracked section prestressed by *CFRP* bars. A deformability model for concrete beams prestressed by *FRP* is also proposed and compared to conventional methods for evaluating ductility. Design recommendations for partially prestressed concrete beams with *CFRP* bars are also presented.

Chapter 8: A summary of the investigation is given. Several conclusions are introduced to give an understanding of the behaviour of concrete beams partially prestressed by *CFRP* reinforcement.

2. ————— FIBRE REINFORCED PLASTIC REINFORCEMENT

2.1 BACKGROUND

Developments in science and technology have accelerated in the last decade, especially in the composites industry. The development of new materials and their applications in aerospace and defence has been growing fast. Much of the research and investment that has taken place has been aimed at these market areas. On the other hand, the rate of development with respect to the needs of the construction industry, namely, mass produced, high quality, relatively low cost composite products to meet sophisticated structural requirements, has been relatively slow. Increasingly, fibre reinforced plastics (*FRP*) have been used in a number of structures, such as bridges, buildings, off-shore structures, and retaining walls in Japan, Germany, the USA, and Canada.

Population growth and the demand for services have meant that infrastructures are overwhelmed with a level of usage never anticipated during construction. Corrosion of steel, sometimes exacerbated by poor design and construction, has led to rapid

deterioration of structures. The cost to repair and replace these structures is staggering. More durable structures which can be maintained indefinitely without disrupting usage are needed. High-quality structural composites are being seen as materials likely to assist in meeting these objectives. However, standard specifications and codes of practice do not yet exist in civil and structural engineering applications of composites; therefore, the vital questions of reliability and performance are difficult to address.

2.2 DEFINITION OF *FRP*

Fibre reinforced plastics (*FRP*) are obtained by inserting fibres of high strength into a polymer matrix. The reinforcement of the matrix is provided by the fibres which are characterized by very high strength-to-weight ratios and very small diameters. The matrix is essentially the binder material of the composite. Similar to the behaviour of many tissues in the body, which are made up of stiff fibres embedded in a lower stiffness matrix, the essence of *FRP* technology is the ability to have strong fibres in the right location, in the right orientation and with the right volume fraction. Since different materials can be used as a matrix for various types of fibres, the scope in terms of properties is almost limitless. In practice, only a few materials are used, and selection is determined by factors such as ease of fabrication, compatibility between matrix and fibres, desired end properties, and cost. Therefore, the most commonly used fibre materials are glass, carbon, and aramid (abbreviation for polyparaphenylene-

terephthalamide). The matrix materials are classified in general into two groups of thermosetting resins, namely, polyesters and epoxides, and thermoplastics resins, namely, nylon, polycarbonate and polypropylene.

A flat arrangement of unidirectional fibres or woven fibre fabrics in a thin layer of matrix material produces a lamina. The properties of the laminae are strongly dependent on the orientation of the embedded fibres. In general, fibre-reinforced laminae display anisotropic behaviour. A series of laminae stacked together, with a prescribed sequence of orientation for the individual laminae, forms a laminate. Laminates can be tailored to provide the directional dependence of strength and stiffness required to match the loading conditions to which the structural element will be subjected. A wide variety of *FRP* structural shapes and pultruded custom shapes are now commercially available. In addition, fibre-reinforced prestressing tendons and cables, rebars, gratings, and reinforcing grids are widely produced in different shapes using carbon, aramid, and glass.

2.3 APPLICATIONS OF *FRP*

There has been a rapid growth in the use of fibre-reinforced materials in engineering applications in the last few years. However, the full potential of *FRP* has yet to be realized in civil and structural engineering applications. *FRP* comes in the form of laminates, structural sections, reinforcing bars and grids and prestressing tendons. Fibre

reinforced materials are not universal substitutes for other materials and should be selected for their own particular qualities. However, the advantages of *FRP* will certainly encourage the designers to achieve structural systems that could not be built using conventional materials.

One of the major problems that readily reduces the life of concrete structures is the corrosion of steel reinforcement. This problem is more serious in cold climates where de-icing salts accelerate the deterioration. Since *FRPs* are non-metallic materials, they are non-corroding which is a major advantage over steel. The potential result of eliminating corrosion is a longer life-time of structures with minimum maintenance, which will significantly offset the high material cost.

FRP has strength-to-weight ratios ranging from three to five times higher than that of prestressing steel. The light weight of the *FRP* makes handling and installation generally much easier and reduces costs of assembly. This also makes *FRP* very attractive as a rehabilitation material. The other important properties of *FRP* are its electro-magnetic neutrality and relatively favourable fatigue behaviour.

FRP has been used in the following structural applications :

1. Short span bridges: Many pedestrian bridges have been constructed using *FRP*. A

Philadelphia company, E.T Techtonics, has constructed pedestrian bridges using Kevlar 49 cables to prestress glass-fibre king-post, queen-post and truss bridges. Bridges of 7- to 10-m span have been constructed (cited in Mufti, Erki, and Jaeger 1991).

Fibre reinforced plastic tendons have been used to reinforce and prestress concrete to produce more durable structures. In addition to the previously mentioned advantages of *FRP*, *FRP* tendons are characterised by high tensile strength, low relaxation under sustained high loads (especially for carbon and glass-based *FRP*) and excellent fatigue properties (especially for carbon and aramid *FRP* tendons) (Rostásy 1988). The low Young's modulus of *FRP* tendons results in a reduction in prestressing losses. These characteristics greatly enhance the use of *FRP* as prestressing tendons for short-span bridges. A number of pedestrian and highway bridges in several countries have been built using *FRP* structural sections and prestressing elements for concrete girders and slabs (Mufti, Erki, and Jaeger 1991 and Minosaku 1992). Table 2-1 shows different types of prestressed concrete bridges with *FRP* prestressing tendons.

2. Long span bridges: As a result of the very high strength-to-weight ratio of *FRP* compared to those of conventional materials, *FRP* can compete with steel and concrete in the construction of long span bridges. *FRP* structural sections can be

utilized in the construction of the bridge girders , while unidirectional *FRP* tendons can be used as cables under tension. To date, the construction of relatively long-span bridges with *FRP* has not been reported. A proposal for a carbon-fibre-reinforced-composite bridge across the strait of Gibraltar at its narrowest site was reported by Prof. Urs Meier (Meier 1988). Prof. Meier outlined the feasibility of constructing cable-stayed and classical suspension bridges of steel, glass-reinforced plastics (*GRP*) and carbon-fibre-reinforced plastics (*CFRP*) and concluded that the most feasible design would be a cable-stayed bridge of *CFRP*. In Fig. 2-1, the specific design loads versus the centre spans for the classical form of suspension bridges made of steel are compared with those made of *GRP* or *CFRP*. The comparison shows that the use of advanced composites would allow the doubling or tripling of the limiting span in comparison to steel structures.

3. Repair of structures: A number of chimneys, columns, slabs and girders have been strengthened against overloads from earthquake or changes in use using *CFRP* products (Mufti, Erki and Jaeger 1992). Many products are available for such retrofitting. These are most often unidirectional fibre tapes, fibre winding strands and fabrics. Flexural and shear strengthening are possible using these materials.

The process used to retrofit a typical chimney starts with the preparation and trowelling of the concrete surface with mortar or epoxy, followed by application of

auto-adhesive tapes in the longitudinal direction and confinement of the chimney by circumferentially wound carbon strands. An automatic winding machine was made to facilitate the strand winding operation, as shown in Fig. 2-2. Finally, a fire-resistant covering material, such as mortar, is applied on the surface.

4. Repair of bridges: Many highway bridges built 40 years ago have deteriorated due to the increased weight of trucks legally permitted on highways. In addition, corrosion caused by de-icing salts has made the deterioration even more severe. Strengthening of deteriorated steel and concrete structures by bonding carbon-fibre-reinforced epoxy laminates to the exterior of the structure has been studied in Switzerland and Germany (Meier and Kaiser 1991). The study has shown that the use of *CFRP* laminates in place of steel plates for such applications can reduce the total cost of a reinforcing project by about 20 percent. Although the *FRP* materials are much costlier than steel, the lighter weight and better corrosion-resistant properties can result in significant reductions in fabrication and long-term costs, as shown in Fig. 2-3.

5. Bridge enclosures: The concept of "Bridge Enclosure" involves hanging a floor from the steel girders of a composite bridge, at the level of the bottom flanges of the girders, to provide access for inspection and maintenance. The floor is sealed to the outside girders to provide protection from the environment. Corrosion rates of steel

within such enclosures have been found to drop to negligible levels. The first system of this type in the world was installed on the A19 Tees Viaduct in Middlesbrough, England, in 1989. The material used was glass-reinforced-plastic (*GRP*) (Maunsell International Consulting Engineers 1989). The structural floor of the enclosure, as shown in Fig. 2-4, is composed of pultruded *GRP* panels which are characterised by light weight and high durability. The modular *GRP* panels were selected on the basis of a cost/benefit analysis, which took into account total costs of inspection and maintenance of the steel plate girders. Other cost-saving attributes to the system were the minimum weight, reliable life to first maintenance (30 years), good fire resistance and good long-term appearance.

6. Tunnel lining: *FRP* grids covered by shotcrete can be used for tunnel lining. *FRP* has advantages over the steel due to its high corrosion-resistance, its flexibility which makes it suitable for curved surfaces, as shown in Fig. 2-5, and its excellent alkali-, acid- and chemical-resisting properties. The material is very in light weight, having approximately one-fourth the specific gravity of steel, and may be cut easily with a hack-saw. *FRP* grids have been used in many tunnel lining projects (NEFMAC, 1987) such as the Kakkonda hydroelectric power plant, where glass *FRP* was used to reinforce the arch, side wall and invert of a water-conveyance tunnel for crack prevention in a total area of 430 m².

7. Marine structures: Glass *FRP* has been used for over 45 years in marine applications. Fibreglass boats are roughly 95 percent of all the boats manufactured in the USA. Durability and performance of fibreglass in salt water has thus been proven with time. Sen, Issa and Iyer (1992) reported a feasibility study of fibreglass pretensioned piles in a marine environment.

8. Special applications: Fibreglass cables were used in the rehabilitation of the Mairie d'Ivry metro station in Paris, as shown in Fig. 2-6, where the non-magnetic nature of the material played an important role in cable selection.

A computer research centre was constructed using glass fibre pultruded sections and is shown in Fig. 2-7. The major advantage of using glass fibres in this structure is that they are invisible to radio waves.

2.4 MATERIAL PROPERTIES

There are a large number of candidate constituent materials in addition to the material configuration variables, including number of fibres, orientation of fibres, combination of fibres, type of matrices, etc, which significantly affect the characteristics of *FRP*. A brief review of the fibre and matrix properties is given followed by the properties of *FRP* prestressing reinforcement.

2.4.1 Fibre Properties

Fibres are the principal constituent in *FRP* material as they occupy the largest volume fraction and carry the major portion of the load acting on a composite structure. Proper selection of the type, number, and orientation of fibres is very important, since it influences the tensile and compressive properties of the *FRP* product as well as its electrical and thermal conductivities and cost.

It has been reported that variability is an important aspect of the mechanical properties of fibres, as tests on individual fibres show a wide range of strengths (Hull 1981). A comparison of the tensile stress-strain behaviours for different fibres is given in Fig. 2-8. The fibres are characterised by linear behaviour up to failure, with all the fibres fracturing in a brittle manner without any yield or flow. Carbon and glass fibres are almost completely brittle and fracture without any reduction in the cross-section; for Kevlar 49 fibres, necking precedes fracture and final separation occurs after a large amount of local drawing. The stress-strain curves show that the high-modulus fibres have a much lower strain at failure. Carbon fibres have the highest specific Young's modulus (modulus / density) and the lowest strain at failure, followed by Kevlar 49 and glass. The variability of the tensile strength is less than that of the modulus of elasticity.

2.4.1.1 Glass

Two types of glass fibres, E-glass and S-glass, are commonly used in the *FRP* industry. E-glass has the lowest cost of all commercially available reinforcing fibres, which is the reason for its widespread use. S-glass has the highest tensile strength among all fibres in use (Mallick 1993). However, the compositional difference and higher manufacturing cost make it more expensive than E-glass.

The average tensile strength of freshly drawn glass fibres may exceed 3.45 GPa. However, surface damage (flaws) produced by abrasion, either by rubbing against each other or by contact with the processing equipment, tends to reduce its tensile strength to values in the range of 1.72 to 2.07 GPa. Strength degradation increases as the surface flaws grow under cyclic loads; this is one of the major disadvantages of using glass fibres in fatigue applications.

The tensile strength of glass fibres is also reduced in the presence of water or under sustained loads (static fatigue). Water bleaches alkalis from the surface and deepens surface flaws already present in the fibres. Under sustained loads, the growth of surface flaws is accelerated due to stress corrosion by atmospheric moisture. As a result, the tensile strength of glass fibres is decreased by increasing load duration (Mallick 1993).

2.4.1.2 Carbon

Carbon fibres are manufactured from two types of fundamental materials, namely, textile PAN-based and PITCH-based materials. The most common textile material is poly-acrylonitrile (PAN). Pitch-based carbon, which is a byproduct of petroleum refining or coal coking, has a lower cost than pan-based carbon.

Carbon fibres are commercially available with tensile moduli varying from 270 to 517 GPa (Mallick 1993). In general, the low-modulus fibres have lower specific gravities, lower cost, higher tensile strengths and higher tensile strains to failure than the high-modulus fibres. However, the manufacturers of carbon fibres report that the tensile strength of the fibres is in the range of 3000 MPa and the tensile elastic modulus about 230 GPa. Among the advantages of carbon fibres are their exceptionally high tensile-strength-weight ratios as well as tensile-modulus-weight ratios, very low coefficient of linear expansion, and high fatigue strengths. The disadvantages are their low impact resistance, high electrical conductivity and high cost.

2.4.1.3 Kevlar 49

Kevlar 49 is a highly crystalline aramid (aromatic polyamide). Among the reinforcing fibres, Kevlar 49 has the lowest specific gravity and the highest tensile

strength-weight ratio (Mallick 1993). The major disadvantages of Kevlar 49 are its low compressive strength and difficulty in machining.

Although the tensile stress-strain behaviour of Kevlar 49 is linear, fibre fracture is usually preceded by longitudinal fragmentation, splintering and even localized drawing. In bending, Kevlar 49 fibres exhibit a high degree of yielding on the compression side. Such a non-catastrophic failure mode is not observed in other fibres and gives Kevlar 49 composites superior damage tolerance against impact or other dynamic loading. Kevlar 49 fibres start to carbonize at about 427°C and the recommended maximum long-term-use temperature is 160°C. It is reported that moisture has little or no effect on the properties of Kevlar 49; however, it is quite sensitive to ultra-violet radiation.

2.4.2 Matrix Properties

The role of the matrix in a fibre reinforced composite is:

1. To transfer stresses among the fibres.
2. To provide a barrier against an adverse environment.
3. To protect the surface of the fibres from mechanical abrasion.

The matrix plays a minor role in the tensile load-carrying capacity of a composite

structure. However, it has a major influence on the interlaminar and in-plane shear properties of a composite structure. Matrix materials are either polymeric, metallic or ceramic. Polymers are the most commonly used, and are divided into thermoplastics and thermosets. The tensile stress-strain diagrams of thermosetting polymer (epoxy) and a thermoplastic polymer (polysulfane) are shown in Fig. 2-9. Increasing the temperature and decreasing the rate of loading result in an increase in the ultimate strain and a decrease in the ultimate stress of the polymeric solids (Mallick 1993).

2.5 CHARACTERISTICS OF *FRP* REINFORCEMENT

FRP prestressing reinforcements currently commercially available are mainly made of parallel filaments of glass, carbon, or aramid, most of which are impregnated with a resin matrix. They are available in the form of bars, ropes, and strands. The general advantages of *FRP* prestressing reinforcements compared to steel are:

1. High ratio of strength-to-mass density (up to 5 times greater than that of steel)
2. Carbon and aramid fibre tendons have excellent fatigue characteristics. However, the fatigue strength of glass *FRP* reinforcement may be significantly below that of steel.
3. Excellent corrosion resistance and electromagnetic neutrality.
4. Low coefficient of thermal expansion in the axial direction, especially for carbon

FRP reinforcement.

The disadvantages of *FRP* prestressing reinforcement include:

1. High cost (5 to 10 times more than that of steel).
2. Low failure strain.
3. Low ratio of lateral-to-axial strength.
4. Low long-term to short-term static strength (especially for glass *FRP*).
5. Glass fibres may deteriorate due to water absorption.

The characteristics of *FRP* reinforcement differ greatly according to the properties of the matrix and fibres and to the volume fraction of the fibres . Moreover, various parameters affect the stress-strain characteristics of *FRP* reinforcement, such as diameter and length of reinforcing bars, temperature, and rate of loading. The material characteristics of reinforcement made of glass-fibre-, carbon-fibre- and aramid-fibre-reinforced plastic (*GFRP*, *CFRP* and *AFRP* respectively) as compared to those of prestressing steel strands are shown in Fig. 2-10. Similarly to the behaviour of the fibres and unlike that of prestressing steel, *FRP* reinforcement does not yield but remains linearly elastic up to failure. Young's modulus of *FRP* reinforcement is much less than that of prestressing steel strand, ranging between 50 and 150 MPa, while the tensile strength is close to that of the steel. The characteristics of different commercial *FRP*

prestressing reinforcement are given in Table 2-2.

2.5.1 Glass-Based *FRP* Prestressing Reinforcement

GFRP is the least expensive type of *FRP* reinforcement. Since *GFRP* has a very low transverse shear strength, which makes it difficult to make efficient anchorages for prestressing, most of the *GFRP* reinforcement commercially available is proposed as non-prestressed reinforcement. Surface treatments such as quartz sand, to give a rough finish, and external fibre winding, to produce a ribbed surface, have been applied to *GFRP* bars to improve their bond to concrete. One commercial application of *GFRP* prestressing reinforcement is "Polystal". Other *GFRP* bars are produced for different applications such as Isorod by Pultall Inc. (Canada), IMCO by IMCO Reinforced Plastics Inc. (USA), Jitec by Cousin Frère (France), Kodiak by IGI International Grating (USA) and Plalloy by Asahi Glass Matrex (Japan). The following is a brief summary of the properties of Polystal *GFRP* prestressing tendons.

Polystal: is produced by Bayer AG in association with Strag Bau-AG in Germany. This tendon consists of bundles of bars, each containing E-type glass fibre filaments in an unsaturated polyester resin matrix. The bar diameter is 7.5 mm, with loosely packed fibres of 68 percent by volume (80 percent by weight). The specific weight of Polystal is 2.0 gm/cm^3 and its coefficient of linear thermal expansion is $0.7 \times 10^{-5} (1/^\circ\text{C})$. The

tensile strength of the Polystal is about 1670 MPa, while its young's modulus is 51 GPa. It is reported (Miessler and Preis 1989) that the time-dependent creep strength, which is called a creep-rupture phenomenon, is about 70 percent of the short-term strength as shown in Fig. 2-11. Polystal survived two million cycles under a stress range of 55 MPa with 10 percent failure probability, when a tensile fatigue test was conducted under a maximum stress (σ_0) = 736 MPa, which is 44 percent of the ultimate strength as shown in Fig. 2-12. It is concluded that a limiting fatigue strength at 2×10^6 load cycles does not exist for *FRP* (Rostásy 1988). Stress loss due to relaxation is predicted to be approximately 3.2 percent after 57 years. Fig. 2-13 shows the relaxation losses of Polystal in comparison to those of prestressing steel of a low-relaxation type.

2.5.2 Carbon-Based *FRP* Prestressing Reinforcement

CFRP prestressing reinforcement has the highest tensile modulus of elasticity of the various types of *FRP* reinforcement (about 70 percent of the modulus of prestressing steel). The maximum strain at failure is between 1.2 and 2 percent. The axial coefficient of thermal expansion is very low compared to that of prestressing steel (0 to 0.6×10^{-6} 1°C), while the radial coefficient of thermal expansion of *CFRP* ranges between 35 and 50×10^{-6} 1°C (Kim and Meier 1991). *CFRP* prestressing reinforcement is made in the form of bars, ropes and cables, using PAN or PITCH-based carbon fibres. Various types of *CFRP* reinforcement are produced, such as *CFCC* by Tokyo Rope (Japan), Leadline

by Mitsubishi Kasei (Japan), Jitec by Cousin Frère (France) and Bri-Ten by British Ropes (UK).

Carbon Fibre Composite Cables (CFCC): are made by Tokyo Rope (Tokyo Rope Mfg. Co., Ltd. 1993) in Japan using carbon fibres of polyacrylonitrile (PAN) supplied by Toho Rayon. The wires are made from roving prepreg, which consist of 12,000 filaments impregnated with resin. The prepreg is twisted to create a fibre core which is wrapped in synthetic yarns, thereby becoming a single cable. The yarn covering protects the core from UV radiation and mechanical damage, and improves the bond of *CFCC* to concrete. Cables consist of either single, seven, nineteen or thirty-seven wires. The wires are twisted to allow better redistribution of stresses through the cross-section. *CFCC* is available in diameters of 3 to 40 mm with a maximum length of 600 m. *CFCC* cables are flexible enough to be coiled on drums for transportation. Prior to heat curing, *CFCC* can be shaped into rectangular or circular spirals to be used as stirrups or confining reinforcement.

The tensile strength of *CFCC* varies according to the diameter of the cable. For the 12.5-mm cable, the tensile strength and modulus are 2100 MPa and 137 GPa, respectively. The coefficient of linear thermal expansion is approximately $0.6 \times 10^{-6} / ^\circ\text{C}$, which is about 1/20 of that of the steel. *CFCC* shows a relaxation of about 3.5 percent after 30 years at 80 percent of the ultimate load, which is 50 percent less than that of

prestressing steel strand, as shown in Fig. 2-14. Fig. 2-15 shows the tensile fatigue characteristics of *CFCC*, where a limit of two million cycles shows higher amplitude of stress for *CFCC* than the amplitude of stress of prestressing steel strand subjected to the same mean stress. Pull-out tests show that *CFCC* has bond strength to the concrete of more than two times higher than that of the steel.

Leadline: produced by Mitsubishi Kasei (Mitsubishi Kasei Corporation 1992), is another application for the use of carbon fibres in prestressing reinforcement. Leadline bars are pultruded using linearly oriented Dialead coal tar PITCH-based continuous carbon fibre and an epoxy resin. Leadline bars have round, ribbed, and indented shapes and a guaranteed tensile strength and modulus of 1970 MPa and 147 GPa, respectively, for 8-mm diameter. Relaxation of an 8-mm Leadline bar at normal temperature and in an alkaline solution (PH=13) with temperature = 60°C, is shown in Fig. 2-16 and 2-17. The anticipated relaxation of Leadline, after 30 years, is between 2 and 3 percent. The fatigue strength of 3-mm-diameter and 400-mm-length Leadline bar is shown in Fig. 2-18. At a constant stress range of 10 percent, the fatigue strength is 57 percent of the static strength at 10 million cycles.

2.5.3 Aramid-Based *FRP* Prestressing Reinforcement

Three different types of Aramid fibres are used in the industry to produce *AFRP*

prestressing reinforcement, namely Kevlar (29-49-149) by Dupont in U.S.A., Twaron by Aramid Maatschappij v.o.f. in the Netherlands, and Technora by Teijin in Japan. The fibre tensile strengths and moduli of elasticity are, respectively, 2650 MPa and 165 GPa for Kevlar 49, 2800 MPa and 125 GPa for Twaron, and 3400 MPa and 73 GPa for Technora. *AFRP* prestressing reinforcement is produced in different shapes such as spiral-wound, braided, and rectangular bars. The phenomenon of creep-rupture failure has been observed for *AFRP* reinforcement. Different *AFRP* prestressing elements are produced such as Technora by Teijin (Japan), FiBRA by Mitsui (Japan), Arapree by AKZO and Hollandsche Beton Groep nv (Holland), Phillystran by United Rope Works (USA), and Parafil Ropes by ICI linear Composites (UK).

Technora: Teijin Limited of Japan produces bars of brand name Technora using Teijin aramid fibres, PPODTA co-poly-paraphenylen/3,4'-oxdiphenylene terephthalamide, impregnated with vinylester resin in a pultrusion method. Both round bars and bars with external spiral windings are available in diameters of 3 to 8 mm. The bars are flexible enough to be wound on a 1.5-meter-diameter drum and may be cut to the required lengths with a grinder. The coefficient of linear thermal expansion is $-15 \times 10^{-6} / ^\circ\text{C}$. Relaxation of Technora *AFRP* prestressing reinforcement ranges between 7 and 14 percent (Kakihara, Kamiyoshi, Kumagai and Noritake 1991), as shown in Fig. 2-19. Fatigue characteristics of 6-mm *AFRP* bar are shown in Fig. 2-20. It is also reported that the number of cycles to fracture is higher than 1 million at practical levels of load, 1000-1200 MPa, and with

an amplitude of 200-300 MPa.

Fibra: is produced by Mitsui construction company by braiding multiple bundles of 600 denier (0.00066 oz/ft) kevlar 49 fibres and impregnating the braided fibres with an Epicote 827 and tetra epoxy resin (Mitsui Construction Co., Ltd.). Fibra bars are available in diameters from 3 to 16 mm, and can be wound on a 1.5 meter drum for easy transportation. Braiding was selected for manufacturing Fibra bars to increase the bond with concrete. Moreover, the bond can be further improved by applying a quartz sand finish to the bars. Relaxation after 100 hours was found to be 10 percent regardless of the initial load, which is two to three times greater than that of prestressing steel, as shown in Fig. 2-21. There was no apparent deterioration when the bars were placed in an alkaline environment with elevated temperature up to 80°C.

Arapree: aramid bar is developed by Akzo in association with Hollandsche Beton Groep nv. Arapree is manufactured by pultrusion, using Twaron HM aramid fibres and an epoxy resin. Arapree tendons are available in flat strips with cross-section ranging from 0.5x20 mm to 5.6x20 mm, and in round bars, with 2.5-, 5- and 7-mm diameters. Relaxation of Arapree in alkaline solutions is higher than relaxation in air (Gerritse and Werner 1991), as shown in Fig. 2-22. The creep-rupture behaviour, which is the relation between the stress level in the fibres and the time it takes for an Arapree bar to fail under the corresponding constant stress, is shown in Fig. 2-23.

2.6 ANCHORAGES OF *FRP* PRESTRESSING Reinforcement

The very low ratio of lateral to axial strength of *FRP* reinforcement (as high as 1:30) (Kim and Meier 1991), translates into a need to redesign the anchoring system for such reinforcement. Conventional systems such as clamps or potted end fittings that are used for steel cables or strands do not ensure reliable anchoring of *FRP* reinforcement. The principal goal is to achieve a stress distribution in the anchoring zone such that failure of the cable will take place outside the anchor zone. A further consideration is the long-term reliability of the anchor. It should be noted that the currently available anchorages can be used only for short-term applications.

Each type of *FRP* prestressing reinforcement commercially available has unique characteristics; to date, there is no single anchorage scheme that can ensure optimal prestressing load transfer for all of them. Most of the systems developed so far have been grout and wedge-type anchorages, as shown in Fig. 2-24 and 2-25, the exception being some non-resin-impregnated aramid tendons (Erki and Rizkalla 1993). One disadvantage of grout-type anchorages is that the tendon and its anchorages have to be supplied as a pre-assembled unit. This could be inconvenient if any late design changes are made or if the anchorages ever need to be replaced during their service life.

Table 2-1 Examples of concrete bridges prestressed by FRP reinforcement

Material	Bridge description	Diameter of reinforcement	Dimensions of the bridge	P/P_u^*
CFRP	BASF post-tensioned prestressed concrete highway bridge, Germany, 1991	Four cables, each is made of 19 1x7 ϕ 12.5	11.2 m wide x 80 m long, four 20 m spans, 2 straight and 2 curved	50 % under design load
	Nagatsugawa pretensioned simple slab pedestrian bridge, Japan, 1989	Cables of 1x7 ϕ 12.5 mm	2.5 m wide x 8.0 m long	60, 55 and 50 %, jacking, initial and at design load
	Kitakyusu prestressed concrete highway bridge, Japan, 1989	8 multi-cables bundled with 8 CFRP rods of 8 mm diameter	35.8 m long, pretensioned girder (18.2 m span) and post-tensioned girder (17.5 m span)	55 % under design load
	Shinmiya pretensioned concrete slab highway bridge, Japan, 1988	eight 1x7 ϕ 12.5	5.76 m span and 7 m wide	60, 55 and 45 %, jacking, initial and at design load
AFRP	Demonstration bridges for Technora, pretensioned composite slab and post-tensioned box girder, Japan, 1990 and 1991	3 ϕ 6 pretensioned strands, 19 ϕ 6 post-tensioned cables and 7 ϕ 6 external cables	11.79 m span for the pretensioned bridge and 24.1 m span for the post-tensioned girder	75, 70, and 60 %, jacking, initial and at design load
	Mito city post-tensioned concrete pedestrian suspended slab bridge, Japan, 1990	16 cables, each is made of 8 bands 4.86 x 19.5 mm	2.1 m wide and 54.5 m long	50 % under design load
	Nasu pretensioned prestressed concrete highway bridge, Japan, 1990	Braided AFRP 14 mm diameter	3 spans 11.98 m each	50 % under design load
GFRP	The Marienfelde pedestrian externally prestressed bridge, Germany, 1989	Cables of 1x19 ϕ 7.5	5 m wide and two spans of 17.6 and 23 m long	n/a [†]
	The Ulenbergstrasse post-tensioned prestressed highway bridge, Germany, 1986	59 cables of 1x19 ϕ 7.5	two spans of 21.3 and 25.6 m long	47 % under design load
	Lünen'sche Gasse single span slab bridge, Germany, 1980	100 rods of 7.5 mm diameter	6.55 m span	n/a [†]

* P/P_u is the ratio of the prestressing force to the ultimate strength of the cables

† not available

Table 2-2 Characteristics of FRP prestressing reinforcement

Commercial name	Fibre	Matrix	V_f^* (%)	Diam. (mm)	Density (gm/cm ³)	Tensile [†] strength (MPa)	Tensile [†] modulus (GPa)	Ultimate tensile strain (%)	Coefficient of thermal expansion (1/°C)	Comments
Polystal (Strabag Bau-AG)	Glass E-type	Polyester	68	7.5 to 25	2.0	1670	51	3.3	7×10^{-6}	Based on 7.5 mm bar
Leadline (Mitsubishi Kasei)	Carbon	Epoxy	65	1 - 17	1.6	1970	147	1.3	0.68×10^{-6}	Based on 8 mm bar
CFCC (Tokyo Rope)	Carbon	Epoxy	64	3 - 40	2.0	2100	137	1.57	0.6×10^{-6}	Based on 12.5 mm cable
Bri-Ten (British Ropes Ltd.)	Carbon	Vinyl-ester	63	51	n/a [§]	1480	136	1.1	0	
Technora (Teijin)	Aramid	Vinyl-ester	65	3 - 8	1.3	1900	54	3.7	-15×10^{-6}	
Fibra (Mitsui)	Aramid Kevlar 49	Epoxy	60	4 - 14	1.3	1255	64.8	2	-5.2×10^{-6}	Based on 8 mm bar
Arapree (AKZO)	Aramid Twaron	Epoxy	37 to 45	5.7 to 7.9	1.23	1000 to 1200	43 to 53	2.3	-2×10^{-6}	Rectangular & circular shapes
Parafil [‡] Rope (ICI)	A Terylene F Kevlar 29 G Kevlar 49	No resin, fibres in sheathing	100	4.5 to 140	0.9 to 1.0	616 to 1926	12 to 126.5	5.1 to 1.5	-5.7×10^{-6}	A, F & G are 3 different types of Parafil

* Fibre content by volume

† Tensile strength and modulus are based on gross sectional area

‡ Parafil may not be classified as FRP tendons, since the fibres are not embedded in a plastic matrix

§ not available

U MEIER

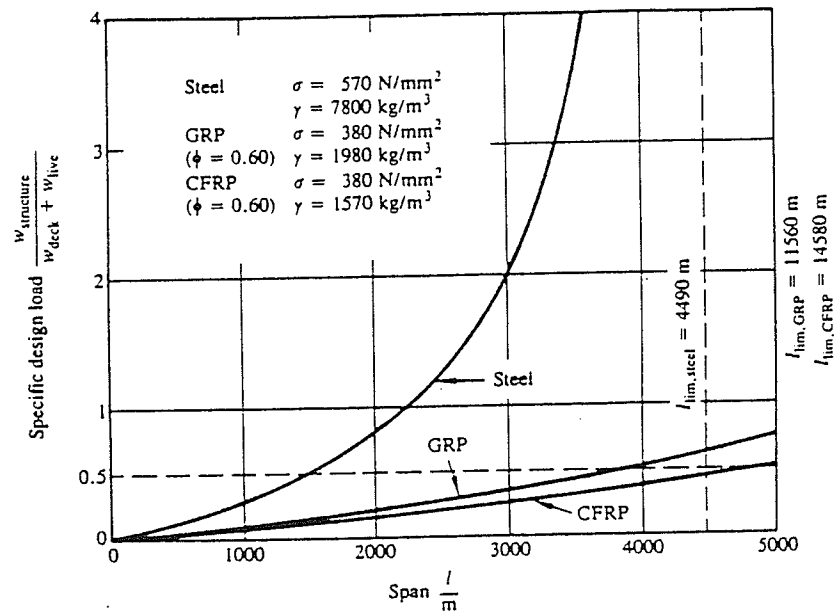


Fig.2-1 Specific design load vs. main span for classical form of suspension bridges

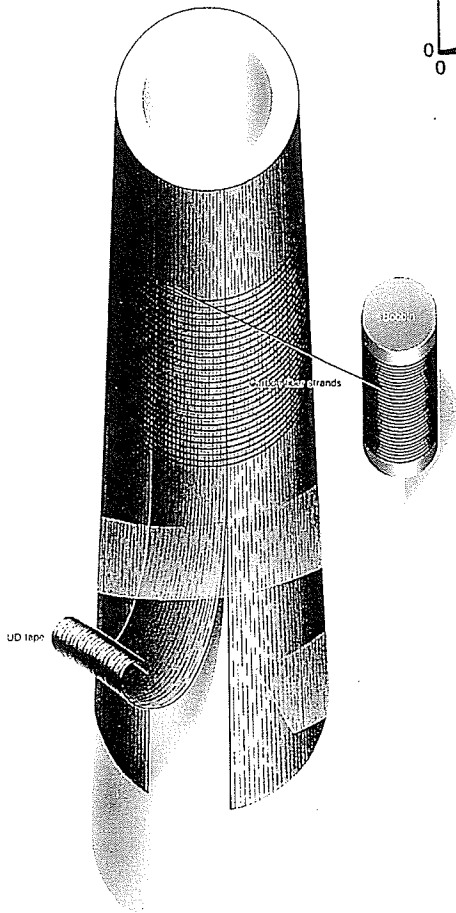


Fig.2-2 Retrofitting of chimney

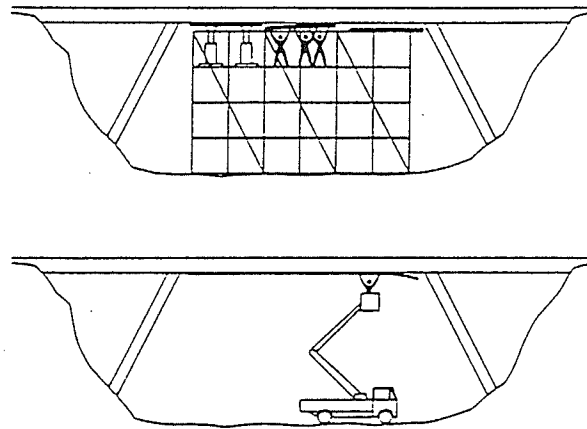


Fig.2-3 Strengthening of existing bridges
 above: strengthening with steel plates
 below: strengthening with unidirectional carbon fibre reinforced epoxy tapes

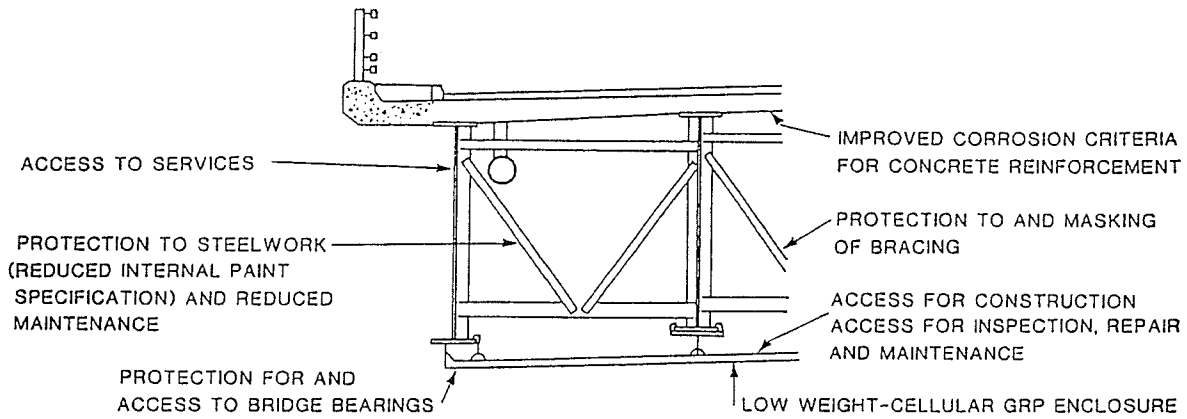


Fig.2-4 Structural floor of bridge enclosure



Fig.2-5 Tunnel lining by FRP grids

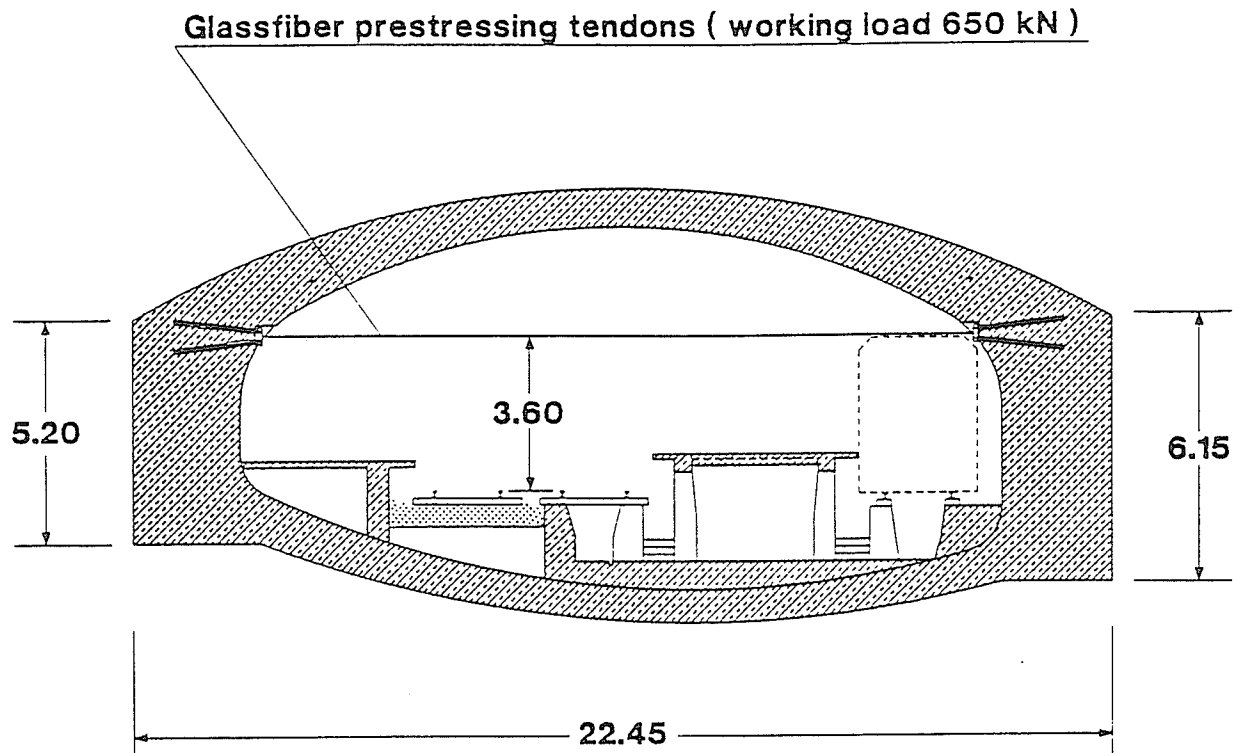


Fig.2-6 Cross section of Marie d'Ivry metro station

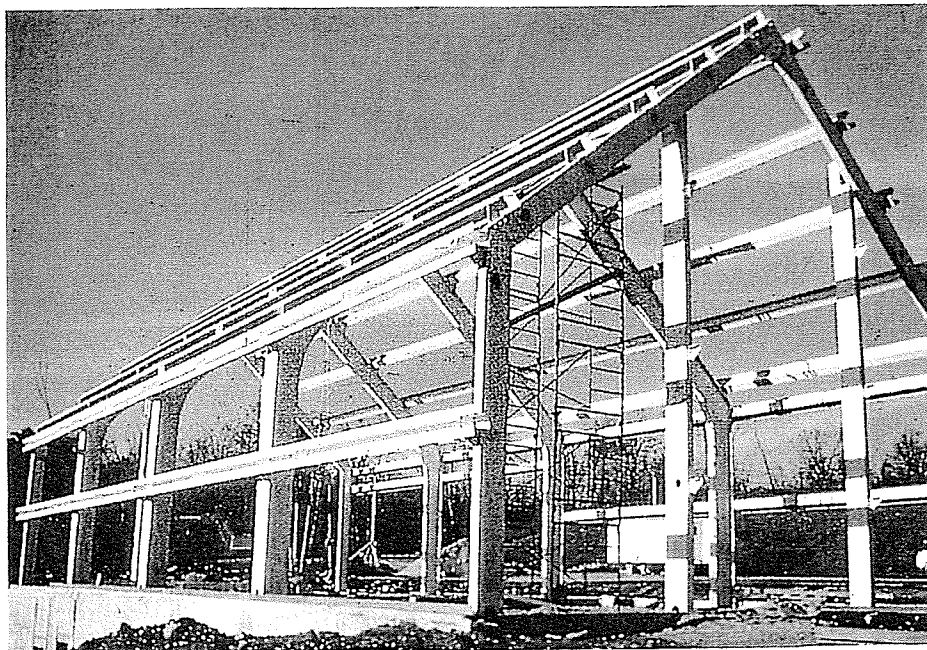


Fig.2-7 One of the four turrets constructed to house communications equipments

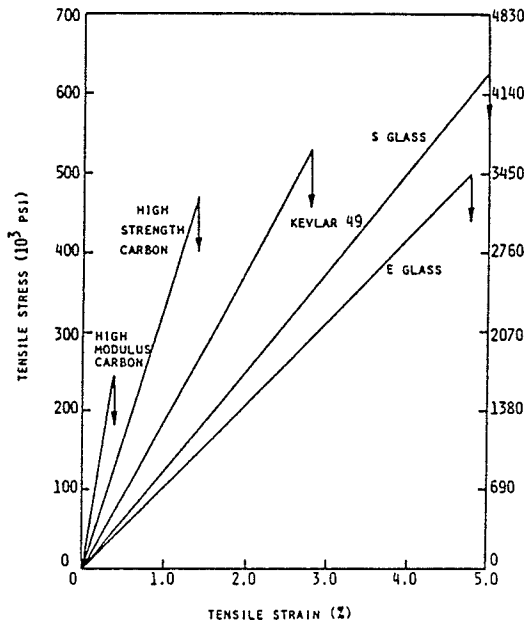


Fig.2-8 Tensile stress-strain diagrams for various reinforcing fibres

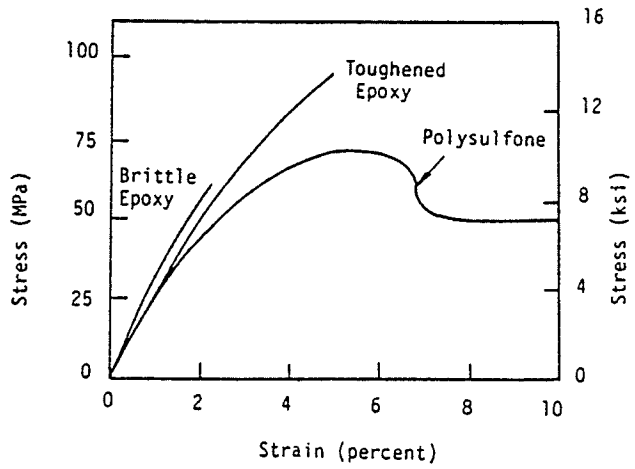


Fig.2-9 Tensile stress-strain diagrams of a thermosetting polymer (epoxy) and a thermoplastic polymer (polysulfone)

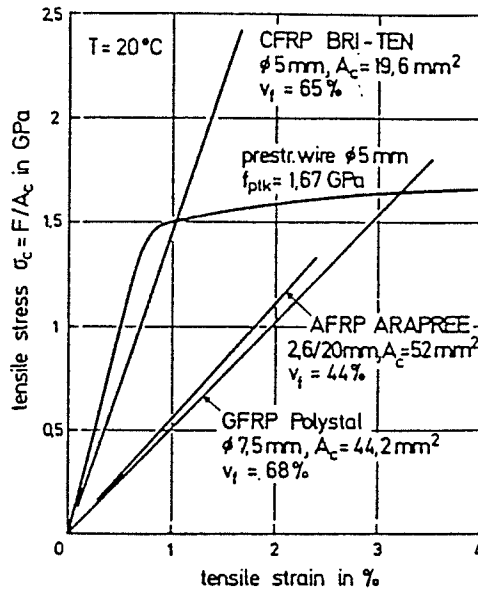


Fig.2-10 Tensile stress-strain diagrams of several FRP and prestressing wire

38

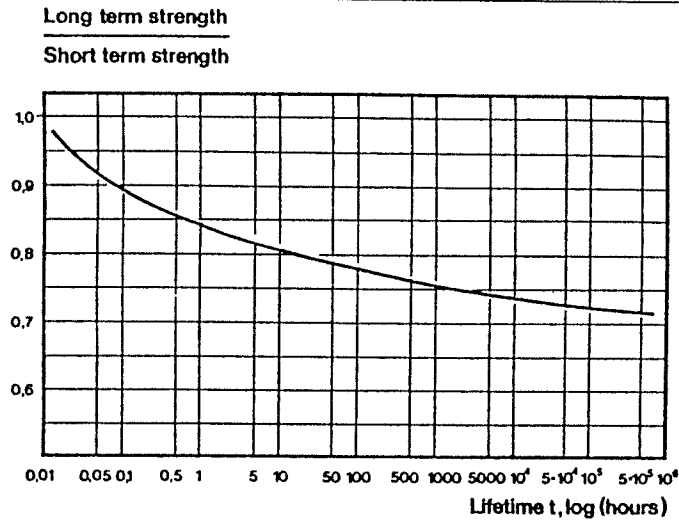


Fig.2-11 Creep strength of GFRP bars (Polystal)

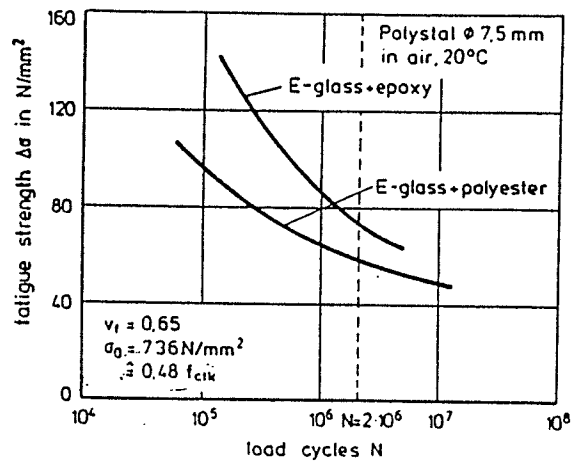


Fig.2-12 Fatigue behaviour of GFRP bars (Polystal)

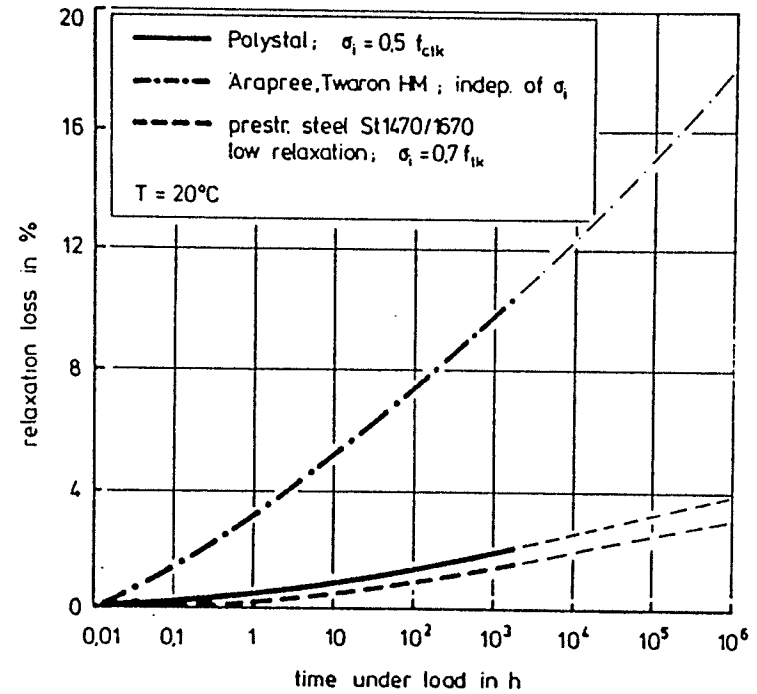


Fig.2-13 Stress relaxation of GFRP (Polystal), AFRP (Arapree) and prestressing steel (low relaxation)

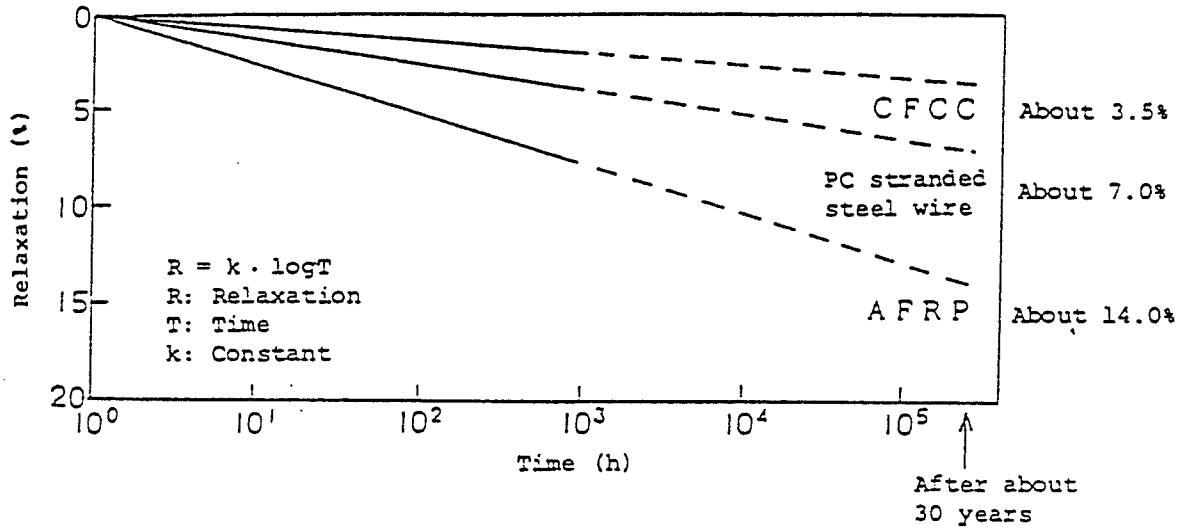


Fig.2-14 Stress relaxation of CFCC in normal temperature

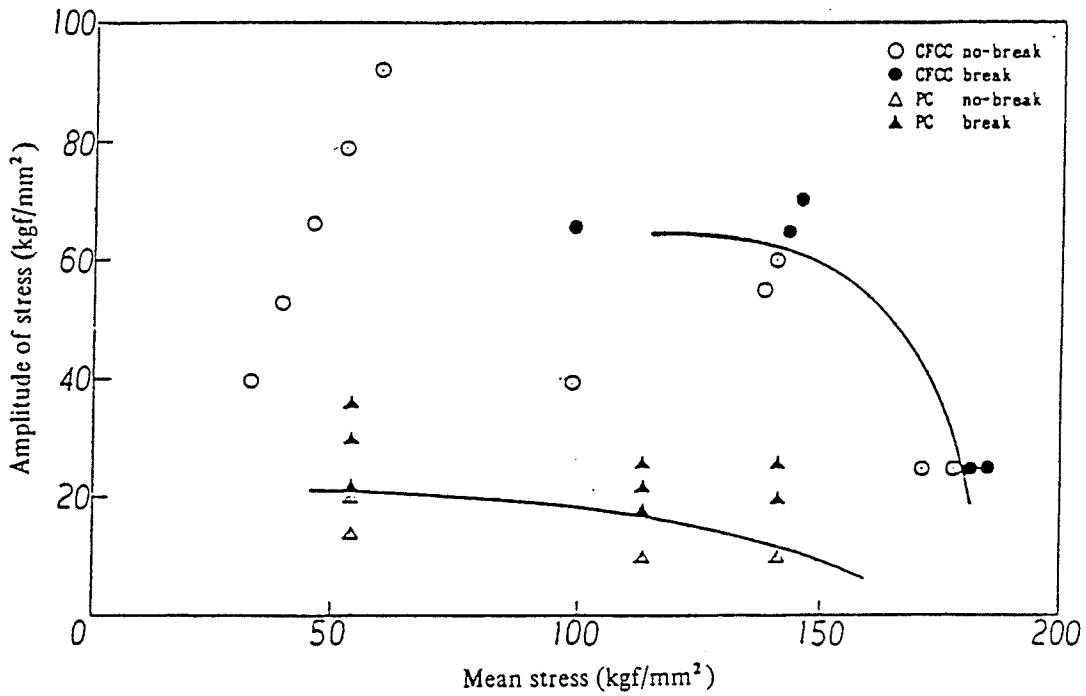


Fig.2-15 Fatigue strength of CFCC

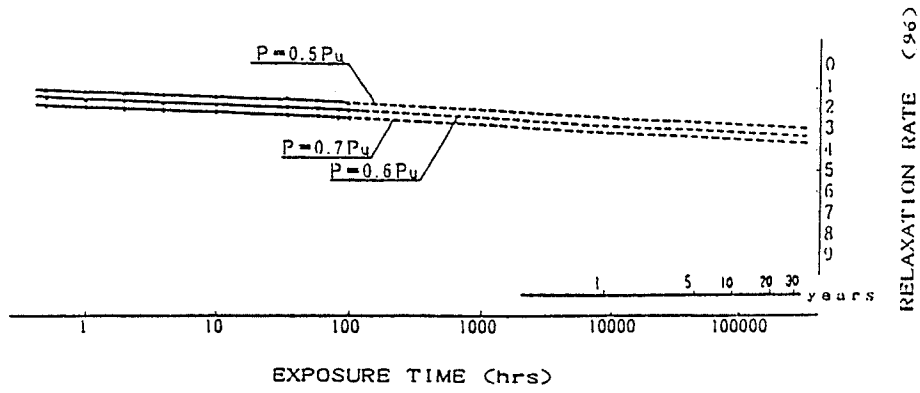


Fig.2-16 Stress relaxation of Leadline

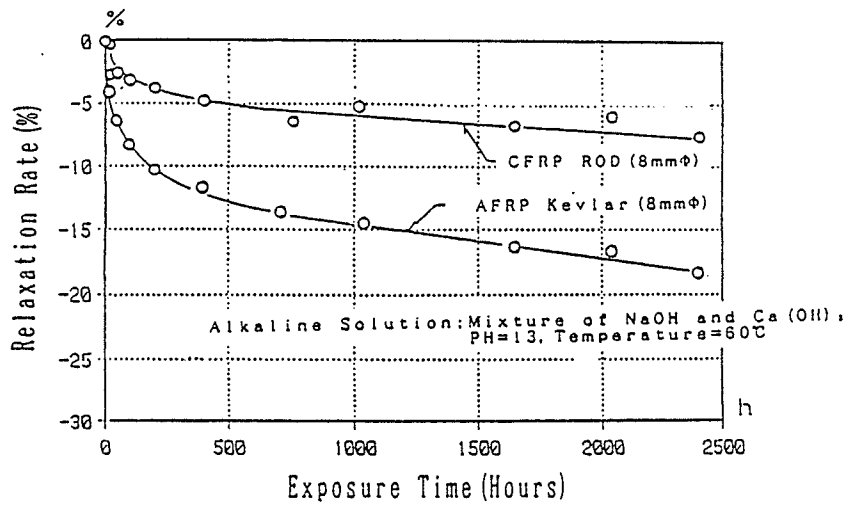


Fig.2-17 Stress relaxation of CFRP (Leadline), AFRP rod in alkaline solution

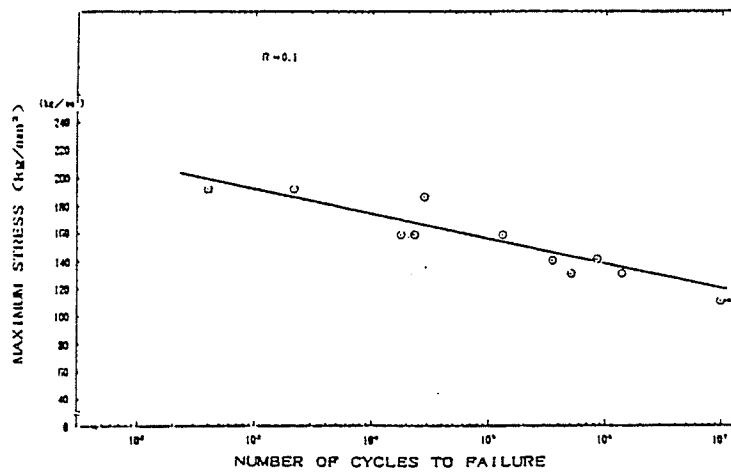


Fig.2-18 Fatigue behaviour of Leadline

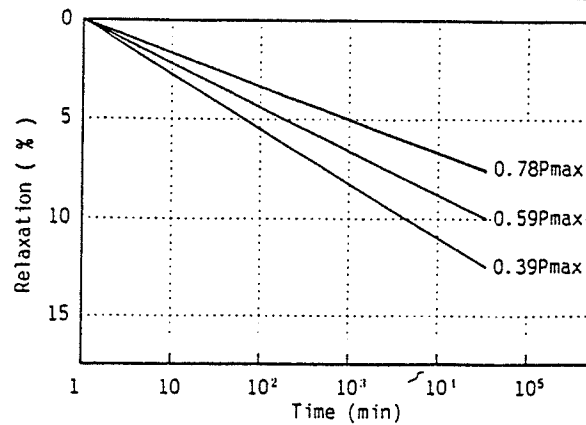


Fig.2-19 Relaxation of Technora

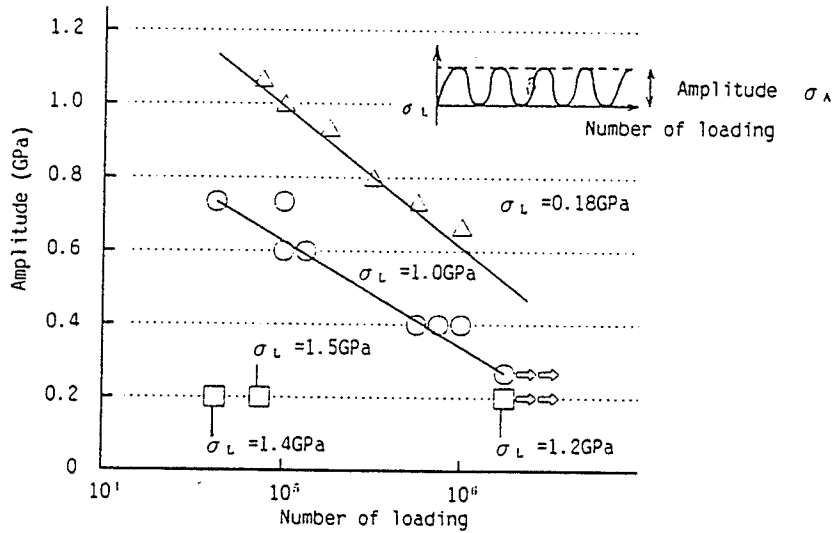
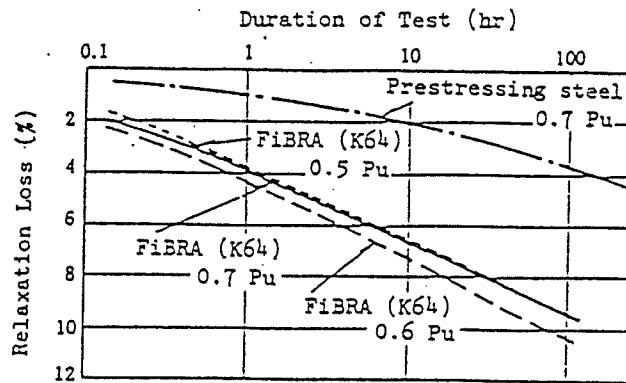
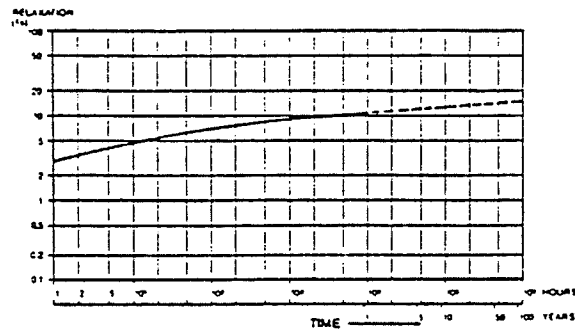


Fig.2-20 Fatigue behaviour of Technora

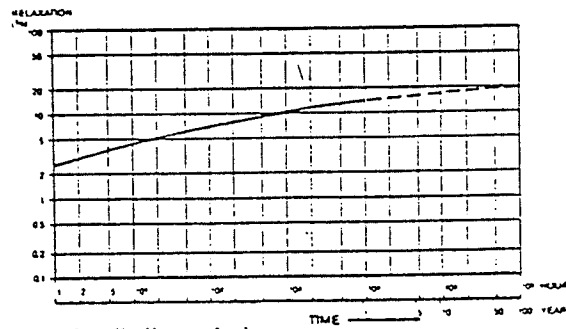


(Note) Tests performed at Shinko Wire.

Fig.2-21 Relaxation of Fibra



Arapree in air



Arapree in alkaline solution

Fig.2-22 Stress relaxation of Arapree

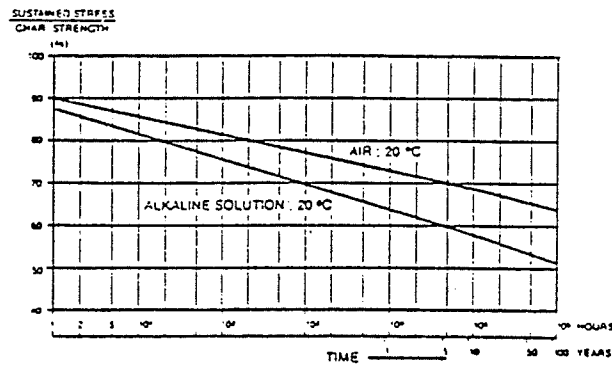


Fig.2-23 Stress-rupture behaviour of Arapree

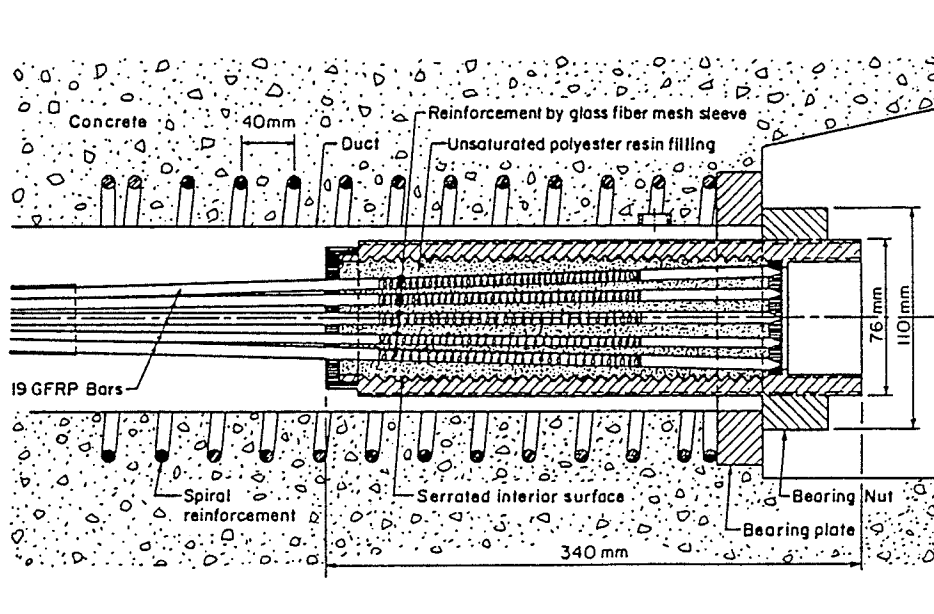


Fig.2-24 Anchor for Polystal prestressing tendon, Strabag Bau-AG, "grout type"

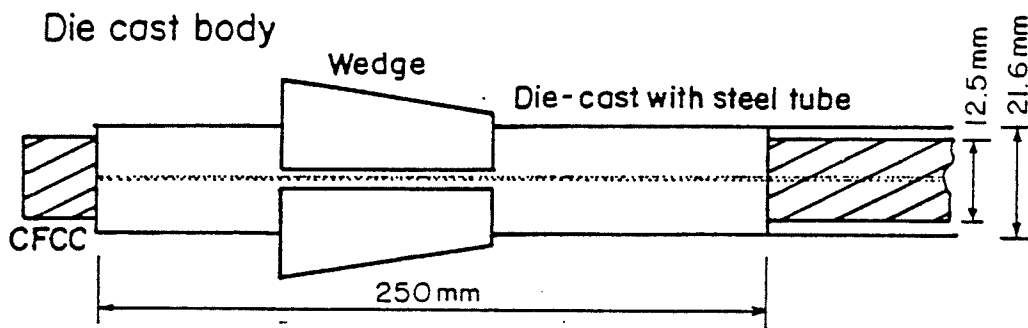


Fig.2-25 Anchorages for CFRP ropes using die-cast wedge by Tokyo Rope

3. _____ BEHAVIOUR OF CONCRETE BEAMS PRESTRESSED BY *FRP* REINFORCEMENT

3.1 GENERAL

One of the first iron bridges was built in England in 1779; since then a revolution in the bridge industry has exploded. Nowadays, the number of bridge structures has grown dramatically to meet the demands of today's infrastructure. However, deterioration of such structures is accelerated due to corrosion of steel. The maintenance cost to protect the steel from corrosion is relatively high. One of the most promising avenues which has been explored is to use *FRP* in the bridge industry. *FRP* tendons may be used either to strengthen deteriorated structures or to construct new bridges. *FRP* tendons are used in the form of prestressing elements to post-tension and pre-tension the concrete. But a crucial issue is to develop the confidence needed for a broad acceptance of advanced composites. Obstacles to future development of *FRP* applications are:

1. Lack of codes and specifications.
2. Lack of experience and education.

3. Relatively high cost compared to conventional materials.
4. Incomplete understanding of the material properties and long-term behaviour.

Research in this field has already been started and several structures have been constructed with *FRP* prestressing reinforcement. Moreover, committees in a number of countries have proposed design recommendations to introduce *FRP* in the building industry. This chapter presents some of the research which has been done in the field of application of *FRP* as prestressing reinforcement.

3.2 FLEXURAL BEHAVIOUR

Since *FRP* reinforcement is characterised by a linearly elastic stress-strain relationship nearly up to failure, failure of prestressed concrete members will occur either due to rupture of *FRP* reinforcements or due to crushing of concrete. Failure due to rupture of *FRP* reinforcement will occur progressively when the *FRP* reinforcement farthest from the neutral axis reaches the ultimate tensile strain. However, the concrete strain will be less than the ultimate value. This type of failure of a concrete beam is very brittle when compared to that of a similar beam with prestressing steel.

The other mode of failure, crushing of concrete, occurs when the concrete strain reaches its ultimate in compression while the ultimate tensile strain in the *FRP*

reinforcement has not been reached. Such a mode of failure is much more comparable to that of a concrete beam with prestressing steel. Reinforced concrete members with steel as reinforcing materials are normally designed in such a way that yielding of the steel will occur before crushing of the concrete in the compression zone. The following subsections present the research done to investigate the flexural behaviour of concrete beams prestressed by different types of *FRP* reinforcement.

3.2.1 Aramid *FRP*

Tanigaki et al. (1989) examined the flexural behaviour of partially prestressed concrete beams reinforced with braided aramid fibre rods (FiBRA). The FiBRA rods were used for post-tensioning and as non-prestressed reinforcement. Six T-beams with a flange width of 765 mm and a total depth of 300 mm were tested. The beams were of 3.0 meters clear span with a projection of 300 mm on both sides of the supports. The prestressing force was altered in three beams where the tendons were stressed to 15, 30, and 45 percent of their tensile strength. The type of prestressing tendons and main reinforcement were also varied where FiBRA with and without silica-sand adhered to the surface of the rods and steel were used. The number of prestressing tendons was two for all specimens and they were straight and laterally aligned beside each other at 100 mm from the bottom face of the beam. The load was applied in five cycles by obtaining a deflection at mid-span of $L/500$, $L/300$, $L/200$ and $L/100$ at the successive cycles, where

L was the span of the beam; the beam was then loaded to failure. The behaviour of the beams was characterised by the following;

1. For beams with FiBRA as prestressing and non-prestressing reinforcement, the load increased linearly from the occurrence of initial cracking up to failure. For the beam with FiBRA as prestressing tendons and steel as non-prestressed reinforcement, the load increased linearly only after yielding of the steel. This is attributed to the linear stress-strain relationship of the FiBRA up to failure.
2. The crack pattern of the beams showed that the crack spacing was almost 100 mm for both beams with steel and with FiBRA as prestressing reinforcement. This indicated that the bond of the silica-sanded FiBRA rod to the concrete is similar to that of a deformed steel bar.
3. In the beams with FiBRA as prestressed and non-prestressed reinforcement, the failure occurred by rupture of the non-prestressed reinforcement for the beam with low prestressing force and by rupture of the prestressed rod for the beam with higher prestressing force. Failure of the beam with steel bars as non-prestressed reinforcement and FiBRA as prestressing reinforcement occurred by rupture of the FiBRA rods.
4. Flexural behaviour of the beams with and without silica-sand adhered to the surface of the FiBRA tendons, was almost identical.

3.2.2 Carbon *FRP*

Younekura et al. (1991) examined the flexural strengths and flexural failure modes of post-tensioned beams using carbon *FRP* (*CFRP*) and aramid *FRP* (*AFRP*) as prestressing reinforcements. The main variables were the cross-sectional area of prestressing tendons, initial prestressing force, and type and cross-sectional area of non-prestressed reinforcement. The program included testing eleven beams with *CFRP* and one beam with *AFRP*. The behaviour of the tested beams was compared to that of similar beams prestressed with steel tendons. Sixteen I-beams with a total depth of 220 mm, a flange width of 150 mm, and a clear span of 1.40 m were tested under static loads using a two-point load configuration. Five levels of prestressing force were used ranging from 0 to 75 percent of the rupture load of the strands. Strains were recorded at different locations of the beams to examine the strain distribution at critical sections at different load levels. The results of this study are summarized as follows:

1. The two classical failure modes of the beams prestressed by *FRP* tendons, rupture of tendons and crushing of concrete, were achieved. However, it was found that failure due to rupture of prestressing tendons could be avoided by suitable arrangement of ample non-prestressed reinforcement.
2. Comparing a beam with prestressing steel to a similar beam with *FRP* tendons, but with less initial prestressing force, the latter showed larger deflections after crack

initiation and less ultimate load. However, as a result of increasing the prestressing force and the cross-sectional area of the prestressing tendons, the difference in the ultimate load and ultimate deflection of the two beams became less and the failure mode became identical.

3. For beams with *CFRP* reinforcement, increasing the magnitude of the prestressing force resulted in less deflection at the same load level and higher ultimate loads. However, the gradient of the load-deflection curves after the occurrence of cracking was unchanged. On the other hand, for beams prestressed by a large number of steel tendons, the strength of the beams did not increase by increasing the prestressing force.
4. The strains in the beams with *FRP* tendons are larger than those with steel tendons at the same load level and the neutral axis depths were less, due to the low elastic modulus of *FRP* tendons.

Mutsuyoshi et al. (1990) tested ten post-tensioned concrete rectangular beams using carbon-fibre-reinforced plastic cables in seven beams, while prestressing steel was used in the other three beams for comparison. The design prestressing force was varied from 40 to 60 percent of the tensile strength of *CFRP* cables. Different surface preparations for the *CFRP* cables were used to alter the bond characteristics between the cables and the concrete, from fully bonded to unbonded cables. The beams were of dimensions 150x200 mm and with 1.5-m clear span with only one cable in each beam. The beams

were tested under the effect of two-point monotonic loads up to failure. The results of this study showed two failure modes of the prestressed concrete beams, namely rupture of the *CFRP* cables and crushing of the concrete. It also showed that reducing the bond between the *CFRP* cables and the concrete resulted in less ultimate capacity for the beams. No data were available concerning the cracking of the beams or the strains in the cables.

Mutsuyoshi et al. (1991) reported the testing of six concrete T-beams externally prestressed by *CFRP*, *AFRP* and steel. The beams were of 2.5-m span, 400-mm depth, and 300-mm flange width. The cables were depressed at two points; the angle of the cables to the center line of the beam was 7.1° in two beams and 11.3° in the other four beams. The prestress in the cables ranged between 36 and 48 percent of their tensile strength. The beams with *CFRP* failed by crushing of concrete simultaneously with breaking of the cables. The breaking load of *CFRP* tendons, attached externally to the beams, was about 80 percent of the average breaking load obtained from uniaxial tensile tests. This was attributed to the stresses induced in the cables at the bending point.

Maissen and De Smet (1995) tested two concrete beams prestressed by carbon *FRP* cables and one beam prestressed by steel strands. The beams had a T-section with an overall depth of 500 mm and a span of 6.0 m. The beams with *CFRP* were post-tensioned by eight 12.5-mm *CFCC* cables of parabolic shape, where the cables were

bonded in one beam and unbonded in the other. The jacking stress was 50 percent of the ultimate strength of the cables, which was reported to be 2170 MPa. The beam prestressed by steel was post-tensioned by six 13-mm strands. The ultimate load of the beam prestressed by bonded *CFCC* was slightly higher than that of the beam prestressed by steel; however, the deflection at ultimate was much less. The failure was due to rupture of the cables for the beam with bonded *CFCC* and due to crushing of the concrete for the beam with unbonded *CFCC*. The unbonded beam exhibited considerably less cracking than the bonded beam and therefore the rotation of the unbonded beam was concentrated at few cracks. Consequently, the compressive stresses in the concrete at the crack location increased and resulted in crushing of the concrete.

3.2.3 Glass *FRP*

Sen et al. (1991) tested six pre-tensioned concrete beams using glass *FRP* (*GFRP*) tendons for three beams and prestressing steel in the other three beams. The dimensions of the beams were 6" x 8", 6" x 10", and 6" x 12" with 8 feet clear span. The beams were tested using two static point loads. The pre-cracking response of the beams with steel and *GFRP* tendons, having the same effective prestress, was identical, while the post-cracking response of the beams with *GFRP* was more flexible than that of the beams with steel. At failure, cracks in the beams with *GFRP* were more widely spaced over the constant moment zone than in the pretensioned beams with steel. A tension mode of

failure of the beams prestressed by *GFRP* was observed and was accompanied by slip of the tendons.

Taerwe and Miessler (1992) reported the testing of three post-tensioned concrete beams using *GFRP* (Polystal) for prestressing. The tested T-beams were 600 mm deep with a 300-mm flange width and a 2.0-m clear span. *GFRP* tendons were bonded to the concrete in two beams, while the tendons were left unbonded in the third beam. All beams failed by rupture of the tendons. The strains in the *GFRP* tendons were recorded by means of optical-fibre sensors, a technique introduced recently to monitor strain in glass fibre bars. Taerwe and Miessler also reported testing of another beam with a clear span of 20.0 m. The beam had a T-shape with a total depth of 1000 mm and a flange width of 800 mm. A *GFRP* tendon consisting of 19 glass fibre bars (7.5 mm in diameter) was used to post-tension the beam. The tendon had a parabolic shape and was stressed to approximately 50 percent of its ultimate strength. The beam was loaded using two point loads until it failed by rupture of the tendon. Strains in the *GFRP* tendon were monitored using optical-fibre sensors.

3.3 BOND AND DEVELOPMENT LENGTH

Bond characteristics of prestressing tendons are of particular interest in pretensioned members as the prestressing force is transmitted from the tendons to the concrete by bond.

Therefore, the evaluation of bond characteristics of *FRP* reinforcement is of prime importance in the design of prestressed concrete beams. However, due to the vast variations between the different products of *FRP* reinforcement, the bond characteristics are quite variable and dependent on the type of *FRP* reinforcement. For prestressed concrete beams with steel prestressing elements, the bond characteristics are influenced by many factors that depend on both the steel and the concrete, such as:

1. Size and type of tendons (wires or strands)
2. Surface conditions (smooth, deformed, rusted, oiled)
3. Tendon stress
4. Method of transfer (sudden or gentle release)
5. Concrete strength
6. Concrete confinement by steel (e.g., helix or stirrups)
7. Type of loading (e.g., static, repeated, impact)
8. Time-dependant effect
9. Amount of concrete coverage around steel

For concrete beams prestressed by *FRP*, the bond characteristics are influenced by the previously mentioned factors in addition to the following:

1. Tensile strength (1500 to 3000 MPa)

2. Tensile modulus (50 to 150 GPa)
3. Poisson's ratio
4. Shape (circular or rectangular)
5. Surface preparations (braided, deformed, smooth)
6. Type and volume of fibre and matrix

The length of tendon at the end zone of a pretensioned member over which the prestress develops is called the transfer length l_t . Within the transfer length, the stresses in the tendons increase from zero at the end of the member to an effective stress f_{se} at the end of the transfer length l_t . In order to develop the full design strength of the member, an additional flexural bond length l_f is required. To develop the design strength of the tendon f_{ps} , summation of the flexural bond length l_f and the transfer length l_t leads to the development length l_d of the prestressed tendon.

Both the ACI and CSA Codes suggest that the transfer length can be estimated as $50d$ for strands, where d is the strand diameter, and $100d$ for individual wires. The European Code (CEB-FIP Model Code 1978), on the other hand, suggests that transfer lengths may vary between $45d$ to $90d$ for strands and $100d$ to $140d$ for individual wires. Prestressing strands are normally characterized by smaller transfer lengths than prestressing wires, because of their twisted shape which allows for good mechanical bond. The ACI and CSA Codes also require that a pretensioned strand have a development

length, l_d , beyond the critical section, equal to

$$l_d = 0.048 f_{se} d + 0.145 (f_{ps} - f_{se}) d \quad 3-1$$

Where f_{se} is the effective prestress in the strand, f_{ps} is the stress in the strand at the critical section in MPa and d is the diameter of the strand in mm. The following subsections present the research done to investigate the bond characteristics of *FRP* reinforcement.

3.3.1 Aramid *FRP*

Nanni, Utsunomiya, Yonekura, and Tanigaki (1992) evaluated the transfer length of braided epoxy-impregnated aramid fibre (FiBRA), produced by the Mitsui company in Japan. They tested beams 4.0 m in length with a cross section of 120 x 210 mm using different tendon sizes, tendon numbers, surface conditions (adhered sand and smooth), and initial prestressing forces. The transfer length of the *AFRP* tendon was affected mainly by the adhered sand on the tendon surface and by the tendon size. They concluded that:

1. For a minimum concrete strength of 29 MPa and an initial prestress load not higher than 50 percent of the ultimate strength of the tendon, the unfactored transfer length of bonded *AFRP* tendons is related to the nominal diameter as follows:

$$l_t = 50d, \text{ for } d = 8 \text{ mm.}$$

$$l_t = 40d, \text{ for } d = 12 \text{ mm, (} 20d \text{ if sand adhered).}$$

$$l_t = 35d, \text{ for } d = 16 \text{ mm.}$$

2. The mechanism of force transfer of *AFRP* tendons is different from that in steel strands. It was found that the friction component of the transfer bond stress of *AFRP* tendons is higher than that of steel. This could be a consequence of lower rigidity of the *AFRP* tendons, which is about one third that of the steel, and higher Poisson's ratio of the *AFRP* tendons, which was measured to be 1.65 that of the steel.
3. Transfer length of steel strands is considerably higher than the transfer length of *AFRP* tendons. It was also found that the transfer length of adhered-sand tendons is significantly smaller than that of smooth tendons.

Nanni and Tanigaki (1992) determined the development length by performing a three-point flexural test (static monotonic load). Based on the transfer length of *AFRP* tendons (Nanni, Utsunomiya, Yonekura, and Tanigaki 1992), the flexural bond length was determined. A total of 21 beams were tested using three different configurations. The damage due to the failure of each beam was limited to one end of the beam so that a second test could be performed at the opposite end. The different modes of failure were bond slip, bond slip accompanied by split cracking, concrete crushing, and combined

concrete crushing and shear failure. The findings of this study were as follows:

1. The unfactored development length of the *AFRP* tendons was related to the nominal tendon diameter as follows:

$$l_d = 120d, \text{ for } d = 8 \text{ mm.}$$

$$l_d = 100d, \text{ for } d = 12 \text{ mm.}$$

$$l_d = 80d, \text{ for } d = 16 \text{ mm.}$$

These values are based on a concrete strength of 30 MPa at the time of tendon release and concrete cover ranging between 24 and 54 mm. These values are valid for an initial prestress level ranging from 25 to 50 percent of the ultimate strength of the tendons. These values of the development length are also valid for sand-adhered tendons, unless shear reinforcement is used, which results in higher bond strength.

2. The ratio of flexural bond length l_f to transfer length l_t ranged between 0.9 and 1.2, when the initial-stress-to-ultimate-nominal-strength ratio was 0.5.
3. When comparing material manufacturing effects on l_f for cables equal in size and prestressing, the smallest value was found for a sand-adhered *FRP* tendon and the largest for steel strand.
4. Increasing the initial prestress results in smaller flexural bond length l_f .

3.3.2 Glass *FRP*

Iyer and Anigol (1991) performed pull-out tests to study the bond characteristics of fibre glass cables and compared the results to data obtained from similar tests with steel and graphite cables. The findings of this research showed that the bond strength of advanced composite cables (fibre-glass and graphite), was comparable to the bond strength of steel cables.

Iyer, Hubchandani and Feng (1991) tested pretensioned concrete beams using fibre glass, steel, and graphite rods. The transfer length of the rods was measured and was found to be $37d$ for fibre-glass, $61d$ for steel, and $59d$ for graphite cables. The effective prestress level of the tendons was 47, 48, and 44 percent of the tensile strength, for fibre-glass, steel, and graphite respectively.

Pleimann (1991) conducted over 70 pull-out tests to examine the bond strength of *GFRP* (E-glass fibre), *AFRP* (kevlar 49), and steel bars. He tested three different diameters of *GFRP* bars, (6.4, 9.5, and 12.7 mm) and one diameter of *AFRP* bars (9.5 mm). Results indicated that bond strengths of *AFRP* and *GFRP* bars are similar and inferior to steel rebar. He recommended the following two equations to calculate a safe embedment length (in inches) for fibre-glass and *AFRP* bars, respectively;

$$l_d = \frac{f_u A_b}{20 \sqrt{f'_c}} \quad (GFRP) \quad 3-2$$

$$l_d = \frac{f_u A_b}{18 \sqrt{f'_c}} \quad (Kevlar) \quad 3-3$$

where f_u is the ultimate stress capacity of the tendon in psi, A_b is the cross-sectional area of the bar in in^2 and f'_c is the 28-day compressive strength of the concrete in psi.

Chaallal et al. (1992) evaluated the development length for *GFRP* bars (E-glass fibres and polyester resin with sand adhered to the surface). Pull-out tests were undertaken using normal-strength concrete, high-strength concrete, and grout. Three different diameters of the bars were used and the anchored length varied from 5 times to 10 times the bar diameter. A development length of $20d$ was recommended for both normal-strength and high-strength concrete.

Daniali (1992) investigated the bond strength of *GFRP* bars (E-glass fibres and vinyl ester binder) by testing 30 concrete beams. The variables in this study were the diameter of the bars and the embedment lengths. The beams were 3.0 m long with a cross section of 203 x 457 mm. The beams were tested according to the recommendation of ACI Committee 208. The study concluded the length required to develop the ultimate tensile strength of a bar to be 203 mm for #4 bar and 440 mm for #6 bar, if shear

reinforcement is provided along the entire length of the specimen. All specimens reinforced with #8 bars failed in bond. The study pointed to the occurrence of premature bond failure under sustained load.

The bond characteristics of *GFRP* bars were investigated at West Virginia university, (Gangarao and Faza 1991), by testing 20 concrete specimens. Variables such as rebar size, type of rebar (ribbed, sand-coated), and embedment length were considered. The concrete specimens were formed in the shape of a cantilever, to simulate the portion of a beam adjacent to a diagonal crack. In addition, twelve pull-out cylinder specimens were tested. The following equation was suggested to calculate the development length for *GFRP* reinforcement:

$$l_d = 0.06 \frac{A_b f_u}{\sqrt{f'_c}} \quad 3-4$$

where A_b is the cross sectional area of the rebar in in^2 , f'_c and f_u , (the rupture strength of the rebar) are in psi.

3.3.3 Carbon *FRP*

Pull-out tests were performed under repeated loading on carbon-fibre-composite cable (*CFCC*) produced by Tokyo Rope (Tokyo Rope MFG.Co., Ltd., 1993). Ten cycles were

applied to a maximum load in each cycle of 60 percent of the simple pull-out load. Then the bond strength was measured. The bond strengths of 12.5-mm-diameter *CFCC* cable and 12.4-mm-diameter prestressing steel strand were compared. The bond strength of *CFCC* cable was found to be higher than that of steel strand.

The design bond length of *CFRP* bars produced by Mitsubishi Kasei under the brand name of Leadline has also been reported to be $70d$ for bars of 8 and 12 mm diameter (Mitsubishi Kasei Corporation, 1992).

3.4 FATIGUE BEHAVIOUR

If a cracked prestressed concrete member is subjected to repeated applications of load, there is a possibility that a fatigue failure of the tendon may occur. Fatigue resistance of beams is typically investigated by calculating the stress range, Δf_p , produced in the prestressing tendon induced by cyclic loads and comparing this stress range with that obtained from the S-N curve for a particular prestressing system. The CEB-FIP Recommendations define the characteristic fatigue strength of prestressing steel as the stress range which can be applied two million times with a maximum stress of $0.85 f_{py}$ and a probability of failure of 10 percent.

For pretensioned beams, the fatigue life of tendons in the beams is shorter than that

of tendons tested individually in air. For post-tensioned beams, the curves in the tendon profile are a principal cause of low fatigue strengths as the rubbing of the tendons against the sheath at a crack location may cause a premature failure. Special attention should be paid to the fatigue resistance of the anchorage as such devices usually develop the full static strength of the tendon, but not the fatigue strength. Little work has been done to define S-N curves for *FRP* tendons.

Rostásy and Budelmann (1991) evaluated the S-N curve for *GFRP* bars. They reported that the fatigue strength of *FRP* tendons is influenced by the properties of the anchorage chosen. However, the fatigue strength of *GFRP* is markedly below that of wedge-anchored prestressing wire. Miesslerer and Preis (1989) reported that *GFRP* bars may be subjected to two million cycles with a 10 percent probability of failure at a stress range of 55 MPa and a maximum stress equal to 0.44 of the tensile strength of the bar. The following subsections describe some of the work done to investigate the fatigue behaviour of concrete beams prestressed by *FRP* reinforcement.

3.4.1 Aramid *FRP*

McKay and Erki (1992) examined the fatigue strength of prestressed concrete beams using *AFRP* rods. Three concrete beams of cross-sectional dimensions 150x300 mm and 1.05 m clear span were tested. The *AFRP* rods were initially stressed to 80 percent of

their guaranteed tensile strength. The first beam was loaded in two stages. In stage 1, the beam was loaded past cracking close to the ultimate load; then the load was released. In stage 2, the beam was loaded up to failure. The other two beams were subjected to two quasi-static load cycles beyond the cracking limit. Then they were subjected to sinusoidal loading at a frequency of 4 Hz. The maximum and minimum loads were set to simulate partially prestressed conditions by having the lower load just below the cracking load, and the upper load producing a stress change in the *AFRP* rod of 200 Mpa, with a maximum stress of about 80 percent of the guaranteed strength. The beams failed after 1.96 and 2.1 million cycles, respectively, by rupture of the rods. The increase in the deflection for both beams was in the order of 10 to 20 percent of the original deflection. The following conclusions were drawn from the study:

1. The fatigue strength of *AFRP* rods in service loading conditions is at least as good as that for steel strands.
2. The relaxation of *AFRP* rods is higher than that of normal steel strands. A reasonable approximation of the relaxation losses of *AFRP* rods with an initial stress in the range of 1200 MPa can be calculated according to the following equation:

$$\frac{f_p}{f_{p_i}} = 1.009 - \frac{\log(t)}{65.19} \quad 3-5$$

where f_{pi} is the fixing stress and t is the time in minutes.

3. The actual tensile strength of *AFRP* rods is about 20 to 50 percent higher than the guaranteed tensile strength. The authors attributed this increase to the more gradual distribution of bond stresses on both sides of a beam crack than in the case of the prestressing anchorage.

Mikami, Kato, Tamura and Ishibashi (1990) tested three prestressed concrete beams using braided *AFRP* tendons under cyclic load. The beams were 200x250 mm in cross-section, each containing one pre-tensioned tendon stressed to approximately 45 percent of its tensile strength. The clear span of the beam was 1.6 m with a 400-mm projection over the end of each support. Two beams having a ratio of maximum applied load to ultimate static capacity of 0.67 did not fail up to two million cycles. The ratio of the deflection at one million cycles to the initial deflection was about 1.3. The third beam which was loaded up to 0.88 of its ultimate static capacity failed at 229,000 cycles.

Noritake and Kumagai (1991) reported testing of two prestressed concrete beams of 10-m span using *AFRP* tendons. A parabolic cable of nineteen 6-mm-diameter rods was used to post-tension the beams. The first beam was tested under static load while the second beam was tested under cyclic load with a lower bound equal to the dead weight of the beam. Three upper load bounds were selected to produce bending moments equal to $0.45 M_u$ (bending moment at first crack), $0.55 M_u$ and $0.6 M_u$, where M_u is the

ultimate moment of the similar beam tested under static conditions. The beam survived two million cycles without failure. When the beam was loaded to failure, it showed a 10 percent decrease in the ultimate load resistance. The anchorage of the *AFRP* cable was not damaged by the fatigue test.

3.4.2 Glass *FRP*

Sen, Issa and Iyer (1992) reported the testing of two pretensioned concrete beams using *GFRP* rods under cyclic load. The beams were of dimensions 6" x 10" and 6" x 12" and 8 feet clear span. The *GFRP* rods were initially stressed to 47 percent of their tensile strength. A sinusoidal load was applied to the beams at a frequency of 3 Hz. The load was varied between 40 and 60 percent of the ultimate static capacity of the beam, which was measured by static tests performed on similar beams. One of the two beams failed after the application of about 1.5 million cycles while the other beam survived two million cycles. Failure occurred suddenly due to loss of bond and slip of the *GFRP* rods. The following conclusions were drawn from the study:

1. The overall fatigue characteristics of fibre-glass pretensioned concrete beams matched those of similarly loaded steel pretensioned beams.
2. Fatigue loading of fibre-glass pretensioned beams in the post-cracking range resulted in much higher deflection and crack widths than in similar beams with prestressing

steel. This was attributed to the low elastic modulus of the *GFRP* rods.

3. Reduction in the ultimate capacity of the beams due to fatigue loading was very little compared to the static capacity of the beams.

3.4.3 Carbon *FRP*

Abdelrahman, Tadros and Rizkalla (1995) tested four beams of 6.3-m length and 330-mm total depth. Two beams were pretensioned using 8-mm-diameter Leadline rods and the other two beams were pretensioned using 15.2-mm diameter carbon fibre composite cables *CFCC*. Both types of *CFRP* reinforcement, Leadline rods and *CFCC* cables, were pretensioned to 60 percent of the guaranteed ultimate strength specified by the manufacturer. For each type of *CFRP*, one beam was tested under static load and the other under cyclic load. Beams tested under cyclic loading were subjected to a maximum and a minimum load equivalent to the cracking and 70 percent of the cracking load of the beam, respectively. After completion of two million cycles, the beams were loaded to failure to evaluate the effect of fatigue loading on the behaviour of the beams.

The beam prestressed by *CFCC*, tested under cyclic loading, showed perfectly elastic response during and after the completion of two million cycles. The beam stiffness remained constant at different number of cycles. This is attributed to the elastic behaviour of *CFCC*. After two million cycles, the camber of the beam was equal to the

initial camber. This indicates that there was no loss in the beam stiffness due to the application of the cyclic load. When the beam was loaded statically to failure, after two million cycles, the beam followed the same path as the beam tested under static loading conditions. The measured failure load and maximum deflection were about 5 and 10 percent less, respectively, for the beam survived two million cycles than those of the beam tested under static load.

Before applying the cyclic loading to the beam prestressed by Leadline rods, the beam was loaded initially close to failure load, as measured from the static test. As a result, the beam was cracked with the cracks extending up to the upper flange. It was observed that the stiffness of the beam, based on the slope of the initial load-deflection relationship, was reduced by increasing the number of cycles. This reduction in stiffness is mainly due to the initial extensive cracking of the concrete. Prior to testing of the beam, the measured camber was 21 mm. The measured camber after applying the cyclic loading was 3 mm. The decrease in the camber was mainly due to reduction of the beam stiffness. When the beam was loaded to failure, after completion of 2 million cycles, there was no reduction in the carrying capacity nor in the deflection of the beam.

3.5 LONG-TERM BEHAVIOUR

The stress-strain response of *FRP* reinforcement depends upon the rate and time-history of loading. An increase in strain under constant stress is known as *creep*. A reduction in stress under constant strain is called *relaxation*. Creep and relaxation of *FRP* tendons differ greatly according to the type of fibre and matrix.

Fibre composites exhibit the phenomenon of creep-rupture. Therefore, their admissible stress must be chosen well below the creep-rupture strength to preclude failure under sustained load. The long-term static strength for a 100-year load duration has been predicted to be about 70 percent of the tensile strength for *GFRP* tendons (Rostásy 1988). Aramid elements exhibit a slightly lower creep-rupture strength at 100 years.

Relaxation of the prestressing reinforcement should be precisely determined for the prediction of the initial and final losses of the prestressing force. Relaxation is negligible for *CFRP* cables; it is comparable to that of steel for *GFRP*. For *AFRP* reinforcement, relaxation is high, ranging from 7 to 14 percent. However, the total loss of prestressing force will not be affected markedly as the elastic modulus of *AFRP* reinforcement is low.

Burgoyne (1992) reported the testing of two beams prestressed with Parafil ropes. The first beam had a single, straight, unbonded tendon placed in a duct on the centreline

of a simple I-beam of 4.57-m clear span and 400-mm depth. The second beam had two external deflected tendons, one on each side of a bulb T-shaped cross section with 600-mm depth and 500-mm flange width. The clear span of the beam was 7.5 m. Both beams were tested in four-point bending rigs and taken through several elastic loading cycles. The second beam was kept under sustained load for 42 days to monitor the effects of creep and relaxation.

The first beam was tested by applying a load that induced the allowable flexural tensile stress in the bottom fibre of the beam. Ninety-five percent of the mid-span deflection was recovered after the load was removed. In the second cycle, and after loading beyond the cracking load, the measured stiffness was reduced considerably. When the beam was unloaded from the cracked state (but still elastic), the stiffness remained low until the cracks were closed, when the full elastic stiffness was recovered. Virtually no permanent deflection was measured after unloading. When the beam was loaded to failure, considerable curvature occurred and large cracks were observed. Finally failure occurred by crushing of the concrete at the top flange.

The second beam was subjected to two cycles at the service load level. The beam was loaded until the pre-compression strain due to prestressing was counteracted without cracking the beam. The load was maintained for 42 days. The total loss of prestress, due to shrinkage and creep of concrete and due to relaxation in the tendon within 42 days, and

after the application of service load, was 11 and 12 percent in the first and second ropes, respectively. Most of these losses occurred one day after prestressing. The beam was loaded to failure, which occurred due to crushing of the concrete at the top flange. As the tendons were external, they were removed and tested after the collapse of the beam. The breaking force of the tendons was greater than the mean value, and even greater than the maximum value observed in tensile tests conducted on similar ropes. The author attributed this phenomenon to the increase in the strain in the more heavily loaded filaments due to creep. In the subsequent loading, the rope acted as a bundle of yarns with less variability and hence increased strength.

Tanigaki, Nomura, Okamoto and Endo (1989) carried out long-term bending tests to study the load resistance behaviour, over considerable length of time, of partially prestressed concrete beams with *AFRP*. Four rectangular prestressed concrete beams of 300-mm depth, were tested. Braided *AFRP* rods with and without silica sand adhered to the surface were used to pretension three beams, while the fourth beam was post-tensioned. *AFRP* rods were also used as the main reinforcement for all the tested beams. The initial prestressing force was altered in two beams. Concentrated loads, equal to P_{cr} (initial cracking load) and $1.5 P_{cr}$ were maintained for 1000 hours and cracking and deflection of the beams were recorded. After 1000 hours, the measured curvature and deflection increased 5 to 8 times for beams loaded to P_{cr} , and about 10 times for the beam loaded to $1.5 P_{cr}$. Gradual formation of new cracks was observed for the first

100 hours; subsequently, very few cracks were formed and the changes in the deflection with time became moderate. In all the specimens, the strain in the concrete increased more rapidly than that in the *AFRP* rod, which indicated that the neutral axis depth increased with time.

3.6 DESIGN CONSIDERATIONS

In spite of the lack of design codes that govern the use of *FRP* reinforcement in prestressed concrete, several structures have been constructed using *FRP* reinforcement to take advantage of the new material. Aramid, carbon and glass *FRP* reinforcement have been successfully used as prestressing elements for a number of bridges in different countries. The design of such structures has been done rationally and conservatively.

The major problem in the design of prestressed beams with *FRP* is their lack of ductility compared to beams with prestressed steel. This is because of the different stress-strain characteristics of *FRP* and steel bars. Design codes require that the strain in the steel reinforcement at the time of failure exceed the yield strain to ensure enough ductility for the concrete section. However, this can not be ensured for beams with *FRP* reinforcement as the stress-strain relationship is linearly elastic up to failure. This feature underlines the need for a different approach to the design of such structures.

3.6.1 Flexural Analysis

Prestressed concrete beams with *FRP* tendons can be analyzed using the same analysis method as for beams with prestressing steel, using the tensile stress-strain properties of *FRP*. Analysis based on a strain compatibility approach has been addressed by many researchers (Tanigaki et al. 1989, Mutsuyoshi et al. 1990 Yonekura et al.1991, Gangarao 1991, McKay et al. 1992 and Noritake et al.1991). The results of rational analysis of prestressed concrete beams with *FRP* reinforcement using the strain compatibility approach showed very good agreement with the experimental results. The cracking and the ultimate moments, as well as the mode of failure of the beams, could be predicted rationally with very good correlation. The cracking and the ultimate moments of a typical concrete beam prestressed by *FRP* and with non-prestressed reinforcement, can be calculated using equations 3-6 and 3-7, respectively, using the notation given in Fig. 3-1.

$$M_{cr} = P_e + \left[\frac{P_e}{A_c} + f_r \right] * S_b \quad 3-6$$

$$M_U = T_p d_p + T_s d - C_c c - C_s d' \quad 3-7$$

where M_{cr} = cracking moment;
 P_e = effective prestressing force;
 A_c = cross sectional area of concrete;
 f_r = rupture strength of concrete;
 S_b = bottom section modulus;
 M_u = ultimate moment;
 c = location of compression in concrete with respect to extreme compression fibre in concrete;
 C_c = compression in concrete;
 C_s = compression in non-prestressed reinforcement; and
 T_p = tension in *FRP* prestressing tendon.

Prestressed concrete beams with *FRP* tendons may fail in one of the following modes:

1. Rupture of *FRP* tendons: if the strains of the prestressed or non-prestressed *FRP* reinforcement exceed its ultimate value before the concrete crushes. This normally happens with a low percentage of reinforcement.
2. Crushing of concrete: if the ultimate compressive strain in the concrete is reached before the *FRP* tendons rupture. Such failure occurs with a high percentage of reinforcement.

3. Simultaneous rupture of the *FRP* reinforcement and crushing of the concrete: when the ultimate strains in the *FRP* reinforcement and the concrete are achieved at the same time.

3.7 DUCTILITY

It is important to ensure that a structure loaded to failure will behave in a ductile manner. This means ensuring that the structure will not fail in a brittle fashion, without warning, but will be capable of undergoing large deformations at near maximum load-carrying capacity. The ductility of a reinforced concrete member is expressed as the ratio of the ultimate deformation to the deformation at the first yield of the steel reinforcement. The ductility may be expressed in terms of the curvature of a section (ϕ_u / ϕ_y) or in terms of the deflection (Δ_u / Δ_y) of a member.

As *FRP* reinforcement does not yield, but ruptures suddenly in a brittle manner, the ductility of members prestressed by *FRP* reinforcement can not be defined in the same way as members with steel. One proposed ductility definition was the ratio between the curvature at failure and the curvature at a serviceability condition (Jaeger 1995).

It was also suggested that deformability, not ductility, should be the appropriate consideration when dealing with members with *FRP* reinforcement. Tadros defined

deformability as the deformation at failure with respect to the deformation at first cracking (Jaeger 1995). Jaeger, Tadros and Mufti (1995) showed also that deformability may be quantified according to equation 3-8. They recommended that the deformability factor be greater than 4.0.

$$\text{Deformability} = \frac{M_1 \phi_1}{M_2 \phi_2} \quad 3-8$$

where M_1 = Maximum resisting moment at failure of the beam;
 ϕ_1 = Maximum curvature of the section;
 M_2 = Moment corresponding to concrete compressive strain of 0.001; and
 ϕ_2 = Curvature of the section at concrete compressive strain of 0.001.

Naaman and Jeong (1995) proposed another definition for the ductility index based on the elastic and inelastic energy calculated at failure of prestressed beams. The energy is obtained from the load-deflection or the moment-curvature relationship of the beams. The definition gives the same value for the ductility index for beams prestressed by steel as the conventional definition using the deformations at ultimate and at yield. The proposed ductility index is given by equation 3-9.

$$\mu = \frac{1}{2} \left(\frac{E_{tot}}{E_{el}} + 1 \right) \quad 3-9$$

where E_{tot} = total energy, computed as the area under the load-deflection curve up to the load defined as the failure load; and

E_{el} = elastic energy, which can be estimated from unloading tests.

3.8 CASE STUDY: THE FIRST HIGHWAY BRIDGE BUILT IN CANADA

The first prestressed concrete highway bridge in Canada using fibre-reinforced plastic tendons for prestressing and optical fibre for monitoring the bridge behaviour was completed in November 1993. Two different types of carbon-fibre-based tendons were used to prestress six precast concrete girders of a two-continuous-span skewed highway bridge for Centre Street/Beddington Trail, in Calgary, Alberta, Canada. The girders were bulb-tee sections of 1100 mm in depth, with spans of 22.83 and 19.23 m. The girders were pretensioned to carry their own weight and the weight of the deck slab. The girders were post-tensioned by conventional prestressing steel tendons to provide continuity over the middle pier for live loads. Two girders were pretensioned by 8-mm-diameter Leadline tendons produced by Mitsubishi Kasei. The other four girders were pretensioned using 15.2-mm-diameter carbon fibre composite cables (*CFCC*) produced by Tokyo Rope.

A multichannel fibre-optic sensing system, including a number of sensors to monitor the change of light and consequently the strain, was used to monitor the behaviour of the bridge over the lifetime of the bridge. The optical fibres were installed and are monitored

by the research group of the University of Toronto Institute for Aerospace Studies.

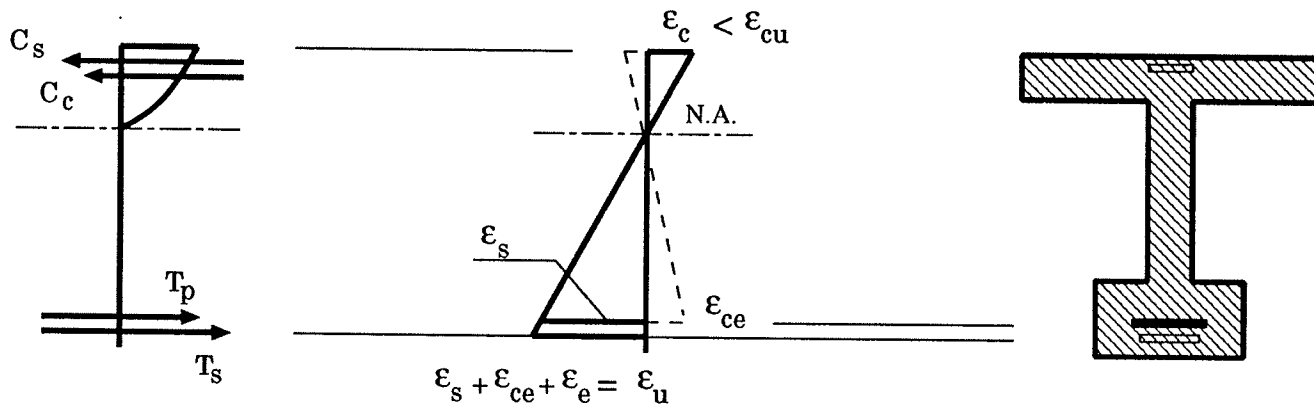
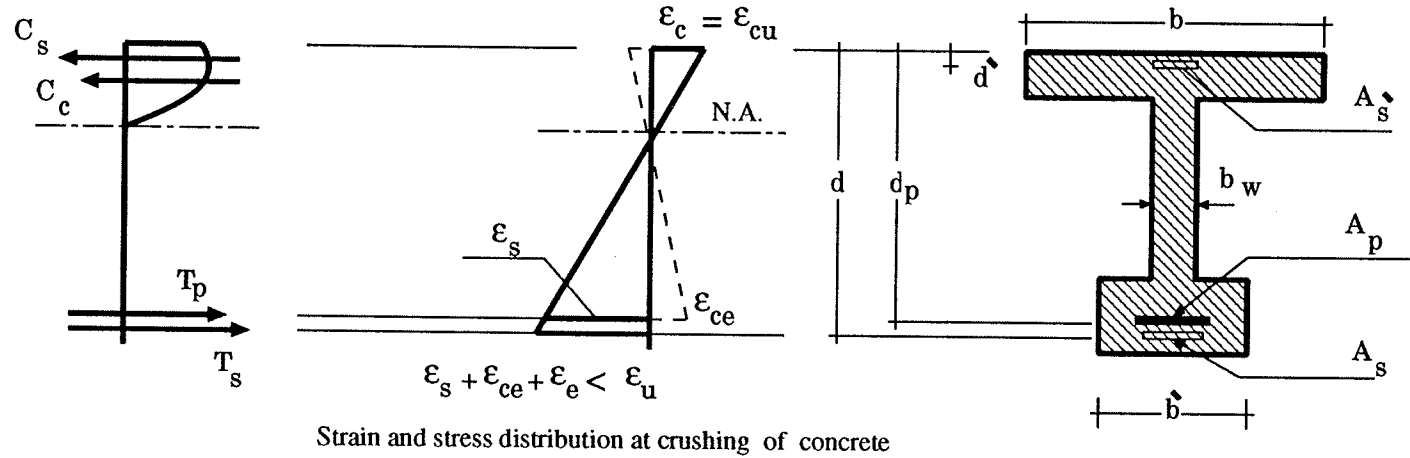


Fig.3-1 Strain and stress distribution for beams prestressed by FRP with different modes of failure

4. ————— SERVICEABILITY OF PRESTRESSED AND PARTIALLY PRESTRESSED CONCRETE BEAMS

4.1 GENERAL

Performance of prestressed and partially prestressed concrete members under service loading conditions should be assessed to ensure their adequate serviceability over their expected life time. The serviceability criteria normally considered are short- and long-term camber or deflection, cracking, fatigue, vibration, corrosion resistance, and durability. These limit states are usually controlled by specifying permissible stresses for concrete and reinforcement, in addition to the strength requirement for the structure. Aesthetically, excessive camber or deflection and large cracks in concrete members are not desirable. Excessive camber or deflection may result in damage of attached non-structural elements or it may result in accumulation of rain water, for bridge girders, and consequent deterioration of the structure. Large cracks can also affect the durability of structures due to corrosion. Prediction of deflection and cracking of prestressed or partially prestressed concrete members is therefore of prime importance and is the subject of this study.

According to the ACI Code "Building Code Requirements for Reinforced Concrete ACI 318M-89" and the Canadian code "Design of Concrete Structures for Buildings, CSA Standard CAN3-A23.3-M84", selection of the concrete cross-section and the area of the prestressing steel is based on allowable stresses for the concrete and steel. The selected member is normally checked for the serviceability requirements and the design altered if necessary. Serviceability requirements specify the allowable deflection and crack width of the given structure at service load conditions. The design is concluded by checking the ultimate strength of the member against the hypothetical factored loads. The European CEB-FIP Code (1990) also requires that the structure is designed according to several limit states including deflection, crack width at service loads, and strength requirements. Other possible limit states such as vibration and fatigue, are to be taken into account. In general, the design should aim to produce a safe, serviceable, durable, economical, and aesthetically pleasing structure.

4.2 PARTIAL PRESTRESSING

The first major prestressed concrete structures were built shortly before the Second World War. Now more than 50 percent of bridges all over the world are constructed using prestressing techniques (Collins and Mitchell 1991). Highway overpasses are normally constructed using precast pretensioned girders. Bridges with spans up to 150 m are constructed using cast-in-place post-tensioned box-girders, while cable-stayed bridges

are used for spans up to 300 m. Other applications of prestressed concrete include parking structures, cylindrical tanks, containment structures, off-shore structures, etc. Compared to reinforced concrete structures, prestressing concrete results in the following:

1. Larger spans;
2. Less deflection at service load;
3. Less cracking at service load; and
4. Use of high-strength materials, which leads to smaller and lighter members.

Full prestressing is achieved when no cracks are allowed under full service loading conditions. Such a criterion is required for the design of tanks and reservoirs where leaks must be avoided, for submerged structures, or for structures subject to a highly corrosive environment. Full prestressing is also required for structures subject to highly repetitive loading. However, full prestressing may result in a significant camber at typical service loads less than the specified design value, which are likely to be the dead load and a fraction of the specified live load. The camber can be also aggravated by the creep of the concrete which magnifies the upward displacement due to the prestressing force, but has less influence on the downward deflection due to live load. In many prestressed concrete structures, it is not likely that the full specified load will be applied during the lifetime of the structure. Therefore, it is possible to design the structural elements such that some cracks may occur under the full specified load; this is known as partial

prestressing. However, such cracks should close when the load is removed. Partial prestressing may be achieved in two ways:

1. By providing non-prestressed reinforcement in addition to the prestressed tendons. This is normally utilized in post-tensioned construction. It may also provide greater economy in the fabrication of long-line pretensioned casting bed when it is desirable to produce elements of different strength. It should be noted, however, that not every beam that has a combination of prestressed and non-prestressed reinforcement may be called a partial prestressed member, since non-prestressed reinforcement may have to be provided in some beams to satisfy the ultimate strength requirements.
2. By reducing the jacking stress of the prestressing reinforcement below the maximum allowable specified by the code and relying on the increase in tendon's stress after decompression and cracking to resist the increase in the applied loads. This is a useful option in pretensioned construction where there may be difficulties in placing non prestressing reinforcement.

The main risk in partial prestressing is that, for an unexpected loss of prestress (due to high friction or inadequate control during tensioning), both the additional stresses in reinforcement and the deformation in the structure are considerably larger for partial prestressing than for full prestressing (Menn 1983). In comparison to fully prestressed

members, partially prestressed members are characterized with the following:

1. More ductility;
2. Lower cost;
3. Less camber;
4. Less prestress force which may allow for an increase in the tendon eccentricity;
5. Less prestress loss due to creep and relaxation (where partial prestressing is achieved using lower tendon stresses); and
6. Less cracking at the end zones in case of post-tensioned and pretensioned elements.

Partial prestressing is considered an intermediate design between the two extremes, namely, reinforced concrete and fully prestressed members. To design a partially prestressed member, the amount of prestressing has to be well quantified. The following section will provide a discussion of the different definitions by which the extent of prestressing can be evaluated according to the literature currently available.

4.2.1 Definition of Partial Prestressing

Several indices have been introduced to quantify the amount of prestressing. These indices normally have a value ranging between zero for reinforced concrete members and unity for fully prestressed concrete members. Some of the indices are a section property

while others depend on the external applied dead and live loads. The indices can be defined as follows:

1. **Partial prestressing ratio (PPR):** Naaman and Siriaksorn (1979) defined *PPR* as the ratio between the nominal moment resistance due to the prestressing reinforcement to the nominal total moment resistance of the section, i.e. due to prestressed and non-prestressed reinforcement, as given by equation 4-1.

$$PPR = \frac{M_{np}}{M_n} = \frac{A_{ps} f_{ps} (d_p - \frac{a}{2})}{A_{ps} f_{ps} (d_p - \frac{a}{2}) + A_{ns} f_y (d - \frac{a}{2})} \quad 4-1$$

where a = depth of the equivalent rectangular stress block in the compression zone of concrete section;

A_{ps} = area of prestressing reinforcement;

A_{ns} = area of non-prestressing reinforcement;

d_p = depth of prestressing reinforcement from extreme compression fibre;

d = depth of non-prestressing reinforcement from extreme compression fibre;

f_{ps} = stress in prestressing reinforcement at ultimate;

f_y = yield stress in non-prestressing reinforcement;

M_{np} = nominal moment resistance of the section based on prestressing reinforcement only; and

M_n = nominal moment resistance of the section.

The partial prestressing ratio is a section property and does not depend on the external applied loads. According to the definition of *PPR*, a prestressed member without non-prestressed reinforcement will automatically be a fully prestressed member, and *PPR* will have a value of unity, even if the stress in the prestressed reinforcement is less than the permissible value. However, it should be mentioned that Naaman and Siriakorn provided the definition for partially prestressed members which contain prestressed and non-prestressed reinforcement.

2. **Degree of prestress (DP):** is the ratio of the decompression moment to the sum of the moments caused by the dead and live loads as given by equation 4-2. The decompression moment is defined as the moment which leads to a zero stress, when combined with the effective prestressing force, at the extreme fibre of the concrete section at which the applied loads cause tensile stresses (Nilson 1987).

$$DP = \frac{M_{dec}}{M_D + M_L} \quad 4-2$$

where M_{dec} = decompression moment;
 M_D = moment due to dead load; and
 M_L = moment due to live load.

One of the advantages of using the degree of prestress to quantify the amount of prestressing is that non-prestressed reinforcement does not necessarily have to be present in the section. For a fully prestressed beam, the value of the degree of prestress may be smaller than, equal to, or greater than unity, depending on the stress at the soffit under service load.

3. **Prestressing Index (i_p):** is the ratio of the yield strength of the prestressing reinforcement to the sum of the yield strengths of the prestressing and non-prestressing reinforcement as given by equation 4-3.

$$i_p = \frac{A_{ps} f_{py}}{A_{ps} f_{py} + A_{ns} f_y} \quad 4-3$$

where f_{py} = yield stress of the prestressing reinforcement.

Similar to *PPR*, the prestressing index (i_p) does not quantify the amount of prestressing in the case of partial prestressing achieved by lowering the stresses in the prestressing reinforcement.

4. **Global reinforcing index (Ω):** is defined by equation 4-4 as the summation of the reinforcing indices for the prestressing and non-prestressing reinforcement at the tension and compression sides, ω_p , ω and ω' which are given by equations 4-5, 4-6 and 4-7, respectively.

$$\Omega = \omega_p + \omega - \omega' \quad 4-4$$

$$\omega_p = \rho_p \frac{f_{ps}}{f'_c} \quad 4-5$$

$$\omega = \rho \frac{f_y}{f'_c} \quad 4-6$$

$$\omega' = \rho' \frac{f_y}{f'_c} \quad 4-7$$

- Where ρ_p = ratio of prestressing reinforcement A_{ps}/bd_p ;
 ρ = ratio of non-prestressing tension reinforcement A_{ns}/bd ;
 ρ' = ratio of non-prestressing compression reinforcement A'_s/bd ;
 A'_s = area of non-prestressing compression reinforcement; and
 b = web width.

The global reinforcing index accounts for all types of reinforcement present in the section. The ACI Code 318M-89 specifies the upper limit of the reinforcing index to be about 0.3. For a flanged section reinforcement indices ω_w , ω_{pw} and ω'_w are computed as for ω , ω_p and ω' except that b shall be the web width and reinforcement shall be that required to develop compressive strength in the web only (ACI Code 318M-89).

4.2.2 Behaviour in Flexure

Load-deflection relations for beams with varying amount of prestress force are presented in Fig. 4-1 (Nilson 1987). Both reinforced and prestressed concrete beams may be under-reinforced, with a relatively small steel area such that failure is preceded by yielding of the steel, or over-reinforced, with a relatively large steel area so that failure is initiated by crushing of the concrete on the compression side of the member before the steel reaches its yield stress. In each case, the amount of prestress force introduced by the given steel area may vary from zero (reinforced concrete) to a very large value (over-prestressing).

Fig. 4-1a shows load-deflection curves for under-reinforced beams, all with the same steel area and concrete dimensions but varying amounts of prestress. Curve (a) represents a beam with zero prestress, while curves (b), (c) and (d) represent partially, fully and over-prestressed beams. Obviously, for beams (b), (c) and (d), the load initiating the first crack of the beam is higher than that for beam (a) because of the initial superimposed compression stresses in the tension zone. The cracking load increases with the increase of the prestressing force. The load causing failure is about the same in all cases. The partially prestressed beam (b) may crack at a load level below the full service load, whereas the fully prestressed beam (c) cracks only when a higher load than the service load is reached. Beam (d), which is the over-prestressed beam, will fail suddenly in a

brittle fashion. A further change in the slope of the load-deflection curve before failure is observed as the steel is stressed to its inelastic range, and as extensive cracking occurs. The corresponding curves for over-reinforced beams, as given in Fig. 4-1b, show brittle failure with less warning than do the under-reinforced beams. The effect of varying the prestress is similar to that for under-reinforced beams, except that the load that causes failure increases to some extent as the prestress force increases (Nilson 1987). Compared to full prestressing, the behaviour of partially prestressed concrete beams with steel reinforcement is characterized with the following:

1. Smaller cracking load and almost the same failure load as fully prestressed beams.
2. Larger deflections at ultimate load, higher ductility, and higher energy absorption than fully prestressed beams because the capacity of flexural members to absorb the energy is directly related to the area under the load-deflection diagram.
3. The fatigue life of cracked partially prestressed beams is generally smaller than that of either fully reinforced or uncracked fully prestressed beams subjected to the same load amplitude (Naaman 1985).

4.3 SERVICEABILITY LIMIT STATES

The most important serviceability limit states, which must be checked for prestressed or partially prestressed concrete members, are the short- and long-term deflection, crack width, and fatigue. Deflection is defined as the total movement induced at a point of a member from its position before application of the load to its position after the application of the load. The point at which maximum deflection occurs along the member is generally of main interest. The deflection due to "short-term" live load and "long-term" dead load plus sustained live load should be calculated. The maximum permissible deflection allowed by the ACI 318-89 and the CSA Standard CAN3-A23.3-M84 is given in Table 4-1. Crack widths are investigated only for partially prestressed concrete members and for non-prestressed concrete members. Limits on the crack width given by the CPCI Metric Design Manual (1989) for non-prestressed and partially prestressed concrete members are summarized in Table 4-2. The crack width should be checked under full service load. The CEB-FIP Code (1978) has recommended the limits of the characteristic crack width at the surface of the concrete as given by Table 4-3. The characteristic crack width is defined as 1.7 times the average crack width and is regarded as the width which only one crack in twenty will exceed. Many attempts have been undertaken by various researchers to address computation methods for the short and long-term deflection and the crack width of prestressed concrete beams. The following summarizes the state-of-the-art methods to calculate the short-term deflection and crack

width of partially prestressed concrete beams.

4.3.1 Short-Term Deflection

The stiffness of partial prestressed concrete members is reduced after cracking resulting in an increase in the deflection which may exceed the acceptable serviceability limit. Hence, the calculation of deflection becomes a matter of practical importance. Deflection, in general, is calculated using the moment-curvature relationship for any flexural member. The curvature at a given section may be estimated either from the strain distribution in the section (the curvature is equal to the slope of the strain diagram), or by the relationship between bending moment and curvature, as given by equation 4-8. The moment-curvature relationship can be used to estimate the curvature along a member corresponding to a given distribution of moments, as shown in Fig. 4-2. The change of slope between any two points along the beam is equal to the area under the curvature diagram between these two points, as given by equation 4-9. The deflection of any point C with respect to another point B, is equal to the first moment of area of the area under the curvature diagram between B and C, as given by equation 4-10.

$$\phi = \frac{\epsilon_c}{c} = \frac{M}{E_c I} \quad 4-8$$

$$\theta_{BC} = \int_{x_C}^{x_B} \phi \, dx \quad 4-9$$

$$\delta_{BC} = \int_{x_C}^{x_B} \phi (x_B - x) \, dx \quad 4-10$$

- where ϕ = curvature of the section;
 ϵ_c = concrete strain at the extreme compression fibre;
 c = neutral axis depth from the extreme compression fibre in concrete;
 θ_{BC} = slope at point C relative to the slope at point B; and
 δ_{BC} = deflection at point C relative to the deflection at point B.

When the bending moment is specified along the beam length, the deflection may be calculated based on the curvature at one section (section of maximum curvature), three sections (section of maximum curvature and two sections at the supports), or more than three sections. The integration may be performed numerically in case of calculation of the deflection using the curvature at different sections along the beam length.

For uncracked sections, the curvature ϕ_g can be estimated using equation 4-8 based on the gross moment of inertia I_g . To calculate the curvature at a cracked section ϕ_{cr} , the cracked moment of inertia I_{cr} , which ignores the concrete in tension, is applied in equation 4-8. However, when cracking occurs in a prestressed concrete member, cracks

develop at several sections along the span. Tensile stresses are introduced into the concrete between cracks by bonded reinforcement. Concrete between the cracks in the tension zone contributes to the stiffness of the member. In addition, cracking does not extend to the neutral axis as assumed in the analysis of cracked concrete sections due to the fact that the concrete tensile strength is not zero. These effects are often called "*tension stiffening*".

4.3.1.1 Tension Stiffening Effect

The bending stiffness of partially prestressed concrete members under service loads is considerably less than that calculated based on uncracked gross cross-sectional properties. This is due to mainly the presence of numerous tensile cracks. However, the actual stiffness is significantly higher than that calculated without consideration of the tensile resistance of the concrete. This phenomenon, known as tension stiffening, is attributed to the fact that concrete does not crack suddenly and completely before it undergoes progressive microcracking (strain softening). Tension stiffening is partly lost when the load is applied repetitively and when it is sustained. The tension stiffening effect depends on the quality of bond of the reinforcing bars. Several empirical methods have been reported to account for tension stiffening in the calculation of the short-term deflection of concrete members, as follows:

Method 1: The effective moment of inertia I_e , which was originally developed by Branson (Branson 1977) for non-prestressed members, accounts for the reduction in the flexural stiffness of partially prestressed members due to cracking. The effective moment of inertia is calculated as given by equation 4-11.

$$I_e = \left(\frac{M_{cr}}{M_s} \right)^m I_g + \left[1 - \left(\frac{M_{cr}}{M_s} \right)^m \right] I_{cr} \leq I_g \quad 4-11$$

where I_{cr} = moment of inertia of the cracked section ignoring concrete in tension;

I_g = gross moment of inertia;

M_{cr} = cracking moment

$$= P_e e + [f_r + P_e / A_g] S_b$$

M_s = service load moment;

m = 3, when calculation is for the entire length of a simply supported member or between inflection points of a continuous member;

4, when calculation is for a given section of the member;

A_g = gross cross-sectional area of concrete;

f_r = rupture strength of concrete;

S_b = cross sectional modulus at the tension side;

P_e = effective prestressing force; and

e = eccentricity of prestressing reinforcement based on gross section properties.

It should be mentioned that the neutral axis, which is based on the depth of the concrete compression zone, does not coincide with the centroid of the transformed cracked section in the presence of the prestressing force. Hence, it is important to note that I_{cr} and I_e are not constants for prestressed concrete sections, but depend on the particular loading at which the deflection is being calculated. Thus, it is not possible to superimpose deflection values after cracking for different loading conditions.

The ACI Code recommends the effective moment of inertia method to calculate the deflection of reinforced or prestressed concrete members. Equation 4-11 has been modified by several researchers to estimate the short-term deflection of partially prestressed beams as follows:

1. Chen, Bennett, Tadros (1982) and Naaman (1982) have proposed that the cracking moment and the service load moment, used in equation 4-11 to calculate the effective moment of inertia, be reduced by an amount equal to the decompression moment M_{dc} . The idea behind obtaining the decompression stage is to attempt to bring the cross-section to a condition identical to that of a conventionally reinforced section subject to a combined axial force and bending moment (Tadros 1982). From that stage on, the cross-section would be analyzed in the same manner as in the working stress analysis of reinforced concrete members. The decompression moment is defined in this case by the moment leading to zero stress at the extreme fibre of

the concrete section, at which the tensile stresses are caused by the applied loads. The decompression moment M_{dc} and the effective moment of inertia I_e are given by equations 4-12 and 4-13, respectively. Accordingly, deflection of the prestressed member, can be calculated using equation 4-14.

$$M_{dc} = P_e e + \frac{P_e S_b}{A_g} \quad 4-12$$

$$I_e = \left(\frac{M_{cr} - M_{dc}}{M_s - M_{dc}} \right)^3 I_g + \left[1 - \left(\frac{M_{cr} - M_{dc}}{M_s - M_{dc}} \right)^3 \right] I_{cr} \leq I_g \quad 4-13$$

$$\Delta = K \frac{M_s L^2}{E_c I_e} \quad 4-14$$

where K = coefficient depending on the support and loading condition; and
 L = effective length of the member.

2. Branson and Trost (1982) have suggested a "zero deflection point" approach for partially prestressed beams, which defines the effective moment of inertia I_e for cracked section as given by equation 4-15.

$$(I_e)_{L2} = \left(\frac{M'_{cr}}{M_{L2}} \right)^3 I_g + \left[1 - \left(\frac{M'_{cr}}{M_{L2}} \right)^3 \right] I_{cr} \leq I_g \quad 4-15$$

- where $(I_e)_{L2}$ = effective moment of inertia compared to a downward (net positive deflection);
- M_{cr}' = net positive moment required to crack the section
 = $[f_r + P_e / A_g] S_b$;
- M_{L2} = part of the live load moment that corresponds to a downward deflection of a prestressed member
 = $M_L - M_{L1}$;
- M_L = live-load moment; and
- M_{L1} = part of the live load moment corresponding to zero deflection
 = $P_e e - M_D$ (for uniformly distributed dead load, live load and equivalent upward prestressed load).

The instantaneous live load deflection, Δ_L is given by equation 4-16. The total deflection due to dead and live loads and prestressing force, Δ , is equal to the deflection due to M_{L2} , Δ_{L2} , and is given by equation 4-17.

$$\Delta_L = K \left[\frac{M_{L1} L^2}{E_c I_g} + \frac{M_{L2} L^2}{E_c (I_e)_{L2}} \right] \quad 4-16$$

$$\Delta = \Delta_{L2} = K \frac{M_{L2} L^2}{E_c (I_e)_{L2}} \quad 4-17$$

3. Branson and Sheikh (Krishna Mohan Rao and Dilger 1992) have proposed a simplified expression for I_e to calculate the instantaneous live load deflection as given by equations 4-18 and 4-19.

$$(I_e)_L = \left(\frac{(M_L)_{cr}}{M_L} \right)^3 I_g + \left[1 - \left(\frac{(M_L)_{cr}}{M_L} \right)^3 \right] I_{cr} \leq I_g \quad 4-18$$

$$\Delta_L = K \frac{M_L L^2}{E_c (I_e)_L} \quad 4-19$$

where $(M_L)_{cr}$ = equivalent live-load cracking moment
 $= M_{cr} - M_D$.

4. Tadros, Ghali and Meyer (1985) took into consideration the shift in the centroid of the cross-section upon cracking that results in a larger prestressing force eccentricity e_{cr} than that of the uncracked member. For prestressed members with flanged cross-sections, ignoring the change of eccentricity while calculating the curvature of the member may result in a significant overestimation of the deflection. Hence, equation 4-20 was suggested to calculate the moment of inertia of the section I_e .

The effective centroidal distance after cracking is calculated as given by equation 4-21 and shown in Fig. 4-3. The change in the eccentricity after cracking can then be calculated using the effective centroidal distance.

$$I_e = \left(\frac{M_{cr} - M_{dc}}{M_s - M_{dc}} \right)^4 I_g + \left[1 - \left(\frac{M_{cr} - M_{dc}}{M_s - M_{dc}} \right)^4 \right] I_{cr} \leq I_g \quad 4-20$$

$$y_e = \left(\frac{M_{cr} - M_{dc}}{M_s - M_{dc}} \right)^4 y_g + \left[1 - \left(\frac{M_{cr} - M_{dc}}{M_s - M_{dc}} \right)^4 \right] y_{cr} \leq y_g \quad 4-21$$

Where y_g = distance to the centroid of the gross section, measured from the extreme compression fibre; and

y_{cr} = distance to the centroid of the cracked section, measured from the extreme compression fibre.

The mean curvature, which takes into account the tension stiffening effect, can be calculated according to equation 4-22. The curvatures at key sections along the span are calculated and integrated to obtain the deflection.

$$\phi_e = \frac{M_s - P_e (d_p - y_e)}{E_c I_e} \quad 4-22$$

Method 2: The effective curvature ϕ_e which takes the tension stiffening effect into consideration is calculated using an interpolation between the uncracked and cracked curvatures ϕ_g and ϕ_{cr} of the sections. The curvatures ϕ_g and ϕ_{cr} are calculated from equation 4-8 using I_g and I_{cr} respectively. The CEB-FIP Model Code (1990) recommends equation 4-23 to calculate the mean curvature at a given section. The interpolation factor ζ is defined by equation 4-24.

$$\phi_e = (1 - \zeta) \phi_g + \zeta \phi_{cr} \quad 4-23$$

$$\zeta = 1 - \beta \left(\frac{M_{cr}}{M} \right)^2 \geq 0.4 \text{ and } M > M_{cr} \quad 4-24$$

where $\beta = \beta_1 \beta_2$, with β_1 (bond factor) = 1 and 0.5, for high bond and plain bars, respectively, and β_2 (loading factor) = 1 and 0.5, for first loading and for loads applied in a sustained manner or for a large number of cycles, respectively.

For most practical applications, $\beta_1 = 1$, $\beta_2 = 0.5$ and hence $\beta = 0.5$.

Ghali (1993) recommended that equation 4-23 be used for deflection computation.

He proposed a definition for the interpolation factor ζ as given by equation 4-25.

$$\zeta = 1 - \left(\beta \frac{f_{cr}}{\sigma_1} \right)^2 \quad 4-25$$

where β = coefficient representing influence of duration of application or repetition of loading; $\beta = 0.8$ at first loading and $\beta = 0.5$ for long-term loading or for a large number of load cycles;

f_{cr} = tensile strength of concrete
 = f_r when a section is subjected to a bending moment without axial force; and

σ_l = tensile stress in the concrete due to applied loads, based on the uncracked section.

The effective curvature is calculated at critical sections and integrated to calculate the deflection as described before.

Method 3: Trost (cited in reference Tadros, Ghali and Meyer 1985) accounts for tension stiffening by interpolation between the deflections δ_g and δ_{cr} of uncracked and cracked members, respectively, as given by equation 4-26.

$$\delta = \frac{(M_n - M_a)^2}{(M_n - M_{cr})^2} \delta_g + \left[1 - \frac{(M_n - M_a)^2}{(M_n - M_{cr})^2} \right] \delta_{cr} \quad 4-26$$

where M_n = moment corresponding to theoretical (nominal) strength; and
 M_a = moment due to applied loads.

Method 4: Tension stiffening of partially prestressed concrete members can be accounted for using the concrete tensile stress-strain relationship. The mean curvature at a given section can be calculated using a strain compatibility approach without ignoring the concrete in tension. Bažant and Oh (1984) used the model shown in Fig. 4-4 for the strain softening in the calculation of the deflection of conventionally reinforced concrete members. Tensile stresses in the concrete were included in the cross-section in the zones where the tensile strains in concrete do not exceed ϵ_{tf} where ϵ_{tf} is defined using the bi-linear uniaxial tensile stress-strain diagram for concrete shown in Fig. 4-4. The model yielded satisfactory results compared to the effective moment of inertia method.

Collins and Mitchell (1991) accounted for tension stiffening using the average concrete stress versus average concrete strain relationship given by equation 4-27, and shown in Fig. 4-5, to estimate the average tensile stress in the concrete after cracking. The tensile stresses are considered only in the effective embedment zone given by the CEB-FIP Code (1978), shown in Fig. 4-6. The average tensile stresses in the cracked concrete outside the effective embedment zone, are ignored. An equivalent uniform distribution of a tensile stress equal to 0.5 times the cracking stress, f_{cr} , is proposed as shown in Fig. 4-7. The curvature can then be calculated and integrated over the beam

length to calculate the member deflection.

$$f_{ct} = \frac{\alpha_1 \alpha_2 f_{cr}}{1 + \sqrt{500 \epsilon_{ct}}} \quad \epsilon_{ct} > \epsilon_{cr} \quad 4-27$$

- where f_{ct} = average tensile stress after cracking;
- ϵ_{ct} = average tensile strain;
- ϵ_{cr} = tensile strain at cracking;
- α_1 = factor accounting for bond characteristics of reinforcement
= 1.0 for deformed reinforcing bars, 0.7 for plain bars, wires, or bonded strands and 0 for unbonded reinforcement; and
- α_2 = factor accounting for sustained or repeated loading
= 1.0 for short-term monotonic loading and 0.7 for sustained and/or repeated loads.

From the previous discussion of the different methods proposed to calculate the deflection, it is concluded that it is difficult to calculate member deflections with a high degree of accuracy even in a controlled testing laboratory. This is due to the random variations of some of the contributory factors such as the concrete modulus of elasticity, creep, and shrinkage. In field conditions, not only are the variations greater, but in addition the number of variables increase. Examples are the uncertainties about level and duration of loading and seasonal weather variations. A calculated deflection should

therefore be viewed as an "estimate" (Tadros, Ghali and Meyer 1985).

4.3.2 Crack Control

Cracking of concrete occurs when the induced strain, which could be due to load and/or shrinkage, exceeds the ultimate tensile strain of concrete. It has been reported in the literature that the measured ultimate tensile strain and modulus of rupture f_r for concrete have very wide and scattered results. Based on statistical evaluation, the modulus of rupture of concrete f_r , related to the compressive cube strength f_{cu} at 28 days, is given by equations 4-28 and 4-29 by Rüh (Leonhardt 1988). This indicates that concrete members normally crack if the tensile strain ϵ_{ct} exceeds the range of 0.01 to 0.012 percent.

$$5\% \text{ probability } f_r = 0.18 f_{cu}^{\frac{2}{3}} \quad \text{MPa} \quad 4-28$$

$$95\% \text{ probability } f_r = 0.36 f_{cu}^{\frac{2}{3}} \quad \text{MPa} \quad 4-29$$

Concrete structures may crack in the first days after placing concrete and before applying any loads on the structure, due to differential temperature caused by the hydration process of cement. The differential temperature may induce higher tensile strain than the strain corresponding to the modulus of rupture. The amount of heat caused by the hydration depends on the member thickness, type of cement, curing process, and

curing environment. Major cracks develop mainly due to the applied loads, which induce internal normal, shearing, torsional, and bending stresses. Cracks may also occur due to tensile stresses produced by restrained deformations due to temperature variation, shrinkage, and creep of the concrete. In general, cracks can not be avoided in concrete structures.

Cracks are typically evaluated by measuring the crack width, w , at the concrete surface. Reinforced and prestressed concrete structures, reinforced by steel bars or tendons, are normally protected against corrosion if the crack width does not exceed 0.4 mm with sufficient concrete cover (Darwin et al. 1985). Design codes aim to control cracks for corrosion protection by limiting the permissible maximum crack width. Replacing the steel by fibre-reinforced-plastic (*FRP*) reinforcement provides an excellent solution to the classical problem of deterioration of concrete structures due to corrosion of steel reinforcement. However, it should be noted that there are many good reasons for controlling widths of cracks other than corrosion protection. For example, it may be necessary to control the crack width to avoid leakage or to avoid impairment of the appearance of the structure (Darwin et al. 1985). It has been reported that crack width is affected by the following factors:

1. Stress in reinforcement;
2. Concrete cover;

3. Diameter, spacing and arrangement of reinforcing bars;
4. Bond properties of reinforcing bars;
5. Concrete strength;
6. Shape of strain distribution;
7. Type and shape of prestressed and non-prestressed reinforcement; and
8. Ratio of prestressed to non-prestressed reinforcement.

4.3.2.1 Crack Width Evaluation

Crack widths should be calculated for partially prestressed and non-prestressed concrete members. The permissible crack width varies between 0.1 and 0.4 mm. When steel reinforcement is designed to provide ultimate strength in accordance with any of the existing codes, load-induced cracks rarely exceed a width of 0.5 mm (Ghali and Favre 1986). Therefore, cracks of larger width occur only when the structure is subjected to loads larger than those it is designed for. Experience indicates that a crack can be visible if its width exceeds 0.2 mm (Darwin et al. 1985). Selection of an appropriate maximum crack width for structures prestressed by *FRP* reinforcement is needed to avoid marring the appearance of the structure. Crack width calculations for partially prestressed members have been related either to a fictitious tensile stress in the concrete or to the stress in the reinforcement.

Fictitious tensile stress method: Control of the crack width using this approach is achieved by limiting the fictitious tensile stress in the concrete, calculated based on uncracked section properties under service loading conditions. This tensile stress is fictitious because it is greater than the modulus of rupture of the concrete. ACI Code 318-83 allows a fictitious tensile stress in the pre-compressed tensile zone of $1.0 \sqrt{f'_c}$ MPa, which is equivalent to $12 \sqrt{f'_c}$ psi, without checking the crack width if the code requirements for minimum cover and deflection are satisfied.

The fictitious tensile stress is insensitive to such parameters as type of reinforcement and its distribution, concrete cover, etc. Naaman and Siriakson (1979) reported that the fictitious tensile stress calculated under full service loads for partially prestressed beams which satisfy ultimate strength and serviceability criteria varied from $5.0 \sqrt{f'_c}$ to $46 \sqrt{f'_c}$ psi, indicating that no limiting tensile stress can be selected to cover all practical cases. Tadros (1982) found that for a partially prestressed doubled T-beam exhibiting a maximum crack width of 0.075 mm, the calculated fictitious tensile stress is $18 \sqrt{f'_c}$ psi. This value is about 50 percent larger than the maximum allowable limit stipulated by the ACI Building Code for prestressed members. Krishna Mohan Rao and Dilger (1992) showed that for a given dimension and reinforcement, the fictitious tensile stress in a T-section is higher than that in I-section, while the calculated crack width for the T-section is less than the crack width for the I-section, under the same load level. Consequently, the use of the fictitious tensile stress method is not acceptable for the

design of prestressed concrete members because it may lead to unsatisfactory crack control (Krishna Mohan Rao and Dilger 1992). An upper limit of the fictitious tensile stress can be too liberal for solid, box and I-type sections and can be too restrictive for T-sections. A survey of the proposed equations to estimate the crack width for partially prestressed concrete members, based on the fictitious tensile stress approach, is given in Table 4-4. It is shown in Table 4-4 whether the given crack width is a maximum or an average value and whether the crack width is predicted at the steel level or at the beam soffit.

Reinforcement stress method: The second approach to estimate the crack width is based on the stress or strain of the reinforcement. Many equations have been proposed to calculate the crack width using this approach. There is a general agreement that the stress in the reinforcement, cover, type of reinforcement and its distribution, and area of concrete in tension are the major variables to be considered in estimating the crack width of concrete members. The crack width is related to the stress in the reinforcement for reinforced concrete members and to the stress change after decompression in the prestressed reinforcement. The decompression is a fictitious state at which the prestressed section becomes similar to a reinforced concrete section subjected to axial force and bending moment. Table 4-5 shows the different methods available in the literature to estimate the crack width using the reinforcement stress approach.

Various methods have been proposed to evaluate the decompression force, based on decompression at the extreme fibre, at reinforcement level, or of the whole section which leads to zero concrete stress throughout the cross-section. Bachmann, Bruggeling, Nilson and Shaikh (Tadros 1982) recommended that the effective prestressing force, P_e , be used instead of the decompression force, P_{dc} , in cracked section stress analysis. Bachmann recommended the use of the effective prestressing force instead of the decompression force since the difference between P_{dc} and P_e is small and P_e is always on the safe side.

The following three methods for estimating the crack width based on the reinforcement stress approach are recommended by the CPCI Design Manual (1989), the CEB-FIP Code (1978) and the ACI building Code (1989).

Method 1: CPCI Design Manual (1989) recommended the use of the method given by Suri and Dilger (1986) to estimate the maximum crack width at the beam soffit. The method is based on statistical analysis and accounts for different combinations of prestressed and non-prestressed reinforcement as given by equation 4-30.

$$w_{\max} = k f_s d_c \sqrt{\frac{A_t}{A_s}} \quad 4-30$$

- where w_{max} = maximum crack width at the beam soffit;
- k = 2.55×10^{-6} for strand and deformed bar combination;
= 2.65×10^{-6} for strands only;
= 3.51×10^{-6} for wire and deformed bar combination;
= 4.50×10^{-6} for wires only;
- f_s = change in the stress in prestressed reinforcement due to an applied moment M_s ;
- d_c = concrete cover measured from centre of reinforcement;
- A_t = area of concrete below the neutral axis; and
- A_s = total area of prestressed A_{ps} and non-prestressed A_{ns} reinforcement.

Design charts are given to calculate the change of the stress in the prestressing reinforcement (Krishna Mohan Rao and Dilger 1992). Rational analysis can also be used to predict the decompression force and the stress in the reinforcement using equations 4-31 and 4-32.

$$P_{dc} = P_i + \Delta P_c + \Delta P_p + \Delta P_s \quad 4-31$$

$$f_s = \left[\frac{-P_{dc}}{A_{cr}} + \frac{-P_{dc} e_{cr} + M_s}{I_{cr}} e_{cr} \right] n \quad 4-32$$

where P_i = initial prestressing force;

ΔP_c = total loss of compression in concrete due to the combined effect of creep, shrinkage of concrete and relaxation of prestressing reinforcement, (negative value);

$$\Delta P_p = f_c (E_{ps} / E_c) A_{ps}$$

force in prestressing reinforcement corresponding to the concrete stress f_c at the level of the prestressed reinforcement under dead load and effective prestress;

$$\Delta P_s = f_c (E_{ns} / E_c) A_{ns}$$

force in non-prestressed reinforcement corresponding to the concrete stress f_c at the level of the non-prestressed reinforcement due to the effect of dead load and effective prestress;

$$f_c = P_e / A + P_e e y_s / I_g - M_d y_s / I_g;$$

A_{cr} = cross-sectional area of transformed cracked section;

e_{cr} = eccentricity of prestressing reinforcement with respect to neutral axis of the transformed cracked section;

n = modular ratio E_s / E_c ; and

E_s = Average modulus of elasticity of prestressed E_{ps} and non-prestressed E_{ns} reinforcement.

Method 2: The CEB-FIP Code 1978 approach for predicting the crack width is based on the strain in the reinforcement. The crack width is calculated based on an assumed crack spacing. An empirical formula is proposed to estimate the crack spacing, as given by equation 4-33, which may be applied for a reinforced or prestressed concrete cross-section subjected to axial force, bending moment, or combination of both.

$$S_{rm} = 2 \left(c + \frac{s}{10} \right) + k_1 k_2 \frac{d_p}{\rho_r} \quad 4-33$$

- where S_{rm} = average spacing between cracks;
- c = concrete cover;
- s = spacing between longitudinal reinforcement. s should be less than or equal to $15d_b$;
- d_b = bar diameter;
- k_1 = coefficient, depending on the bond quality of reinforcement
= 0.4 for high-bond bars and 0.8 for plain bars or plain prestressing wires;
- k_2 = coefficient, depends on the shape of the strain diagram.
= 0.125, in case of bending without axial force, 0.25, in case of axial tension and $0.25 [(\epsilon_1 + \epsilon_2) / 2\epsilon_1]$, in case of eccentric tension or for a zone from web of a beam. ϵ_1 and ϵ_2 are strain values in the cracked state at the top and bottom, respectively, of the zone considered;

$$\rho_r = A_s / A_{cef}; \text{ and}$$

A_{cef} = effective area of concrete, where reinforcement influence the crack width as given in Fig. 4-6.

The average crack width (w_m) is estimated using equation 4-34, which is based on the strain in the prestressing reinforcement, ϵ_{s2} , after decompression. The characteristic crack width (w_k), which is defined as the crack width that only 5 percent of the cracks will exceed, is given by equation 4-35.

$$w_m = S_{rm} \zeta \epsilon_{s2} \quad 4-34$$

$$w_k = 1.7 w_m \quad 4-35$$

where ζ is given by equation 4-24.

Method 3: The ACI 318M-89 and CSA Standard CAN3-A23.3-M84 recommend the use of the method proposed by Gergely and Lutz (1966), given by equation 4-36, for the calculation of the crack width of reinforced concrete beams. It is also proposed to use the same equation for partially prestressed concrete beams (CPCI Design Manual 1989).

$$w = R \frac{h_2}{h_1} f_s \sqrt[3]{d_c A} \quad 4-36$$

where $R = 11 \times 10^{-6}$ for steel;
 $h_1 =$ distance from centroid of tensile reinforcement to neutral axis;
 $h_2 =$ distance from extreme tensile fibre to neutral axis;
 $A =$ average effective area around one reinforcing bar
 $= 2 b d_c / m$; and
 $m =$ number of reinforcing bars.

The factor R in equation 4-36, which depends on the bond of the prestressing reinforcement, was proposed by Suri and Dilger (1986) for different combinations of the prestressed and non-prestressed steel reinforcement. It is reported that there is a poor correlation between the crack width and the variable A , which is the average effective area around one reinforcing bar.

Another expression was proposed (CPCI Design Manual 1989) to control the crack width of partially prestressed concrete beams; it is based on the recommendations of Gergely and Lutz expression and given by equation 4-37. The recommended values of the quantity, z , given by the CPCI Handbook are 15 and 20 kN/mm, which correspond to a maximum crack width of 0.2 and 0.27 mm, respectively, for prestressed elements subjected to exterior and interior exposure. The parameters used in equation 4-37 are similar to the parameters used for calculating the crack width using the Gergely and Lutz equation.

$$z = .001 f_s \sqrt[3]{d_c A} \quad 4-37$$

4.4 SERVICEABILITY OF BEAMS PARTIALLY PRESTRESSED BY *FRP*

Application of fibre-reinforced-plastic reinforcement in prestressed concrete structures is relatively recent. Therefore, design engineers deal with this new material with caution, especially with the lack of knowledge about the long-term characteristics of *FRP* in structural applications. As a result, it is almost a common practice to keep the jacking stresses as low as 60 percent of the nominal tensile strength of *FRP* prestressing reinforcement, as shown in Table 2-1 and recommended by the Japanese proposal, "Design Concept for Concrete Members Using Continuous Fibre Reinforcing Materials" (JSCE 1992). It is advantageous to use *FRP* for partial prestressing to reduce the cost and increase the ductility of the prestressed members, especially since preliminary investigations showed that the fatigue strength of carbon *FRP* is much better than that of steel. This approach imposes a demand for good predictive ability of deflection and crack width for partially prestressed beams at service loading conditions.

Since the elastic modulus of *FRP* prestressing reinforcement is generally lower than that of steel, the deformations of members prestressed by *FRP*, after initiation of cracks, are expected to be greater than those of similar members prestressed by steel strands. In

the case of using *FRP* for stirrups, the shear deformation of the member may also become significant. Yet there is very little information in the literature to predict the deflection of beams partially prestressed by *FRP* reinforcement.

FRP prestressing reinforcement is non-corroding; however, large cracks are not aesthetically desirable. An appropriate allowable crack width will be selected according to the type of structure to achieve an acceptable appearance. In general, the allowable crack width may be taken between 0.3 and 0.5 mm (JSCE 1992). The width and spacing of flexural cracks are directly influenced by the bond properties of the reinforcing materials. Bond characteristics should be considered individually for each type of *FRP* prestressing reinforcement due to the wide variation of shapes and surface configurations such as strand, bars, braided, sand-adhered, grid, etc. Calculation of the flexural crack width may be done by selecting the proper constants for bond.

4.4.1 Deflection Prediction

Mutsuyoshi et al. (1990) reported testing of ten beams reinforced and prestressed by CFCC, which were described previously in chapter 3. The moment-curvature relationship of the bonded reinforced concrete beams was predicted using the strain compatibility approach without accounting for tension stiffening. The predicted behaviour was in good agreement with the experimental; however, the predicted curvature after cracking was overestimated.

Benmokrane et al. tested beams 3.3 m long having two different cross-sections, 200x300 and 200x550 mm reinforced by glass *FRP*. Based on the observed deflection of the beams, a modified expression for the effective moment of inertia of a simply supported beam was developed as given by equation 4-37.

$$I_e = \alpha I_{cr} + \left(\frac{I_g}{\beta} - \alpha I_{cr} \right) \left(\frac{M_{cr}}{M_s} \right)^3 \quad 4-37$$

The constants α and β were evaluated for the glass *FRP* reinforcement and found to be 0.84 and 7, respectively.

Gangarao and Faza (1991) tested concrete beams reinforced by glass *FRP* and evaluated the deflection at mid-span using the effective moment of inertia (I_e) method. They reported that, due to the nature of the crack pattern and the height of the neutral axis, which is very small for *FRP* reinforced concrete beams, the deflection should be calculated using different moments of inertia along the beam length. They suggested that the cracked moment of inertia (I_{cr}) be considered at the middle third for three-point loadings and the effective moment of inertia (I_e) for the end sections. For a beam subjected to a uniformly distributed load, the deflection is calculated using I_{cr} in the middle half of the beam and I_e in the end quarters. If the beam is subjected to a single concentrated load at the mid-span, I_{cr} is used in the middle third of the span and I_e in the end thirds.

Currier, Dolan and O'Neil (1995) reported testing nine beams prestressed by different types of *FRP* reinforcement, namely CFCC carbon fibre, FiBRA aramid fibre and Lightline E-glass, and three more beams prestressed by steel strands. The beams were 254 mm high and 5.49 m long. The deflections of the beams were monitored for a period of one year. Two beams of each group were subjected to uniform dead load producing tensile stresses at the bottom of the beams and the remaining beams carried self-weight only. The observed long-term deflections of the beams prestressed by *FRP* were less than those of beams prestressed by steel. The initial results indicated that current methods for determining long-term deflections, such as the multiplier method reported in the PCI Design Handbook and Branson's equation, under-predict the deflections of members prestressed by *FRP* tendons.

4.4.2 Crack Width Prediction

Nakai et al. (1993) tested five pretensioned concrete T-beams of 500 mm total thickness and 3-m span. Four beams were prestressed by aramid *FRP* and one beam was prestressed by carbon *FRP*. Equation 4-38, which is based on the JSCE (Japanese Society of Civil Engineering) standard specifications, was used to predict the crack width of the tested beams.

$$w = k [4 d_c + 0.7 (s - d_b)] \frac{f_s}{E_s} \quad 4-38$$

where k = factor depends on the bond properties;

d_b = bar diameter; and

c = concrete cover measured from the surface of the reinforcement.

The ratio of the measured to the predicted crack width was about 0.75 and 0.5 for beams prestressed by carbon and aramid *FRP*, respectively.

Tadashi et al. (1993) reported the testing of six concrete beams reinforced and prestressed by braided aramid *FRP* rods. Four beams were of a rectangular cross section, 3.6 m long and 300 mm deep. The other two beams were of T cross-section, 800 mm deep and 10 m long. The full-scale beams were reinforced for shear using spiral aramid *FRP* reinforcement. The beams were subjected to sustained loads ranging from $0.67 P_{cr}$ to $1.5 P_{cr}$ for up to 10,000 hours. The crack width was calculated based on equation 4-39, according to the CEB-FIP Model Code 1990.

$$w_m = l_{av} (\epsilon_{s2} - \beta \epsilon_{sr2} - \epsilon_{sh}) \quad 4-39$$

and

$$l_{av} = 2 (c + 0.1 s) + \frac{0.1 d_b}{\rho_e} \quad \text{for steel} \quad 4-40$$

$$l_{av} = 2 (c + 0.1 s) + \frac{0.05 d_b}{\rho_e} \quad \text{for sand adhered AFRP} \quad 4-41$$

where l_{av} = average spacing between cracks;

β = 0.38 for long term loading;

ϵ_{sr2} = strain of reinforcement at cracking load, based on cracked section properties;

ϵ_{sh} = concrete shrinkage; and

$\rho_e = A_s / A_{cef}$.

Equation 4-40, which calculates the average spacing between cracks for beams with steel, was modified to equation 4-41 for sand-adhered braided aramid *FRP* rods by changing the bond coefficient from 0.1 to 0.05. The reduction in the bond coefficient indicates that the bond properties of the sand-adhered braided aramid *FRP* rods are better than those of steel. The predicted crack width was in good agreement with the measured values.

Table 4-1 Maximum allowable computed deflection recommended by ACI and CSA Code

Type of Element	Deflection to be Considered	Deflection limitation
Flat roofs not supporting or attached to non-structural elements likely to be damaged by large deflections	Immediate deflection due to the live load	$\frac{\ell^{(1)}}{180}$
Floors not supporting or attached to non-structural elements likely to be damaged by large deflections	Immediate deflection due to the live load	$\frac{\ell}{360}$
Roof or floor construction supporting or attached to non-structural elements likely to be damaged by large deflections	That part of the total deflection which occurs after attachment of the non-structural elements, the sum of the long-time deflection due to all sustained loads and the immediate deflection due to any additional live load ⁽²⁾	$\frac{\ell^{(3)}}{480}$
Roof or floor construction supporting or attached to non-structural elements not likely to be damaged by large deflections		$\frac{\ell^{(4)}}{240}$
<p>⁽¹⁾This limit is not intended to safeguard against ponding. Ponding should be checked by suitable calculations of deflection including the added deflection due to ponded water, and considering long-time effects of all sustained loads, camber, construction tolerances, and reliability of provisions for drainage.</p> <p>⁽²⁾The long-time deflection may be reduced by the amount of deflection which occurs before attachment of the non-structural elements. This amount shall be determined on the basis of accepted engineering data relating to the time-deflection characteristics of members similar to those being considered.</p> <p>⁽³⁾This limit may be exceeded if adequate measures are taken to prevent damage to supported or attached elements.</p> <p>⁽⁴⁾But not greater than the tolerance provided for the non-structural elements. This limit may be exceeded if camber is provided so that the total deflection minus the camber does not exceed the limitation.</p>		

Table 4-2 Maximum recommended crack width (CPCI Metric Design Manual).

Type of element and exposure	Maximum value of z (kN/mm)	Corresponding value of w (mm)
Critical appearance		
Exterior exposure	9	0.12
Interior exposure	18	0.24
Prestressed elements		
Exterior exposure	15	0.20
Interior exposure	20	0.27
Non-prestressed elements		
Exterior exposure	25	0.33
Interior exposure	30	0.40

Table 4-3 Recommended limits of crack width given by the CEB-FIP Code 1978.

Exposure Conditions	Load to Be Considered	Limits for Reinforcement Highly Sensitive to Corrosion [†]	Limits for Reinforcement Moderately Sensitive to Corrosion [†]
Mild Usual interior exposure Low-humidity exterior exposure	Frequent (dead load plus frequently occurring live load)	0.2 → 0.3 mm (0.008 → 0.012 in.)	0.4 → 0.6 mm (0.016 → 0.024 in.)
	Permanent (dead load plus sustained live load)	0.1 → 0.15 mm (0.004 → 0.006 in.)	need not be checked
Moderate High humidity or slightly corrosive interior exposure Running water Ordinary soil exposure Usual exterior exposure	Frequent	0.1 → 0.15 mm (0.004 → 0.006 in.)	0.2 → 0.3 mm (0.008 → 0.012 in.)
	Permanent	No tension in concrete	need not be checked
Severe Seawater exposure Slightly acidic liquids Deicing chemicals Corrosive gases Corrosive soils	Rare (dead load plus maximum possible live load)	0.1 → 0.15 mm (0.004 → 0.006 in.)	0.2 → 0.3 mm (0.008 → 0.012 in.)
	Frequent	No tension in concrete	0.1 → 0.15 mm (0.004 → 0.006 in.)

*The limits given refer to the characteristic crack widths, w_k . The lower limit is for a cover equal to the minimum required by CEB, while the upper limit is for a cover at least 1.5 times the minimum cover.

[†]Reinforcement considered to be highly sensitive to corrosion includes prestressing steel, small diameter (< 5 mm or 0.2 in.) bars or wires, and treated steels (heat treated or cold worked). Normal reinforcing bars are considered to be moderately sensitive to corrosion.

Table 4-4 Crack width calculations based on fictitious tensile stress approach

Researcher	Equation	Whether maximum or average crack width	At reinforcement level or beam soffit	Type of prestressed reinforcement	Type of non-prestressed reinforcement
Bennett and Chadrasekhar (1972)	$w = k d_c f_{ct}$ $k = 435 \times 10^{-6}$ for reinforcing bars 725×10^{-6} for strands 1160×10^{-6} for wires	Average width of 8 major cracks	Beam soffit	wires	Deformed bars, strands and wires
Meier and Gergley (1981)	$w = c_1 \epsilon_{ct} d_c$ $c_1 = 12$ for reinforcing bars $= 16$ for strands	Maximum	Beam soffit	Not specific	Deformed bars and strands
	$w = c_2 \epsilon_{ct} d_c (A)^{1/6}$ $c_2 = 0.032$ for reinforcing bars $= 0.0546$ for strands	Maximum	Beam soffit	Not specific	Deformed bars and strands
Scholz (1991)	$w = 0.00024 \frac{A_{t,ucr} f_{ct} h_2}{\sum A_s h_1}$	Maximum	Beam soffit	Not specific	Not specific

Table 4-5 Crack width Calculations based on reinforcement stress/strain approach

Researcher	Equation	Whether maximum or average crack width	At reinforcement level or beam soffit	Type of prestressed reinforcement	Type of non-prestressed reinforcement
CEB-FIP (1970)	$w = (\Delta f_s - 40) \times 10^{-3}$ for non-repetitive loads $w = \Delta f_s \times 10^{-3}$ for repetitive loads	Probabilistic crack width with 95 % chance of not being exceeded	Steel level	Not specific	Not specific
Bennett and Veerasubramanian (1972)	$w = \beta_1 + \beta_2 \epsilon_{ns} c$ $\beta_1 = 0.02, \beta_2 = 6.5$ "calculated based on crack width observed at the second cycle of loading"	Maximum	Beam soffit	Strands	Deformed bars
Hassoun and Sahebjam (1989)	$w = 1.92 c \phi h_1$	Maximum	Beam soffit	Strands	Deformed bars
Nawy (1989)	$w = k \frac{A_t}{\Sigma O} \Delta f_{ps}$ $k = 5.85 \times 10^{-5}$ (pretensioned beams) $= 6.51 \times 10^{-5}$ (post-tensioned beams) $= 6.83 \times 10^{-5}$ (Unbonded post-tensioned beams)	Maximum	Steel level	Strands	Deformed bars

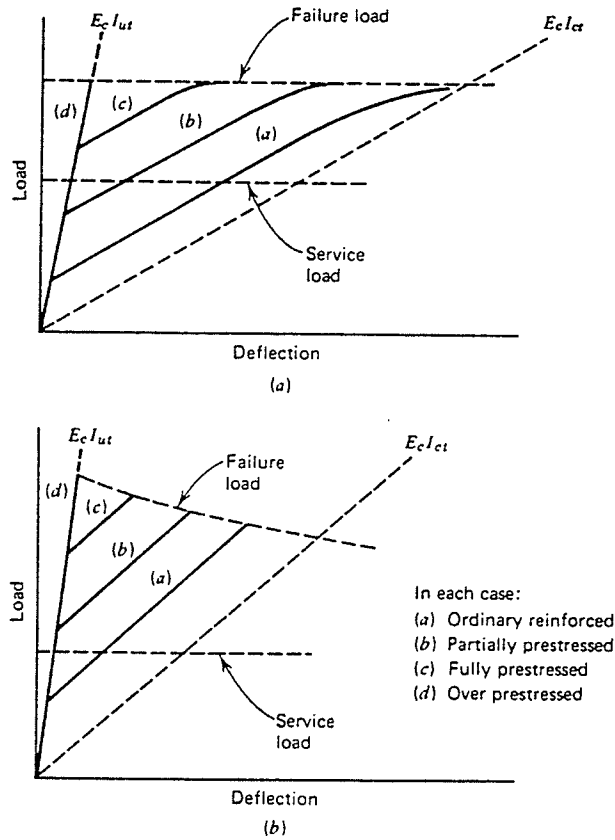


Fig.4-1 Idealized load-deflection curves for beams with varying amounts of prestress force (Nilson 1987)
 (a) under-reinforced beams (b) over-reinforced beams

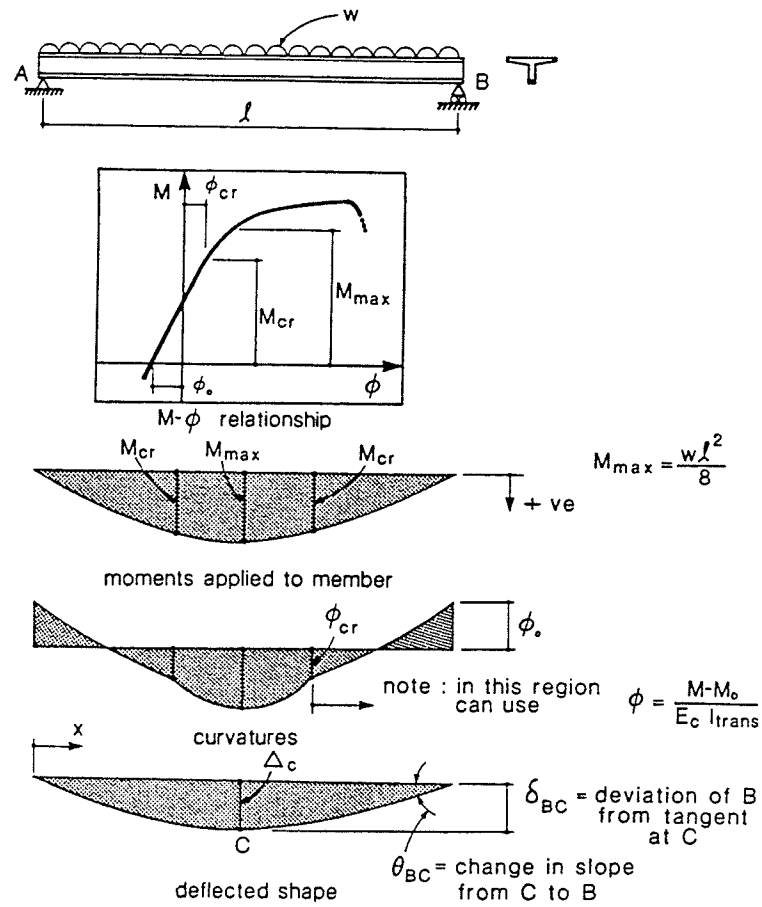


Fig.4-2 Calculating deflection from the curvature (Collins and Mitchell 1991)

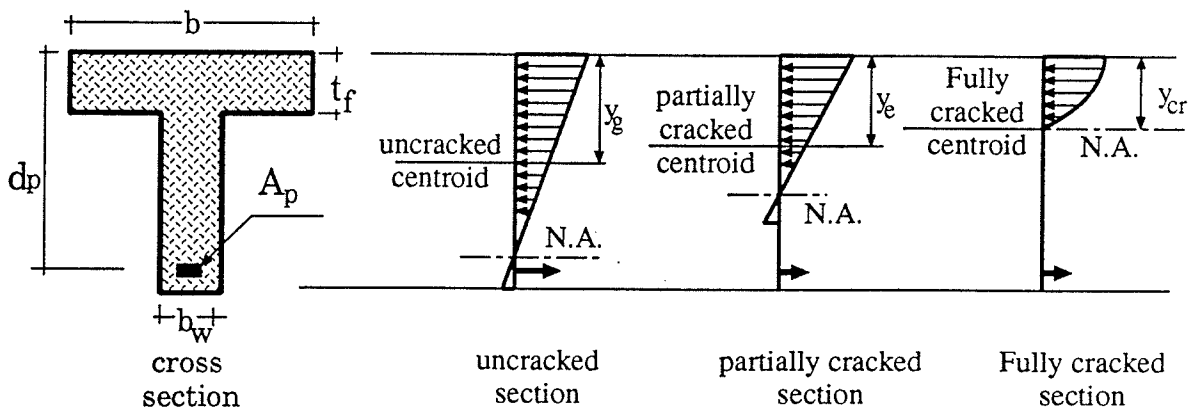


Fig.4-3 Centroidal distances for uncracked, partially cracked and fully cracked sections

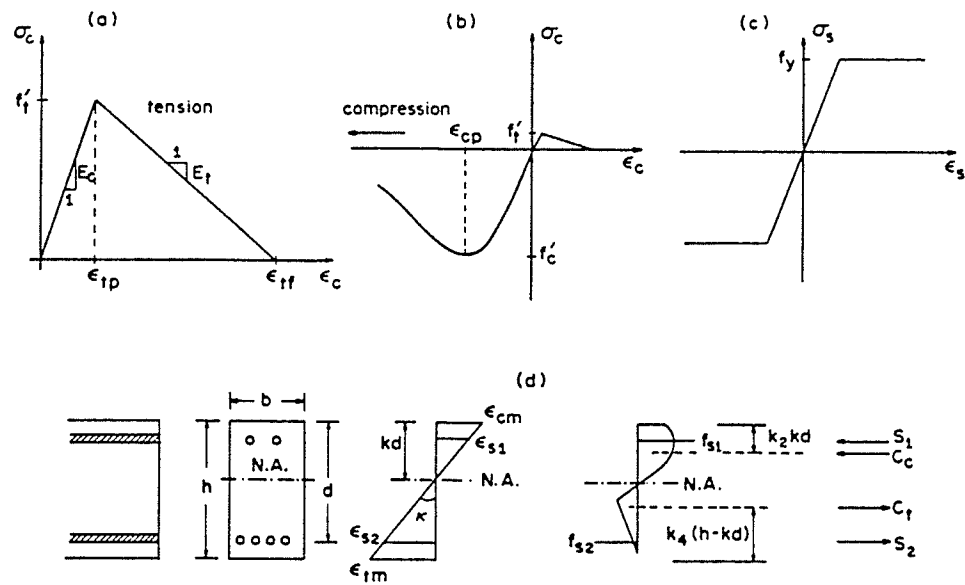


Fig.4-4 Assumed uniaxial stress-strain relations for concrete in tension and compression (a,b) and for steel (c); and stress and strain distributions in the cross section of beams (d). (Bažant and Oh 1984)

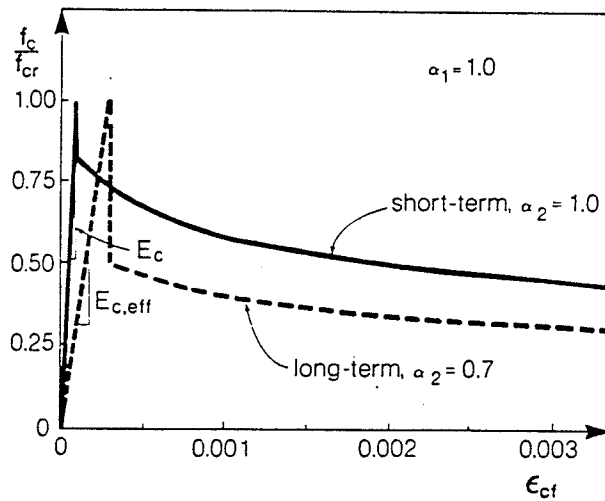


Fig.4-5 Average stress vs. average strain relationship for concrete in tension (Collins and Mitchell 1991)

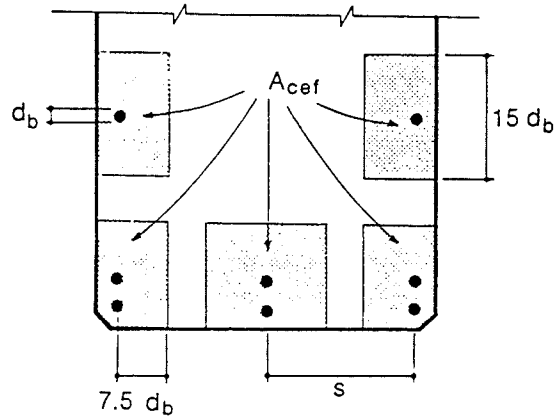


Fig.4-6 Effective embedment zone defined by the CEB-FIP Code (1978)

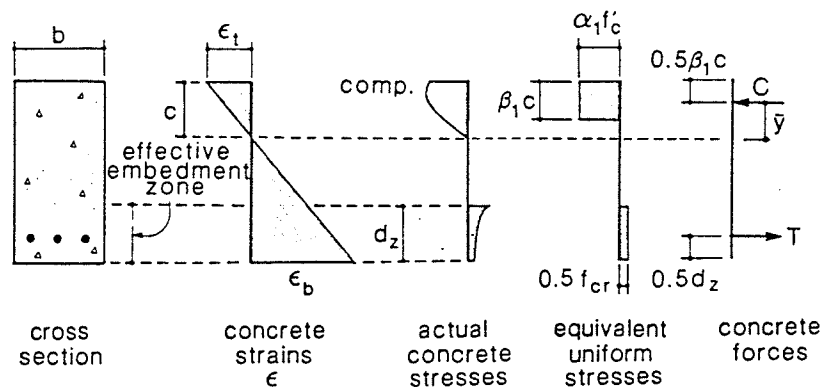


Fig.4-7 Equivalent uniform stress distribution (Collins and Mitchell 1991)

5. _____ THE EXPERIMENTAL PROGRAM

5.1 GENERAL

The experimental program was undertaken to study the flexural behaviour of prestressed and partially prestressed concrete beams with carbon fibre-reinforced-plastic (*CFRP*) prestressing bars. The serviceability limit states in terms of crack width, crack spacing and deflection prior to and after cracking were examined. The modes of failure and the ultimate carrying capacity of the beams were also investigated. The test specimens consisted of eight beams prestressed by *CFRP* bars and two additional beams prestressed by conventional steel strands. The parameters considered in this experimental program were the prestressing ratio and the degree of prestressing. Several control specimens were tested to evaluate the material properties of the concrete, *CFRP* reinforcement, and prestressing steel. This chapter presents details of jacking, testing set-up and different instrumentations used to measure the response of the beams. This chapter also presents the properties of the materials used in this study based on testing of the control specimens.

5.2 TEST SPECIMENS

Ten pretensioned prestressed concrete T-beams with a total length of 6.2 m and a depth of 330 mm were tested. The beams were simply supported with a 5.8-m span and a 200-mm projection from each end. The beams had the same span-to-depth ratio as is typically used by industry for bridge girders. The beams had a flange width varying from 200 mm to 600 mm, as shown in Fig. 5-1. Eight of the tested beams were prestressed by 8-mm Leadline *CFRP* bars produced by Mitsubishi Kasei, Japan; and two beams were prestressed by 13-mm conventional steel strands. The beams were reinforced for shear using double-legged steel stirrups, 6 mm in diameter, uniformly spaced 100 mm apart. The steel stirrups were tied to two longitudinal steel bars, 6 mm in diameter, 25 mm from the top surface of the beam. The nominal yield stress of the steel stirrups and longitudinal bars was 400 MPa. The top flange was reinforced by welded wire fabric (WWF) 102x102, MW 18.7 x MW 18.7 (CPCI Metric Design Manual 1989). The end zone of the beam was reinforced by two steel plates of 12.5-mm (1/2") thickness and two steel bars of 10 mm diameter, as shown in Fig. 5-2. The beams had an adequate factor of safety for shear and bond. The variables of the test program were as follows:

1. Degree of prestressing: two levels of jacking stresses of *CFRP* bars were used, 50 and 70 percent of the guaranteed ultimate strength of the Leadline as reported by the manufacturing company.

2. Number of Leadline bars: two and four bars were used.
3. Distribution of the Leadline bars in the tension zone: where Leadline bars were placed in two and four layers, as shown in Fig. 5-1.
4. Flange width of the beams: two widths were used, 200 mm and 600 mm.

Detailed information about the tested beams is given in Table 5-1. The designation of the beams have the first letter either T, R, or S, refers to T-section of 600-mm flange width, Rectangular section of 200-mm flange width and beams prestressed by Steel reinforcement, respectively. The first number of the beam designation is either 2 or 4, which refers to the number of prestressing bars, while the second number, .5 or .7, refers to the ratio of the jacking stress to the guaranteed ultimate strength. The last letter in the beam designation, H or V, refers to the configuration of the bars in the tension zone, either Horizontal or Vertical.

5.3 JACKING SET-UP

The casting bed and the support system used to jack two beams at the same time is shown in Fig. 5-3. The prestressed tendon consisted of two 8-mm Leadline bars, each anchored by 75-mm-long steel wedges in one anchor head, as shown in Fig. 5-4. A special system of hinges was used to ensure equal distribution of the prestressing force in each tendon, as shown in Fig. 5-5. The prestressing forces were applied using four

hydraulic screw jacks of 50-ton (500 kN) capacity each, with locking nuts to maintain the force constant after jacking. The load was applied in increments using Enerpac hydraulic air pumps. The movement of a spreader beam at the jacking end was recorded by means of linear variable differential transducers (LVDTs). After the required force was applied, the screw jacks were locked with nuts. The prestressing force in each beam was monitored by load cells of 1000-kN capacity each, and by means of strain gauges mounted on each Leadline bar. A data acquisition system of 48-channel capacity and sampling rate of 40 samples per second using a Data Scan 7000 digital card of 16-bit resolution at a range of 10 volts \pm 0.3 m.volt was used to record the readings of the of the load cells, strain gauges and LVDTs during jacking. A software "Labtech Notebook" was used to store the data at a rate of 1 sample every 2 seconds. After jacking, the readings of the strain gauges and the load cell were continuously recorded until the release of the prestressing force at a rate of 1 reading every 10 minutes. The overall jacking set-up used for prestressing is shown in Fig. 5-6.

Before the concrete was cast, the steel form was lubricated and the steel cage, including WWF, was assembled and tied in place. After jacking the Leadline bars by a time period of approximately 12 hours, the concrete was cast for the two beams at the same time. After the concrete had reached a minimum strength of 30 MPa, three to four days after casting, the prestressing forces were gently released by releasing the pressure of the four jacks gradually at both ends of the beams. The beams were taken out of the

form, using an overhead crane of 1.0-ton (10 kN) capacity, by lifting the beams at two points 500 mm from the beam ends. A hair crack was observed at the top surface of one beam, R-4-.5-H, due to the lifting process.

5.4 TESTING SCHEME

The beams were tested using two quasi-static monotonic concentrated loads, 1.0 m apart. The load was applied under stroke control with a rate of 1.0 mm/min up to the cracking load and thereafter at a rate of 2.0 mm/min up to failure. The load was cycled three times between an upper load level of 60 percent of the predicted strength of the beams, which is equivalent to 1.5 to 2 times the cracking load, depending on the prestressing level, and a lower load level of 80 percent of the cracking load of the beam, as shown in Fig. 5-7. The second and the third cycles were applied using the same rate of loading as in the initial cycle. The aim of the repeated loading at the service load limit was to study the deflection, after loss of beam stiffness due to cracking and the cracking behaviour after stabilization of cracks.

A closed-loop MTS 5000-kN (1.2 million pound) cyclic loading testing machine was used to apply the load. The range cards used for testing were 1000 kN for load and 200 mm for stroke. The beams were simply supported on rollers at each end of the beam; the rollers rested on concrete blocks anchored to the floor, as shown schematically in

Fig. 5-8. The load was applied through hollow structural sections 101.6x101.6 mm on the full width of the beam. Cement pads were used at the loading locations and at the bearings to distribute the load evenly. The beams were laterally braced at the location of the supports and 800 mm off the centre of the beams. The beams were painted white to enhance visibility of the cracks. The test set-up, including the MTS machine, is shown in Fig. 5-9.

5.5 INSTRUMENTATION

Nine electrical strain gauges produced by Showa Measuring Instruments Co. Ltd., Tokyo, Japan, of the type N11-FA-5-120-11 and a resistance of 120 ohms, were installed on the Leadline bars for each beam. Seven strain gauges were staggered in the middle zone of the beam and two strain gauges were installed at several distances close to the end of the beam to measure the transfer length of the Leadline bars. The strain gauges were glued to the smooth part on the surface of the Leadline bars using M-Bond 200. The strain gauges were covered by a waterproof coating to protect them from water and damage during the casting of the concrete. The strain gauges were permanently attached to either strain indicators or the data acquisition system to monitor the loss of the prestressing force until the day of testing.

During the test, the strain in the concrete was measured at several locations at each

increment of load. The concrete strains in the compression zone at the top surface of the beam and in the tension zone at the level of the bottom Leadline *CFRP* prestressing bars were measured using demec-point stations, as shown in Fig. 5-10. The concrete strains were measured using a dial gauge with 0.8×10^{-5} mm/mm accuracy to measure the deformation along a 200-mm gauge length. The strains, measured by the dial gauge, were recorded every 2- to 5-kN increment within the service load range followed by increments of 10 kN up to the failure load. The strain in the *CFRP* prestressing bars was monitored, within the constant moment zone, by means of the electrical strain gauges. Dial gauges were also installed at the ends of the bottom Leadline prestressing bars, to monitor any possible slip of the reinforcement.

Measurements were recorded during the test using the same data acquisition system used during prestressing at a rate of 1 sample every 2 seconds. The load and stroke of the cross-head of the machine were recorded. The deflection at midspan was monitored on both sides of the beam, using two linear variable differential transducers (LVDTs) of 125-mm stroke. The vertical movement of the supports was also monitored using two LVDTs, one at each end of the beam. The instrumentation used in the beam test is shown in Fig. 5-8.

Cracking behaviour was monitored in terms of crack pattern, height, and width. The crack width was measured within the constant moment zone at two levels, at the extreme

tension fibre of concrete for all beams, and at the level of the bottom Leadline prestressing bars, 50 mm from the bottom surface of the concrete, for four beams. A microscope of a magnification factor of 50, moving on a system of rollers, was used to measure the crack width, as shown in Fig. 5-11. The crack width measurements were taken every 2 to 5 kN in the first cycle and every 10 kN in the second and third cycles, within the service load limits.

5.6 MATERIALS

CFRP reinforcement is characterized by having the highest tensile elastic modulus, compared to other commercially available *FRP* tendons; however, it has the smallest ultimate tensile strain. *CFRP* reinforcement, in general, is characterized by excellent fatigue characteristics and low relaxation. The axial coefficient of thermal expansion of *CFRP* reinforcement is practically zero (Mufti et al. 1991). The characteristics of the *CFRP* and other materials used in this study are discussed in the following sections.

5.6.1 Leadline

CFRP Leadline bars, having an indented shape and 8-mm nominal diameter, were used in this investigation to pretension the concrete beams. The Leadline bars are produced by Mitsubishi Kasei, Japan. The Leadline bar is pultruded using linearly

oriented Dialead coal-tar-pitch-based continuous fibre and epoxy resin. The actual diameter of the Leadline bar is 7.8 mm with an area of 47.3 mm², according to the manufacturer. The characteristics of the Leadline bars in terms of bond, fatigue, linear density and coefficient of thermal expansion are reported in chapter 2. Steel wedges were used to anchor two Leadline bars in one anchor head. The anchorage is 75 mm in length and 60 mm in diameter, supplied by the same company as the Leadline bars. An aluminum tube was used between the Leadline bar and the steel wedges as a soft material to reduce the transverse stresses on the Leadline bar. A plastic sleeve was used between the steel wedge and the anchorage to prevent slippage of the Leadline bar. The assembly of the Leadline anchorage is shown in Fig. 5-4.

5.6.1.1 Tensile properties

The stress-strain relationship of the Leadline is linearly elastic up to failure as reported by the manufacturing company and as proved by tension tests. Three types of anchorage of the Leadline bars were used in the tension tests. The first and the second types of anchorage were made of reinforced concrete; the third type was a steel wedge similar to those used for steel strands. Two different configurations were used for the concrete anchorage.

The first configuration of the concrete anchorage had a cross-section of 150x150 mm

and a length of 1200 mm, as shown in Fig. 5-12. The concrete anchorage was reinforced by a 4-mm steel spiral of 100-mm diameter and 25-mm pitch. The steel spiral was used to confine the concrete along the length of the concrete anchorage to increase the bond strength and to prevent slippage. The assembly was tested horizontally as shown in Fig. 5-12. Two hydraulic jacks of 50-ton (500 kN) capacity were used to apply the load. The jacks were fixed to a steel abutment and pushed against two movable channels. Two LVDTs were used to monitor the distance between the fixed abutment and the movable channels to make sure that the channels and the concrete blocks were always perpendicular to the Leadline bar, as shown in Fig. 5-13. The loading rate was 10 kN per minute. Two strain gauges, one on each side of the Leadline bar, were used to measure the strain up to failure. The failure of the Leadline bar occurred typically at the face of the concrete block; however, no slip was observed. The average tensile stress and strain at ultimate of three tests were 2950 MPa and 1.56 percent, respectively. The average tensile elastic modulus of the Leadline bars, based on linear regression analysis up to failure, was 187 GPa. A typical stress-strain diagram for the Leadline bar using the concrete block anchorage is shown in Fig. 5-14. The stress-strain relationship of the Leadline is linear up to 1000 MPa with an average elastic modulus of 170 GPa and linear up to failure with an elastic modulus of 190 GPa. This bilinear behaviour could be due to misalignment of some carbon fibres with respect to the longitudinal direction of the bars. Those fibres may be stretched at a higher load level resulting in an increase in the elastic modulus.

The second configuration of concrete anchorage is shown schematically in Fig. 5-15. The difference between the two configurations was that, in the second configuration, the Leadline bar was bonded to the concrete along the entire length, as shown in Fig. 5-16. The maximum observed tensile strength of the Leadline was also 2950 MPa, based on one test. Failure occurred by rupture of the Leadline bar and no bond slip was observed during the test.

The third type of anchorage was the steel wedge type which was used for a single Leadline bar. The same assembly of aluminum tube and plastic wedge used for the anchorage of two Leadline bars was used for the anchorage of one Leadline bar. The tests were conducted and reported by Mitsubishi Kasei company and verified by tests conducted at the University of Manitoba, using the same type of anchorage. The average tensile stress and strain at ultimate, as reported by the manufacturer, were 2250 MPa and 1.3 percent respectively. The company guarantees ultimate tensile strength and elastic modulus of 1970 MPa and 147 GPa, respectively. The results also showed a bi-linear behaviour of the Leadline bars. Table 5-2 shows the results of the tension tests of 8-mm Leadline bars using the three anchorage configurations.

5.6.1.2 Transfer Length

The transfer length is defined as the length required to transfer the full prestressing force to the concrete. The transfer length of the 8-mm Leadline bars was estimated by measuring the strain change in the bars at the ends of the beams before and after release of the prestressing force. After transfer of the prestressing force, the strain at the free end of the bars at the end of the beam is zero and increases gradually within the transfer length until it reaches a constant value along the beam. The strain in the Leadline was measured using strain gauges mounted on the Leadline bars close to the end of the beams. The data were collected from different beams which had the same jacking stress. The Leadline bars were jacked to 980 MPa for six beams, which is 50 percent of the guaranteed strength, and 1380 MPa for two beams, which is 70 percent of the guaranteed strength. When the concrete strength was between 37 and 50 MPa, the force in the Leadline bars was released gently by releasing the pressure of the jacks. The percentage of the strain of the Leadline bars after release, compared to the strain before release, for the different beams, is shown in Fig. 5-17. The loss in the Leadline strain at the midspan of the beams represents the loss due to elastic shortening. A linear regression analysis was carried out for the data collected at the end of the beams and for the data collected at the midspan of the beams. The intersection of the two regression lines represents the transfer length. The transfer length was estimated to be 360 mm (46 bar diameters) when the stress after release was 950 MPa, and 500 mm (64 bar diameters)

when the stress after release was 1310 MPa. The transfer bond strength in the transfer zone was calculated at the two levels of stress, 50 and 70 percent of the guaranteed strength, and was found to be equal to 5.15 and 5.12 MPa, respectively.

For the same levels of stress, 950 and 1310 MPa, the transfer lengths for steel strands are estimated, according to the ACI and CSA Codes, to be 46 and 63 times the diameter of the strand, respectively. The bond strength of steel strands in the transfer zone was reported to be 5.21 MPa (Collins and Mitchell 1991). The ACI and CSA codes also report an average value of the transfer length of steel strands and steel wires as 50 and 100 times the diameter, respectively. The CEB-FIP Code, on the other hand, suggests that transfer lengths may vary between 45 and 90 times the diameter for strands and between 100 and 140 times the diameter for individual wires. The transfer lengths of the Leadline bars are thus comparable to those of steel strands and much smaller than those of steel wires. Also, the bond strength of the Leadline bars in the transfer zone is comparable to that of steel strands and higher than that of steel wires. This conclusion may be attributed to the lower elastic modulus of the Leadline which permits more longitudinal deformation and consequently more transverse deformation than in steel for the same stress level, as Poisson's ratio is approximately the same for Leadline and steel. The wedging action created by the greater lateral expansion of the bar improves the bond strength in the transfer zone; this is known as Hoyer effect.

5.6.1.3 Flexural Bond Strength

The flexural bond strength of 8-mm Leadline bar was compared to that of 13-mm steel strand by testing four reinforced concrete beams, two of them of 800-mm span and two of 1200-mm span. Two beams, one of each span, were reinforced by Leadline and the other two reinforced by steel. The rectangular cross-section of the beams was 120 mm wide and 150 mm deep. The beams were reinforced by 6-mm steel stirrups every 60 mm. The beams were simply supported with a 50-mm projection from each end. The beams were loaded by a single concentrated load at the midspan, using 266-kN universal testing machine. The load and the slip of the reinforcement were recorded during the test. The slip was measured by dial gauges having 1/1000 of an inch accuracy, mounted on the reinforcement at the beam ends.

The two beams reinforced by Leadline and the 800-mm-span beam reinforced by steel failed in bond, as shown in Fig. 5-18, while the 1200-mm-span beam reinforced by steel failed by crushing of the concrete at the top surface. The bond stresses in the Leadline and steel were calculated using plane-section analysis and are compared for the two 800-mm-span beams in Fig. 5-19. The average value of the flexural bond stress for the Leadline at first slip, based on results of the two beams, was 5.0 MPa compared to 5.9 MPa for the steel strand. The bond stress of the steel strands was calculated based on the nominal circumference of the strand (πd_b), where d_b is the nominal diameter of

the prestressing strand. These results suggest that the flexural bond strength of Leadline is less than that of steel strand. This can be attributed to the shape of the seven-wire steel strand which may cause an increase in the bond strength due to mechanical interlocking. It can be also attributed to the lower elastic modulus of the Leadline which causes more longitudinal deformation and consequently more transverse deformation than in steel at the same stress level, as Poisson's ratios of Leadline and steel are similar and approximately equal to 0.3. The higher transverse deformations, which result in reduction of the cross-sectional diameter, could cause a reduction of the bond strength due to friction.

5.6.2 Concrete

Concrete was provided by a local supplier and cast 12 hours after jacking. The concrete had a 14-mm maximum aggregate size and a 200-mm slump. The water/cement ratio was about 0.37 and the cement content was 400 kg/m³. The mix proportion by weight was 1 (portland cement) : 2.9 (coarse aggregate) : 1.7 (fine aggregate). Rheobuilt 1000 superplasticizer at 3 litre/m³ was used to increase the concrete workability. The target compressive strength of the concrete was 30 MPa after 3 days. Twelve concrete cylinders were cast from each batch. Six cylinders were tested in compression, three before release of the prestressing force and three on the day of testing, according to ASTM C39-86. The elastic modulus of the concrete was also evaluated on the day of

testing according to ASTM C469-87a using three concrete cylinders. The average compressive strength of the concrete cylinders ranged between 37 and 50 MPa at the time of release and 47 and 70 MPa at the time of testing. The average elastic modulus ranged from 29 to 38.5 GPa. Table 5-3 shows the properties of the concrete for the tested beams.

5.6.2.1 Tensile strength

The tensile strength of the concrete was measured using the splitting test for three concrete cylinders on the day of testing and from a plain-concrete beam test according to ASTM C496-90 and ASTM C78-84, respectively. The average tensile strength, based on the split-cylinder test, ranged from 3.2 MPa to 4.3 MPa, while it ranged between 5.1 MPa and 7.5 MPa based on the plain-concrete beam test. This indicates that the tensile strength of the concrete measured using the split-cylinder test is about 50 to 80 percent of the tensile strength based on the beam test. These results agree with the values given by Park and Paulay (1975), where they indicated that the split-cylinder tensile strength ranges from 50 to 75 percent of the modulus of rupture.

5.6.3 Steel

The tensile properties of the prestressing steel strands were evaluated based on

tension test of 13-mm-diameter steel strand using conventional steel wedge anchorages. The tensile strength and modulus were 1900 MPa and 180 GPa, respectively. The strain in the steel strand was measured using an LVDT of 300-mm gauge length. The modified Ramberg-Osgood function (Mattock 1979, cited in Collins and Mitchell 1991) for the tested steel strand is given by equation 5-1.

$$f_p = 180,000 \varepsilon_p \left[0.03 + \frac{0.97}{\left(1 + (102 \varepsilon_p)^{10} \right)^{0.1}} \right] \leq f_{pu} \quad 5-1$$

where f_p = stress in the steel strand;
 ε_p = strain the steel strand; and
 f_{pu} = ultimate stress in the steel strand.

5.7 PRESTRESSING LOSSES

The jacking forces were measured for each beam individually using a load cell as previously described. The loss of the prestressing forces was calculated based on the strain loss in the Leadline bars, measured by strain gauges mounted on each Leadline bar, using equation 5-2. The effective prestressing forces in the tested beams were calculated based on the loss of the prestressing forces on the day of testing, as given by equation 5-3. For the beams prestressed by steel, the loss of the prestressing force was predicted according to the CSA Code using computer software CONCISE (Computer

Analysis and Design for Precast Prestressed Concrete) developed by the Canadian Prestressed Concrete Institute (CPCI) since no strain gauges were used for the steel strands.

$$l = \frac{\epsilon_i - \epsilon_e}{\epsilon_i} P_i \quad 5-2$$

$$P_e = P_i - l \quad 5-3$$

- where
- l = loss in the prestressing force;
 - ϵ_i = average of the initial strains in the Leadline bars;
 - ϵ_e = average of the Leadline strains on the day of testing;
 - P_i = initial prestressing force; and
 - P_e = effective prestressing force on the day of testing.

The jacking and effective prestressing forces and the prestress losses are given in Table 5-4. The prestress losses of the beams prestressed by Leadline bars ranged between 8.0 and 17.8 percent except for beam R-4-.5-H, where the loss of the prestressing force was 25.5 percent due to the occurrence of one crack at the top surface of the beam while lifting the beam out of the form.

Table 5-1 Test program

Beam No.	Flange width	Beam Designation	Type of prestressing Tendons	No. of prestressing Tendons	$\rho_p = \frac{A_p}{bd}$ (%)	Jacking stress to Guaranteed strength (%)
1	600	T-4-.5-H	Leadline	4-D-8	0.12	50
2	600	T-4-.5-V		4-D-8	0.13	50
3	600	T-2-.5-V		2-D-8	0.06	50
4	600	T-4-.7-V		4-D-8	0.13	70
5	600	S-T-2-.5	Steel	2-D-13	0.13	50
6	200	R-4-.5-H	Leadline	4-D-8	0.37	50
7	200	R-4-.5-V		4-D-8	0.39	50
8	200	R-2-.5-V		2-D-8	0.18	50
9	200	R-4-.7-V		4-D-8	0.39	70
10	200	S-R-2-.5	Steel	2-D-13	0.39	50

Table 5-2 Tensile properties of Leadline

Anchorage Type	Ultimate stress (MPa)		Ultimate strain (%)		Elastic modulus (GPa)	
	Mean	σ_n	Mean	σ_n	Mean	σ_n
1- concrete block (first configuration)	2950	24.3	1.56	0.04	187	6.1
2- concrete block (second configuration)	2950	n/a *	n/a	n/a	185	n/a
3- steel wedge type, (reported by the manufacturer)	1970 (guaranteed)		n/a	n/a	147	n/a
	2250 (mean)		1.3	n/a	147	n/a
	(tested at U of M)	2280	223	1.29	0.12	177

* not available

Table 5-3 Concrete properties

Type of test		Beams T&R-4-.5-H	Beams T&R-4-.5-V	Beams T&R-4-.7	Beams T&R-2-.5	Beams S-T&R-2-.5
Compression at release	Mean	37	50	50	54	52
	σ_n^*	0.7	1.6	0.9	1.0	0.8
Compression at testing	Mean	47	61	64	70	67
	σ_n	2.7	2.7	3.5	3.3	1.2
Elastic modulus	Mean	29,040	33,770	36,850	38,480	37,950
	σ_n	2960	n/a [†]	n/a	n/a	1300
Tensile strength (Splitting)	Mean	3.2	4.3	4.0	3.8	3.5
	σ_n	0.16	0.35	n/a	0.2	0.25
Tensile strength (beam test)	Mean	n/a	5.1	7.5	5.2	6.2
	σ_n	n/a	0.08	n/a	n/a	0.61

* σ_n is the standard deviation

† not available

Table 5-4 Prestressing forces in the tested beams

Beam	Jacking force, P_j (kN)	effective prestressing force, P_e (kN)	Prestress loss (%)
T-4-.5-H	185.1	155.6*	16.0
R-4-.5-H	185.9	138.5*	25.5 [†]
T-4-.5-V	186.7	153.4*	17.8
R-4-.5-V	185.1	160.6*	13.3
T-4-.7-V	257.6	236.9*	8.0
R-4-.7-V	257.1	224.6*	12.6
T-2-.5-V	93.0	80.50*	13.5
R-2-.5-V	92.7	83.53*	9.9
S-T-2-.5	188.5	156.5 [‡]	17.0
S-R-2-.5	188.9	157.4 [‡]	16.6

* based on measured strains

† cracked at the tension zone during lifting process

‡ based on calculation of the losses

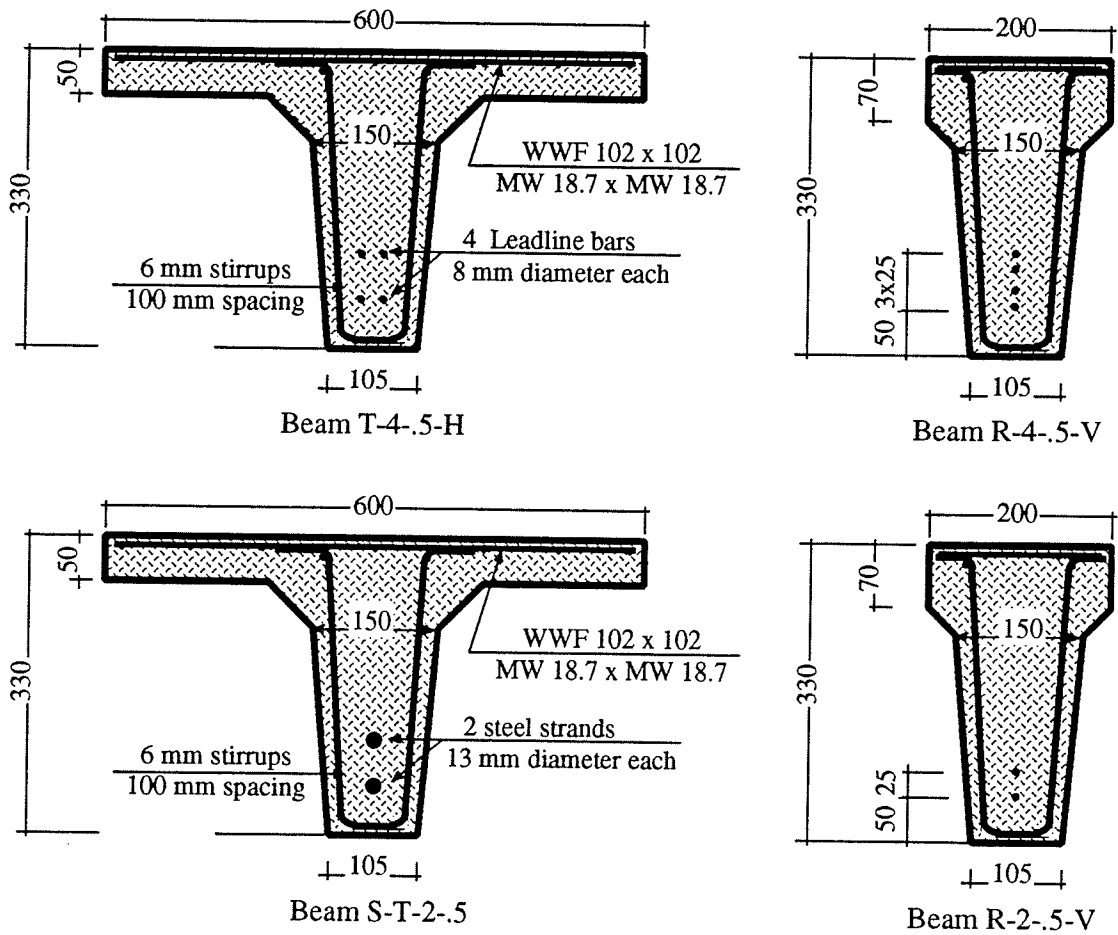


Fig.5-1 Cross sections of the tested beams

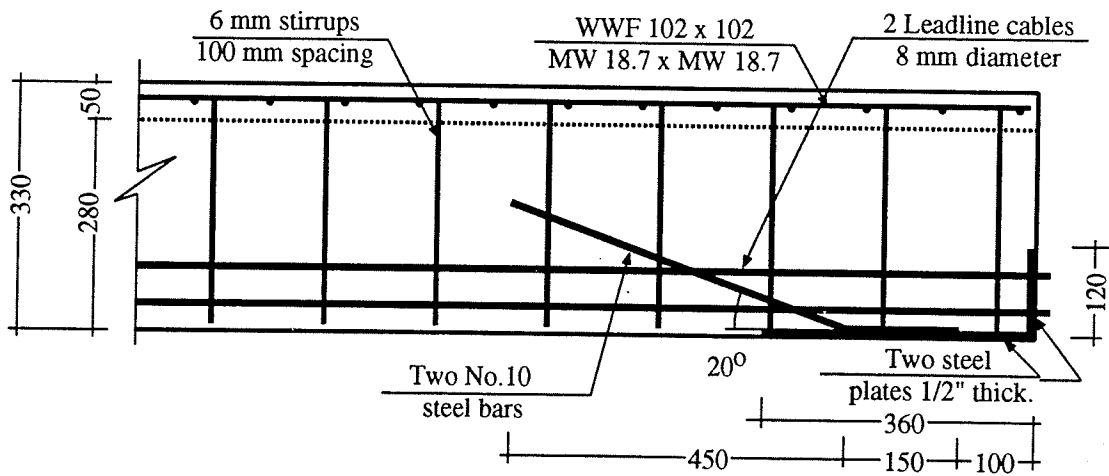


Fig.5-2 Details of the end zone of the beam

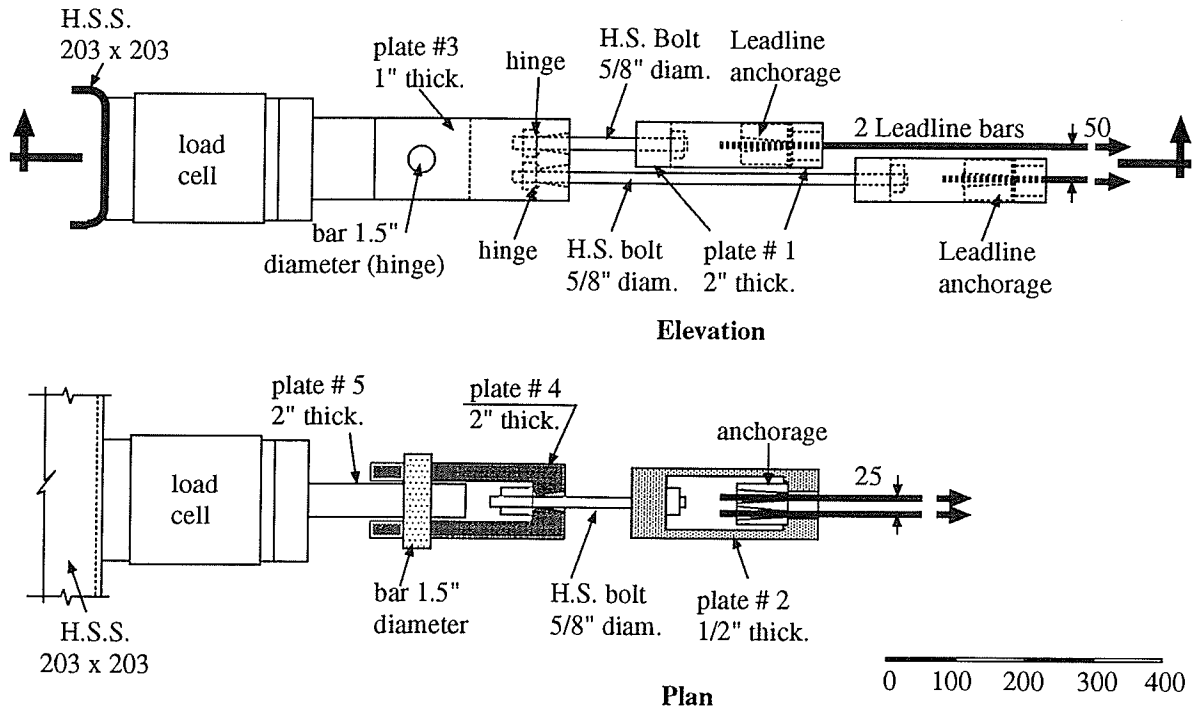


Fig.5-5 Details of the hinge system

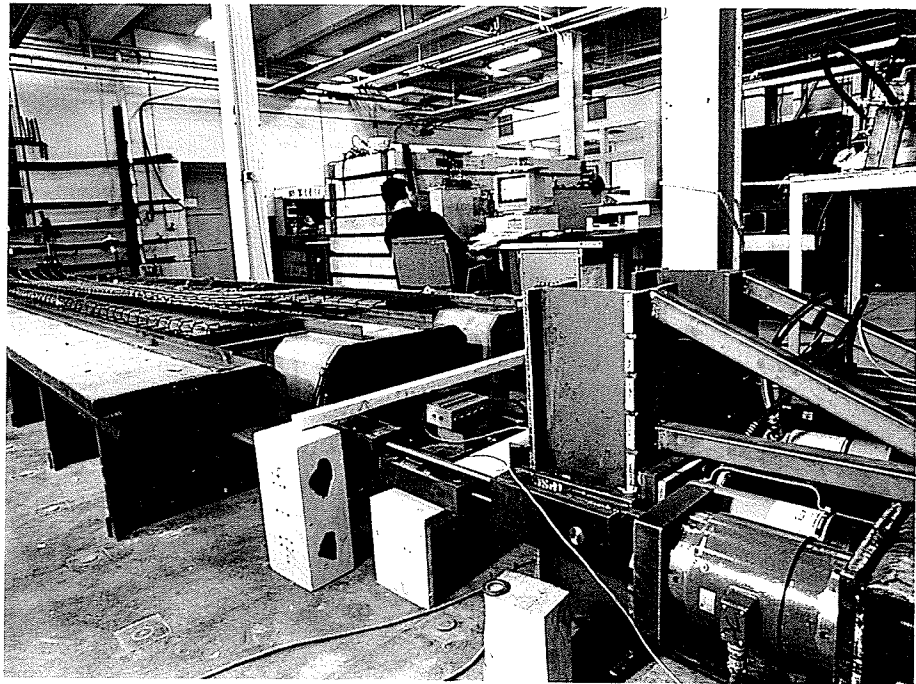


Fig.5-6 jacking set-up

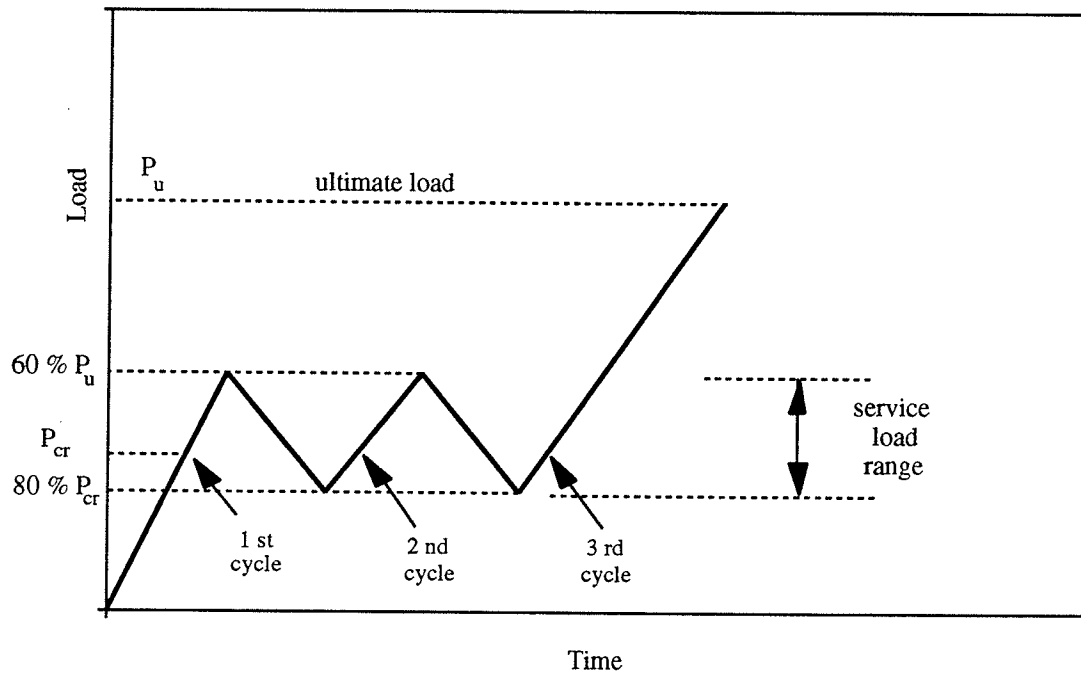


Fig.5-7 Load history

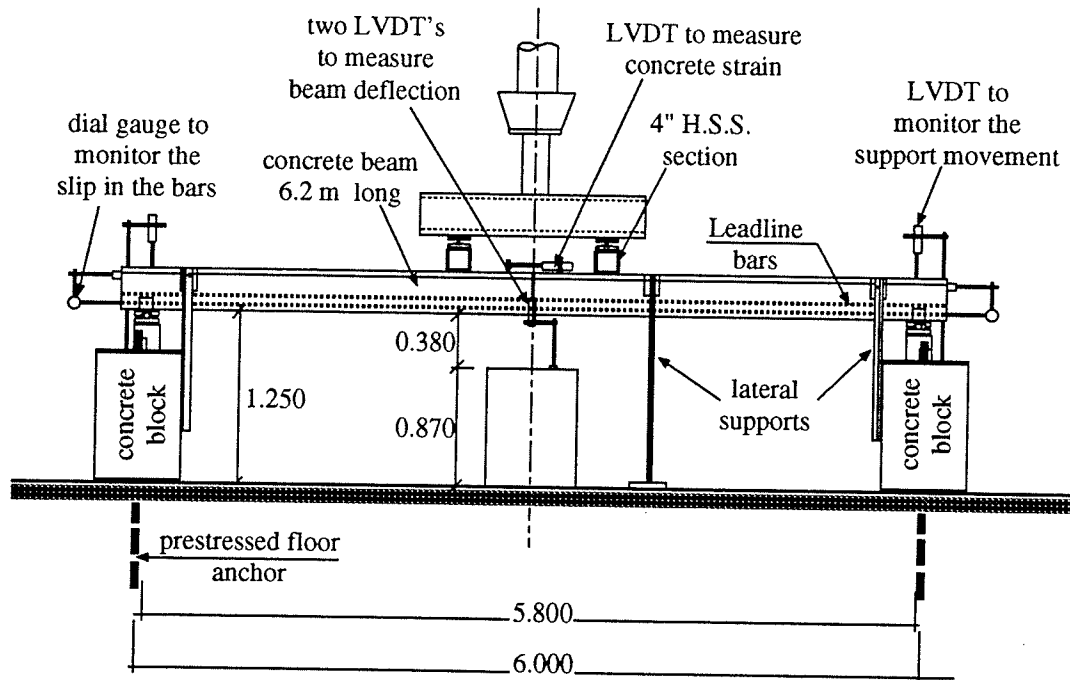


Fig.5-8 Schematic of the test set-up

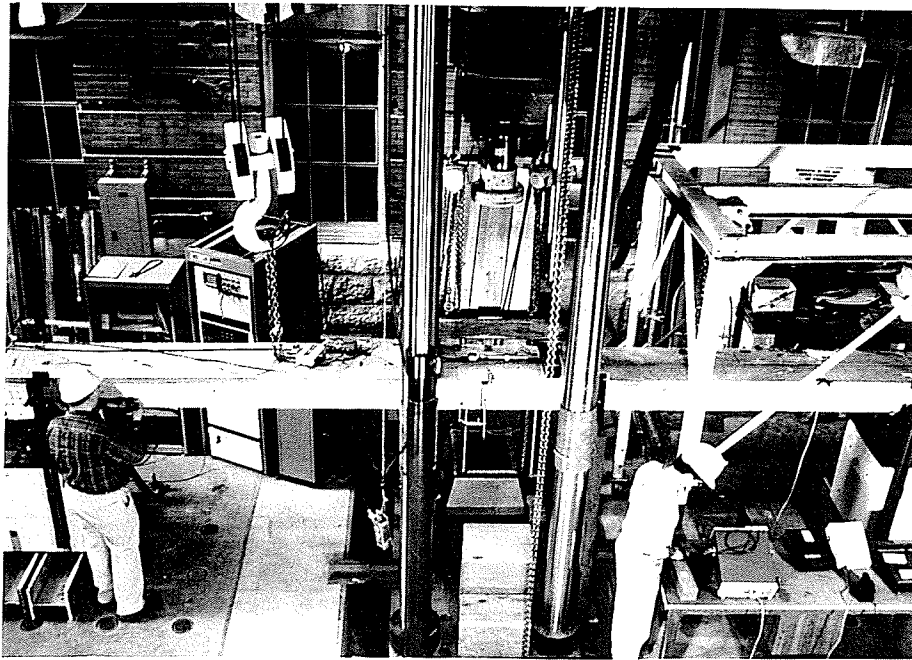


Fig.5-9 Test set-up

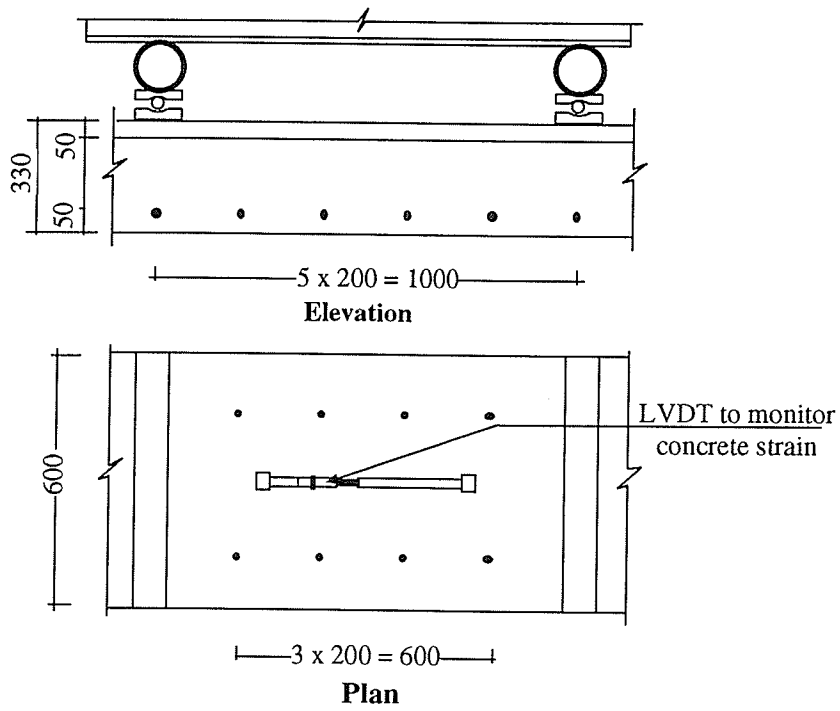


Fig.5-10 Location of the demec point stations

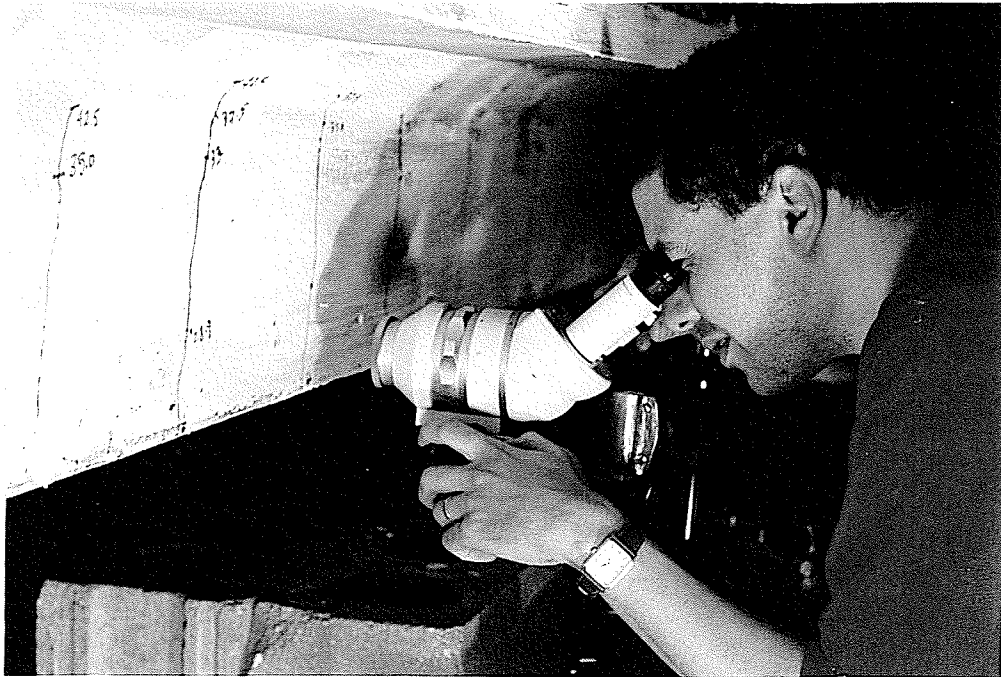


Fig.5-11 Microscope for measuring the crack width

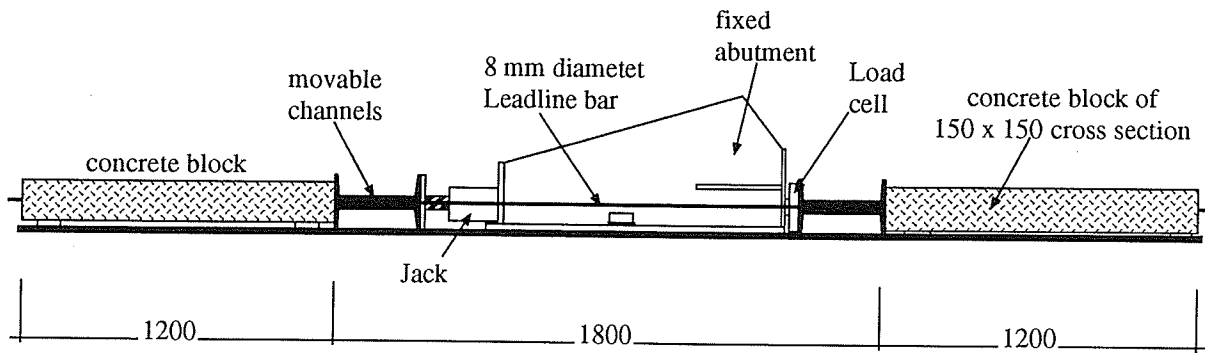


Fig.5-12 Schematic of the tension test of the Leadline using concrete anchorage (configuration #1)

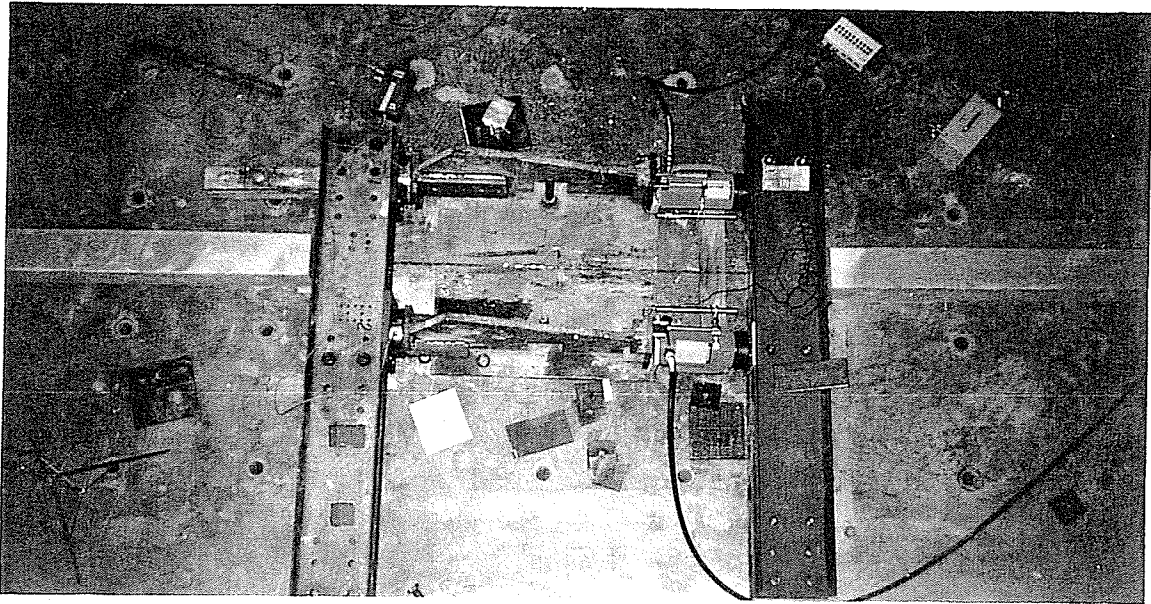


Fig.5-13 Tension test of the Leadline bar using concrete anchorage (configuration #1)

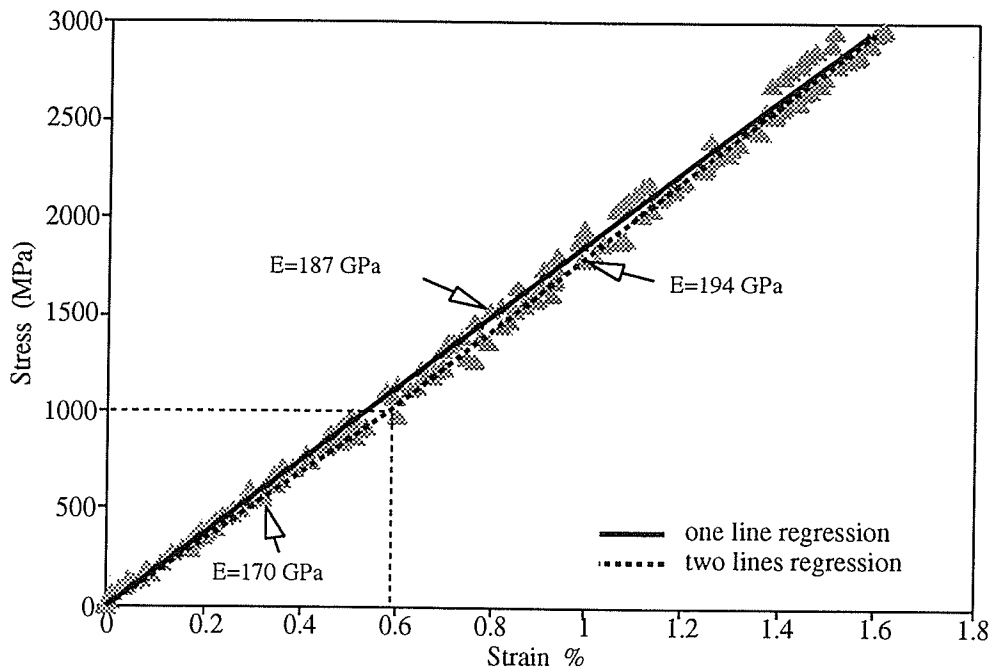


Fig.5-14 Stress-strain relationship of the Leadline bar

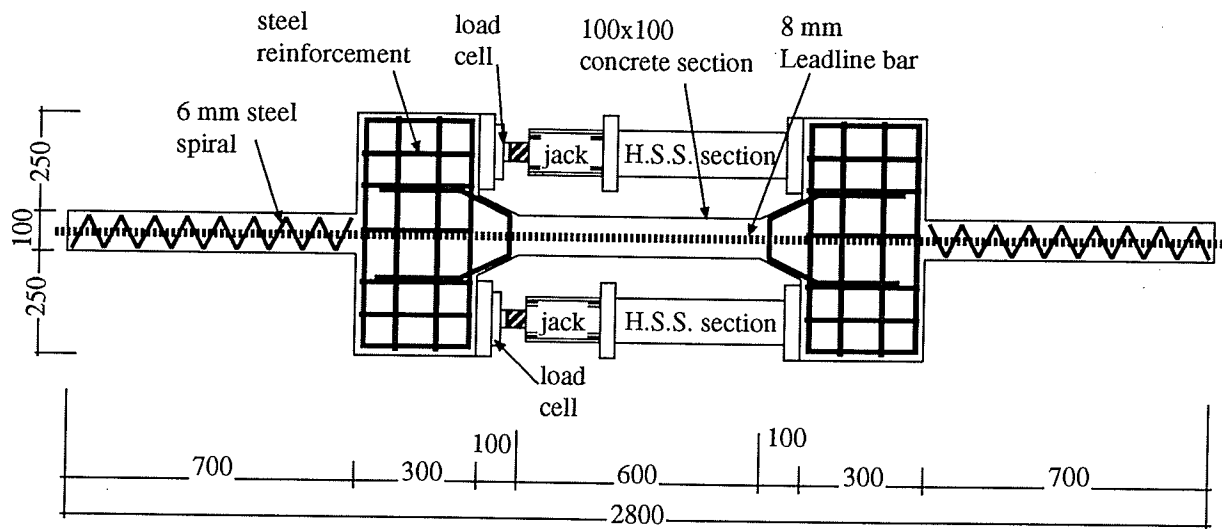


Fig.5-15 Schematic of the tension test of the Leadline using concrete anchorage (configuration #2)

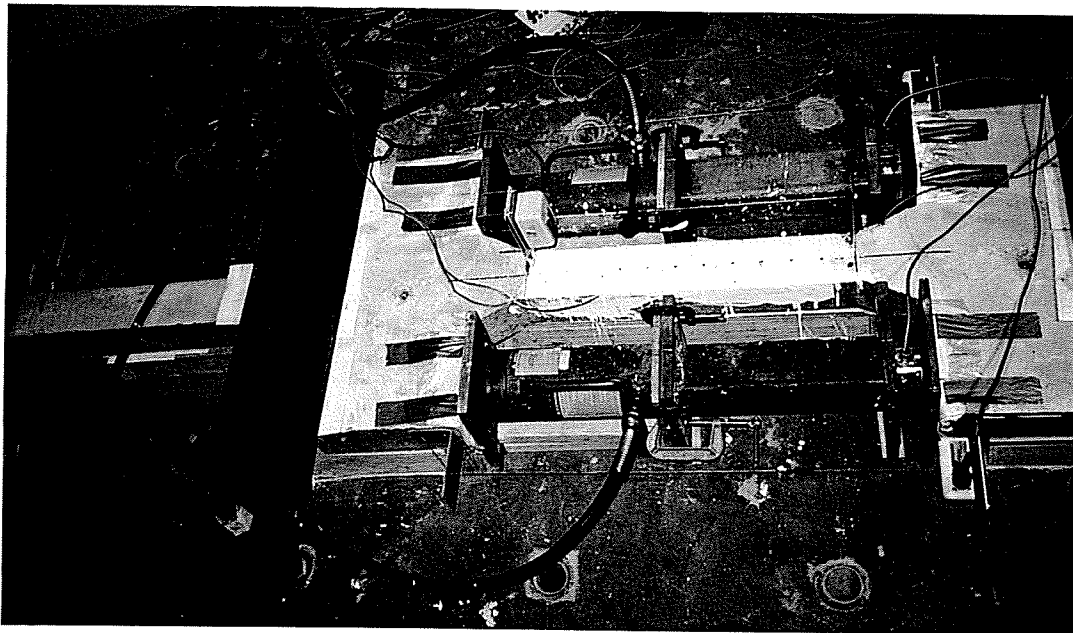


Fig.5-16 Tension test of the Leadline bar using concrete anchorage (configuration #2)

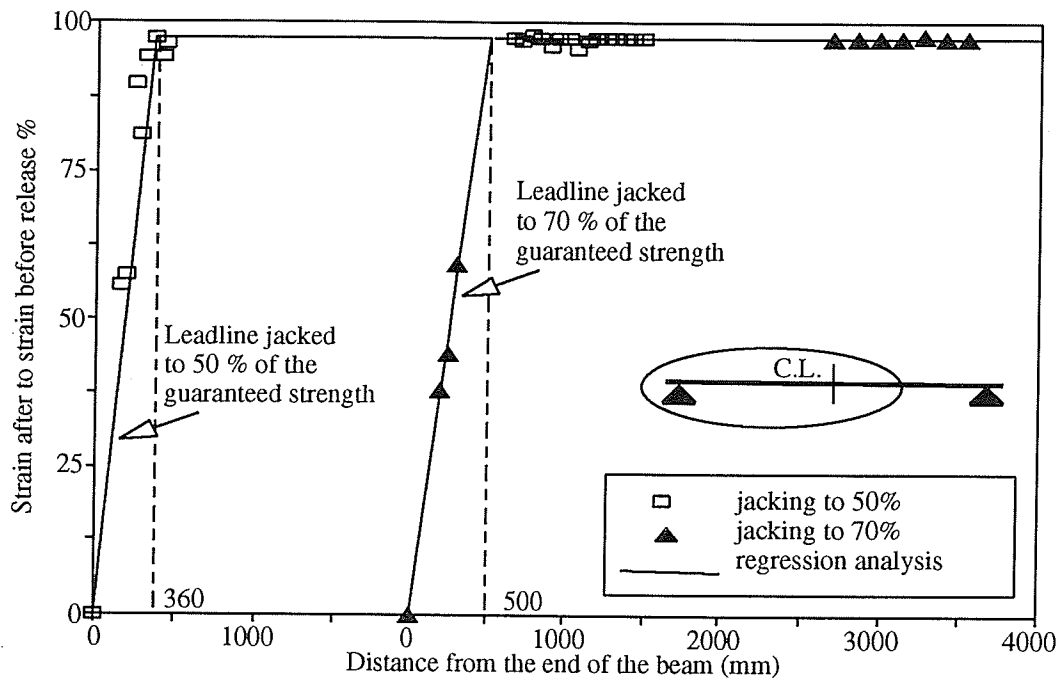


Fig.5-17 Transfer length of Leadline

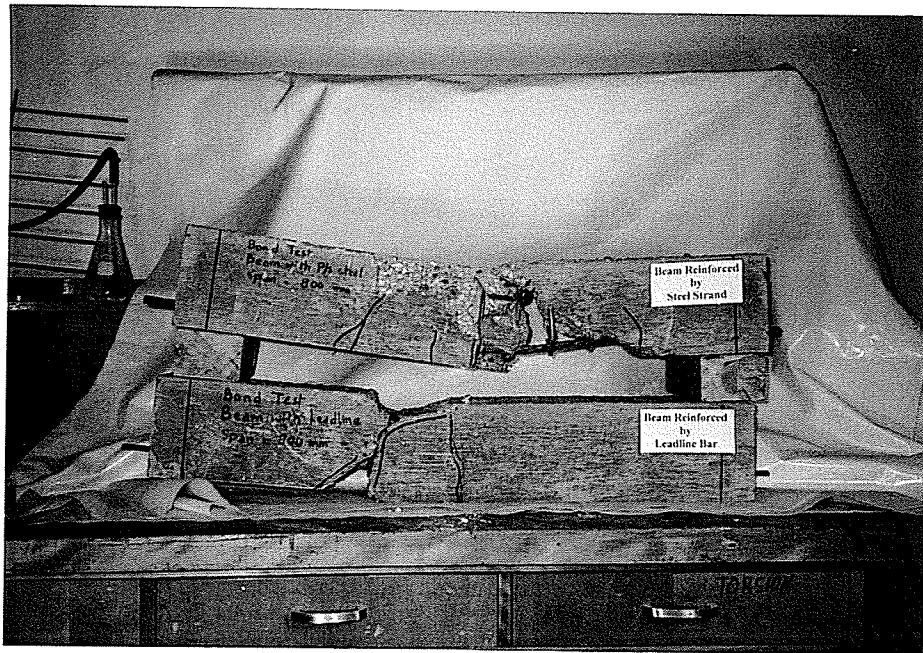


Fig.5-18 Failure mode of two beams with 800 mm span reinforced by Leadline and steel

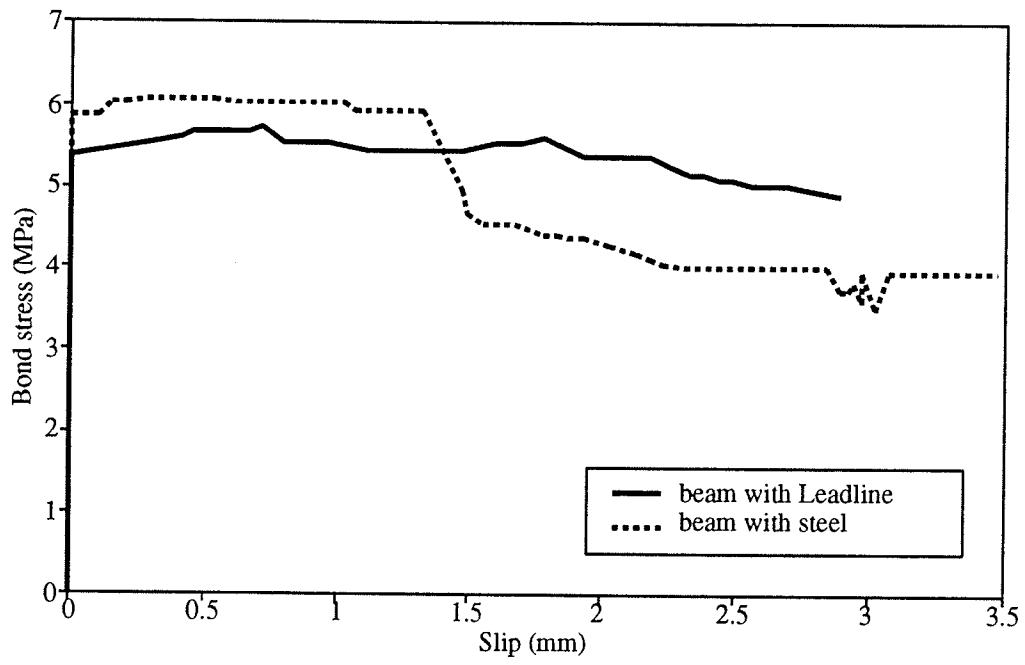


Fig.5-19 Bond stress of Leadline bars and steel strands

6. ————— RESULTS OF THE EXPERIMENTAL PROGRAM

6.1 GENERAL

Eight concrete beams prestressed by 8-mm Leadline bars and two beams prestressed by 13-mm steel strands were tested. The two beams prestressed by steel strands had the same prestressing force and eccentricity as two beams prestressed by Leadline bars. The two jacking stresses of the Leadline bars were 50 and 70 percent of the guaranteed ultimate strength. The level of prestressing, in terms of concrete stresses at the top and bottom fibres after jacking, was also varied by changing the number of Leadline bars from two to four bars. In addition, the distribution of the Leadline bars in the tension zone was varied to study its effect on the cracking behaviour of the beams. The beams were designed to have a tensile stress on the top fibre and a compressive stress on the bottom fibre of concrete within the allowable stresses specified by code. The beams were simply supported and tested using two quasi-static concentrated loads 1.0 meter apart. The beams were tested after a period of time ranging from 30 to 60 days from the time of casting. This chapter discusses the test results for the ten beams tested in this program.

6.2 FLEXURAL BEHAVIOUR

The typical behaviour of the beams prestressed by *CFRP* bars is shown by the load-deflection relationship for a typical beam, T-4-.5-H, in Fig. 6-1. In general, the concrete beams prestressed by Leadline bars behaved linearly up to cracking, and again after cracking with a reduced stiffness up to failure. This bilinear behaviour is attributed to the linearly elastic behaviour of the Leadline bars. The beams were cycled three times between a lower load level corresponding to 80 percent of the cracking load, P_{cr} , and an upper load level equivalent to 60 percent of the predicted ultimate load, P_u , which coincides with 1.5 to 2 times the cracking load depending on the prestressing level. The deflection of the beams during the second and third cycles was identical and higher than the deflection at the initial cycle at a given applied load. The stiffnesses of the beams in the second and third cycles, presented by the slope of the load-deflection diagrams, were higher than those of the beams in the initial cycle after cracking but lower than the initial stiffness based on gross section properties. After application of the cyclic loading within the service load range and after attaining the magnitude of the repeated load, the beams followed the monotonic load-deflection path. The general behaviour of each beam is summarized in the following subsections:

Beam T-4-.5-H: was jacked up to 50 percent of the guaranteed strength of the Leadline. The beam had a flange width of 600 mm and was prestressed by four Leadline bars, two

bars at 50 mm and two at 100 mm from the bottom fibre of the beam. The beam cracked at a load level of 25.3 kN and was cycled three times between lower and upper load levels of 25.0 and 50.0 kN, respectively. The beam had five cracks in the constant moment zone within the service load limit, as shown in Fig. 6-2. The second and third cracks occurred at 30.0 kN, while the fourth and fifth cracks occurred at 33.2 and 40.0 kN, respectively. The beam failed when one of the bottom Leadline bars ruptured at a load level of 106.1 kN. The applied load dropped until the second Leadline bar at the bottom level failed at 101.0 kN. The applied load dropped for the second time to 43.0 kN and the top Leadline bars carried more load until the test was stopped at 50.4 kN. The maximum deflection at failure of the beam was 176.5 mm, or 1/33 of the beam span.

Beam R-4.5-H: was also jacked to 50 percent of the guaranteed strength of the Leadline. The beam had a flange width of 200 mm and was prestressed by four Leadline bars, two at 50 mm and two at 100 mm from the bottom of the beam. The camber was measured before testing the beam, 73 days after casting, and was found to be 13.2 mm, compared to an estimated value of 4.6 mm after release. This increase in camber is due to creep of the concrete. Five cracks occurred in the constant moment zone, as shown in Fig. 6-3. The first crack occurred at 23.4 kN. The second and third cracks occurred at 29.0 kN while the last two cracks occurred at 30.0 kN. The beam was cycled 3 times between 20.0 and 50.0 kN, which corresponds to $0.8 P_{cr}$ to $2 P_{cr}$ ($0.6 P_u$). The beam

failed at a load equal to 89.2 kN; the corresponding deflection was 168.0 mm, or 1/35 of the beam span. The beam failed by crushing of the concrete at the top flange in the maximum moment zone in an area 260 mm wide and 160 mm in depth.

Beam T-4.5-V: had a flange width of 600 mm and was prestressed by four Leadline bars located at 50, 78, 100, and 128 mm from the bottom fibres of the beam. The Leadline bars were jacked to 50 percent of the guaranteed strength. Before testing, the camber was 5.5 mm 33 days after casting. The beam cracked at a load level of 27.3 kN and failed at a load level of 97.9 kN. Five cracks occurred in the constant moment zone as shown in Fig. 6-4. The first three cracks occurred at a load level of 27.3 kN. The other two cracks occurred at a load level ranging between 29.0 and 33.0 kN. The beam was cycled three times between lower and upper load limits of 23.0 and 45.0 kN, respectively.

The beam was unloaded at 68.6 kN, which is 70 percent of the measured failure load, and loaded again to failure to evaluate the released elastic and the consumed inelastic energy of the beam. The corresponding deflection of the beam at 68.6 kN, before unloading, was 91.8 mm. The behaviour of the beam was not completely elastic as the residual deflection of the beam at zero load was 10.5 mm. The energy released at unloading of the beam was mainly elastic. The inelastic energy consumed by the beam was very small and occurred mainly due to cracking of concrete. After reloading, the

deflection of the beam at 68.6 kN was only 5 percent higher than that before unloading despite the severe cracking of the beam at this load level. This is attributed to the elastic behaviour of the Leadline. The beam failed by rupture of the Leadline bar, which is the closest to the extreme tension fibre of concrete, at a load level of 97.6 kN. The load dropped to 58.2 kN and increased until the second Leadline bar from the bottom failed at a load level of 68.2 kN. The load dropped again to 30.8 kN and increased until the third Leadline bar failed at 43.0 kN. The load dropped for the third time to 16.8 kN and the test was stopped at a load of 19.2 kN. Before failure, flexural shear cracks were observed outside the constant moment zone. The deflection of the beam at failure of the first Leadline bar was 171.4 mm, or 1/34 of the beam span.

Beam R-4-.5-V: had a 200-mm flange width and was prestressed by four Leadline bars jacked to 50 percent of the guaranteed strength and located as in beam T-4-.5-V. The camber of beam R-4-.5-V was measured prior to testing, 40 days after casting, and was found to be 10.0 mm. The beam had a cracking load of 23.1 kN and five cracks occurred between 23.4 kN and 30.0 kN, as shown in Fig. 6-5. The beam was cycled between lower and upper load levels of 20.0 and 45.0 kN. The beam failed by rupture of the bottom Leadline bar at a load level of 90.2 kN accompanied by a horizontal crack at about 50 mm from the bottom surface of the beam. The load dropped to 50.9 kN. The beam carried more load until crushing of the concrete at the top surface of the beam between the two concentrated loads occurred at a load level of 53.7 kN. The deflection

of the beam was 186.2 mm, or 1/31 of the beam span. This deflection was the largest observed deflection compared to that of the other beams prestressed by Leadline and jacked to 50 percent of the guaranteed ultimate strength. This is attributed to the type of failure where both the concrete and the Leadline were strained to the full capacity.

Beam T-4-7: was prestressed by four Leadline bars jacked to 70 percent of the guaranteed ultimate strength and located as in beam T-4-.5-V. The beam had a 600-mm flange width. The beam cracked at a load level of 37.9 kN. This beam had only three cracks occurring at load levels ranging between 37.9 and 41.7 kN, as shown in Fig. 6-6. The beam was cycled three times between 30 and 55 kN. The beam failed by rupture of the bottom Leadline bar at a load level of 102.2 kN. The load dropped to 64.0 kN and the second bar ruptured at a load of 72.2 kN. The load dropped after the failure of the second bar to 61.7 and the test was stopped at 62.3 kN. The deflection at the ultimate load was 140.1, or 1/41 of the beam span.

Beam R-4-7: had a 200-mm flange width and a prestressing force identical to that of beam T-4-7. The beam was prestressed by four Leadline bars located as in beam T-4-.5-V. The measured camber of the beam on the day of testing, 36 days after casting, was 13 mm. The beam cracked at 32.1 kN and failed at 98.1 kN by rupture of the bottom Leadline bar. Five cracks were observed in the constant moment zone, as shown in Fig. 6-7. The second to fifth cracks occurred at load levels ranging from 34.2 kN to

39.0 kN. The beam was cycled three times between 25.0 and 50.0 kN. At onset of failure, two cracks in the constant moment zone extended to the top surface of the flange and the load dropped to zero. The deflection at failure was 164.5 mm, or 1/35 of the span of the beam.

Beam T-2-.5: was prestressed by two Leadline bars at 50 and 78 mm from the bottom fibre of the beam, jacked to 50 percent of the guaranteed strength. The beam had a 200-mm flange width. Three cracks occurred at a load of 13.1 kN and another two cracks occurred at 21.0 and 22.0 kN respectively. The third crack formed at 13.1 kN closed when a crack occurred at 16.0 kN outside the constant moment zone, as shown in Fig. 6-8. The camber of the beam, 33 days after casting, was 5 mm. The beam was cycled three times between 10.0 and 24.0 kN. The beam failed by rupture of the bottom Leadline bar at a load level of 56.3 kN. The load dropped to 21.0 kN and the test was stopped. The deflection at failure was 151.0 mm, or 1/38 of the beam span. Several flexure-shear cracks were observed outside the constant moment zone before failure of the beam.

Beam R-2-.5: was prestressed with the same force and the same location of bars as beam T-2-.5. The camber of the beam was 7 mm 36 days after casting. The beam cracked at 12.7 kN and failed at 56.8 kN. Five cracks were observed in the constant moment zone, as shown in Fig. 6-9; four of them occurred at load levels ranging between 12.7 and

15.9 kN, while the fifth crack occurred at 23.4 kN with a loud noise. The load was cycled three times between 10.0 and 24.0 kN. Again the beam failed by rupture of the bottom Leadline bar, accompanied by flexure and flexure-shear cracks extending to the top flange of the beam. The load dropped to 22.0 kN and the beam carried more load until the test was stopped. The deflection at failure was 164.6 mm, or 1/35 of the beam span.

Beam S-T-2-.5: was prestressed by two 13-mm steel strands at 50 and 100 mm from the bottom of the beam. The strands were jacked to 51 percent of their ultimate strength to have the same prestressing force as beams T-4-.5-H, R-4-.5-H, T-4-.5-V and R-4-.5-V. Beam S-T-2-.5 cracked at a load of 30.7 kN and had ten cracks within the constant moment zone. Unlike in the beams prestressed by Leadline, the number of cracks increased with increase of the applied load. Six cracks occurred between 30.7 kN and 39.0 kN and three cracks occurred between 43.0 kN and 47.5 kN; the last crack occurred at 60.0 kN, as shown in Fig. 6-10. Unlike for beams prestressed by Leadline, the load-deflection relationship was linear up to cracking and non-linear after cracking up to failure as shown in Fig. 6-11. The camber of the beam was 10.7 mm 33 days after casting. The load was cycled three times between 25.0 and 50.0 kN. The beam was unloaded at 76.5 kN after the steel had yielded. After unloading, the permanent deformation was 204.0 mm at zero load. The inelastic energy consumed by the beam was much higher than the released elastic energy. The maximum load carried by the beam

was 77.1 kN. The bottom steel strand ruptured at 76.3 kN, followed by a drop of the load to 30.4 kN. The beam carried more load until the second strand ruptured at 31.4 kN. After yielding of the steel strands, the deflection of the beam increased without a significant increase of the applied load. The number of the flexure and flexure-shear cracks before failure of the beam was higher than that for a similar beam prestressed by Leadline. One of the cracks in the constant moment zone extended up to the top surface of the beam across the flange. The deflection of the beam at failure was 346.4 mm, or 1/17 of the span.

Beam S-R-2-.5: was prestressed by identical prestressing force and steel strands as beam S-T-2-.5. The beam had a flange width of 200 mm. The behaviour of the beam was linear before cracking and non-linear after cracking up to failure as was that of beam S-T-2-.5. The camber of the beam was 12.2 mm before testing the beam, 37 days after casting. The beam cracked at a load level of 27.9 kN. Ten cracks were observed within the constant moment zone. Five cracks occurred between 27.9 kN and 34.0 kN and three cracks occurred between 40.0 and 42.0 kN, as shown in Fig. 6-12. Two more cracks occurred at a load level of 52.0 kN. The beam was cycled between 22.0 and 42.0 kN. The beam failed at a load level of 70.1 kN by crushing of concrete in the constant moment zone. At failure, the steel strands was just past the yield stress. The strain in the steel increased without a significant increase in the applied load until the concrete failed. The deflection of the beam at ultimate was 170.6 mm, or 1/34 of the span.

6.3 FAILURE MODES

In general, the two observed modes of failure were either rupture of the Leadline bar farthest from the neutral axis or crushing of the concrete at the top surface within the constant moment zone. Typical behaviour for beams failing by rupture of the Leadline bars was sudden drop of the load resistance immediately after failure of the first bar. After redistribution of the internal forces, the beam carried more load until the second Leadline bar ruptured. At the onset of rupture of the bottom Leadline bar, a horizontal crack occurred in some of the beams at the level of the prestressing bar as well as extensive cracks extending to the top flange of the beam. The horizontal cracks occurred mainly due to release of the elastic strain energy after rupture of the bars. The released elastic energy, which is partly absorbed by the concrete, induced the horizontal cracks at the level of the reinforcement. This is confirmed by the findings of the research conducted at the University of Michigan (Naaman and Jeong 1995) on the behaviour of beams prestressed and partially prestressed by *CFRP* tendons. Progressive failure of the other Leadline bars occurred in some of the beams, accompanied by horizontal cracks in the constant moment zone. Flexure-shear cracks were observed outside the constant moment zone. Fig. 6-13 shows the typical crack pattern at the failure of a beam due to rupture of the Leadline bars.

The second mode of failure, crushing of the concrete, occurred for only one of the

beams, R-4-.5-H, with 200-mm flange width and four Leadline bars jacked to 50 percent of the guaranteed strength and placed in two layers. The failure occurred in the constant moment zone when the concrete strain reached its maximum value (about 0.004). At the onset of failure, the top steel bars and the steel stirrups were exposed, followed by buckling of the top steel bars and the welded wire fabric used to reinforce the top flange. Cracking of the beam that failed by crushing of the concrete was not as extensive as that of beams which failed by rupture of the Leadline bars. Flexure-shear cracks were also observed before failure of the beam. Fig. 6-14 shows the failure of beam R-4-.5-H due to crushing of the concrete. Crushing of the concrete also occurred for beam R-4-.5-V with 200-mm flange width and four Leadline bars oriented vertically on top of each other and jacked to 50 percent of the guaranteed strength. However, the crushing of the concrete occurred after rupture of the bottom Leadline bar. Fig. 6-15 shows beam R-4-.5-V after failure. No slip of the Leadline bars was observed during any of the beam tests.

Beams prestressed by steel strands had the same two modes of failure as the beams prestressed by Leadline. The beam with a large flange width failed by rupture of the bottom strand, while the beam with a small flange width failed by crushing of the concrete. The prestressing steel in both beams yielded before failure. The cracking of the beams at the onset of failure is shown for the two modes of failure in Fig. 6-16 and 6-17, respectively.

The cracking load, deflection at cracking, ultimate load, and deflection at ultimate of the different beams, are given in Table 6-1. The mode of failure is also given for the different beams. Based on the flexural capacity of the beams, the tensile strength of the Leadline bars was calculated and is given in the last column of Table 6-1. The mean tensile strength of the Leadline bars was 3230 MPa with a standard deviation of 100 MPa. The characteristic value of the tensile strength, based on 5 percent probability, was 3050 MPa.

6.4 STRAIN DISTRIBUTION

The strain in the Leadline bars was measured in all the beams by means of strain gauges. Each Leadline bar had at least one strain gauge in the constant moment zone. The typical load-strain relationship of the Leadline is shown in Fig. 6-18. The strain started from a value representing the effective strain of the Leadline bars on the day of testing. Similarly to the load-deflection behaviour, the load-strain behaviour of the Leadline was linear up to cracking and after cracking up to failure. The strain in the Leadline bars in the second and third cycles was identical and was higher than that in the initial cycle, due to the presence of cracks. For beams which failed by rupture of the Leadline bars, the maximum recorded value of the Leadline strain ranged from 0.0153 to 0.0185 for the different beams. However, it should be noted that strains obtained from any strain gauge are localized and depend on whether the gauge is at the exact location

of a crack or in between cracks. Therefore, the measured strains should be carefully interpreted in view of their location with respect to the cracks.

The concrete strains, measured using demec gauges at the top surface of the beam and at 50 mm from the bottom fibres of the beam, are shown in Fig. 6-19 and 6-20, respectively, for one of the beams prestressed by Leadline. The concrete strain at the top of the concrete surface represents the maximum of three values measured at three different locations within the constant moment zone. The concrete strain at 50 mm from the bottom of the beam represents the maximum strain, over a 200-mm gauge length, at five different locations within the constant moment zone. The solid lines in the figures connect the measured values of the strains, while the broken lines represent the anticipated values before failure of the beams, based on linear regression analysis of the strain readings after cracking. The measured concrete strain in compression for the beams which failed by crushing of the concrete ranged between 0.0040 and 0.0044.

The neutral axis location was calculated based on the demec point readings at different load levels after cracking. The location of the neutral axis is shown in Fig. 6-21 versus the applied load for two beams with 600- and 200-mm flange width. It can be seen that the neutral axis rises rapidly after cracking with increase of the applied load. The neutral axis tends to be stationary beyond a certain load level after the cracking of the beam. This phenomenon can be explained as the increase of the internal moment

resistance is achieved by an increase of the tensile resultant force due to increase of Leadline stress and therefore the neutral axis remains nearly stationary up to failure of the beam.

6.5 CRACKING BEHAVIOUR

Cracking behaviour of the beams prestressed by Leadline was examined within the constant moment zone. In general, flexural cracks of beams prestressed by Leadline bars were evenly distributed in the constant moment zone. Cracks started perpendicular to the centre-line of the beam and extended into the top flange. It was observed that steel stirrups act as crack initiators for most of the flexural cracks regardless of the type of prestressing reinforcement, as shown in Fig. 6-22. Typical average and maximum crack widths, measured at the extreme tension fibre for the three cycles, are shown in Fig. 6-23 and 6-24, respectively. It can be seen that the crack width increases non-linearly with increase of the applied load during the initial cycle; however, it decreases linearly with decrease of the applied load for the two subsequent cycles up to the level of the cracking load. It can be also seen that crack widths during the second and third cycles were the same and were higher than the crack width during the initial cycle. Crack widths at the upper load levels were the same for the three cycles; this is attributed to the elastic behaviour of the Leadline and the concrete. The crack width, measured at the level of the prestressing reinforcement, was linearly proportional to the crack width at the extreme

tension fibre. The relation between the crack widths at the two levels was governed by the ratio of the distances from the neutral axis to the extreme tension fibre and the distance from the neutral axis to the level of the prestressing reinforcement, as shown in Fig. 6-25.

At high load levels, cracks in beams prestressed by Leadline bifurcated at the top, parallel to the neutral axis. At high load levels, the neutral axis became stationary and the cracks could not propagate vertically due to the constant compression zone depth; in order to reduce the tensile stresses at the tip of the cracks with increase in the applied load, the cracks extended laterally in a forked configuration, as shown in Fig. 6-22. It was reported by (Beeby 1979) that tensile stresses perpendicular to the neutral axis exist at the head of the cracks when the ratio of crack spacing to crack height reduces below about 2. These stresses become greater than those on the surface at mid-spacing between cracks.

The number of and spacing between cracks, and the load at which the cracks were stabilized, are reported in Table 6-2. Stabilization of cracks is defined by the stage at which the number of cracks did not increase with increasing load (Leonhardt 1977). The maximum crack width at stabilization of cracks is also given in Table 6-2. It can be seen that crack stabilization occurred at a lower load for beams prestressed by Leadline than for beams prestressed by steel. This can be attributed to the low flexural bond strength

of the Leadline compared to that of the steel strands. At stabilization of cracks, the crack width of the beams prestressed by Leadline was much smaller than that of beams prestressed by steel. The crack distribution at the load producing a maximum crack width of 0.4 mm is shown in Fig. 6-26 and 6-27 for the beams with 600- and 200-mm flange width respectively. Based on crack control, the service load is defined in this study as the load at which the maximum crack width is 0.4 mm. The number of and spacing between cracks at service load limit are given in Table 6-3. It can be seen that, at service load, the cracks were stabilized for beams prestressed by Leadline, except for the two beams having low prestressed reinforcement ratios; however, for beams prestressed by steel strands, the cracks were not stabilized at the service load.

6.6 COMPARISON BETWEEN BEAMS PRESTRESSED BY LEADLINE AND STEEL

Since Leadline bars are characterized by linear stress-strain behaviour up to failure with neither yielding nor strain hardening, in contrast to the steel strands, and because of the difference in the bond properties of steel and Leadline, the behaviour of the two types of prestressed beams was different under service loading conditions and at ultimate. In general, the failure of prestressed beams is governed by either the ultimate tensile strain of the reinforcement or the ultimate compressive strain of concrete. However, the performance of the beams prestressed by Leadline was different from that of those with

steel, in terms of deflection after cracking, strain distribution, and cracking behaviour. A comparison of the behaviour of the beams prestressed by Leadline and by steel is given in the following subsections.

6.6.1 Load-Deflection

The load-deflection behaviours of two beams with the same jacking force and eccentricity, one prestressed by Leadline bars and the other with steel strands, are shown in Fig. 6-28a for beams with a 600-mm flange width and Fig. 6-28b for beams with a 200-mm flange width. The ultimate tensile strength of the steel strands was approximately equal to the guaranteed tensile strength of the Leadline bars but less than the measured tensile strength. Before cracking, the deflection of the beams prestressed by Leadline was slightly higher than that with steel strands, for the same flange width. The slight difference in deflection is mainly attributed to the difference in the elastic modulus of the concrete, which was 29,040 MPa for the beams with Leadline and 37,950 MPa for the beams with steel.

The cracking load of the beams prestressed by steel was higher than that of those prestressed by Leadline. The calculated concrete rupture strengths were 5.6 MPa and 4.1 MPa for beams prestressed by steel and Leadline, respectively. After cracking, the stiffness of the beams prestressed by Leadline was 30 percent less than that of beams with

steel for beams with a 600-mm flange width, and 15 percent less, for beams with a 200-mm flange width. The lower stiffness of the beams after cracking is attributed to the lower elastic modulus of the Leadline bars, which is about 22 percent less than that of steel strands. Consequently, the deflection of beams prestressed by Leadline after cracking was higher.

For beams with a 600-mm flange width, the deflection at ultimate load of the beam prestressed by steel strands was much higher than that of the beam prestressed by Leadline. This is attributed to the higher ultimate strain of the steel compared to that of the Leadline, as both beams failed by rupture of the prestressing reinforcement and consequently the ultimate strain of both types of reinforcement was achieved. For beams with a 200-mm flange width, the deflection at ultimate load was almost the same for beams prestressed by Leadline and steel. Both beams had the same mode of failure, namely, crushing of the concrete, which points to the fact that the ultimate strain in the concrete controlled the failure of both beams. Therefore, the curvature of the two beams at ultimate load and hence the deflection of the beams at failure was the same. Despite the fact that the ultimate strength of the 2-D-13 prestressing steel strand was equal to the guaranteed strength of the 4-D-8 Leadline bars, the ultimate load of the beam prestressed by Leadline was 25 percent higher. The reason is that the actual tensile strength was much higher for the Leadline than for the steel. For beam S-R-2-.5, the increase in the applied load was negligible after yielding of the steel; however, the applied load increased

for beam R-4-.5-H until the concrete failed. This is attributed to the linear stress-strain behaviour of the Leadline up to failure.

6.6.2 Strain Distribution

The average concrete strain at the top surface of the beam and at 50 mm from the bottom surface, for beams prestressed by Leadline and by steel, is shown in Fig. 6-29 and 6-30. The higher concrete strain before cracking, for beams prestressed by Leadline, is attributed to the lower concrete elastic modulus than that for beams prestressed by steel, as discussed earlier. The higher concrete strain for beams with Leadline after cracking is attributed to the lower elastic modulus of Leadline.

The strain distribution in the constant moment zone, measured at 1.4 times the cracking load and at ultimate load, is shown in Fig. 6-31 for the beams with 600- and 200-mm flange width. The strain distribution at ultimate is given at three different sections within the constant moment zone away from the concentrated loads and is also given in terms of the average strain over the constant moment zone. All the strain values were calculated based on the measured strains using demec point stations and taking into consideration the initial elastic strain in the concrete due to the effective prestressing force. At failure, the location of the neutral axis of the beam prestressed by steel with 600-mm flange width was 18.9 mm in comparison to a value of 43.0 mm for a similar

beam prestressed by Leadline. This is attributed to the higher strain in the steel strands at rupture compared to that in the Leadline. The high strain in the tension zone for the beam with steel resulted in higher curvature at ultimate and less compression zone depth than for the beam prestressed by Leadline. For beams with 200-mm flange width, the neutral axis locations for the two beams prestressed by Leadline and steel were almost equal; consequently the curvature at ultimate was also equal. This is attributed to the mode of failure, where the maximum concrete compressive strain controlled the strain distribution for the two beams at ultimate.

Based on an average value of the measured strains, the neutral axis location of beams prestressed by Leadline and steel is shown in Fig. 6-32 for beams with 600- and 200-mm flange width. It can be seen that the neutral axis shifts towards the compression zone with increase of the applied load. For beams prestressed by Leadline, the neutral axis depth decreases more rapidly than for beams prestressed by steel. This is attributed to the lower elastic modulus of the Leadline. Thus, for a given concrete strain in the extreme compression fibre, more strain will be developed in the Leadline than in the steel to achieve the same resistance. This behaviour will lead to a smaller compression zone depth for beams prestressed by Leadline than for beams prestressed by steel subjected to the same load.

As the load increases, the neutral axis continues to move, causing reduction of the

compression zone depth for beams prestressed by steel, while it remains nearly stationary for beams prestressed by Leadline. After yielding of the steel strands, increase of the internal moment resistance with increase of the applied load can be achieved only by increasing the internal lever arm length, correspondingly decreasing the compression zone depth. In the case of Leadline, the increase of the internal moment resistance is achieved by an increase of the tensile resultant force due to increase of Leadline stress; therefore the neutral axis remains nearly stationary up to the rupture of the bar.

6.6.3 Cracking Behaviour

Concrete cracks at a section within the constant moment zone when the induced tensile stress exceeds the tensile strength of concrete. Increasing the applied load above the cracking load results in initiation of other cracks away from the vicinity of the first crack. Increasing the applied load may result in one of two developments: (1) either cracks will increase in height which will reduce the tensile stresses in the concrete between the cracks, or (2) cracks will fork at an angle with the original crack. This latter behaviour may occur because of the principal tensile stresses which are at an angle with respect to the neutral axis at the head of the cracks. For a certain crack pattern, the increased applied load may not result in formation of new cracks, which is called a "stabilized crack pattern" (Leonhardt 1977). Test results indicated that stabilization of the flexural cracks in beams prestressed by Leadline bars occurs at a significantly lower strain

level than in beams prestressed by steel. The number of cracks of all the beams tested is shown in Fig. 6-33 in relation to the strain in the prestressing reinforcement after decompression. Stabilization of cracks occurred at an average strain value of 0.001 for beams prestressed by Leadline compared to a strain value of 0.0038 for beams prestressed by steel strands.

For beams prestressed by Leadline, the crack pattern was characterized by fewer cracks than for beams prestressed by steel, resulting in a larger spacing, as shown in Fig. 6-34. This may be attributed to the lower flexural bond of the Leadline than that of steel. After formation of the stabilized crack pattern, the tensile strain in the concrete adjacent to the Leadline bars may not increase due to the possible occurrence of slip of the Leadline bars between cracks in the constant moment zone. The smaller number of cracks in the beams prestressed by Leadline may be also attributed to the rapid increase in the crack heights after cracking due to the rapid decrease in the compression zone depth. With the increase of the applied load, the neutral axis location remained constant and the existing cracks forked to reduce the tensile stresses at the tip of the cracks. The early "forking of cracks" is attributed to the small compression zone depth which was almost stationary; consequently the cracks height did not propagate vertically. Forking of cracks is also due to the presence of inclined principal tensile stresses at the tip of the cracks and the high compression in the concrete above the neutral axis. This behaviour suggests that the energy dissipated by the cracks forking is lower than the energy

dissipated at the initiation of a new crack at this level. It should be mentioned that for beam T-2-.5, where the reinforcement ratio is 0.06 percent, the decrease of the compression zone depth was very rapid. The spacing between the first and the second cracks was 404 mm. At a load level of 22.0 kN, which is about 1.7 times the cracking load, a new crack was initiated accompanied by a loud sound and a sudden drop of the load from 22.0 kN to 19.5 kN. The crack height was 222 mm while its width was 0.36 mm. This reflects the significant energy dissipated to initiate the crack. This energy could not be dissipated by forming the forking cracks due the fact that the reinforcement ratio of the beam was low and therefore the compression of the concrete was also low.

For beams prestressed by steel, movement of the neutral axis was observed with increase of the applied load as shown in Fig. 6-32. As a result, after the stabilized crack pattern was achieved, the cracks propagated vertically with the decrease in the compression zone depth. The cracks were perpendicular to the neutral axis and extended to the top flange. The decrease of the compression zone depth at high loads was considerable. For beam S-T-2-.5, the cracks forked in the top flange at about 80 percent of the ultimate load, after the cracks were stabilized. For beam S-R-2-.5, however, the cracks did not fork until the beam failed. This is attributed to the high tensile stresses and the small compression zone depth developed in beam S-T-2-.5 compared to those in beam S-R-2-.5.

6.6.3.1 Crack Spacing

Crack stabilization of the beams prestressed by Leadline with a high reinforcement ratio occurred at a low load level, as given in column 4 of Table 6-2. The maximum observed crack width at crack stabilization was ranged between 0.08 and 0.40 mm, which is considered to be within the service load range, as shown in column 6, Table 6-2. However, for beams prestressed by steel strands with a similar reinforcement ratio, the crack stabilization occurred at a higher load level and the corresponding crack width was ranged between 0.76 and 0.95 mm which greatly exceeds the service range. Therefore, at crack stabilization, the spacing between cracks was almost twice as large for beams prestressed by Leadline as for beams prestressed by steel, as shown in the last two columns of Table 6-2. For beams prestressed by Leadline with a small reinforcement ratio, crack stabilization occurred at a load higher than the service load level, as shown in Table 6-2. The corresponding crack width was between 0.60 and 0.74 mm. This behaviour is attributed to the sudden and high increase of the stress in the Leadline immediately after the initiation of the first crack, resulting in wider cracks for this category of beams. This behaviour confirms the findings by (Leonhardt 1977) for beams prestressed by steel with a small percentage of reinforcement.

The concept of random formation of cracks in reinforced concrete members has been discussed by many researchers (Beeby 1979 and Goto 1971). The final crack pattern is

expected to vary from a minimum crack spacing S_{min} to a maximum crack spacing S_{max} , which can be in ratio of up to two. At a load level corresponding to a crack width of 0.40 mm, which is assumed to be the limiting value for service load conditions, the ratios of S_{min}/S_{avg} and S_{max}/S_{avg} were computed for each beam and are given in Fig. 6-35 as a function of the measured average crack spacing S_{avg} . The average ratios of S_{min}/S_{avg} and S_{max}/S_{avg} were 0.79 and 1.17, respectively, for beams prestressed by Leadline and much wider range of 0.65 and 1.50 for beams prestressed by steel. However, after stabilization of cracks, these ratios were in the range of 0.70 and 1.25 for both types of beams, as shown in Fig. 6-36. This indicates that the cracking behaviour, after stabilization of cracks, is the same for beams prestressed by Leadline and by steel strands.

6.6.3.2 Crack Width

The relationship between the maximum, minimum and average crack width, w_{max} , w_{min} and w_{avg} , is shown in Fig. 6-37 for beams prestressed by Leadline and steel, respectively, for all the flexural cracks observed within the constant moment zone at different load levels. The average values of the ratios between w_{max}/w_{avg} and w_{min}/w_{avg} were 1.19 and 0.80, respectively for beams prestressed by Leadline, and 1.60 and 0.56, respectively, for beams prestressed by steel. The large variation of the crack width for beams prestressed by steel is attributed to the significant variation of the crack spacing before stabilization of the cracks. In contrast, the small variation of the crack width for

beams prestressed by Leadline is attributed to the equal distribution of cracks, which is again due to the early formation of the stabilized crack pattern.

The relationship between the maximum crack width of beams prestressed by Leadline and steel and the average concrete tensile strain at 50 mm from the bottom of the beam, taking into consideration the elastic strain in the concrete due to prestressing, is shown in Fig. 6-38. It can be seen that the maximum crack width increases linearly with the strain. The scatter of the data is represented by the value of " R^2 " which has the range from 0 to 1, with 1 being optimal. The value of R^2 was 0.953 and 0.667 for beams prestressed by Leadline and steel, respectively, which indicates less scatter of the crack width of beams prestressed by Leadline.

6.7 EFFECT OF FLANGE WIDTH

The tested beams had two different cross sections with respect to the flange width, 600 and 200 mm. For beams with a 600-mm flange width, failure was always due to rupture of the prestressing bars. The mode of failure changed to crushing of concrete for the beam R-4-.5-H with a 200-mm flange width as the area of concrete resisting compression was much smaller. The cracking and ultimate moment capacities of beams with a 200-mm flange width were less than those of beams with a 600-mm flange width, due to the smaller section modulus. The load-deflection behaviour of two beams with

different flange widths is shown in Fig. 6-39. The stiffness of the beam with the smaller flange width, before and after cracking, was less than that for beam with the larger flange width. At the same load level, the concrete strain at the top surface and reinforcement level was higher for beams with a 200-mm flange width due to the smaller section modulus, as shown in Fig. 6-40a and 6-40b respectively. Consequently, the deflection of beams with a smaller flange width was higher at the same load level than that of beams with a large flange width, as shown in Fig. 6-39. The maximum crack width of beams with 600- and 200-mm flange widths was the same for a given concrete strain at the level of the reinforcement, as shown in Fig. 6-41. This is due to the fact that the crack width depends on the tensile strain in the prestressing reinforcement after decompression regardless of the shape of the cross section, provided that the concrete cover and the reinforcement area remain the same. The compression zone depth of the beams with a smaller flange width was larger than that of beams with a large flange width at the same load level, as shown in Fig. 6-42.

6.8 EFFECT OF DEGREE OF PRESTRESSING

The degree of prestressing was examined by using two levels of the jacking stress of the Leadline bars, 50 and 70 percent of the guaranteed strength, for two beams having the same eccentricity of the prestressing reinforcement as well as the same dimensions. Beams prestressed by Leadline jacked to 70 percent of the guaranteed strength had a

38 percent higher cracking load and a 4 to 8 percent higher ultimate load than did beams jacked to 50 percent of the guaranteed strength. However, the deflection at failure of beams with the higher jacking stress was about 11 to 18 percent less, as shown in Fig. 6-43. This indicates that the deformability of the beams can be increased by lowering the jacking stress. The maximum spacing between cracks was larger for beams with the higher jacking stress, as shown in Table 6-2, which may be attributed to the higher prestressing force, which results in fewer cracks. At the same load level, concrete strains were higher for beams jacked to 50 percent of the guaranteed strength, as shown in Fig. 6-44, which is attributed to the early cracking of the beams. Fig. 6-44 also shows that the tensile strain measured on the concrete surface before failure, at the level of the Leadline bars, ranged between 1.85 and 1.95 percent. That the Leadline bars in the constant moment zone were debonded is demonstrated by the fact that the maximum measured tensile strain in the Leadline was only 1.85 percent while the calculated strain, based on the concrete strain and assuming complete bond between the concrete and the Leadline, was about 2.5 percent after adding the initial strain due to jacking. The increase of the tensile strain measured on the concrete surface in the constant moment zone was due to the slip of the Leadline bars between cracks. The location of the neutral axis in beams with different jacking stresses was the same at ultimate, as shown in Fig. 6-45. The mode of failure of the beams with different jacking stresses was the same, due to rupture of the Leadline bars.

The degree of prestressing was also examined by using two and four bars in two identical beams. The cracking and ultimate loads were certainly less for the beams with two Leadline bars. The stiffness of the beams with less reinforcement, compared to that of the beams with four Leadline bars, was similar before cracking and less after cracking, as shown in Fig. 6-46. The stabilized crack pattern was achieved at a much higher strain for the beam with less reinforcement. Consequently, the crack width at stabilization of cracks was larger for beams with less reinforcement, as shown in Table 6-2. For a beam with fewer prestressing bars, the maximum bond strength in the region between any two flexural cracks was higher than that for a beam with large number of bars due to less interference between the bond stresses around each bar. The high strain at crack stabilization for the beams with fewer bars could be also attributed to the sudden increase and high strain in the reinforcement after cracking.

6.9 EFFECT OF DISTRIBUTION OF PRESTRESSING BARS IN THE TENSION ZONE

The distribution of the prestressing bars in the tension zone was studied by testing four beams with 600- and 200-mm flange widths, all prestressed by four bars. The four Leadline bars were placed in two layers in two of the beams and in four layers in the other two beams. The ultimate carrying capacity of the beam with two layers of reinforcement and a 600-mm flange width, T-4-.5-H, was higher than that of the beam

with four layers, T-4-.5-V, as shown in Table 6-1, due to the larger eccentricity. Despite the failure mode of the two beams with 200-mm flange width, R-4-.5-H and R-4-.5-V, being different, as shown in Table 6-1, the maximum compressive strain in the concrete at ultimate was in the range of 0.0042 for both beams; consequently, the two beams had similar failure loads. The failure of the beams with 600-mm flange widths was progressive since the failure of the Leadline bars occurred at different load levels for every layer, as shown in Fig. 6-47.

The concrete tensile strain at the reinforcement level was higher for beams with Leadline bars placed in four layers than for beams with Leadline bars placed in two layers, at the same load level, due to the lower eccentricity. Consequently the maximum crack width was less for beams with two layers of reinforcement, at the same load level, as shown in Fig. 6-48.

Table 6-1 Experimental results of the tested beams

Beam	Cracking load (kN)	Deflection at cracking (mm)	Ultimate load (kN)	Deflection at ultimate (mm)	Failure mode	Tensile strength (MPa)
T-4-.5-H	25.31	5.23	106.1	176.5	R*	3140
R-4-.5-H	23.40	7.96	89.3	168.0	C†	-
T-4-.5-V	27.33	4.75	97.9	171.4	R	3270
R-4-.5-V	23.16	6.37	90.2	186.2	R	3050
T-4-.7-V	37.90	6.93	102.2	140.1	R	3260
R-4-.7-V	32.10	8.62	98.1	164.5	R	3215
T-2-.5-V	13.08	2.55	56.3	151.0	R	3270
R-2-.5-V	12.69	3.46	56.8	164.6	R	3175
S-T-2-.5	30.71	5.74	77.1	346.4	R	2065
S-R-2-.5	27.86	7.04	70.1	170.6	C	-

* "R" refers to rupture of the prestressing bar (or strand)

† "C" refers to crushing of concrete at the top surface of the beam

Table 6-2 Measured response at stabilization of cracks

Beam	reinforcement ratio ρ_p * (%)	Load P_s † (kN)	P_s/P_{cr} ‡	Number of cracks	Maximum crack width (mm)	Average crack spacing (mm)	Maximum crack spacing (mm)
T-4-.5-H	0.12	40.0	1.58	5	0.40	174	221
R-4-.5-H	0.37	29.9	1.28	5	0.16	201	270
T-4-.5-V	0.13	33.0	1.21	5	0.10	230	275
R-4-.5-V	0.39	27.5	1.19	5	0.08	204	220
T-4-.7-V	0.13	42.0	1.11	3	0.14	329	340
R-4-.7-V	0.39	39.0	1.21	5	0.14	208	255
T-2-.5-V	0.06	22.0	1.68	5	0.60	206	215
R-2-.5-V	0.18	23.4	1.84	5	0.74	207	290
S-T-2-.5	0.13	60.0	1.95	10	0.76	103	133
S-R-2-.5	0.39	53.0	1.90	10	0.95	103	126

* $\rho_p = A_p / (bd)$, where A_p , b and d are the area of prestressing reinforcement, flange width and the depth of prestressing reinforcement.

† P_s is the measured load at stabilization of cracks.

‡ P_{cr} is the cracking load of the beams.

Table 6-3 Cracking behaviour of the beams at maximum crack width of 0.4 mm

Beam	At maximum crack width of 0.4 mm					
	Load	Number of cracks	Average crack width	Average crack spacing	Maximum crack spacing	Check crack stabilization
T-4-.5-H	40.0	5	0.30	174	221	Yes
R-4-.5-H	36.0	5	0.26	201	270	Yes
T-4-.5-V	37.5	5	0.36	230	275	Yes
R-4-.5-V	34.7	5	0.37	204	220	Yes
T-4-.7-V	48.3	3	0.37	329	340	Yes
R-4-.7-V	46.2	5	0.37	208	255	Yes
T-2-.5-V	19.2	3	0.27	310	404	No
R-2-.5-V	18.9	4	0.35	275	330	No
S-T-2-.5	46.7	8	0.26	133	213	No
S-R-2-.5	40.0	6	0.23	166	232	No

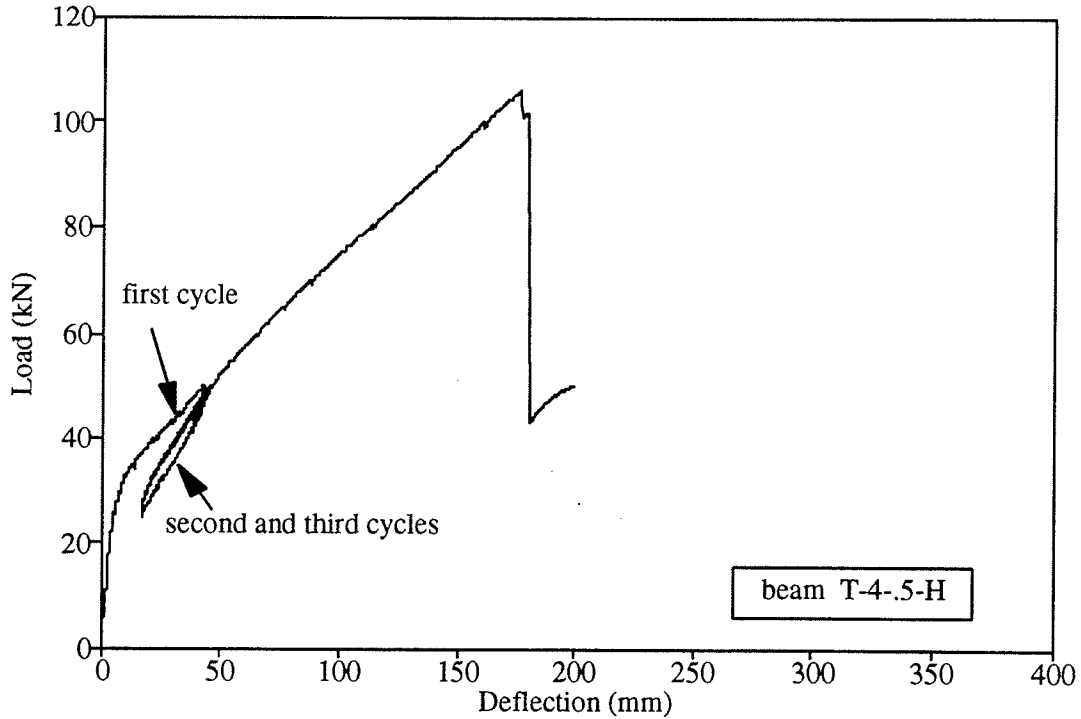


Fig.6-1 Typical load-deflection of beam prestressed by Leadline

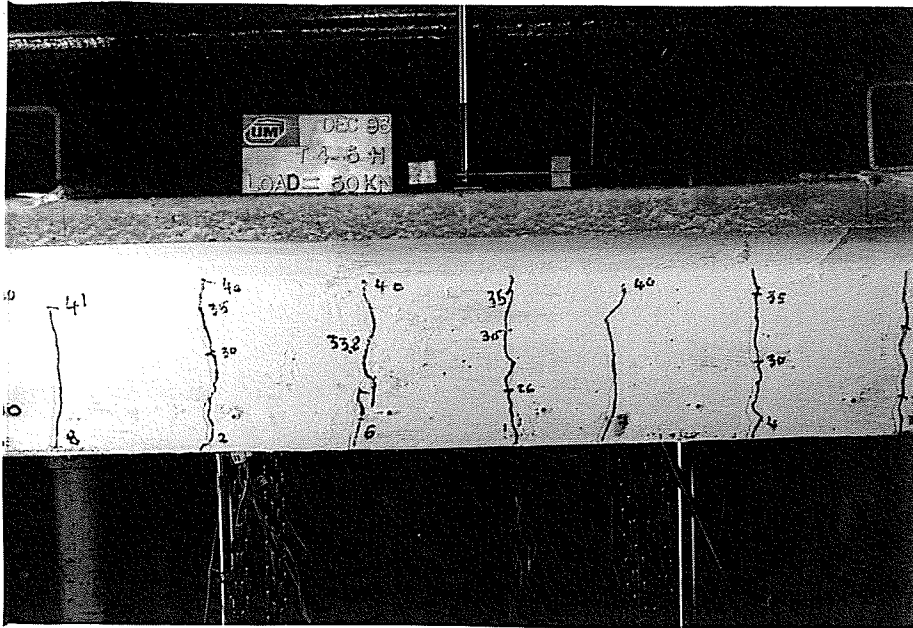


Fig.6-2 Cracking of beam T-4.5-H

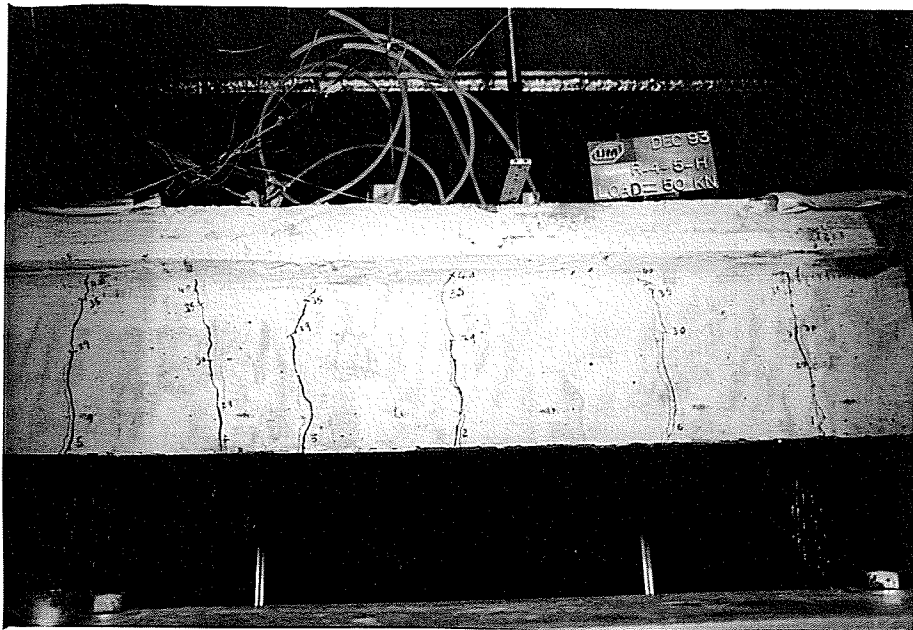


Fig.6-3 Cracking of beam R-4.5-H

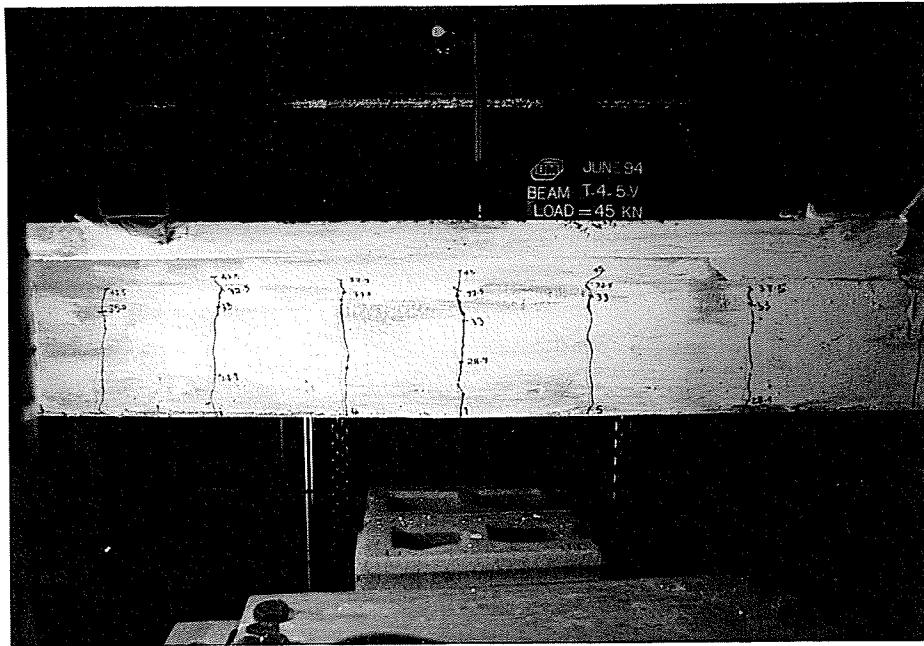


Fig.6-4 Cracking of beam T-4-.5-V

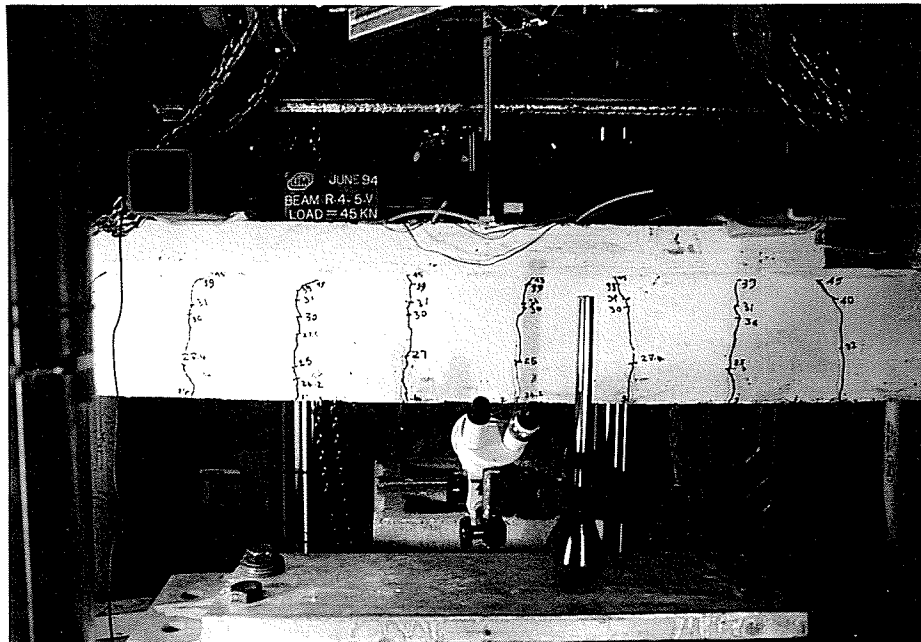


Fig.6-5 Cracking of beam R-4-.5-V

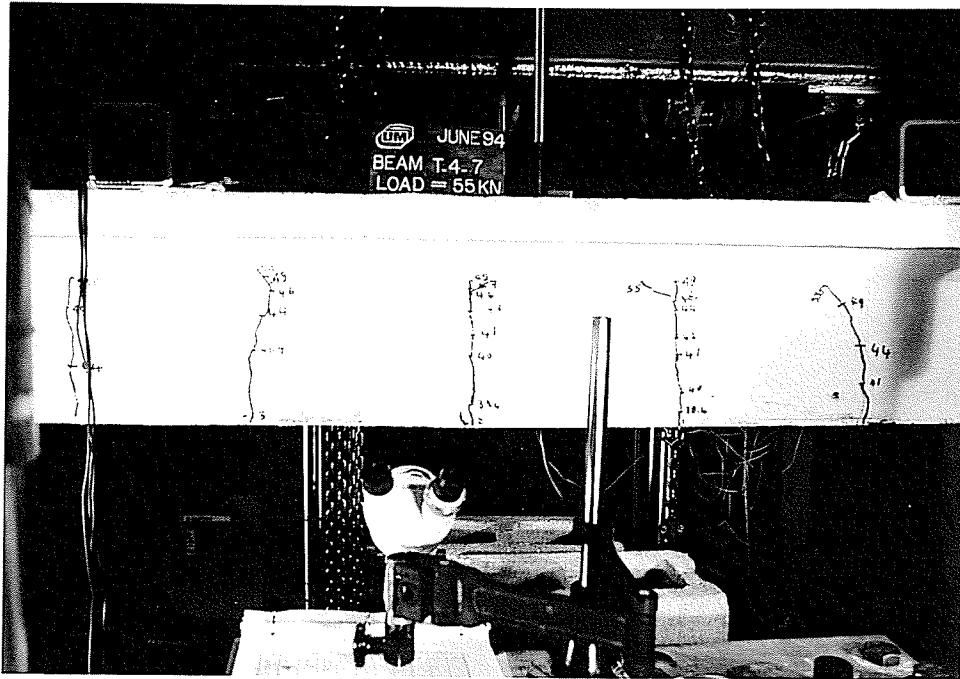


Fig.6-6 Cracking of beam T-4-.7-V

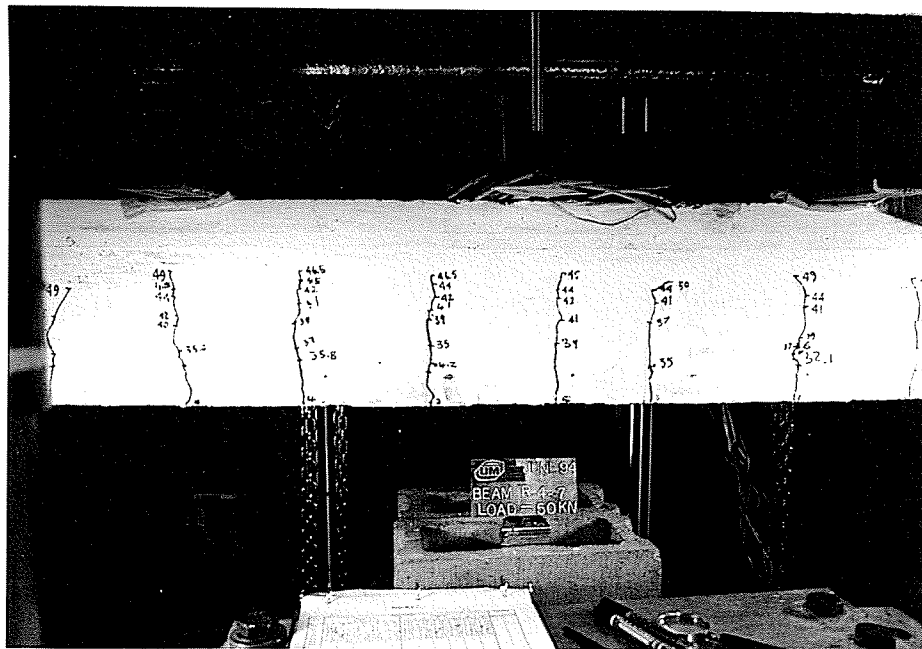


Fig.6-7 Cracking of beam R-4-.7-V

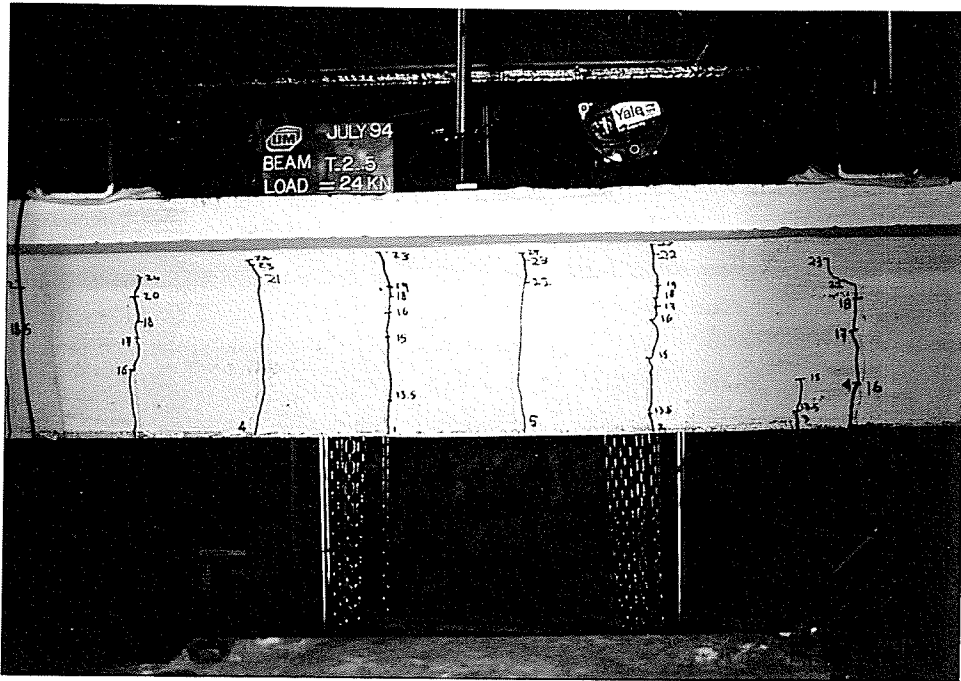


Fig.6-8 Cracking of beam T-2-.5-V

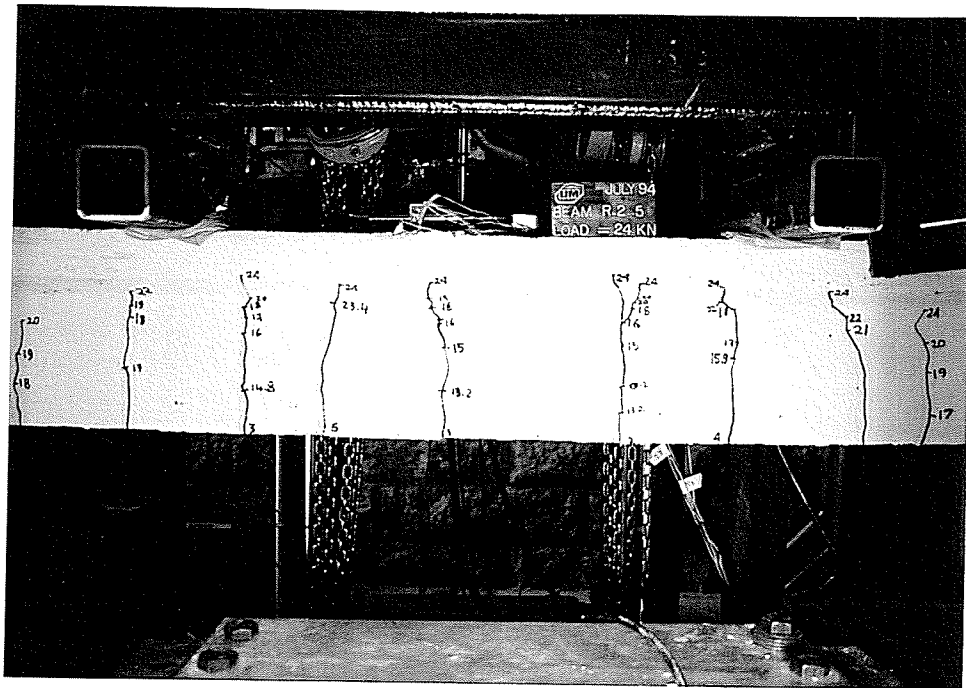


Fig.6-9 Cracking of beam R-2-.5-V

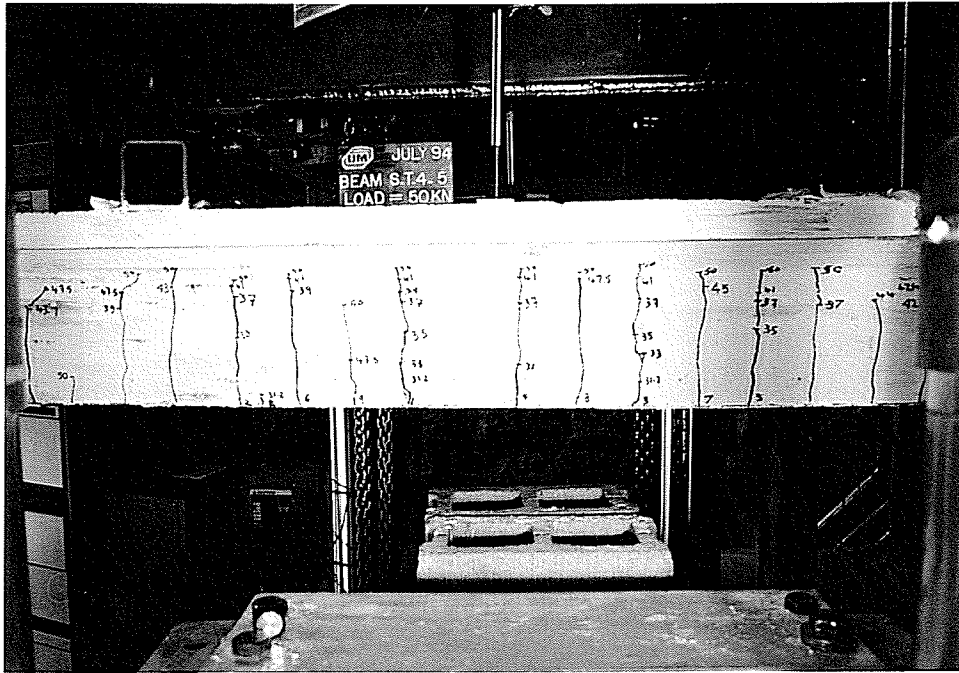


Fig.6-10 Cracking of beam S-T-2-5

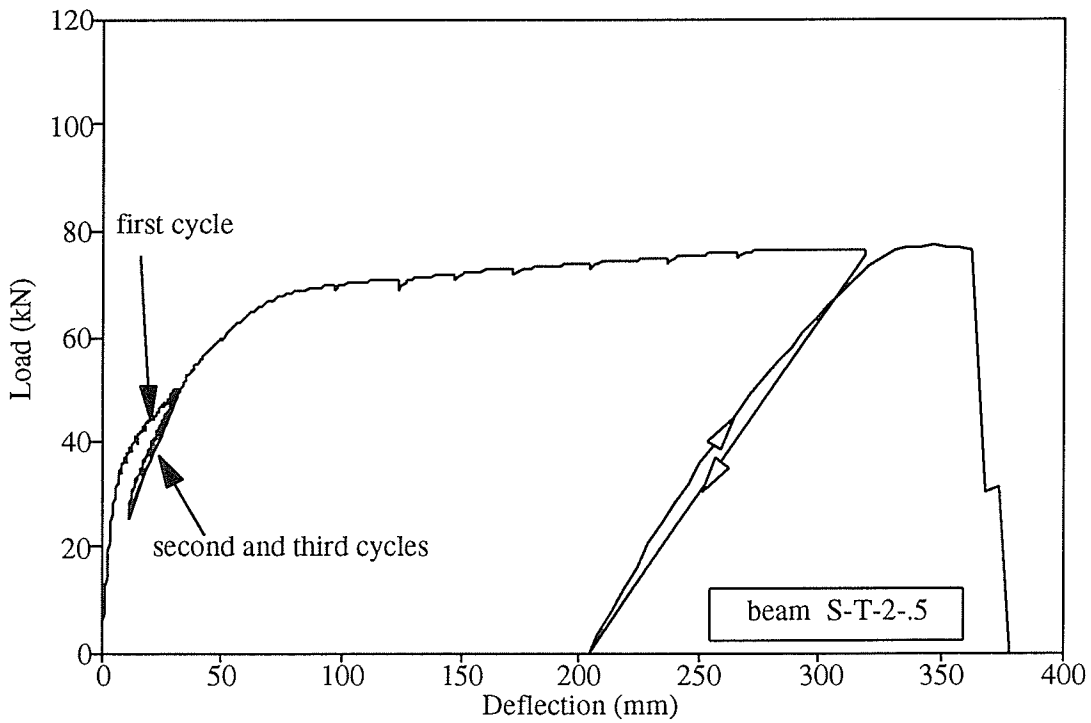


Fig.6-11 Typical Load-deflection of beam prestressed by steel

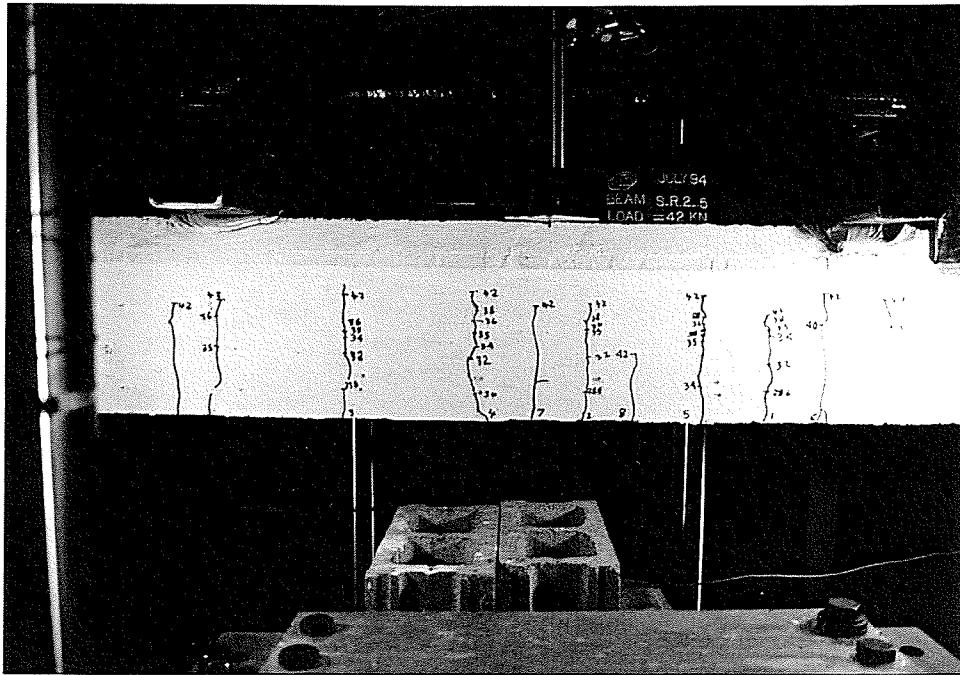


Fig.6-12 Cracking of beam S-R-2-5

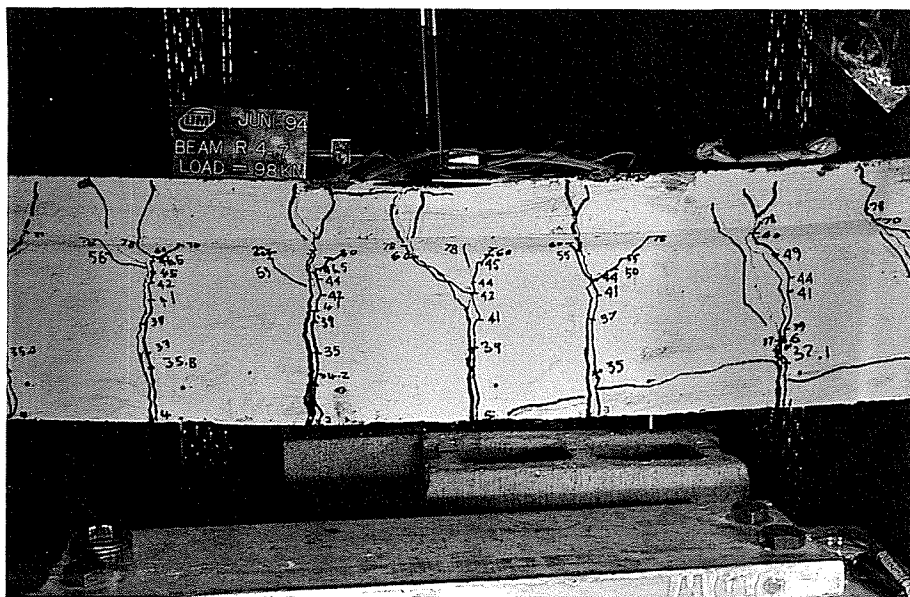


Fig.6-13 Failure due to rupture of Leadline bars

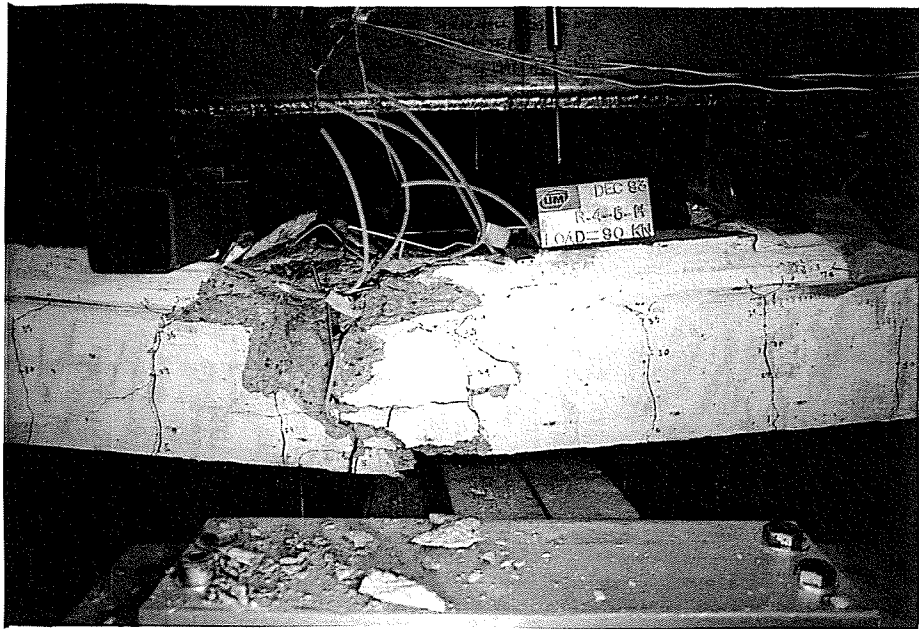


Fig.6-14 Failure due to crushing of concrete (beam prestressed by Leadline)

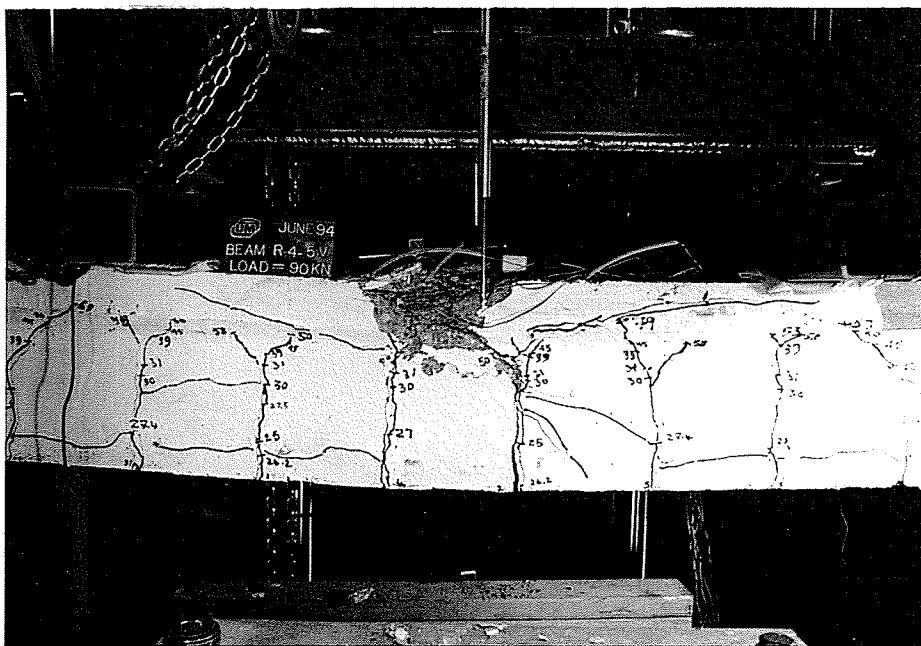


Fig.6-15 Beam R-4-5-V at failure

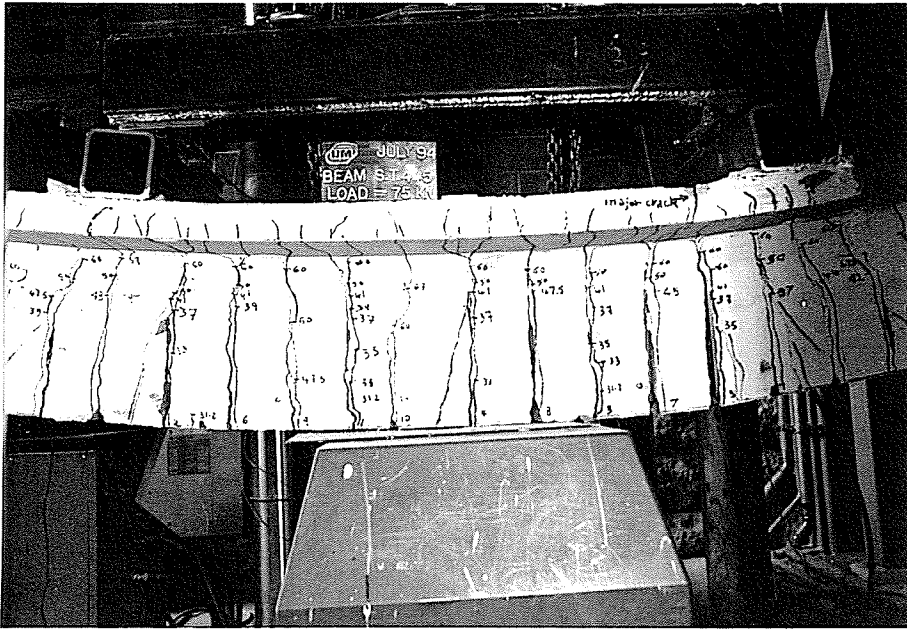


Fig.6-16 Failure of beam S-T-2-.5 prestressed by steel

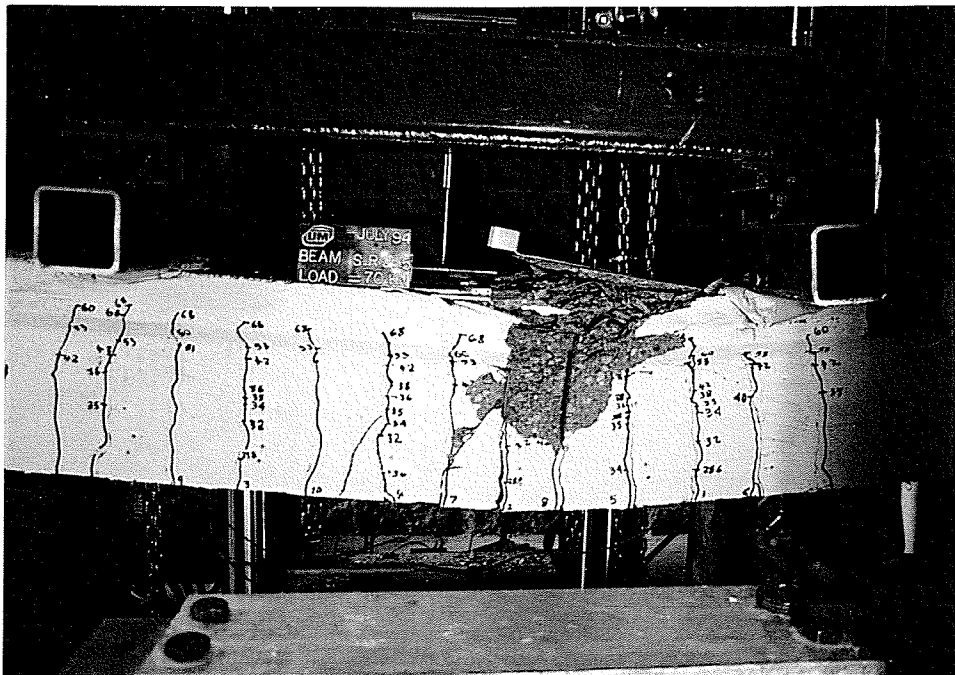


Fig.6-17 Failure of beam S-R-2-.5 prestressed by steel

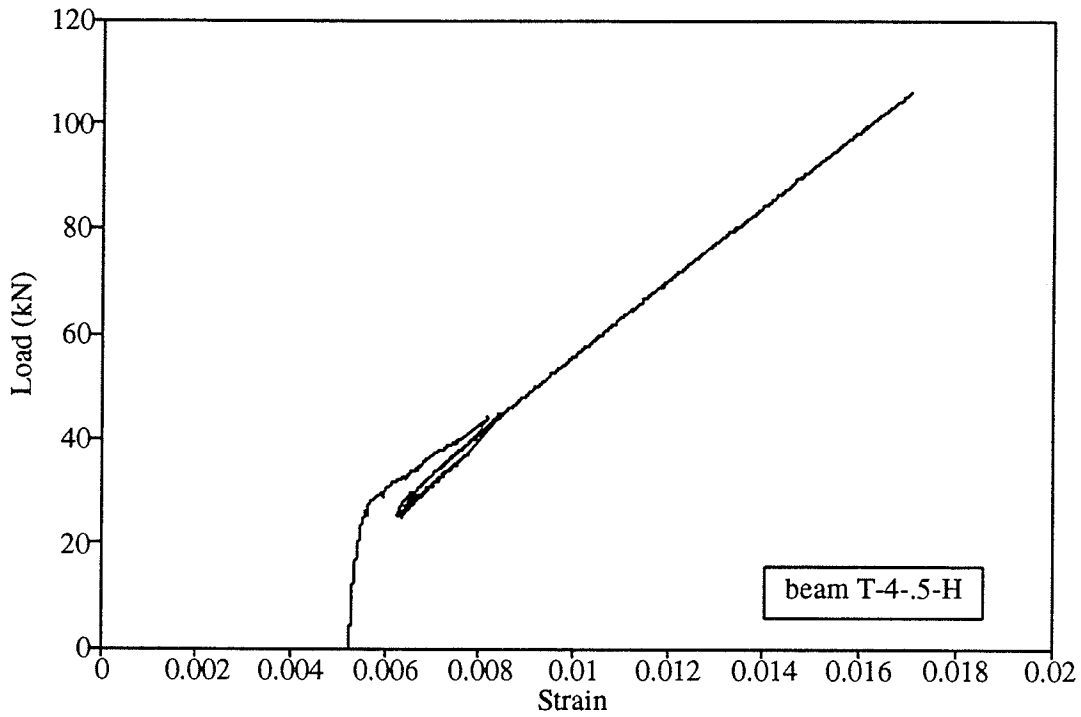


Fig.6-18 Typical load-strain relationship of beam prestressed by Leadline

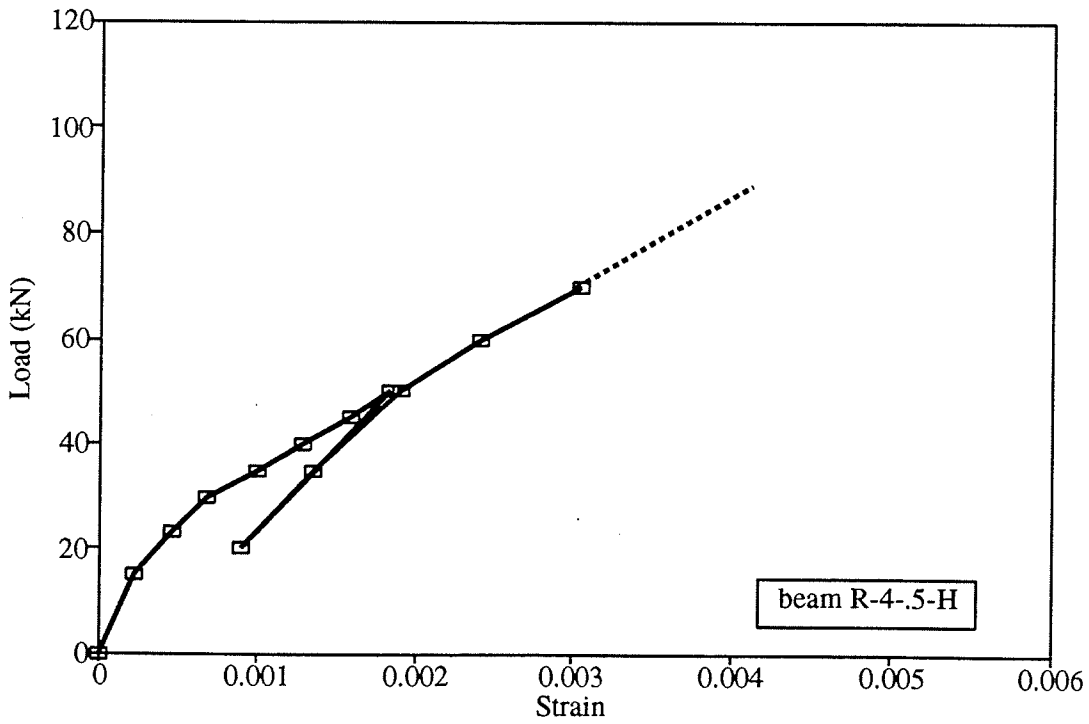


Fig.6-19 Concrete strain at the top surface for typical beam prestressed by Leadline

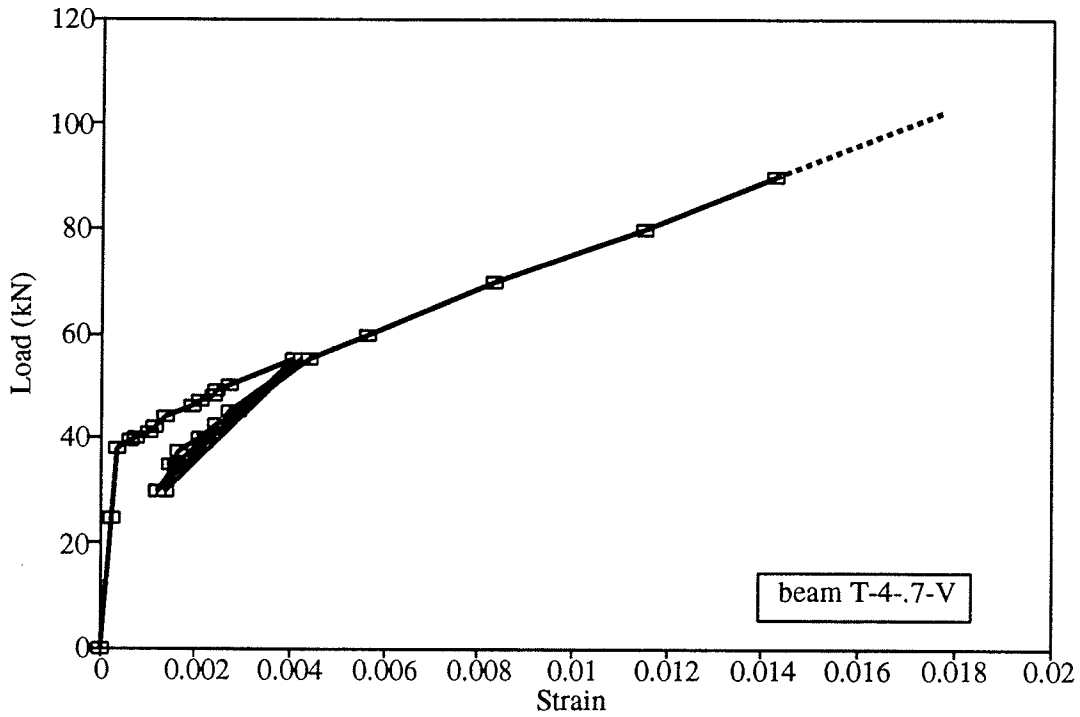


Fig.6-20 Concrete strain at reinforcement level for typical beam prestressed by Leadline

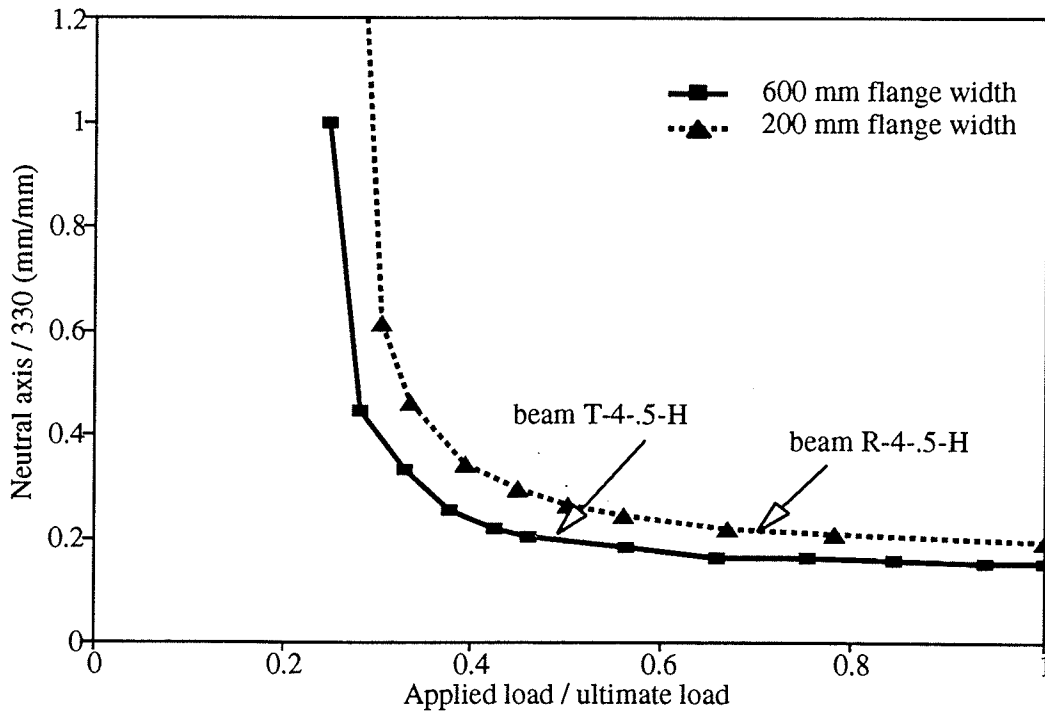


Fig.6-21 Neutral axis of beams with 600 and 200 mm flange width

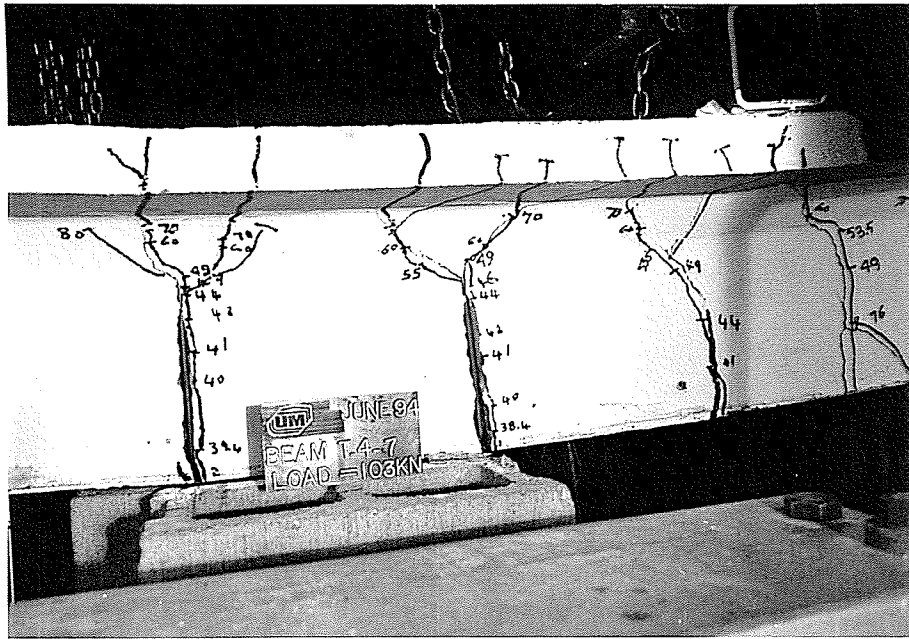


Fig.6-22 Beam T-4-7-V at failure

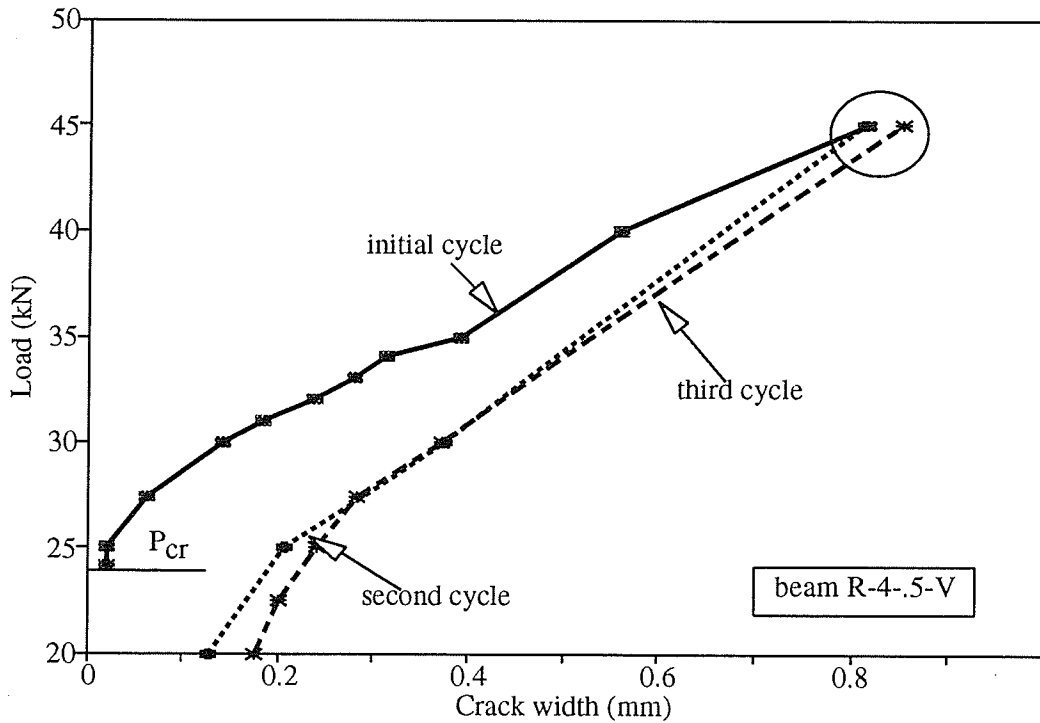


Fig.6-23 Average crack width for typical beam prestressed by Leadline

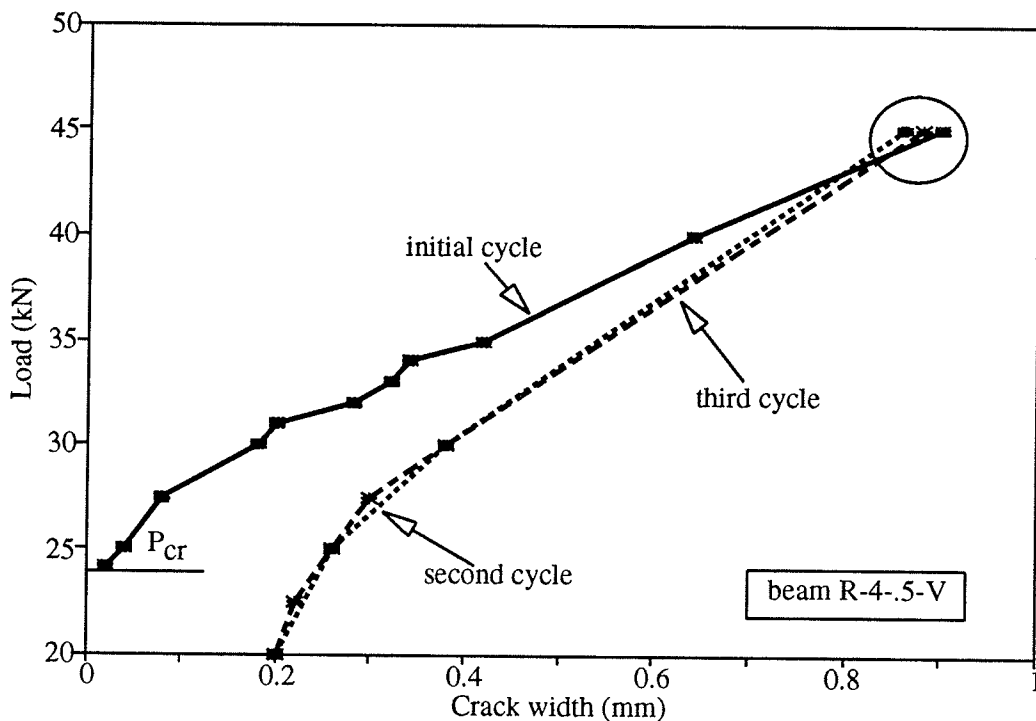


Fig.6-24 Maximum crack width for typical beam prestressed by Leadline

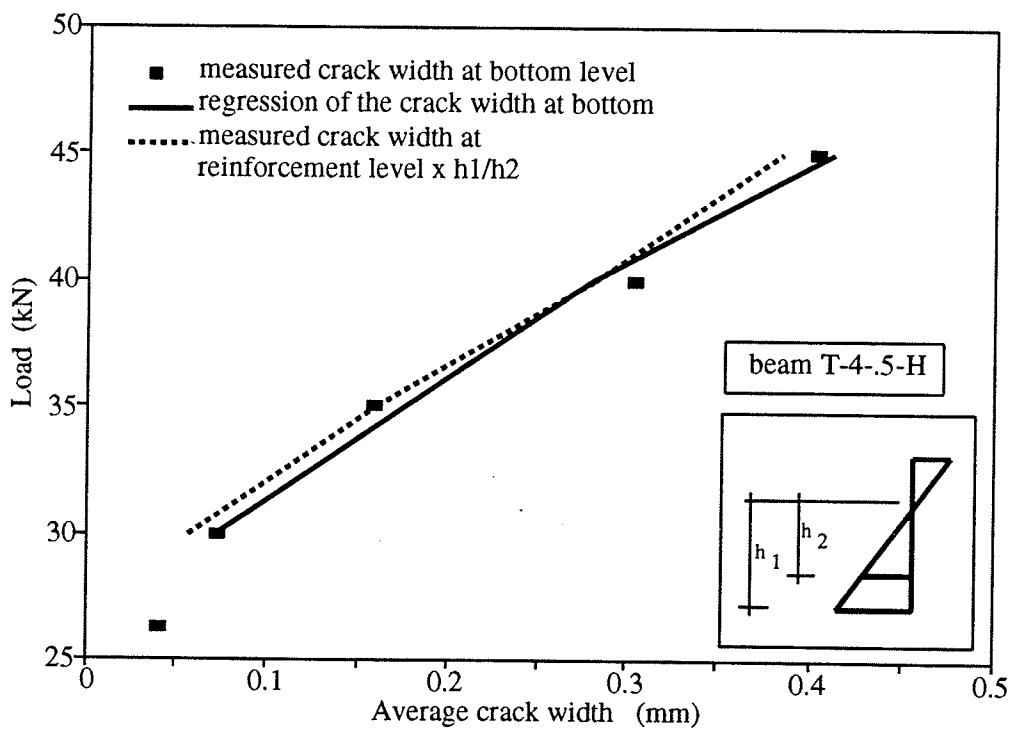


Fig.6-25 Average crack width measured at two levels below the neutral axis

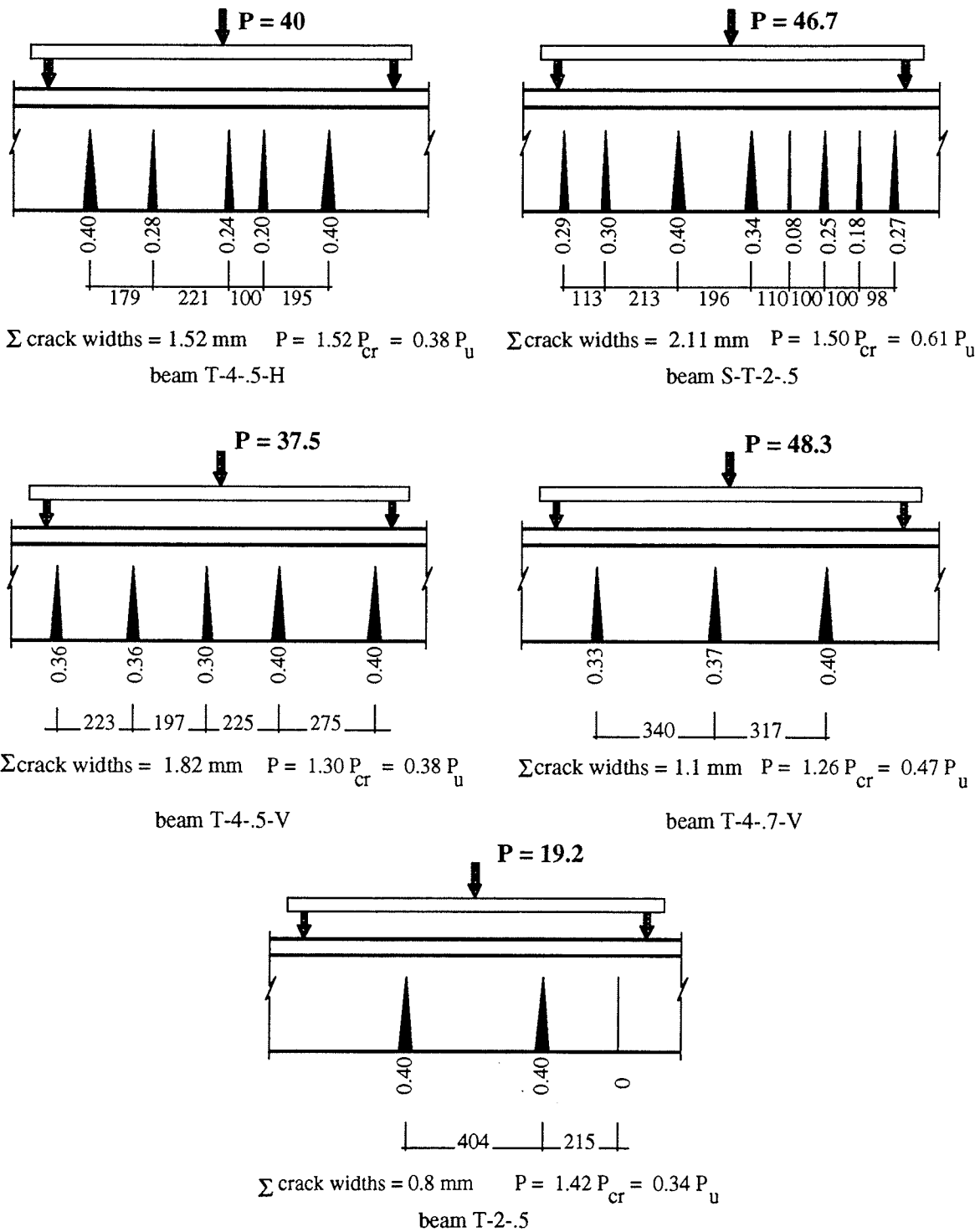


Fig.6-26 Crack distribution at service load for beams with 600 mm flange width

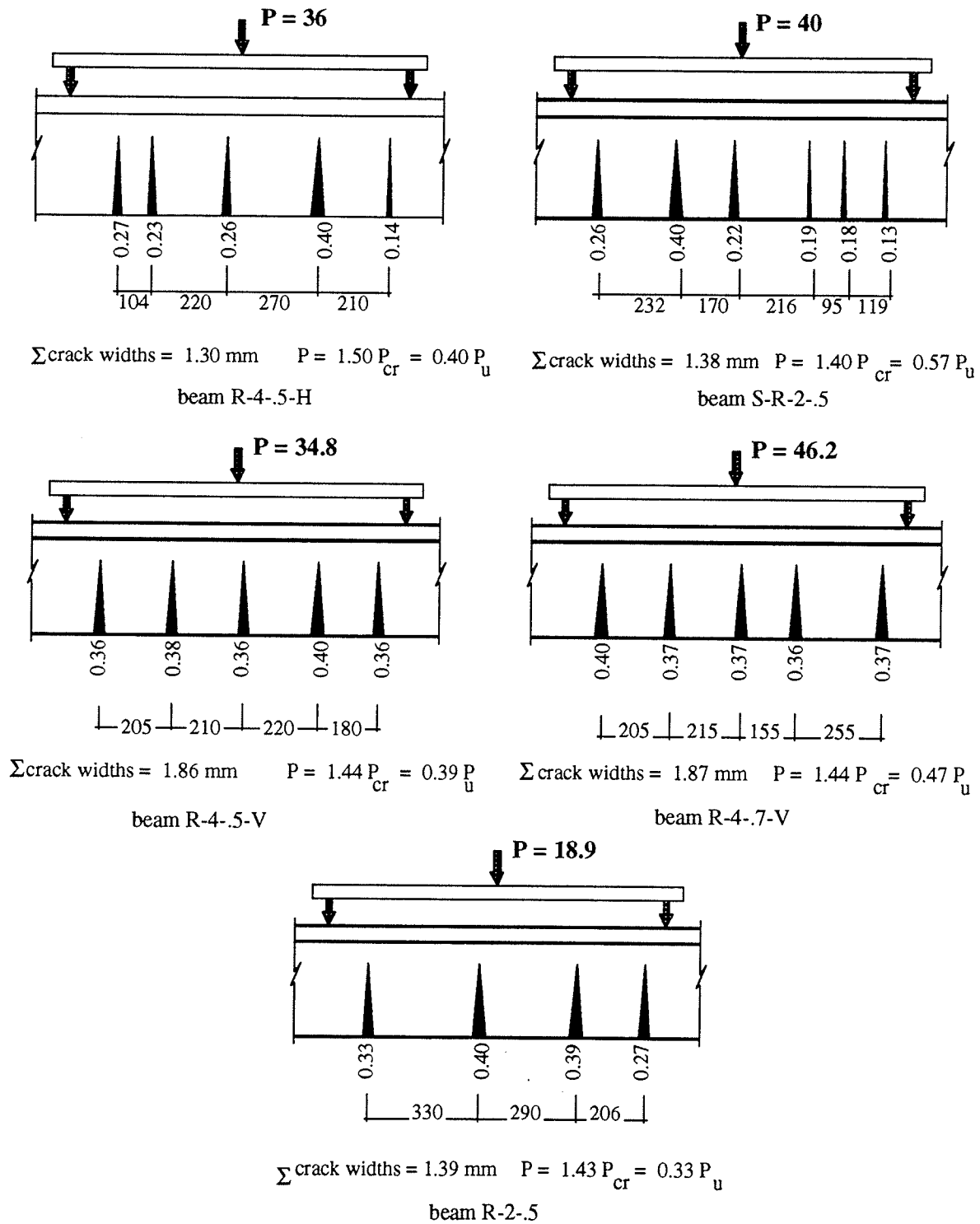


Fig.6-27 Crack distribution at service load for beams with 200 mm flange width

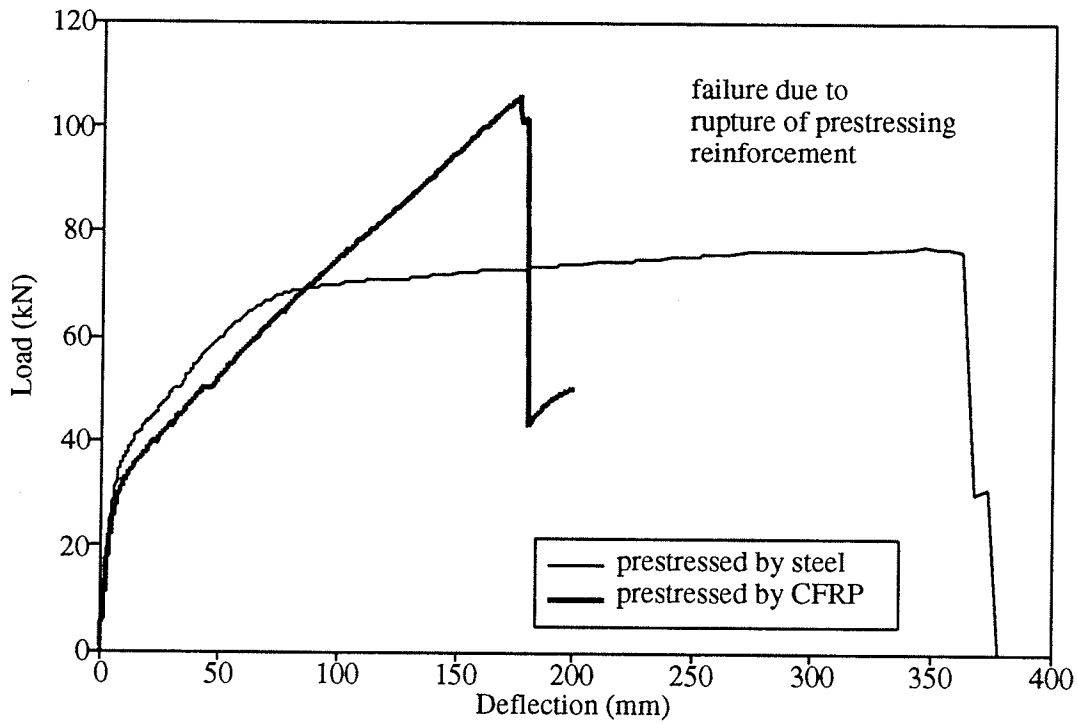


Fig.6-28a Load-deflection of beams prestressed by Leadline & steel (flange width = 600mm)

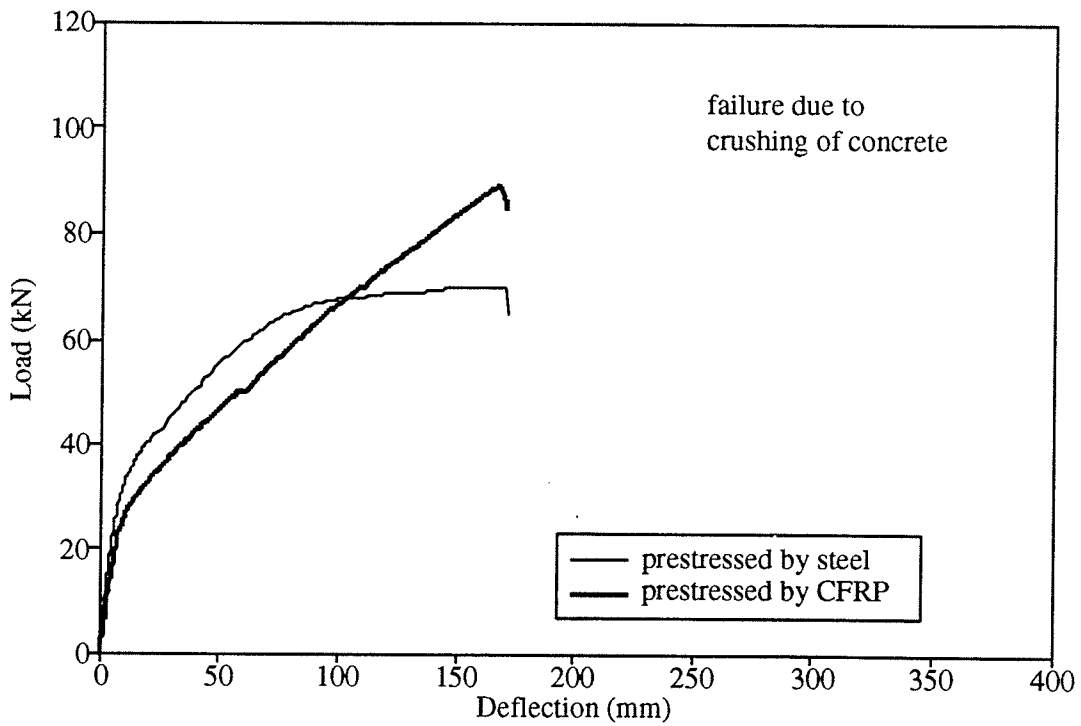


Fig.6-28b Load-deflection of beams prestressed by Leadline & steel (flange width = 200mm)

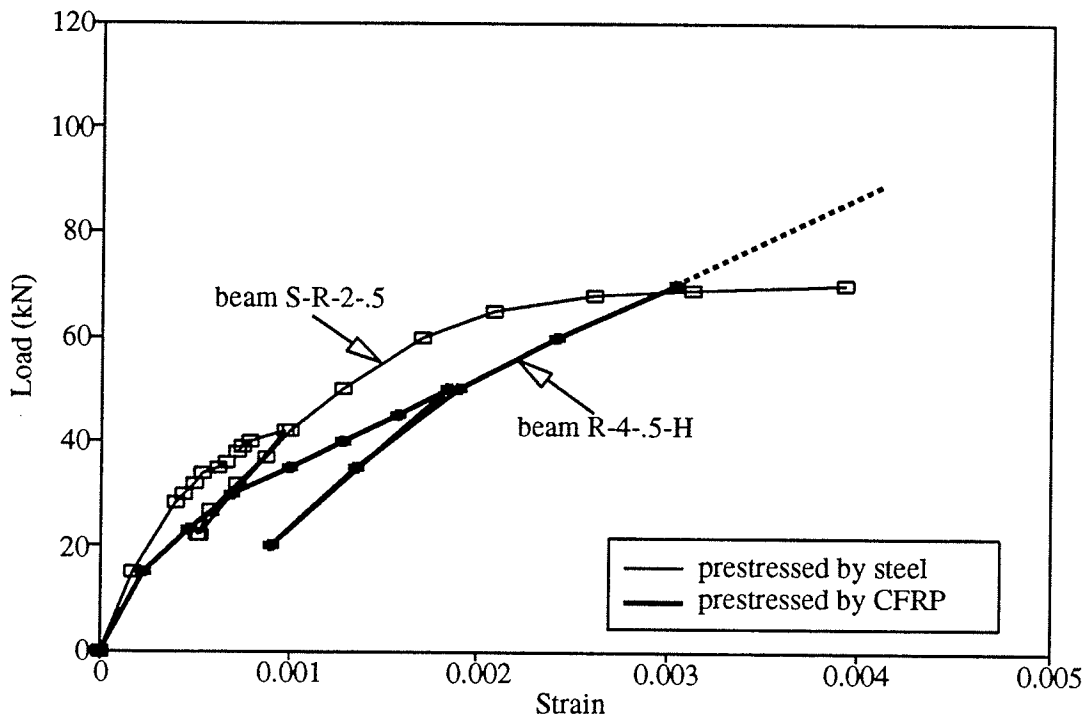


Fig.6-29 Concrete strain at the top surface of beams prestressed by Leadline & steel

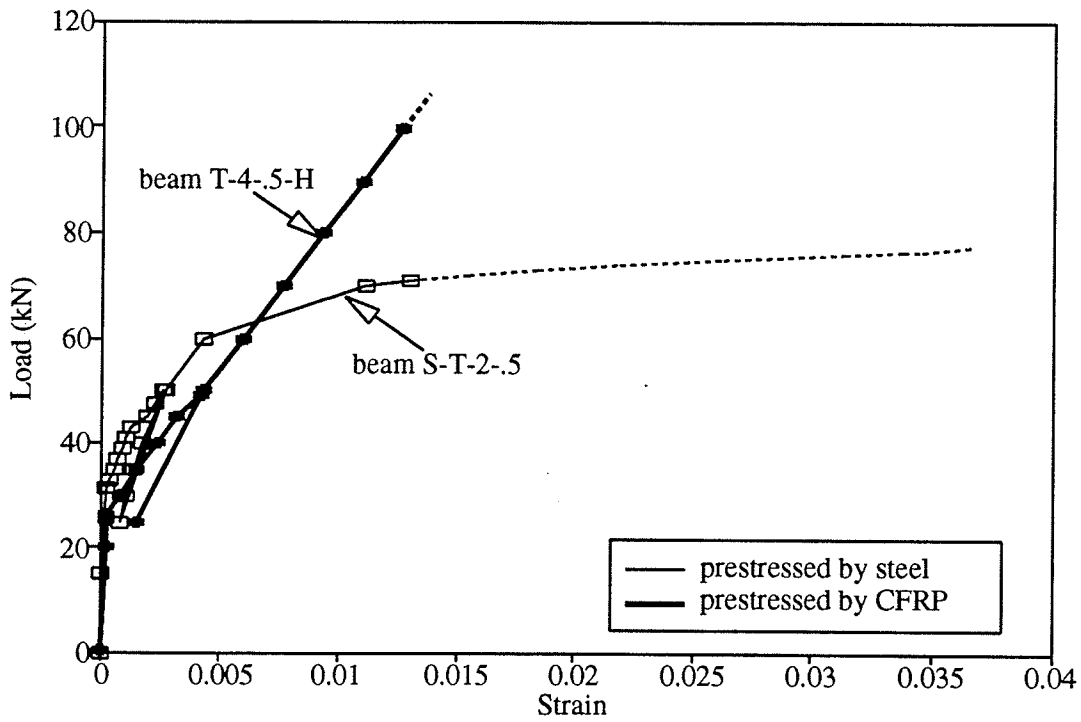


Fig.6-30 Concrete tensile strain of beams prestressed by Leadline & steel

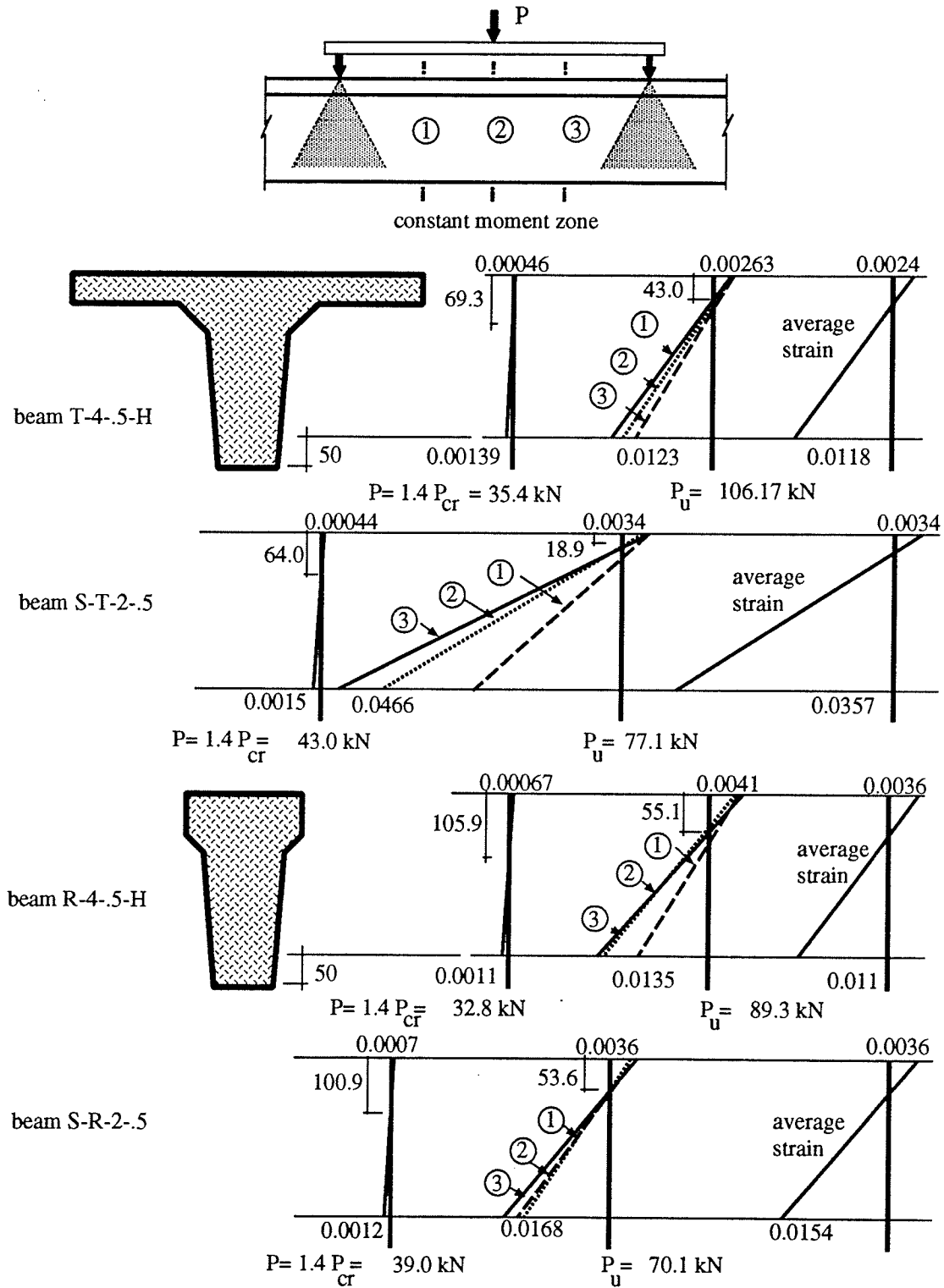


Fig.6-31 Strain distribution at the critical section of beams prestressed by Leadline & steel

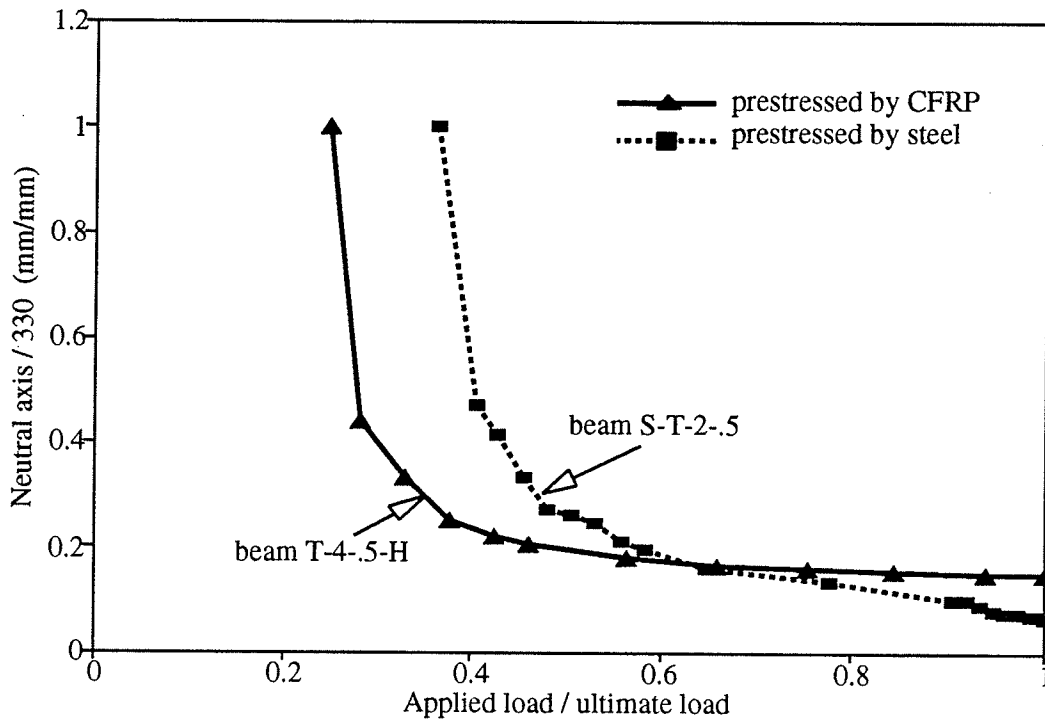


Fig.6-32a Neutral axis of beams with 600 mm flange width and prestressed by Leadline & steel

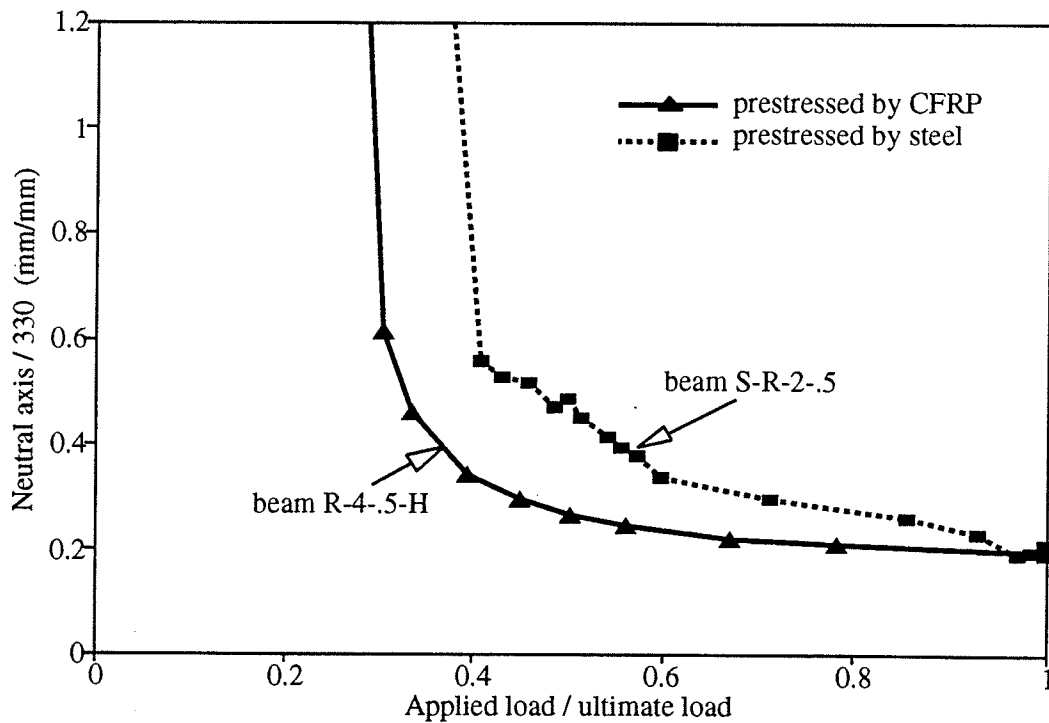


Fig.6-32b Neutral axis of beams with 200 mm flange width and prestressed by Leadline & steel

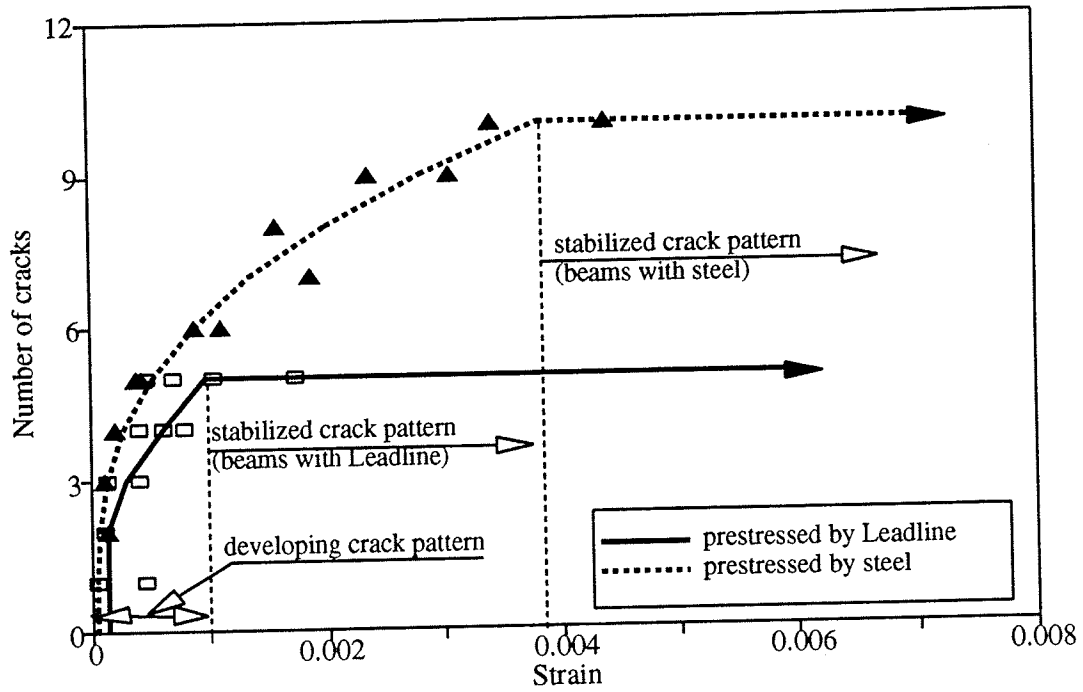


Fig.6-33 Number of cracks of beams prestressed by Leadline and steel

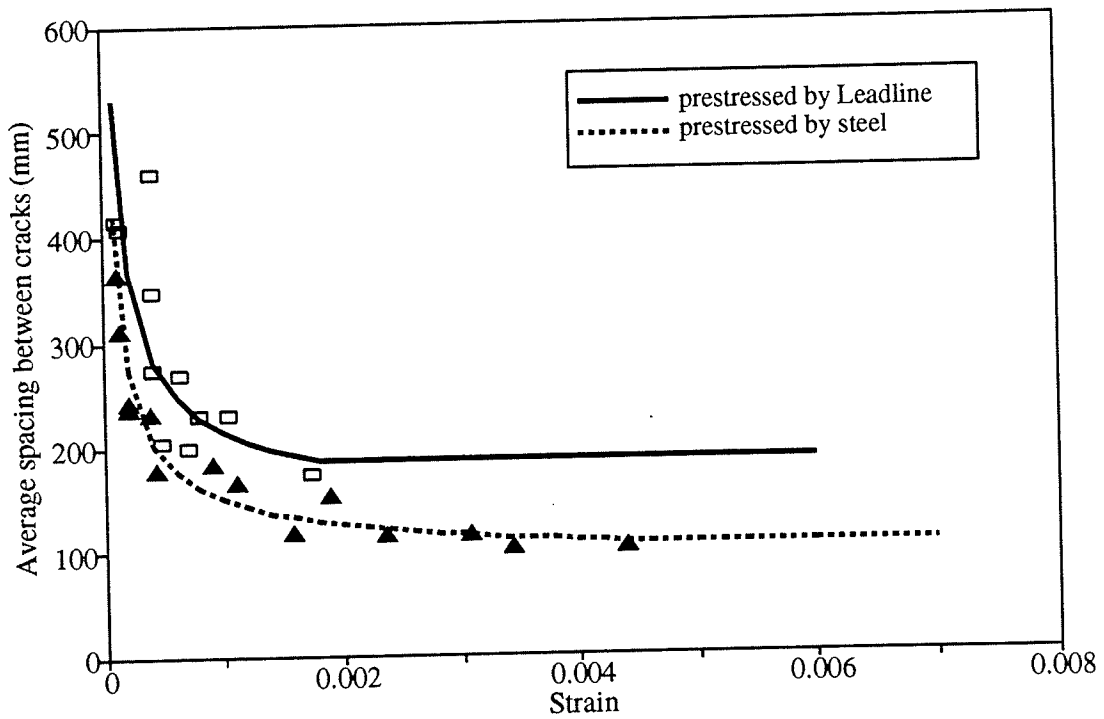


Fig.6-34 Spacing between cracks for beams prestressed by Leadline and steel

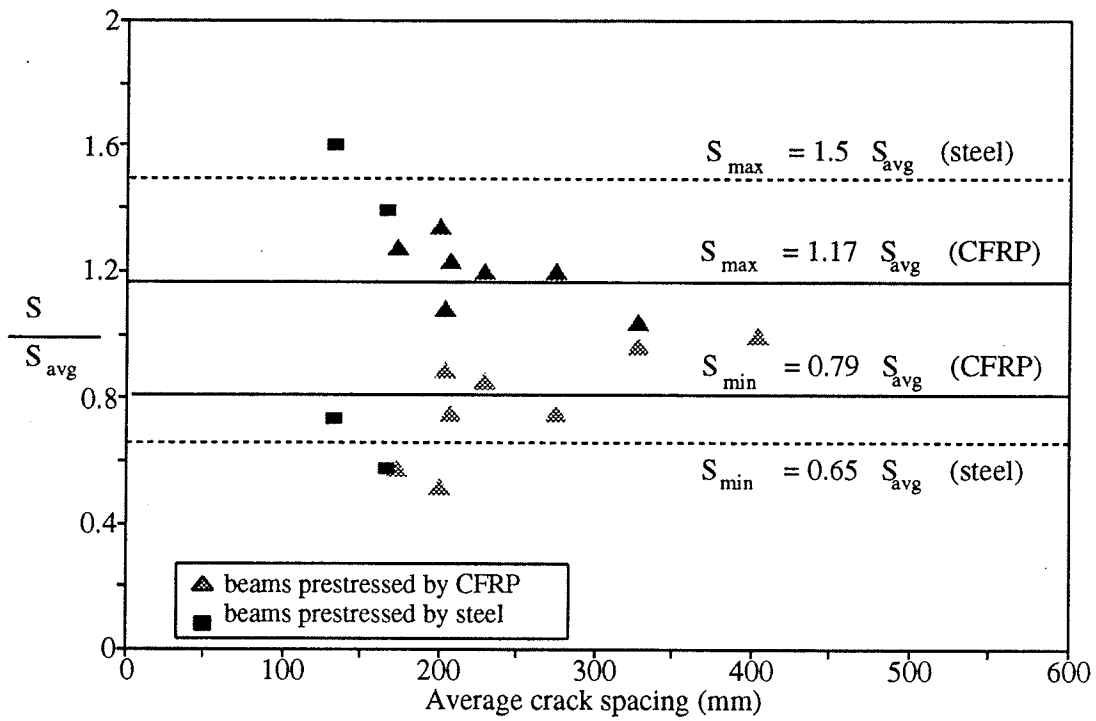


Fig.6-35 Variation of the crack spacing at service load limit

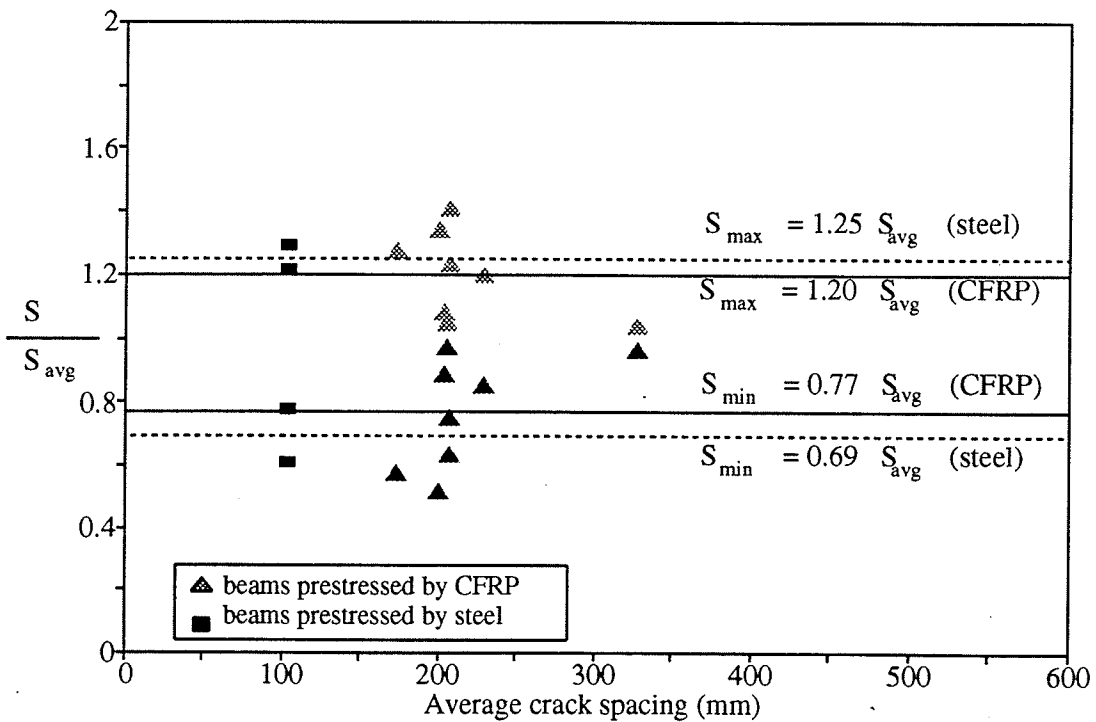


Fig.6-36 Variation of the crack spacing at ultimate load

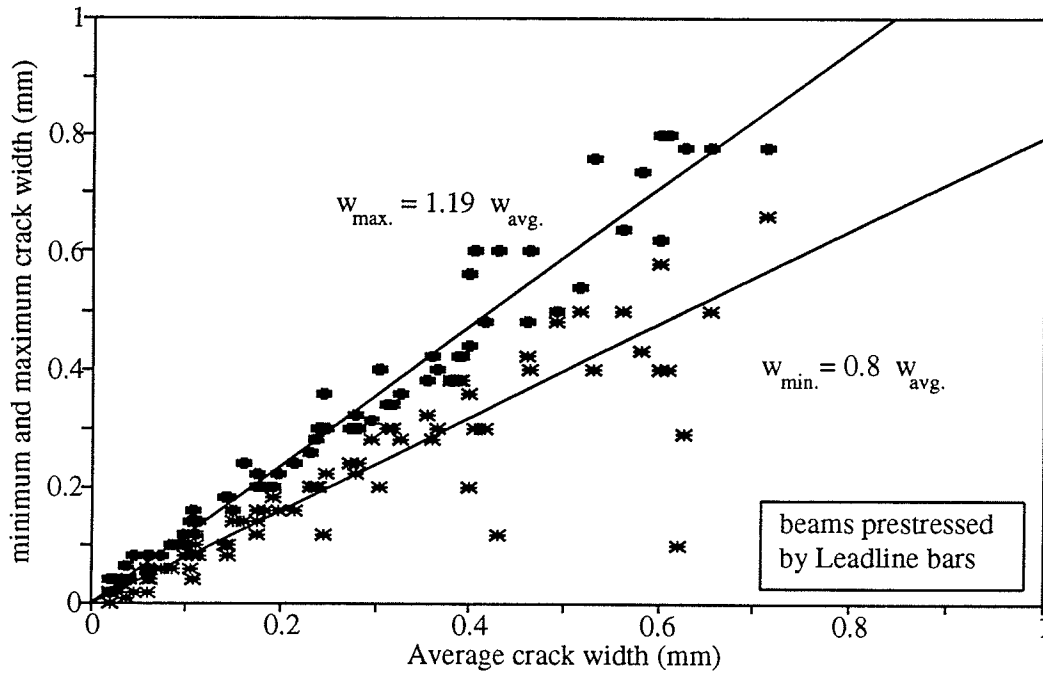


Fig.6-37a Variation of the crack width of beams prestressed by Leadline

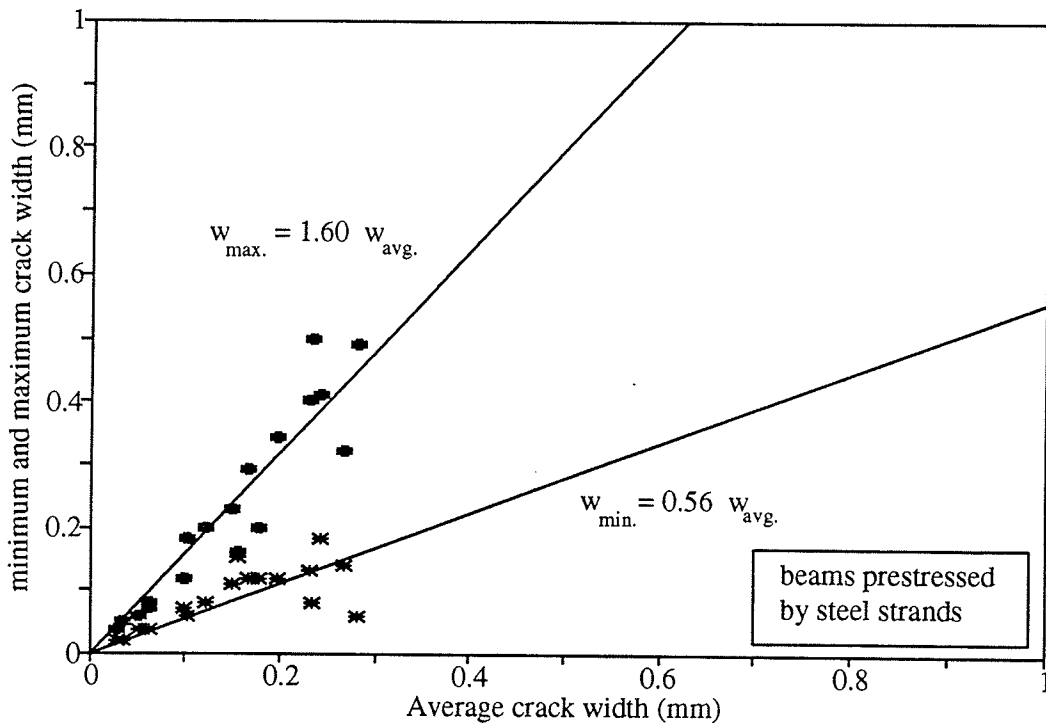


Fig.6-37b Variation of the crack width of beams prestressed by steel

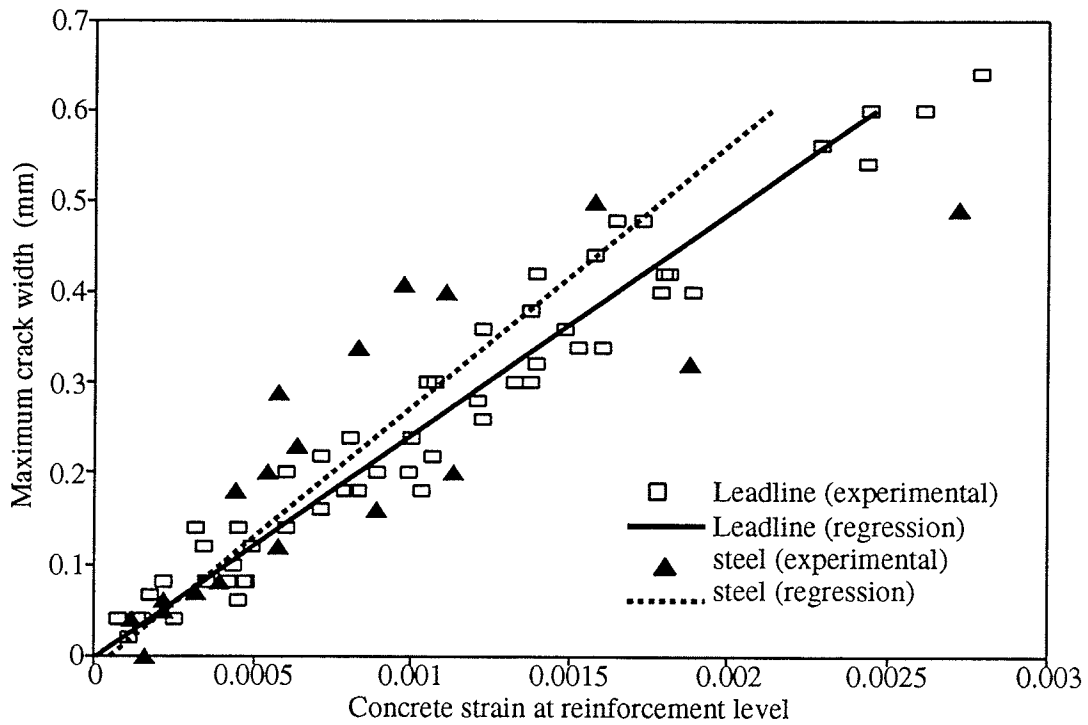


Fig.6-38 Maximum crack width vs. the measured strain of beams prestressed by Leadline & steel

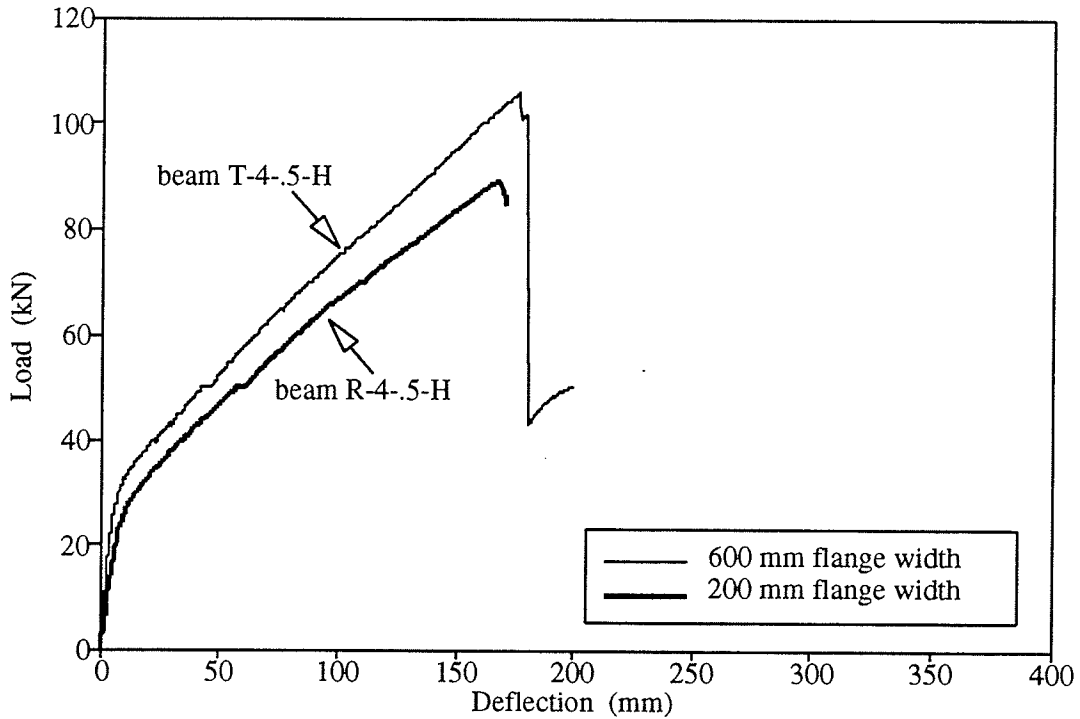


Fig.6-39 Load-deflection of beams with 600 and 200 mm flange width

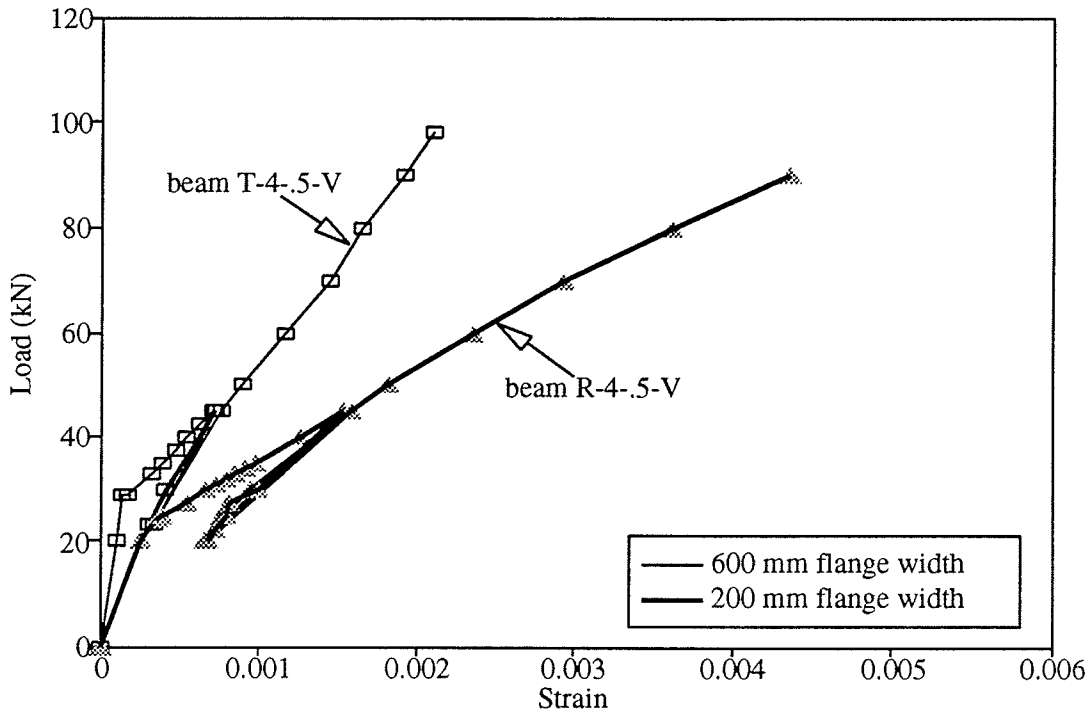


Fig.6-40a Concrete strain at the top surface of beams with 600 and 200 mm flange width

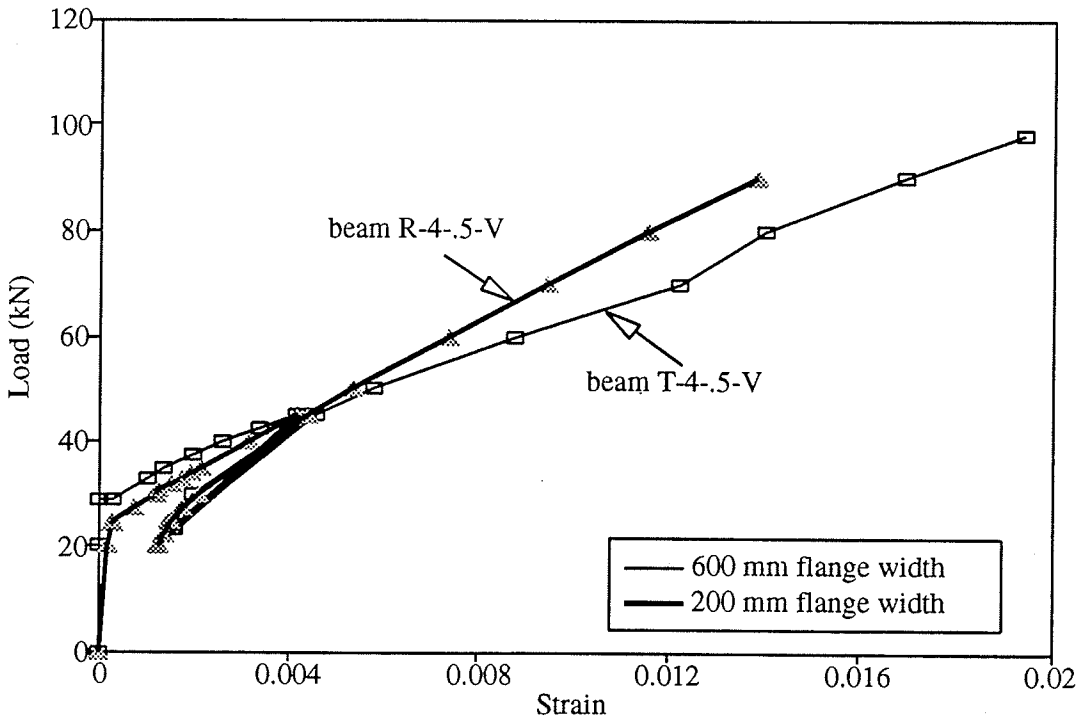


Fig.6-40b Concrete strain at reinforcement level of beams with 600 and 200 mm flange width

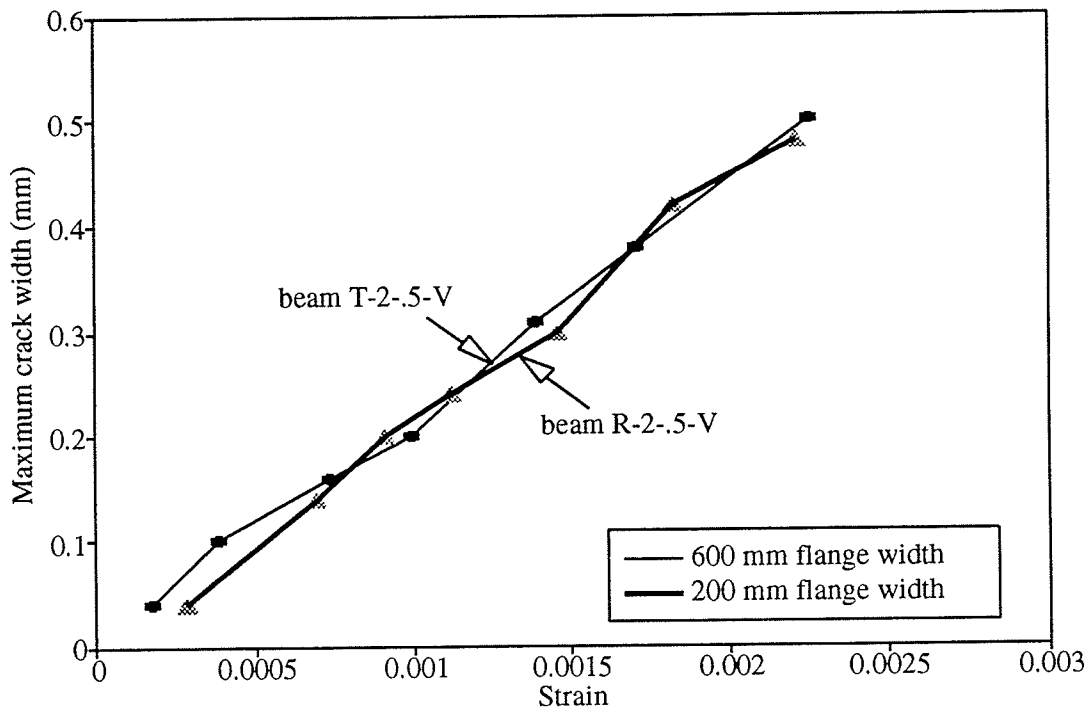


Fig.6-41 Maximum crack width of beams with 600 and 200 mm flange width

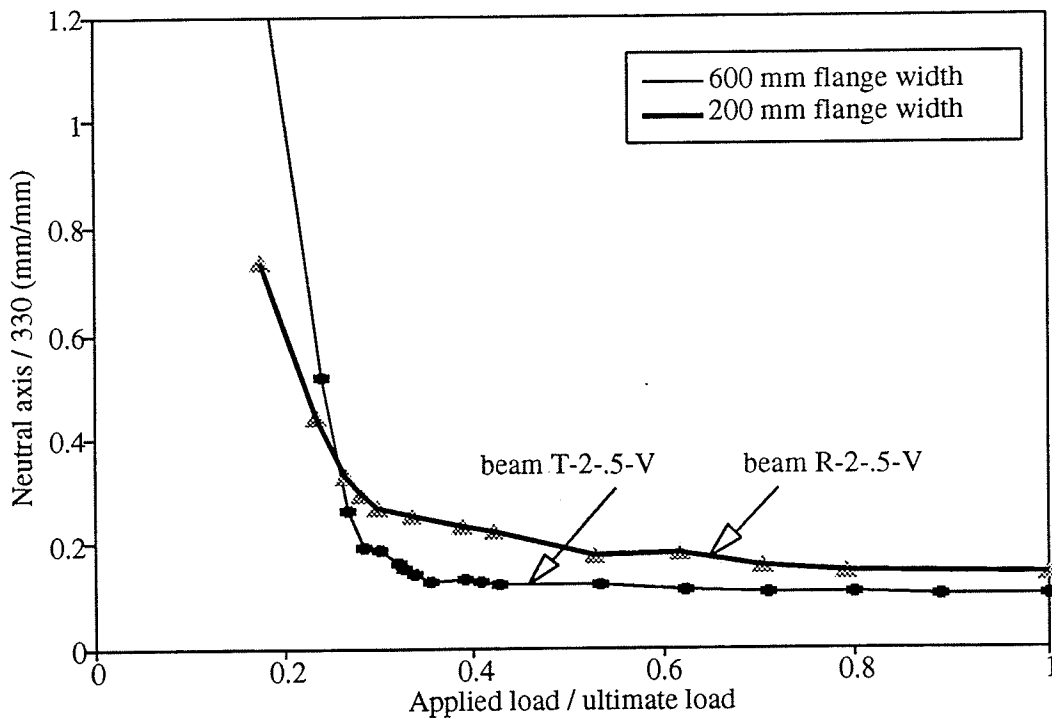


Fig.6-42 Neutral axis of beams with 600 and 200 mm flange width

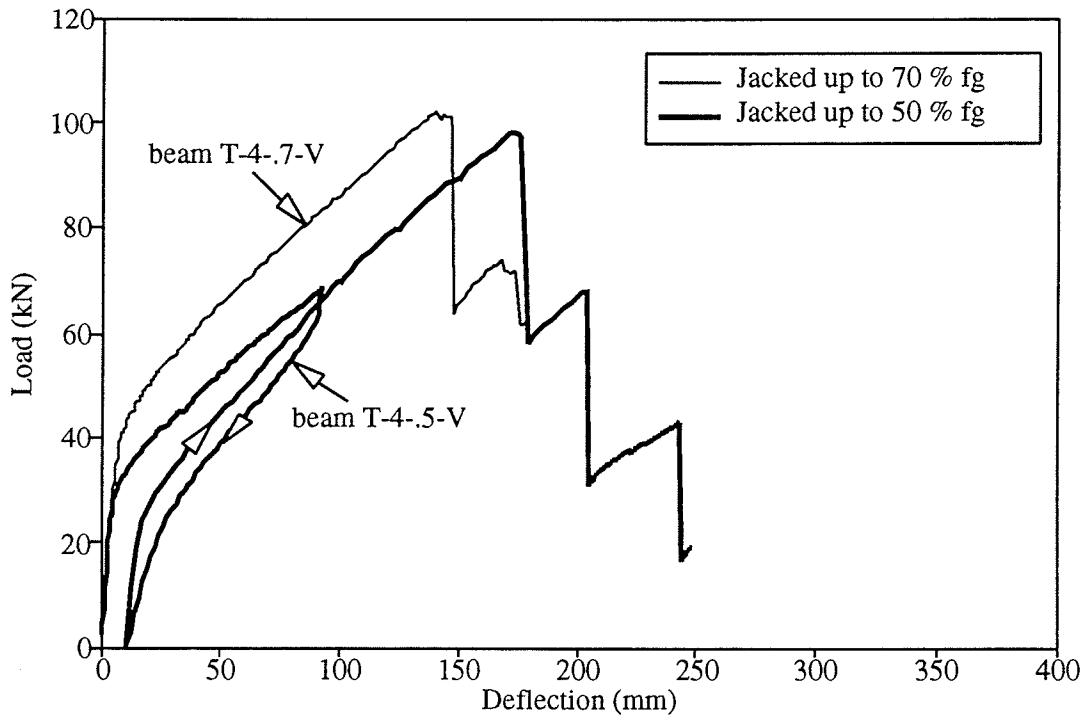


Fig.6-43 Load-deflection of beams with different jacking stress

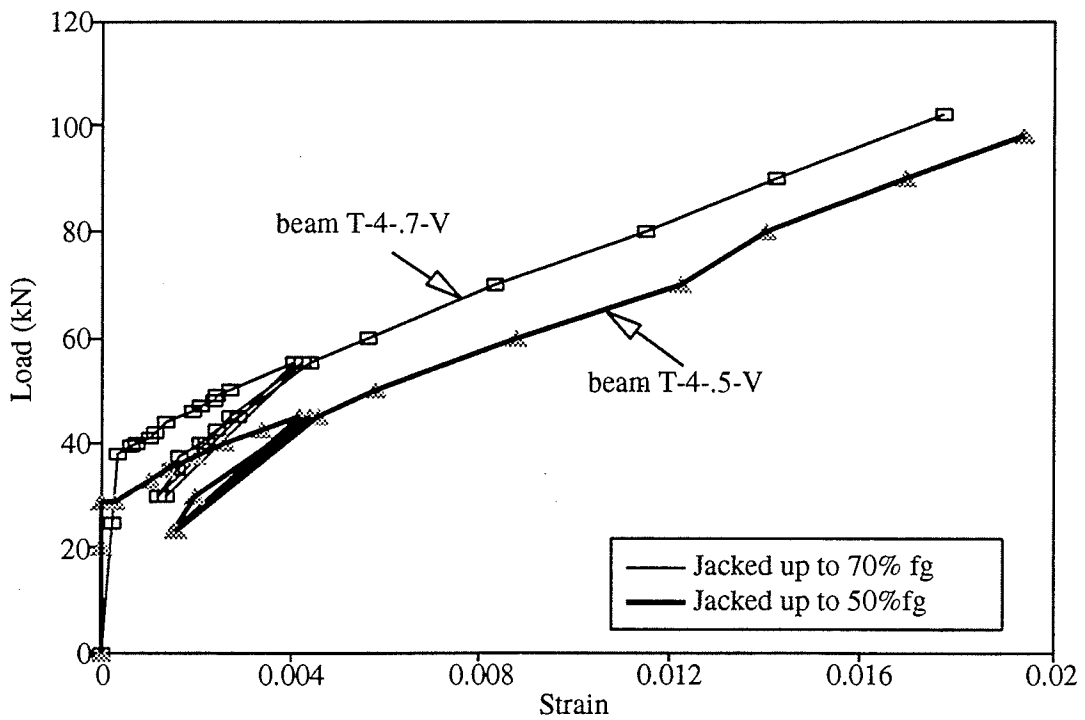


Fig.6-44 Concrete strain at reinforcement level of beams with different jacking stress

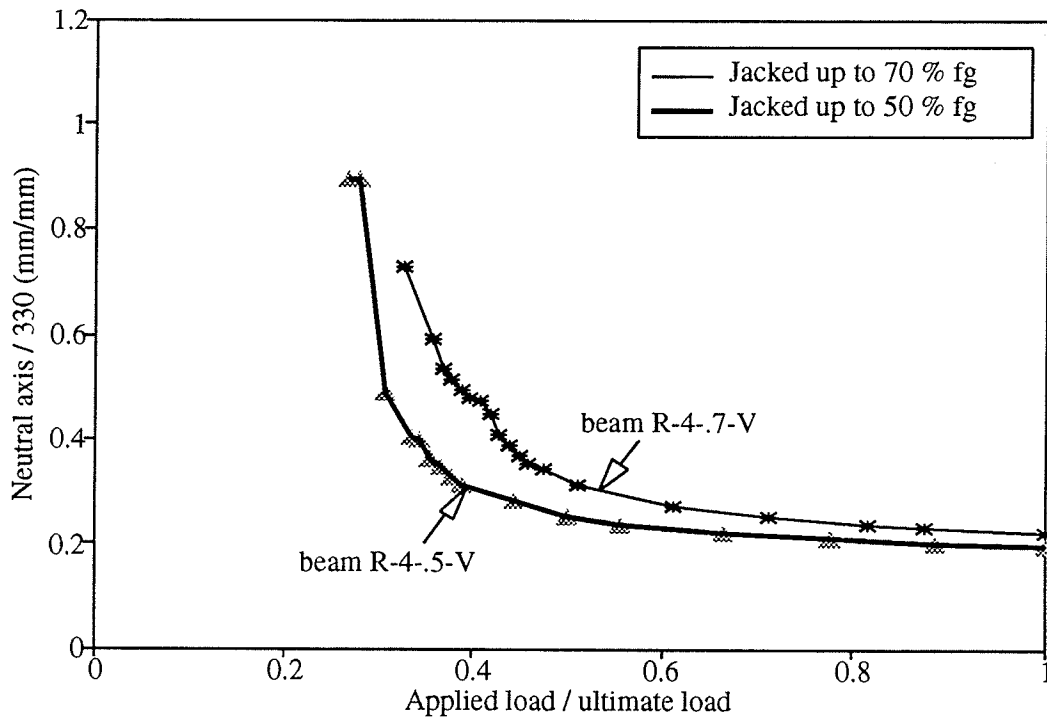


Fig.6-45 Neutral axis of beams with different jacking stress

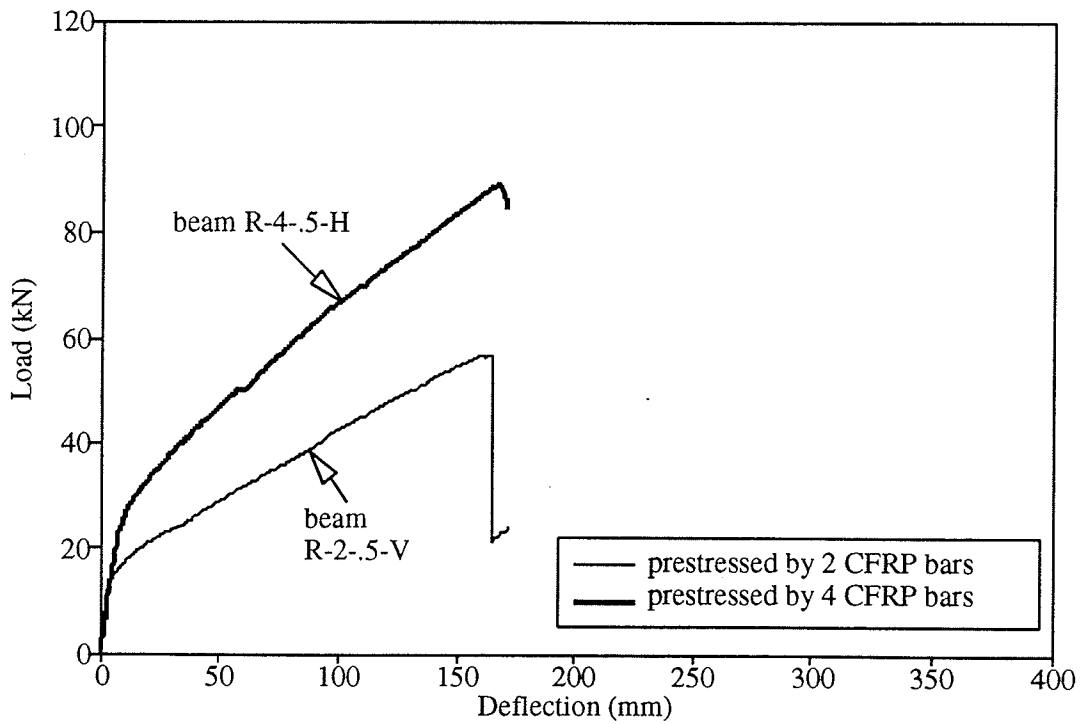


Fig.6-46 Load-deflection of beams with different number of Leadline bars

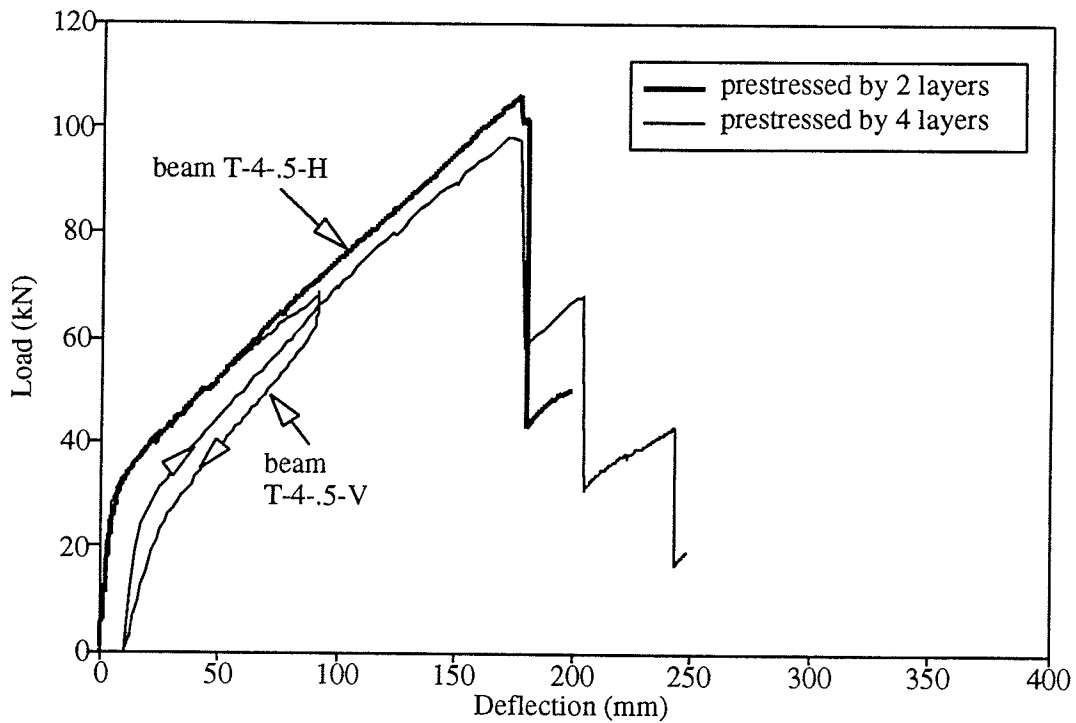


Fig.6-47 Load-deflection of beams with different distribution of the Leadline bars in the tension zone

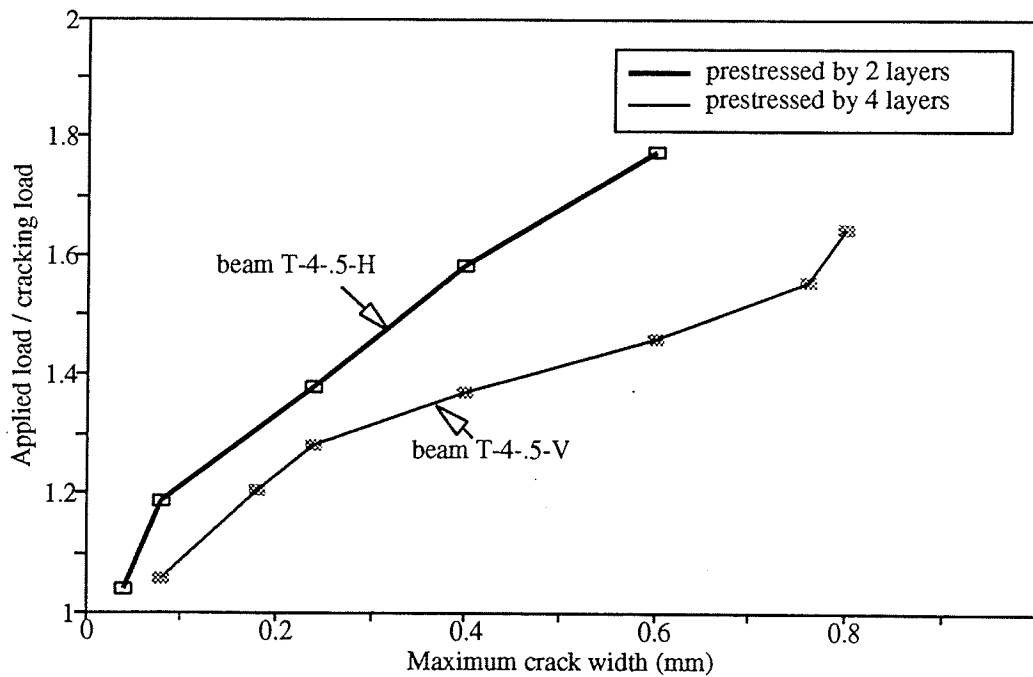


Fig.6-48 Maximum crack width of beams with different distribution of the Leadline bars in the tension zone

7. _____ FLEXURAL ANALYSIS

7.1 ANALYSIS PROCEDURE

The tested beams were analyzed using a strain compatibility approach to predict the flexural response up to failure. The concrete is assumed to be subjected to uniaxial strains uniform over the entire width of the section. The analysis also assumes that the strains are linear over the depth of the section, which means that plane sections remain plane after bending. This method is widely used for prestressed members subjected to flexure and is described in many text books (eg. Collins and Mitchell 1991). The analysis procedure was performed using a computer program to predict the response of the beams, according to the following steps:

1. Assume a strain at the extreme compression fibre of the concrete.
2. Assume a neutral axis depth.
3. Determine the internal forces in the compression and the tension zones based on the tensile strains at every layer of the prestressing reinforcement as shown in Fig. 7-1.
4. Check the equilibrium of the section according to equation 7-1, taking into

consideration the initial strain in the prestressing reinforcement as shown in equation 7-2.

5. Revise the assumption of the neutral axis depth until equilibrium is satisfied.
6. Calculate the internal moment of the section according to equation 7-3.
7. Increase the concrete strain at the top fibre and repeat steps b to f.
8. Calculate the moment-curvature relationship, ignoring the tension stiffening at every strain increment using equation 7-4.

$$\int_{A_c} f_c dA_c + \int_{A_p} f_p dA_p = 0 \quad 7-1$$

$$\epsilon_p = \epsilon_c \frac{d_p - c}{c} + \epsilon_{ce} + \epsilon_e \quad 7-2$$

$$\int_{A_c} f_c y dA_c + \int_{A_p} f_p y dA_p = M \quad 7-3$$

$$\phi = \frac{\epsilon_c}{c} \quad 7-4$$

where y = distance, measured from the neutral axis;
 M = bending moment;
 f_c = concrete stress in compression;
 A_c = area of concrete;

-
- f_p = stress of the prestressed reinforcement;
- A_p = area of the prestressed reinforcement;
- ϵ_p = total strain in the prestressing reinforcement;
- ϵ_c = concrete strain at the compression fibre;
- ϵ_{ce} = concrete strain at the level of the prestressing reinforcement, due to the prestressing force;
- ϵ_e = effective strain in the prestressing reinforcement after losses;
- c = neutral axis depth from the compression fibre;
- d_p = depth of the prestressing reinforcement from compression fibre; and
- ϕ = curvature at the given strain increment.

7.1.1 Cracking Moment Calculation

The cracking moment calculated using two methods. The first method was based on the equilibrium and compatibility conditions as described above. The strain in the extreme tension fibre of concrete was assumed to be equal to the rupture strain of the concrete. The rupture strain of the concrete was calculated using a tensile elastic modulus equal to the elastic modulus of the concrete in compression, measured from testing the concrete cylinders. The neutral axis depth was calculated by trial and error until equilibrium of the section was achieved. The internal forces considered in the analysis were the compression and tension in the concrete, the tensile force in the prestressed

reinforcement, and the compressive force in the non-prestressed reinforcement.

In the second method, the cracking moment was calculated based on the gross section properties using equation 7-5.

$$M_{cr} = P_e e + \left[f_r + \frac{P_e}{A_g} \right] S_b \quad 7-5$$

- where M_{cr} = cracking moment;
- P_e = effective prestressing force;
- e = eccentricity of the prestressing reinforcement based on gross section properties;
- f_r = rupture strength of concrete;
- A_g = gross cross sectional area; and
- S_b = section modulus of the tension side.

7.1.2 Failure Criteria

The failure modes of beams prestressed by Leadline bars are similar to beams prestressed by steel reinforcement. The three modes are crushing of concrete, rupture of Leadline, and simultaneous crushing of concrete and rupture of Leadline. Therefore, the failure of the beams is controlled by either the compressive strain in the concrete at the

extreme compression fibre or the tensile strain at the Leadline bar farthest from the neutral axis. Specifically, the failure criteria of beams prestressed by Leadline are any of the following:

- 1- Crushing of concrete when the concrete strain in compression reaches the ultimate value.
- 2- Rupture of the Leadline when the tensile strain of the Leadline bar at the layer of prestressing reinforcement farthest from the neutral axis reaches a value of 2.0 percent, which corresponds to an ultimate tensile strength of 2950 MPa, taking into consideration the initial strain due to jacking. After rupture of the Leadline bar farthest from the neutral axis, the beam continues to carry load until the next Leadline bars rupture.
- 3- Balanced failure can occur if the reinforcement achieves 2.0 percent strain simultaneously with the ultimate compressive strain at the extreme fibres of the concrete.

7.2 MATERIAL MODELLING

The three materials used in the study were concrete, Leadline bars and prestressing steel strands. The materials were modelled using measured values from the control specimens and the analytical models available in the literature.

7.2.1 Concrete

The stress-strain relationship of the concrete was modelled using the parabolic relationship in compression illustrated in Fig. 7-2. The internal compression force in the concrete was evaluated using the stress-block factors introduced by Collins and Mitchell (1991). Instead of using the parabolic stress distribution, an equivalent uniform stress distribution was employed, as shown in Fig. 7-1. For a given parabolic compression stress distribution, the stress block factors α_1 and β_1 were calculated such that the magnitude and location of the resultant force did not change. The resultant force of the uniform stress block was maintained equal to the force resulting from the parabolic concrete stress distribution using equation 7-6. For a parabolic stress-strain curve and constant beam width b , equation 7-6 can be reduced to equation 7-7. To satisfy the requirement that the location of the resultant force is the same for the uniform and parabolic distributions, equation 7-8 was used which can also be reduced to equation 7-9.

$$\int_0^c f_c b dy = \alpha_1 f_c' \beta_1 c b \quad 7-6$$

$$\alpha_1 \beta_1 = \frac{\epsilon_c}{\epsilon_c'} - \frac{1}{3} \left(\frac{\epsilon_c}{\epsilon_c'} \right)^2 \quad 7-7$$

$$\bar{y} = \frac{\int_0^c f_c b y dy}{\int_0^c f_c b dy} \quad 7-8$$

$$\beta_1 = \frac{4 - \frac{\epsilon_c}{\epsilon'_c}}{6 - \frac{2 \epsilon_c}{\epsilon'_c}} \quad 7-9$$

where ϵ_c = concrete strain for a given loading condition;
 ϵ'_c = concrete strain corresponding to the maximum stress; and
 ϵ_{cu} = ultimate strain of the concrete in compression.

Since the stress-strain relationship of the concrete changes with the change of rate of loading, the maximum concrete strain in compression was measured and was found to be about 0.004. The rupture strength, f_r , and the elastic modulus of concrete, E_c , were determined based on control specimens for each batch of concrete as given in chapter 5. The concrete strain corresponding to the maximum stress was related to the measured concrete strength and elastic modulus in compression, as given by equation 7-10 (Park and Paulay 1975).

$$\epsilon'_c = \frac{2 f'_c}{E_c} \quad 7-10$$

The rupture strength of concrete was assumed according to the Canadian Code CSA (1984) and given by equation 7-11. The factor a in equation 7-11 is given as 0.6. The tensile elastic modulus of concrete was assumed to be equal to the elastic modulus in compression (Park and Paulay 1975 and Collins and Mitchell 1991). After cracking, concrete in tension was neglected.

$$f_r = a \sqrt{f'_c} \quad 7-11$$

7.2.2 Leadline

The stress-strain behaviour of the Leadline bars was assumed to be linearly elastic up to failure. A tensile elastic modulus of 147 GPa was used, based on the value reported by the manufacturer. An ultimate tensile strength of 2950 MPa was also used in the analysis, based on the tensile test performed with a concrete anchorage. The ultimate tensile strain was calculated based on the assumed elastic modulus and tensile strength and was found to be 2.0 percent. It should be noted that the guaranteed tensile strength of the Leadline, which was the basis for the calculation of the jacking force, was 1970 MPa.

7.2.3 Steel

The tensile properties were based on testing of 13-mm-diameter steel strands in tension, as given in chapter 5. The tensile strength and modulus used in the analysis were 1900 MPa and 180 GPa, respectively. The strain of the steel strand at rupture was 4.3 percent. The modified Ramberg-Osgood function, given in chapter 5 for the tested steel strand, was used to model the behaviour.

7.3 COMPARISON BETWEEN ANALYTICAL AND EXPERIMENTAL RESULTS

The cracking moment of all beams tested was calculated, using the two methods described above, based on an assumed rupture strength of the concrete, according to the CSA Code. For beams prestressed by Leadline bars, using the strain compatibility and equilibrium conditions, method #1 overestimated the predicted cracking load by an average value of 22 percent with standard deviation of 20 percent, while using equation 7-5, method #2 overestimated the predicted cracking load by an average value of 9.0 percent with standard deviation of 17 percent as shown in Table 7-1. The cracking loads of the two beams prestressed by two Leadline bars were overestimated by about 55 percent using the first method and 35 percent using the second method. Since the two beams were cast using one batch of concrete, the difference between the predicted and

the observed cracking load may be attributed to the variability of the rupture strength as reported by Rüşh (Leonhardt 1988) and discussed in chapter 4. This phenomenon could also be attributed to the increased shrinkage cracks in the beams with two Leadline bars compared to the beams prestressed by four bars. The predicted cracking load of the two beams prestressed by steel was overestimated by 7 percent, using strain compatibility and equilibrium conditions, and underestimated by 5 percent using the second method, as shown in Table 7-1.

The rupture strength of the concrete was calculated based on the observed cracking load, using the two methods described above. A linear interpolation was performed between the calculated rupture strength and square root of the compression strength of the concrete. The factor a in equation 7-11 was found to be 0.40 and 0.54 using methods 1 and 2, respectively, as shown in Fig. 7-3. It should be noted that the variability of the rupture strength is high as shown in Fig. 7-3.

The predicted failure mode of the tested beams prestressed by Leadline and steel agreed with the observed failure mode given in chapter 6, Table 6-1. Accordingly, one beam prestressed by Leadline, R-4-.5-H, failed by crushing of the concrete. All the other beams prestressed by Leadline failed by rupture of the Leadline bars. Also, the beam with a 200-mm flange width prestressed by steel strands failed by crushing of the concrete, while the beam with a 600-mm flange width failed by rupture of the steel strands.

The failure loads of beams prestressed by Leadline that failed by rupture of the Leadline bars were underestimated by an average value of 10 percent, as shown in Table 7-1. This may be attributed to the higher tensile strength of the Leadline bars than the assumed value of 2950 MPa. The predicted failure load of the beam prestressed by Leadline that failed by crushing of concrete was the same as the observed failure load, as shown in Table 7-1. The predicted failure load of the beams prestressed by steel was 7 percent less than the observed value for the beam that failed by rupture of the steel strands and it was the same as the measured value for the beam that failed by crushing of the concrete.

The failure loads of the tested beams were also predicted based on the guaranteed tensile strength of the Leadline of 1970 MPa. The ultimate loads were underestimated by an average value of 40 percent of the measured failure loads. Reducing the ultimate strength of the Leadline resulted in the predicted mode of failure of beam R-4-.5-H changing from crushing of the concrete to rupture of the Leadline bars; the predicted failure load was about 70 percent of the measured load at failure.

7.4 DEFLECTION PREDICTION

The deflection was calculated using two different techniques, integration of the curvature at many sections along the beam span, and a simplified method where the deflection was calculated using an equivalent moment of inertia for the entire beam. Using the first technique, the deflection was calculated with and without accounting for tension stiffening. The curvature was calculated using the strain compatibility approach described previously. To calculate the effective curvature for a given section accounting for tension stiffening, three different methods were used, namely, the effective moment of inertia I_e method, the CEB-FIP Code, and strain compatibility including the tension in the concrete after cracking. In the second technique, where the deflection was calculated using an effective moment of inertia, for the entire beam, tension stiffening was included.

The cracking load of the beams was assumed to be equal to the observed cracking load in order not to accumulate the error in calculating the deflection. Deflections due to self-weight of the beam, weight of the spreader beam used for applying the concentrated loads, and effective prestressing were deducted from the calculated total deflection at every load increment. The different methods for deflection calculation were compared to each other using an error percentage (e), which is given by equation 7-12.

$$e \% = \frac{\Delta_{predicted} - \Delta_{exp}}{\Delta_{exp}} \times 100 \quad 7-12$$

7.4.1 Integration of Curvature

In this method the moment-curvature relationship was calculated for every beam with and without accounting for tension stiffening. For each load increment, the curvature at different sections along the entire length of the beam was determined up to the failure load using a computer program. The deflection was determined by integration of the curvature from the support to the mid-span section to obtain the maximum deflection due to the specified load. The curvature integration was performed numerically using equation 7-13 and is illustrated in Fig. 7-4. In this case, the integration was performed at 40 sections along half the beam span. Increasing the number of sections increases the accuracy of the calculations. The deflection can also be determined by integration of the curvature at four distinct sections using equation 7-14. In general, the sections should be selected at any expected abrupt change of the curvature. The selected sections were at the support, cracking moment, location of the concentrated load and midspan, as shown in Fig. 7-5.

$$\Delta = \sum \frac{\phi_i x_i + \phi_{i+1} x_{i+1}}{2} \Delta x_i \quad 7-13$$

$$\Delta = \frac{\phi_1 x_1 + \phi_2 x_2}{2} \Delta x_1 + \frac{\phi_2 x_2 + \phi_3 x_3}{2} \Delta x_2 + \frac{\phi_3 x_3 + \phi_4 x_4}{2} \Delta x_3 \quad 7-14$$

7.4.1.1 Ignoring Tension Stiffening

The curvature was calculated without accounting for tension stiffening based on the slope of the strain diagram obtained at each load increment, as described in section 7.1. The predicted deflection before cracking was in very good agreement with the measured values. After cracking, however, the predicted deflection based on integration of the curvature at 40 sections was, in general, overestimated due to ignoring the contribution of the tension stiffening of the concrete between cracks. The overestimate averaged 30 percent within the service load range and 21 percent up to the ultimate load, as given in Table 7-2 and Table 7-3. The histogram of the error distribution of the predicted deflection ignoring the tension stiffening for beams prestressed by Leadline bars is given in Fig. 7-6. It can be seen from the figure that 35 percent of the predicted deflection has an error between 10 and 20 percent.

7.4.1.2 Accounting for Tension Stiffening

The contribution of the concrete between cracks to the stiffness of the beams is referred to as tension stiffening. Because cracks of concrete beams occur randomly, there

is no rationale to calculate the tension stiffening and it is usually included empirically. Tension stiffening was included in the deflection calculations using three different methods. These methods are described in the following sections:

7.4.1.2.1 Method #1: Effective Moment of Inertia " I_e "

The effective moment of inertia I_e method, modified by Tadros, Ghali and Meyer (1985), was used to predict the deflection of the beams. It was reported (Krishna Mohan Rao and W.H.Dilger 1992) that this method gives the most accurate prediction of the deflection compared to other methods using the I_e approach. The effective moment of inertia method has been adopted by the ACI and CSA Codes for reinforced concrete members and by the CPCI Design Manual for reinforced and prestressed concrete members. This method interpolates between the cracked and the uncracked moment of inertia of the section to calculate the effective moment of inertia using Branson's formula as given by equation 4-20. At a given section, the applied moment is reduced by the decompression moment to account for the initial curvature induced by prestressing.

After cracking, eccentricity of the prestressing reinforcement is calculated as the distance between the centroid of the prestressed reinforcement to the effective centroid of the section, which is interpolated between the cracked and the uncracked centroids of the section using the same interpolation factor as is used for I_e , as given by equation 4-21.

The effective curvature ϕ_e was calculated using the applied moment and the rigidity of the section $E_c I_e$, as given by equation 4-22. The effective curvature was integrated at 40 sections over one-half the beam span to predict the mid-span deflection.

The cracked moment of inertia I_{cr} , required to calculate I_e in equation 4-20, was calculated with respect to the cracked centroid of the section which is at a distance y_{cr} from the extreme compression fibre of the concrete, as given in equation 7-15 and 7-16 for T-sections and using the notation given in Fig. 7-1.

$$y_{cr} = \frac{\frac{1}{2} b t_f^2 + b_w (c - t_f) \left(t_f + \frac{c - t_f}{2} \right) + n A_p d_p}{b t_f + b_w (c - t_f) + n A_p} \quad 7-15$$

$$I_{cr} = \frac{1}{12} b t_f^3 + b t_f \left(y_{cr} - \frac{t_f}{2} \right)^2 + \frac{1}{12} b_w (c - t_f)^3 + b_w (c - t_f) \left(y_{cr} - t_f - \frac{c - t_f}{2} \right)^2 + n A_p (d_p - y_{cr})^2 \quad 7-16$$

where $n = E_p / E_c$; and

$E_p =$ Elastic modulus of *FRP* prestressing reinforcement.

The predicted deflections were in good agreement with the observed deflections. A comparison between the experimental and the predicted deflection for one of the tested beams is shown in Fig. 7-7. After cracking and up to the failure load, the predicted

deflection is very close to the measured value. The mean value and the standard deviation of the error in the deflection calculation based on this method were 6 and 10 percent up to the predicted failure load, and 0 and 13 percent within the service load range, respectively, as given in Tables 7-2 and 7-3. The histogram of the error distribution is shown in Fig. 7-8. Up to the ultimate load, 85 percent of the predicted deflections were within a 20 percent error. This increased to 89 percent within the service load range.

7.4.1.2.2 Method #2: CEB-FIP Code

The CEB-FIP Code 1990 approach for calculating the effective curvature ϕ_e was applied for the tested beams, using the interpolation factor ζ between the gross and the cracked curvatures, ϕ_g and ϕ_{cr} , as given by equation 4-23. The mean curvature was calculated at 40 sections over the length of the beam. Numerical integration over one-half the beam span was used to calculate the deflection at mid-span. For reinforced concrete structures, the interpolation factor ζ depends on the ratio between the cracking and the service moments; however, for prestressed sections, the moment on the section should be reduced to account for the prestressing force (CEB Manual 1985). The interpolation factor used in this study to calculate the deflection of beams prestressed by *CFRP* bars depends on the decompression moment M_{dc} as given by equation 7-17. This decompression moment is commonly used to convert the prestressed section to a

reinforced concrete section subject to moment and normal force. Several opinions exist on how to calculate the decompression state of prestressed sections. The decompression defined by Nawy and Huang (1977) represents the condition at which the stresses in the concrete at the level of reinforcement are equal to zero. Naaman and Siriakorn (1979) defined the decompression moment by the state at which zero stress occurs at the level of the extreme tension fibre. The concept of decompression of the full concrete section was first proposed by Tadros (1982) and used by others (Ghali 1989 and Suri and Dilger 1986). In this study, the decompression moment is the moment which produces zero stress at the extreme concrete fibre of the precompressed zone. It should be noted that this moment does not result in complete decompression of the whole section. However, this method eliminates the complicated calculations required to compute the decompression force which is required for decompression of the entire section and provides satisfactory results in comparison to the other methods.

$$\zeta = 1 - \beta_1 \beta_2 \left(\frac{M_{cr} - M_{dc}}{M_s - M_{dc}} \right)^2 \geq 0.4 \quad 7-17$$

The factor β_1 refers to the bond condition of the reinforcement; the factor β_2 refers to the type of applied load. As the beams were tested under static short-term loading, the coefficient β_2 was taken equal to 1.0, as recommended by the code. The factor β_1 was evaluated for the beams prestressed by *CFRP* bars and found to be equal to 1.0. The estimated deflection of the beams was in good agreement with the measured values, as

shown for two of the tested beams with large and small flange widths in Fig. 7-9 and 7-10, respectively. It can be also seen from the figures that the calculated deflection for beams with a large flange width was slightly overestimated, unlike the deflection of beams with a small flange width. The mean value and the standard deviation of the error were, respectively, 8 and 8 percent calculated up to the failure load, and 7 and 12 percent calculated within the service load range, as given in Tables 7-2 and 7-3. A histogram of the error distribution is shown in Fig. 7-11. Up to the ultimate load, 94 percent of the predicted deflections were within a 20 percent margin of error, while 83 percent of the predicted deflections within the service load were within ± 20 percent error.

The deflections were also calculated using integration of the curvature at selected sections, as shown in Fig. 7-12. Up to the ultimate load, 76 percent of the predicted deflections were in the margin of 20 percent error and 80 percent of the predicted deflections within the service load range had ± 20 percent error. The accuracy of the predicted deflection is reduced in comparison to the calculated deflection using integration at 40 sections due to the approximation of the curvature profile along the beam span, as shown in Fig. 7-13. The mean value and the standard deviation of the error were, respectively, 10 and 11 percent calculated up to the predicted failure load, and 10 and 15 percent if calculated within the service load range, as given in Tables 7-2 and 7-3. A histogram of the error distribution is shown in Fig. 7-14.

7.4.1.2.3 Method #3: Strain Compatibility Accounting For Concrete in Tension

The mean curvature was calculated based on strain compatibility, including the tensile stresses of the concrete below the neutral axis. The proposed stress distribution within the cross section is shown in Fig. 7-15. The tensile stresses in the concrete are introduced in two locations in the beam, below the neutral axis where the tensile stresses in concrete increases linearly up to the rupture strength, and within the effective embedment zone around the reinforcement as introduced by CEB-FIP Code (1978) and shown in Fig. 4-6. The average tensile stress-strain relationship of concrete after cracking, given by equation 4-27 (Collins and Mitchell 1991), was used to predict the tensile stresses in concrete in the effective embedment zone. The concrete tensile strain was calculated at four levels within the effective embedment zone. A linear distribution of the tensile stresses was assumed between every two levels to simplify the calculation of the tensile forces in the concrete shown in Fig. 7-15. The two values selected for the bond factor α_1 were 0 and 1.0, while a value of 1.0 was used for α_2 , for the case of short-term loading. The mean errors of the predicted deflection using the two values of α_1 were 35 and -23 percent, respectively, as shown in Fig. 7-16. In order to minimize the error of the predicted deflection, α_1 was interpolated as 0.6 and 0.7, respectively, for beams prestressed by Leadline bars and steel strands.

The predicted deflections using integration of the curvature at 40 sections along half

the beam span and α_1 of 0.6, are compared to the measured deflections for a typical beam in Fig. 7-17. A very good correlation between the predicted and the measured deflection is observed. The mean value and the standard deviation of the error of the predicted deflections of beams prestressed by Leadline were 1 and 11 percent calculated up to the failure load and -2 and 13 percent within the service load limit, respectively. Up to the ultimate load, 92 percent of the predicted deflections were within a 20 percent error while, within the service load range, 88 percent of the predicted deflection were in the margin of 20 percent error. A histogram of the error distribution of the predicted deflection is shown in Fig. 7-18.

The accuracy of this method was also examined by comparing the predicted to the measured deflections of a prestressed composite beam tested by others (Fam, Rizkalla and Saltzberg 1995) as shown in Fig. 7-19. The beam was 9.3 m long, 550 mm deep and prestressed by six longitudinal 8-mm Leadline bars and four draped 8-mm Leadline bars. Good agreement between the predicted and the measured deflections is observed.

7.4.2 Simplified Method

Since deflection calculation using integration of the curvature requires a computer program or a programmable calculator to perform the computations, a simplified method is normally used to estimate the deflection at the preliminary design stage. The simplified

method is based on using the beam flexural rigidity $E_c I_e$ at the section of maximum moment. Equation 7-18 is used to estimate the deflection for any beam for given loading and boundary conditions. The coefficients k_p , k_D and k_L , which depend on the boundary and loading conditions, could be found in many text books (Branson 1977, CPCI Metric Design Manual 1989, Naaman 1982 and Nilson 1987). The coefficients k_p , k_D , and k_L were calculated for the tested beams and were found to be equal to 1/8, 5/48, 1/10.37, respectively. The effective moment of inertia I_e was calculated using equation 4-13.

$$\Delta = -k_p \frac{P_e (d_p - y'_e) L^2}{E_c I_e} + k_D \frac{M_D L^2}{E_c I_e} + k_L \frac{M_L L^2}{E_c I_e} \quad 7-18$$

- where
- Δ = deflection of the beam;
 - P_e = effective prestressing force;
 - y'_e = effective centroidal distance from the extreme compression fibre;
 - M_D = Moment due to dead load on the beam;
 - M_L = applied external moment;
 - y_{cr} = cracked centroidal distance from the extreme compression fibre;
 - y_g = gross centroidal distance from the extreme compression fibre; and
 - M_{dc} = decompression moment.

The deflection due to live load is calculated in two steps as the difference between the deflection due to the total service load and the deflection due to dead load, which are

calculated using equation 7-18. This deflection can not be calculated in one step using one value for the moment of inertia. This is not only due to the change of the effective moment of inertia, I_e , but also due to the continuous change of the eccentricity of the prestressing force after cracking due to the movement of the neutral axis with the increase of the applied load. The effective centroidal distance y'_e , for beams prestressed by *CFRP* bars is determined in the following section.

7.4.2.1 Centroidal Distance of Prestressed Cracked Beams

After cracking and due to tension stiffening, the average distance between the centroid of the transformed section and the extreme compression fibre y'_e has an intermediate value between the cracked and uncracked centroidal distances y_{cr} and y_g respectively. Different interpolation factors have been proposed for calculation of y'_e (Branson and Trost 1982 and Tadros, Ghali and Meyer 1985). Based on the average value of the measured strain, the compression zone depth was computed; consequently, the effective centroidal distance is proposed as given by equation 7-19. The effective centroidal distance is interpolated between the cracked and uncracked centroidal distances using the interpolation factor ψ given by equation 7-20.

$$y'_e = y_{cr} + \psi^2 (y_g - y_{cr}) \leq y_g \quad 7-19$$

$$\psi = \left(\frac{M_{cr} - M_{dc}}{M_s - M_{dc}} \right) \quad 7-20$$

The measured values were compared to the cracked and uncracked centroidal distances, y_{cr} and y_g , for eight beams as well as to values calculated from the proposed equation for y'_e , as shown in Fig. 7-20 for one of the tested beams prestressed by *CFRP* bars. The interpolation factor in equation 7-19 has the power of 2 instead of the value of 2.5 used for beams prestressed by steel. This suggests that y'_e is closer to y_g for beams prestressed by *CFRP* than beams prestressed by steel subjected to the same prestressing and loading conditions. This behaviour can be attributed to the larger crack spacing observed for beams prestressed by *CFRP* bars and the consequently larger uncracked portion of the beam.

The cracked section properties, y_{cr} and I_{cr} , were determined accurately using the compression zone depth obtained at each load increment using the strain compatibility approach. The properties of a cracked prestressed section can also be evaluated using design charts proposed in the CPCI Metric Design Manual 1989. In order to illustrate the use of this method, an example of the calculation of the deflection of a beam prestressed by *CFRP* bars is given in Appendix A.

The measured deflection of a typical beam prestressed by Leadline was compared

to the predicted deflection using I_e (Tadros et al.) method and the simplified method, as shown in Fig. 7-21. The mean value and the standard deviation of the calculated error were -4 and 13 percent calculated up to the ultimate load level and -16 and 13 percent calculated within the service load limit, respectively. Up to the ultimate load, 73 percent of the predicted deflections were within a 20 percent error, while 56 percent of the predicted deflections within the service load range were within the same margin of error. A histogram of the error distribution is shown in Fig. 7-22.

7.4.3 Design Recommendations

Deflection calculation using integration of the curvature along the beam span gives an accurate prediction as the margin of error is within 20 percent. This method is therefore recommended for prediction of the short-term deflection of concrete beams partially prestressed by *CFRP* Leadline bars. The simplified method has also been shown to be a good tool for preliminary design as 80 percent of the predicted deflection in the service load range is within a ± 30 percent error. It should be noted that the CEB-FIP Code method and the strain compatibility method are dependent on the bond factors which are function of the characteristics of the reinforcement, while the equivalent moment of inertia I_e (Tadros et al.) method and the simplified method are applicable to any type of reinforcement independently of the bond properties of the reinforcement.

The measured deflection is plotted versus the predicted deflection in Fig. 7-23 for a typical beam using all the methods described above. It can be seen that the predicted deflection ignoring the tension stiffening effect is the upper bound. Fig. 7-24 shows the distribution of the error using the different methods, at various load levels. A negative value of the error means that the predicted deflection is underestimated, while a positive value means that the predicted deflection is overestimated. It is obvious that the error within the range of the service load is considerably higher than the error beyond service load limit. This is due to the small magnitude of the deflection in the service load range, which is in the denominator of the equation calculating the error. Fig. 7-24 also shows that tension stiffening has a significant effect in the deflection computations. Tables 7-2 and 7-3 show the statistics of the error in terms of the mean value and the standard deviation. The minimum and the maximum error are also presented. The predicted deflection using the CEB-FIP Code has the least mean and standard deviation of error. The predicted deflections within 20 percent error are shown for the different methods within the service load range and up to failure in Fig. 7-25 and 7-26, respectively.

7.5 CRACK WIDTH

Cracks in concrete structures prestressed by steel are normally controlled to minimize the corrosion of the steel. Replacing the steel by *FRP* reinforcement provides an excellent solution to the classical deterioration problem of concrete structures as *FRP* reinforcement does not corrode. However, there are good reasons for controlling widths of cracks other than corrosion prevention. Control of the crack width might be required to prevent leakage or to preserve the appearance of the structure. Several aspects should be assessed for the choice of permissible crack widths in prestressed structures, such as surface texture of the concrete and distance of the cracks from possible observers. It is reported that cracks wider than 0.25 to 0.3 mm can lead to public concern (Padilla and Robles 1971).

Many formulae are currently available to calculate the crack width of prestressed concrete beams, as shown in chapter 4. Due to the local and random occurrence of cracks, the level of accuracy of crack width prediction of reinforced or prestressed concrete structures is less than that of deflection prediction (CEB Manual 1985). The various parameters affecting the cracking behaviour are the reinforcement stress or strain after decompression, effective concrete area in tension, area of reinforcement, concrete cover, and bond characteristics of the reinforcement. There is no universal agreement on the mathematical relationship of these variables to the crack width. For example, the

effective area of concrete in tension has a square root and a cubic root relationship in Suri and Dilger equation (1986) and in Gergely and Lutz equation (1966), respectively, while it is raised to the power of one in the CEB-FIP Code (1978). Moreover, the definition of concrete area in tension is proposed to be the area below the neutral axis by Suri and Dilger, while considered in the CEB-FIP Code and in Gergely and Lutz equation as the effective area of concrete in tension around the reinforcement.

7.5.1 Influence of Major Parameters

The relationship between the major parameters and the measured crack width of beams prestressed by *CFRP* bars is examined. The relationship between the steel stress, after decompression, f_s , to the crack width of beams prestressed by steel wires or strands with or without non-prestressed deformed steel bars, proposed by Suri and Dilger (1986), is given in equation 7-21. Similarly, the stress in the *CFRP* bars, after decompression, f_f was found to be related to the maximum measured crack width by equation 7-22, as shown in Fig. 7-27.

$$w_{\max} = 0.109 \times 10^{-3} f_s^{1.38} - 0.01 \quad \text{beams prestressed by steel} \quad 7-21$$

$$w_{\max} = 0.525 \times 10^{-3} f_f^{1.13} - 0.023 \quad \text{beams prestressed by Leadline} \quad 7-22$$

Since the stress in the reinforcement is typically related linearly to the crack width by most researchers, a linear regression was performed for beams prestressed by *CFRP* and compared to the data given, by Suri and Dilger (1986) for beams prestressed by steel strands in equations 7-23 and 7-24 and shown in Fig. 7-28. The linear relationship between the crack width and the reinforcement stress provided a standard error of 0.07 for beams prestressed by Leadline in comparison to a value of 0.10 for beams prestressed by steel strands.

$$w_{\max} = 0.116 \times 10^{-2} f_s \quad \text{beams prestressed by steel} \quad 7-23$$

$$w_{\max} = 0.124 \times 10^{-2} f_f - 0.053 \quad \text{beams prestressed by Leadline} \quad 7-24$$

The concrete area in tension, A_t , which is considered another major parameter, is related to the crack width as shown in Fig. 7-29 for beams prestressed by Leadline. Despite of scattering of the results of all the tested beams, the non-linear regression provided equation 7-25 which compared well to equation 7-26 proposed for beams prestressed by steel by Suri and Dilger (1986).

$$w_{\max} = 0.033 \left[\frac{A_f}{A_t} \right]^{-0.4} \quad \text{beams prestressed by Leadline} \quad 7-25$$

$$w_{\max} = 0.017 \left[\frac{A_s}{A_t} \right]^{0.5} \quad \text{beams prestressed by steel} \quad 7-26$$

where A_f = area of *FRP* in the tension zone; and

A_s = total area of prestressed and non-prestressed steel in the tension zone.

The CEB-FIP Code (1978) relates the strain in the reinforcement to the crack width. The calculated strain after decompression was interpolated as shown in Fig. 7-30. It is observed that, for a given crack width, the associated strain is similar for beams prestressed by Leadline and steel when the crack width is less than 0.4 mm; however, for larger crack width, the resulting strain for beams prestressed by Leadline is higher. This may be attributed to the lower flexural bond strength of the Leadline which results in early crack stabilization with respect to beams prestressed by steel and hence the crack spacing is more uniform for beams with Leadline. Consequently, the increase in the strain of beams with Leadline results in equal increase of the width of all cracks. Conversely, the increase in the strain of beams prestressed by steel results in an unequal increase of the crack width; as a result, the maximum crack width becomes larger. The maximum crack width is given as a function of the strain for beams prestressed by steel and Leadline in equations 7-27 and 7-28, respectively. The crack-width-strain relationship for beams with steel is calculated by converting the steel stress in equation 7-21 (Suri and Dilger 1986) to strain using an elastic modulus of 180 GPa.

$$w_{\max} = 2100 \epsilon_s^{1.38} - 0.01 \quad \text{beams prestressed by steel} \quad 7-27$$

$$w_{\max} = 370 \epsilon_f^{1.13} - 0.023 \quad \text{beams prestressed by Leadline} \quad 7-28$$

where ϵ_s = strain of steel after decompression; and

ϵ_f = strain of *FRP* after decompression.

7.5.2 Calculation of The Stress in The Reinforcement

The stress in the reinforcement was calculated for crack width prediction as the incremental stress resulting from the difference between the moment at which the crack width is to be determined and the decompression moment. The stress in the reinforcement was calculated based on the strain compatibility approach using the method described at the beginning of this chapter. The effective strain in the prestressed reinforcement was calculated based on the average of the strain gauge readings on the day of testing. The strain in the reinforcement after decompression, ϵ_f , and consequently the stress, was calculated taking into account the strain in the concrete due to prestressing, ϵ_{ce} , as shown in Fig. 7-1.

7.5.3 Crack Width Calculation

The crack width was calculated for all the beams prestressed by *CFRP* bars using three methods given by Suri and Dilger (1986), CEB-FIP Code (1987) and Gergely and Lutz (1966). Since bond properties of the reinforcement are considered to be among the most important parameters affecting the cracking behaviour of partially prestressed beams, the three methods were used to determine the equivalent bond factors for *CFRP* bars. The bond factors were found to be different from those of steel reinforcement since bond is significantly affected by surface conditions (smooth or ribbed) and type of reinforcement (strand or bar). The other two factors which can also affect the bond characteristics are the elastic modulus and Poisson's ratio. Bond factors are introduced into the equations predicting the crack width, such as " k " in the method introduced by Suri and Dilger and given in equation 4-30, " k_1 " in the CEB-FIP Code as given by equation 4-33, and " R " in the method introduced by Gergely and Lutz and given by equation 4-36. The following subsections discuss the results of each of the above methods.

7.5.3.1 Method #1: Suri and Dilger (1986)

The CPCI Design Manual (1989) recommended the use of the method presented by Suri and Dilger (1986) to estimate the maximum crack width at the beam soffit and given

by equation 4-30. The relationship between the measured crack width and both the steel stress and the concrete area in tension show that equation 4-30 can be applied for beams prestressed by Leadline using the same variables with the same exponent; however, the bond factor k has to be calculated. The bond factor was calculated using linear regression analysis of the test results, as shown in Fig. 7-31. A value of 1.41×10^{-6} was obtained for the Leadline compared to values ranging from 2.55×10^{-6} to 4.50×10^{-6} for various combinations of prestressed and non-prestressed steel. The predicted crack width using equation 4-30 is plotted versus the observed crack width in Fig. 7-32. It can be observed that the agreement between the calculated and the measured crack width is almost within ± 40 percent margin.

The crack width calculated using this method was also examined by comparing the predicted to the measured maximum crack width of a beam prestressed by Leadline bars and tested by others (Fam, Rizkalla and Saltzberg 1995) as shown in Fig. 7-33. Good agreement between the predicted and the measured crack width is observed.

7.5.3.2 Method #2: The CEB-FIP Code (1978)

The CEB-FIP Code expression for calculating the crack width using the average spacing between cracks is given by equation 4-33. The average crack width w_m at the beam soffit is estimated using the strain in the prestressing reinforcement after

decompression and the crack spacing as given by equation 4-34. The interpolation factor ζ in equation 4-34 is defined by equation 7-17. To evaluate the bond factor k_1 in equation 4-33, two values, 0.2 and 0.8, were selected as initial values for the bond factor. It should be noted that the bond factor k_1 ranges between 0.4 and 0.8 for deformed and plain steel bars, respectively. The mean error of the predicted crack width using the two values of k_1 , 0.2 and 0.8, were -9.3 and 60 percent, respectively, as shown in Fig. 7-34. In order to minimize the error of the predicted deflection, which is represented by the broken line in Fig. 7-34, k_1 was interpolated as 0.28 for beams prestressed by Leadline bars. The bond factor k_1 of prestressing steel was also evaluated using the data obtained from the two tested beams prestressed by steel strands and found to be equal to 0.1. The average crack width of the tested beams was predicted and found to be in the range of ± 40 percent of the measured crack width as shown in Fig. 7-35.

7.5.3.3 Method #3: Gergely and Lutz (1966)

Gergely and Lutz (1966) recommended the use of equation 4-36 for the calculation of the maximum crack width at the beam soffit for reinforced concrete beams. The same equation is proposed for concrete beams partially prestressed by steel reinforcement by the CPCI Design Manual (1989). The bond factor R was linearly interpolated using the measured maximum crack width, as shown in Fig. 7-36, and it was found to be equal to 12.5×10^{-6} for beams prestressed by Leadline. The bond factor R was modified by Suri

and Dilger (1986) for beams prestressed by steel and was reported to be in the range of 13.7×10^{-6} to 25×10^{-6} . The crack width for the tested beams, predicted using equation 4-36 is compared to the measured values in Fig. 7-37; an agreement within ± 40 percent can be observed.

7.5.4 Design Recommendations

The error of the predicted crack width is compared for the different methods in Table 7-4. It can be seen that the predicted crack width has a large margin of error; the smallest standard deviation of the error was 15 percent for the Gergely and Lutz method. Therefore, it is essential to verify the proposed values for bond factors by testing other beams with a wide range of span-to-depth ratios and different configurations. A comparison of the accuracy of the three different methods is shown in Fig. 7-38. Any of the above three methods can be used for crack width prediction of concrete beams partially prestressed by *CFRP* Leadline bars knowing that the accuracy is within ± 40 percent.

7.6 STRAIN DISTRIBUTION

The tensile strains in the prestressing reinforcement as well as the compressive strains in the concrete should be evaluated at full service load and at the nominal ultimate

carrying capacity of the beams in order to examine the margin of safety of the beams. The proposed ACI Code, Committee 318, 1995 (Mast 1992) requires a minimum net tensile strain after decompression of 0.005. Therefore, the calculation of the flexural strains is a design requirement for prestressed concrete beams. This section compares the measured to the predicted strains with and without accounting for tension stiffening. The strains were calculated using the strain compatibility method described at the beginning of this chapter. The tension stiffening effect was included by accounting for concrete in tension in two locations in the cross-section of the beam, below the neutral axis where the tensile stresses in concrete increases linearly up to the rupture strength, and within the effective embedment zone around reinforcement, as shown in Fig. 7-15.

The predicted strains are compared to the measured concrete strains at the extreme compression fibre and at the level of the bottom *CFRP* bars, as shown in Fig. 7-39 and 7-40, respectively, for one of the tested beams. It can be seen that the predicted strains are in good correlation with the measured values. It can be also seen that ignoring the tension stiffening effect overestimates the strains after cracking and within the service load range; however, the effect of the tension stiffening on the calculated strains diminishes prior to the ultimate load. The predicted strain profiles with and without accounting for tension stiffening are also compared to the strains measured at three different locations in the constant moment zone for six partially prestressed beams jacked to 50 percent of the guaranteed strength of the *CFRP* bars, as shown in Fig. 7-41. The

strains are compared at two load levels, at the service load which is defined as the load at which the maximum crack width is 0.40 mm and at approximately 90 percent of the failure load of the beams. It can be seen that the calculated strains accounting for tension stiffening are less than the calculated strains if the tension stiffening is ignored. Also, the calculated strains are in good agreement with the measured strains, especially when the tension stiffening is included in the calculation.

7.7 FREQUENT LOADING AND UNLOADING

Since partially prestressed beams are designed to crack under superimposed dead and live loads, the behaviour of the beams under service loading can not be considered perfectly elastic due to the permanent cracks. To satisfy the serviceability requirements, it is important to be able to determine the deflection and crack width at a fraction of the live load after the beam has been subjected to the full service load. Beams may also be accidentally subjected to loads higher than the specified service load and consequently serviceability requirements should be checked due to unloading conditions. This frequent loading and unloading will be referred to as repeated loading. The following sections discuss prediction of the deflection and the crack width of concrete beams partially prestressed by *CFRP* bars under limited repeated loading.

7.7.1 Deflection Prediction

Response of beams prestressed by *CFRP* bars can be reasonably predicted before cracking using the gross moment of inertia or, more accurately, using the uncracked transformed moment of inertia. Behaviour of the beams at this loading stage is elastic and linear. However, after cracking, which occurs in the case of partially prestressed beams, the load-deflection behaviour under repeated loading is not perfectly elastic despite the fact that the *CFRP* material is elastic up to failure. The test results indicated that, during unloading of the beams within the service load range, the deflection does not follow the same path as the initial cycle. This may be attributed to cracking of the beams and the non-recoverable creep of the concrete occurring due to the time involved in the loading cycle. The measured deflections of the beams in the second and third cycles were found to be identical. The deflections of the beams, after reloading to the same load level, follow the same path as in the initial cycle. This behaviour is typical for beams prestressed by either *CFRP* bars or steel strands as shown in Fig. 7-42. The cyclic loading shown in the figure has a lower load level equivalent to 80 percent of the cracking load and an upper load level equivalent to 60 percent of the predicted ultimate load which represents 1.5 to 2 times the cracking load, depending on the prestressing level. This behaviour was also reported by Branson (1977) for beams prestressed by steel.

The available information in the literature for deflection calculation of prestressed beams under repeated loading is very limited. Kripanarayanan and Branson (1979) recommended the use of constant stiffness during unloading and reloading of the beams. They proposed using a constant moment of inertia I_{rep} for repeated load which is higher than the moment of inertia of the section at the initial cycle I_e . However, the proposed method did not account for the change in the eccentricity of the decompression force due to increasing the applied load.

7.7.1.1 Proposed Model

The typical behaviour of concrete beams prestressed by *CFRP* bars is shown in Fig. 7-43. In order to illustrate this behaviour, consider the beam to be loaded from point O, which represents zero load, to point A, which is the cracking load and to point B, which is higher than the cracking load, as shown in Fig. 7-43. The slope of the line OB is proportional not only to the effective moment of inertia, I_e , but also to the eccentricity of the prestressing force calculated at point B. If the beam is unloaded at point B and the behaviour of the beam is perfectly elastic, the beam will follow the path BAO, which is the same path as the first loading and the total deformation of the beam should be completely recovered. Conversely, if the behaviour of the beam is perfectly inelastic, the beam will follow the path BE, which is parallel to the line OA, and the beam will have a residual deformation corresponding to the deflection OE. The actual

behaviour of the beam is between the two cases and is represented by the path BCD. In spite of the fact that the *FRP* reinforcement and the concrete are linear at this load level, the beam will have a residual deformation equivalent to OD. This residual deformation is proportional to the load at which the beam is unloaded.

The bilinear behaviour at unloading and reloading of the prestressed beams shown in Fig. 7-43 was observed for all the tested beams including the beams prestressed by steel strands. The load-deflection relationship is considered to be linear from point D, up to a load, P_{dc} , causing the decompression moment, M_{dc} , defined by point C based on zero stress at the extreme concrete fibres of the precompressed zone. The deflection within the range DC can be estimated using the uncracked moment of inertia, I_g . The deflection is also assumed to be linear between point C and point B at which the beam is unloaded. The stiffness of the beam at point B, which is proportional to the line DB, is based on a moment of inertia, I_{rep} , which is higher than the inertia I_e at the same point. The deflection at any point between point C and point B can be estimated using linear interpolation between the deflections at point B and point C.

The deflection at point B can be calculated using equation 7-29, which is dependent on a higher moment of inertia, I_{rep} , than the moment of inertia, I_e . Based on the current research, the moment of inertia, I_{rep} , at the load level where the beam is unloaded is proposed as given by equation 7-30. The proposed equation is based on the measured

deflection for all the beams tested under repeated loading in this investigation. The interpolation factor, ψ , used in equation 7-30, is selected similarly to the interpolation factor in equation 7-20. The interpolation factor has a value of 1 if unloading of the beam occurs right after cracking. At this stage, I_{rep} will be equal to I_g . At higher load levels, ψ has a value less than 1 and I_{rep} will be calculated according to the proposed model.

$$\Delta = -k_p \frac{P_e (d_p - y'_e) L^2}{E_c I_{rep}} + k_s \frac{M_{rep} L^2}{E_c I_{rep}} \quad 7-29$$

$$I_{rep} = I_{cr} + \psi^{2.5} (I_g - I_{cr}) \leq I_g \quad 7-30$$

The effective centroidal distance y'_e , which is the distance between the centroid of the cracked section and the extreme compression fibre, was found to be smaller under repeated load than that for the initial loading, as shown in Fig. 7-44 for one of the tested beams. It was found that the value of y'_e did not change after applying two cycles as shown in the figure. Therefore, equation 7-19, which is used to calculate y'_e at first loading, can be applied to estimate y'_e at the unloading level, P_{rep} .

The following steps are proposed to estimate the load-deflection response of beams prestressed by *CFRP* bars under repeated loading. A numerical example is given in Appendix A.

1. Calculate the residual deflection after complete unloading of the applied load, which corresponds to the deflection OD shown in Fig. 7-43. This deflection is equivalent to the difference between the deflection at point B using equation 7-18 and the deflection at the same point B using equation 7-29.
2. Calculate the deflection at point C at the load level, P_{dc} , causing the decompression moment, M_{dc} . This deflection is the summation of the residual deflection calculated in step 1 and the deflection due to M_{dc} using the gross moment of inertia I_g .
3. The proposed model assumes a linear relationship between point C and the level where the beam was unloaded, point B, which corresponds to P_{rep} . Deflection of the beam at any intermediate load level between C and B can be linearly interpolated.

The proposed model was applied to the tested beams and found to be in good agreement with the measured deflection. The average value and the standard deviation of the difference between the predicted and the measured deflections were 1 and 11 percent, respectively. The minimum and maximum error of the predicted deflection were -23 and 11 percent, respectively. A typical predicted load-deflection relationship for one of the tested beams prestressed by *CFRP* bars under repeated load is shown in Fig. 7-45. The beam shown in Fig. 7-45 was unloaded at two load levels, 60 percent of the predicted

ultimate load and at the ultimate load level, based on the guaranteed strength of the *CFRP* bars. The predicted and the measured values are in good agreement as shown in Fig. 7-45.

7.7.2 Crack Width Prediction

Since *FRP* is non-corroding material, controlling of the crack width is mainly for the aesthetics of the structure and not for corrosion prevention. Crack width may be checked at a fraction of the live load, not at the full live load, similar to the requirements of calculating the stress limitations for fatigue of partially prestressed beams. It has been reported that the actual live load varies between 20 and 70 percent of the specified live load in more than 95 percent of the cases for some structures, and that the most frequent value falls between 40 to 50 percent (Leonhardt 1977, cited in Naaman and Siriakorn 1979). Therefore, estimation of the crack width of partially prestressed beams should include the effect of repeated loading to simulate the case of unloading the beam from full service load to a load level representing that of the dead load in addition to the most frequent portion of live load. The proposed equations in the literature for crack width calculation of partially prestressed beams are typically based on experimental programs for beams tested under a single cycle. The following section discusses a proposed model to calculate the crack width of beams partially prestressed by *CFRP* bars, including the effect of unloading.

7.7.2.1 Proposed Model

Measured crack widths at repeated loading are generally higher than the crack width at first loading as indicated in chapter 6 for the tested beams. Test results indicated that crack widths in the second and third cycles were almost identical. The results also showed that the crack width in the initial and the two consecutive cycles were the same at the unloading load level, P_{rep} . Measurements of the crack widths within the repeated load range indicated that the load-crack width relationships are almost linear beyond the cracking load and non-linear below the cracking level for beams prestressed by *CFRP*. The proposed model for crack width prediction for beams prestressed by *CFRP* bars subjected to repeated loading is based on a linear relationship between the load P_{rep} and the load P_{dc} which causes the decompression moment M_{dc} , as shown in Fig. 7-46 and given by equation 7-31. In this analysis, the decompression moment is based on zero stress at the extreme precompressed concrete fibres.

$$w = w_{rep} \left(\frac{M_s - M_{dc}}{M_{rep} - M_{dc}} \right) \quad M_s > M_{cr} \quad 7-31$$

The crack width at a load where the beam is unloaded, P_{rep} , can be predicted using any of the previously described methods in section 7.5.3. Therefore, accuracy of the predicted crack width due to repeated loading is dependent on the accuracy of the estimated crack width at first loading. The proposed linear model, shown in Fig. 7-46,

is not applicable at load levels less than the cracking load due to the nonlinear behaviour within this range. The proposed model is shown for one of the tested beams in Fig. 7-47. It can be seen that the proposed model agrees well with the measured crack width due to repeated cycles.

7.8 DEFORMABILITY OF BEAMS PRESTRESSED BY *CFRP*

Failure of concrete beams prestressed by *CFRP* is typically governed by one of three modes of failure, crushing of the concrete, rupture of the *CFRP* reinforcement, or simultaneous crushing of the concrete and rupture of the reinforcement. This behaviour is illustrated in Fig. 7-48 for beams prestressed by Leadline bars. As a typical example of *FRP* reinforcements the behaviour is based on an effective prestressing force of 50 percent of the guaranteed tensile strength of the reinforcement. The figure shows that up to a reinforcement ratio of 0.19 percent, failure of the beams occurs due to rupture of Leadline bars and therefore the ultimate carrying capacity of the prestressing reinforcement is used. Increasing the area of Leadline certainly increases the ultimate resistance of the beam; however, the mode of failure changes from rupture of the reinforcement to crushing of the concrete. The corresponding stress in the Leadline bars at failure of the beams decreases with the increase of the reinforcement ratio as shown in Fig. 7-48.

Behaviour of concrete beams prestressed by *CFRP* reinforcement is similar to that of beams prestressed by steel in terms of modes of failure; however, the performance of the beams is different in terms of the deformational behaviour and the ultimate carrying capacity of the beams. In order to illustrate this difference, the ultimate carrying capacity of rectangular beams prestressed by Leadline and steel, as well as their deformability, in terms of the section curvature at ultimate of the beams, are shown in Fig. 7-49. The relation is given for the case of effective prestressing force of 50 percent of the guaranteed tensile strength of the Leadline bars and 60 percent of the ultimate strength of steel strands, which are commonly used cases for both types of reinforcement. For a reinforcement ratio less than 0.19 percent, the capacity of beams prestressed by Leadline is higher than that of beams prestressed by steel strands, which is the case of beams with wide flanges; however, the section curvature at failure is much less for beams prestressed by Leadline. Increasing the reinforcement ratio results in the section curvature at ultimate of beams prestressed by Leadline fairly matching the behaviour of beams prestressed by steel, which is similar to behaviour of the tested beams with a small flange width, as shown in Fig. 7-49.

The maximum reinforcement ratio currently considered by the ACI Code Committee 318 (Mast 1992) was also applied for beams prestressed by Leadline as shown in Fig. 7-49. According to the proposed model, a minimum net tensile strain of 0.005, after decompression, should be achieved before failure. Based on this proposed requirement,

the maximum limit of the reinforcement ratio of beams prestressed by Leadline was calculated and found to be 0.63 percent as shown in Fig. 7-49. At this level of reinforcement, there is virtually no difference in the deformability of beams prestressed by Leadline and steel.

Since beams with a low reinforcement ratio and beams with a large flange width have a small compression zone depth at failure and consequently very high tensile strain at the level of the prestressed bars, failure of those beams normally occurs due to rupture of *CFRP* prestressing reinforcement. However, the results of the tested beams indicated sufficient deformability before failure of such beams and acceptable safety margins measured in the following forms:

- 1- Deflections prior to failure were in the range of $1/30$ to $1/40$ of the span, which is considered to be significant deflection and quite sufficient to provide warning before failure. It should be mentioned that the ACI and CSA codes limit deflection due to live load to $1/180$ of the span.
- 2- The beams were extensively cracked before failure and the cracks were uniformly distributed, typically observed for beams prestressed by steel strands.
- 3- The maximum measured crack width in the constant moment zone was in the range

of 0.8 to 1.2 mm for partially prestressed beams with *CFRP* bars at 50 percent of the failure load, which is significantly higher than the maximum specified value at service load. The large crack width provides sufficient warning before failure.

The deformability ratio proposed by Jaeger, Tadros and Mufti (1995) and given by equation 3-8 is calculated for the tested beams and given in the second column, Table 7-5. The model was developed for reinforced concrete beams with rectangular cross sections and a specific mode of failure, namely, crushing of concrete. However, this model was used for the tested beams to check its applicability for beams prestressed by *CFRP* with different modes of failure. It can be seen that the calculated deformability ratio for the beam prestressed by Leadline with a 600-mm flange width is about 50 percent less than the deformability of the beam prestressed by steel. However, for beams with a 200-mm flange width, the deformability ratios for beams prestressed by Leadline and steel are comparable. Increasing the jacking stress from 50 to 70 percent of the guaranteed strength results in a reduction in the deformability ratio by 25 percent for the beams with a 600-mm flange width. It can be also seen from the table that the deformability of beams with a 200-mm flange width is more than twice the deformability of beams with a 600-mm flange width. This finding does not agree with the conventional definition of ductility of beams prestressed by steel based on the deformation at ultimate, Δ_u , and the deformation at yield, Δ_y , and given in the last column in Table 7-5, where the ductility of the beam with a 600-mm flange width is 2.6 times that for the beam with

a 200-mm flange width. This disagreement is because the denominator in the proposed model by Jaeger et al. contains the moment and curvature at a compressive concrete strain of 0.001. This strain is achieved at a low load level for beams with a small flange width; therefore, the corresponding moment and the curvature are small in comparison to beams with a large flange width.

7.8.1 Proposed Deformability Ratio

Since *CFRP* reinforcement behaves elastically and rupture of the reinforcement occurs without the typical yield plateau for steel, the ductility of this material can not be defined in terms of the inelastic deformation prior to failure as in the case of steel. Behaviour of concrete beams prestressed by *CFRP* reinforcement is non-linearly elastic up to failure, where the non-linearity arises from cracking of the concrete. The inelastic energy consumed prior to failure of beams prestressed by *CFRP* is very small in comparison to beams prestressed by steel provided that the prestressing steel has yielded before failure. Conversely, the elastic energy released at failure of beams prestressed by *CFRP* bars is tremendous, which makes the failure of such beams similar to the brittle shear failure of prestressed beams. However, a quantification of the safety margin is needed for the design of such beams and it is identified here by the deformability ratio.

No universal definition has yet been established to identify the deformability of such

beams. The proposed deformability ratio relies on the equivalent deformation at ultimate load of the beam based on uncracked section properties and the actual deformation at ultimate, as shown in Fig. 7-50. Deformability of the beams can be defined in terms of section member properties as given by equations 7-32 and 7-33, respectively.

$$\mu_{\phi} = \frac{\phi_2}{\phi_1} \quad 7-32$$

$$\mu_{\Delta} = \frac{\Delta_2}{\Delta_1} \quad 7-33$$

where ϕ_1 and Δ_1 are the equivalent curvature and deflection of the uncracked section at a load equal to the ultimate load and ϕ_2 and Δ_2 are the ultimate curvature and deflection.

The deformability of the tested beams was calculated according to the proposed model and is given in Table 7-5. The table shows that the deformability of beams with a large flange width is higher than the deformability of beams with a small flange width. It can be also seen from the table that the deformability of the beams prestressed by two Leadline bars is higher than the deformability of the beams prestressed by four bars. The ductility of beams prestressed by steel based on the deflection at yield were 6.56 and 2.49 for the two beams with 600- and 200-mm flange widths, respectively. The calculated deformabilities for the same two beams using the proposed approach were 25.59 and

10.32, respectively, which is about four times the ductility ratio. This indicates that the proposed deformability definition overestimates the ductility of beams prestressed by steel reinforcement.

The deformability of beams prestressed by Leadline is compared to the deformability of beams prestressed by steel, having the same cross-section and prestressing force in Fig. 7-51. It can be observed that the deformability of the beam prestressed by Leadline with a large flange width is much less than that for the beam prestressed by steel. Increasing the reinforcement ratio or reducing the flange width of the beams results in the deformability ratios of the two beams becoming comparable.

The deformabilities of beams with different jacking stresses are also compared in Fig. 7-52. It can be seen that the deformability ratio increased by about 15 percent with the decrease of the jacking stress from 70 to 50 percent of the guaranteed strength of the *CFRP* bars.

Table 7-1 Comparison between the predicted and the experimental results

Beam	$P_{cr,exp}$ (kN)	$P_{cr,prd}$ (kN) method#1	$P_{cr,prd}$ (kN) method#2	P_{cr} prd/exp method #1	P_{cr} prd/exp method#2	$P_{u,exp}$ (kN)	$P_{u,prd}$ (kN)	P_u prd/ exp	Failure mode
T-4-.5-H	25.31	30.85	27.71	1.22	1.09	106.2	97.9	0.92	R*
R-4-.5-H	23.40	24.03	21.49	1.03	0.92	89.3	89.7	1.00	c†
T-4-.5-V	27.33	30.50	27.16	1.11	0.99	97.9	86.1	0.88	R
R-4-.5-V	23.16	25.98	23.02	1.12	0.99	90.2	86.6	0.96	R
T-4-.7-V	37.90	42.70	38.96	1.13	1.03	102.2	89.9	0.88	R
R-4-.7-V	32.10	34.71	31.66	1.08	0.99	98.1	87.4	0.89	R
T-2-.5-V	13.08	20.82	18.39	1.59	1.40	56.3	49.5	0.88	R
R-2-.5-V	12.69	19.05	16.70	1.50	1.31	56.8	51.3	0.90	R
S-T-2-.5	30.71	33.61	29.63	1.09	0.96	77.1	71.4	0.93	R
S-R-2-.5	27.86	29.32	25.86	1.05	0.93	70.1	70.8	1.00	C
Mean value				1.22‡	1.09‡			0.90§	
Standard deviation				0.20‡	0.17‡			0.03§	

* Rupture of prestressing reinforcement

† Crushing of concrete

‡ Mean value and standard deviation for beams prestressed by Leadline

§ Mean value and standard deviation for beams prestressed by Leadline failed by rupture of bars

Table 7-2 Error of the predicted deflection within service load

	Curvature integration at 40 sections				CEB-FIP Code (curvature integration at key sections)	Simplified method
	No tension stiffening	I_e Tadros et al.	CEB-FIP Code	Strain compatibility		
Number of data	89	89	89	89	89	89
mean error (%)	30.5	0	7.7	-2.0	10.6	-16.1
Standard deviation	22	13.2	12.1	12.9	15.3	12.9
Minimum error	-15.6	-23.0	-15.6	-28.6	-15.9	-38.1
Maximum error	89.3	31.4	41.8	24.2	53.6	7.9

Table 7-3 Error of the predicted deflection up to the ultimate load

	Curvature integration at 40 sections				CEB-FIP Code (curvature integration at key sections)	Simplified method
	No tension stiffening	I_e Tadros et al.	CEB-FIP Code	Strain compatibility		
Number of data	245	245	245	240	245	245
mean error (%)	20.6	6.0	8.4	1.2	10.8	-4.5
Standard deviation	16.2	10.0	8.3	11.1	11.0	13.5
Minimum error	-15.6	-23.0	-15.6	-28.8	-15.9	-38.1
Maximum error	89.3	31.4	41.8	24.2	53.6	16.5

Table 7-4 Statistical data of the error of crack width prediction

Method	Number of data	Mean error (%)	Standard deviation	Minimum error	Maximum error
Suri and Dilger (1986)	42	0	20	-20	51
CEB-FIP Code (1978)	42	0	24	-38	69
Gergely and Lutz (1966)	42	0	15	-19	42

Table 7-5 Member deformability of the tested beams

Beam	Deformability ratio (Jaeger et al. 1995) $M_1\phi_1 / M_2\phi_2^*$	Proposed deformability ratio Δ_2 / Δ_1	Ductility ratio Δ_u / Δ_y
T-4-.5-H	3.82	8.05	n/a [†]
R-4-.5-H	9.53	5.74	n/a
T-4-.5-V	3.38	9.79	n/a
R-4-.5-V	7.92	7.42	n/a
T-4-.7-V	2.45	8.27	n/a
R-4-.7-V	7.76	6.59	n/a
T-2-.5-V	1.65	14.63	n/a
R-2-.5-V	4.04	9.99	n/a
S-T-2-.5	5.80	25.59	6.56
S-R-2-.5	9.29	10.32	2.49

* M_1 and ϕ_1 are the moments and the curvature at ultimate, respectively and M_2 and ϕ_2 are the moment and curvature at concrete compressive strain of 0.001

† not applicable

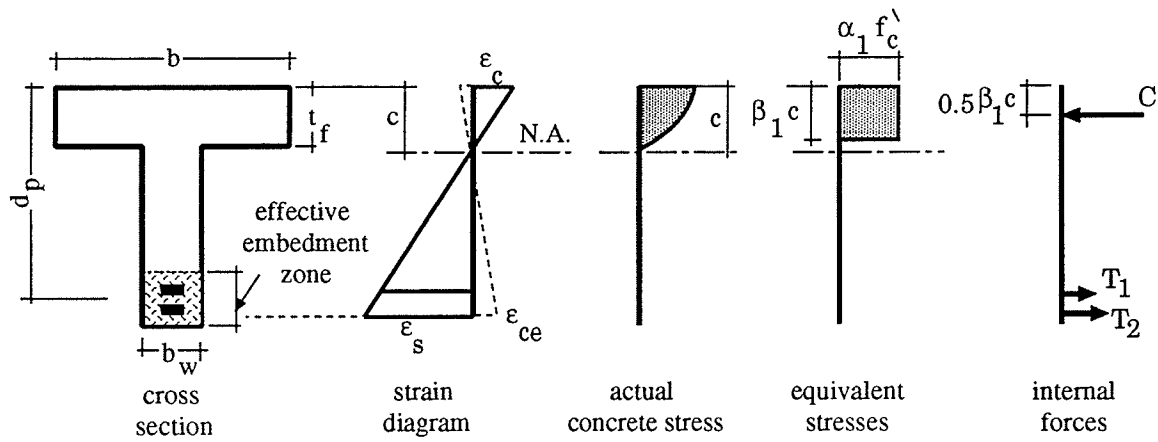


Fig.7-1 Strain compatibility of concrete section prestressed by FRP.

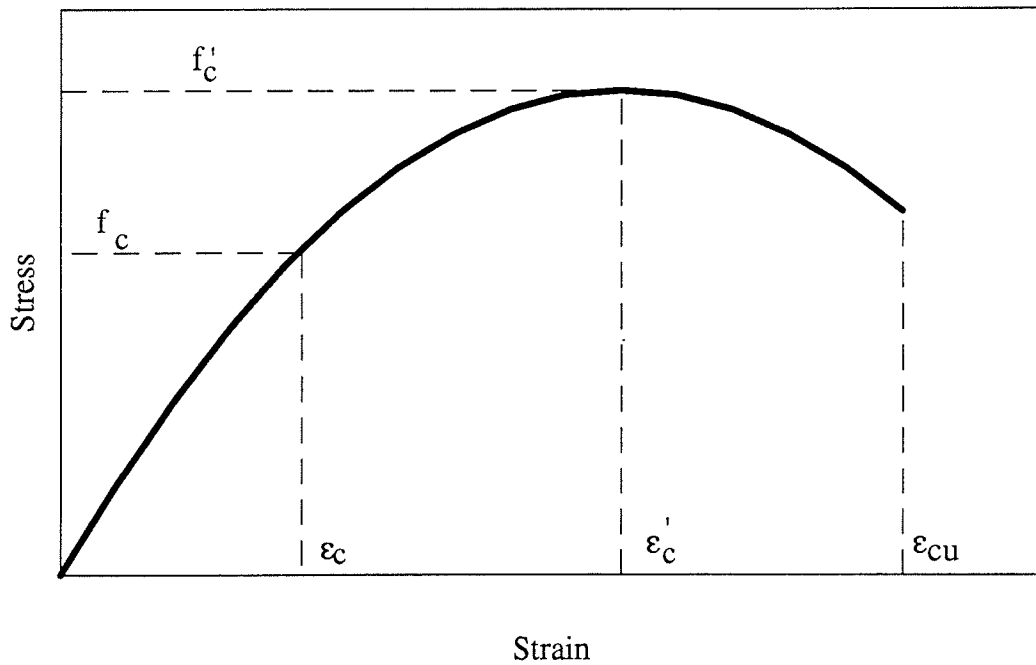


Fig.7-2 Stress-strain of the concrete in compression

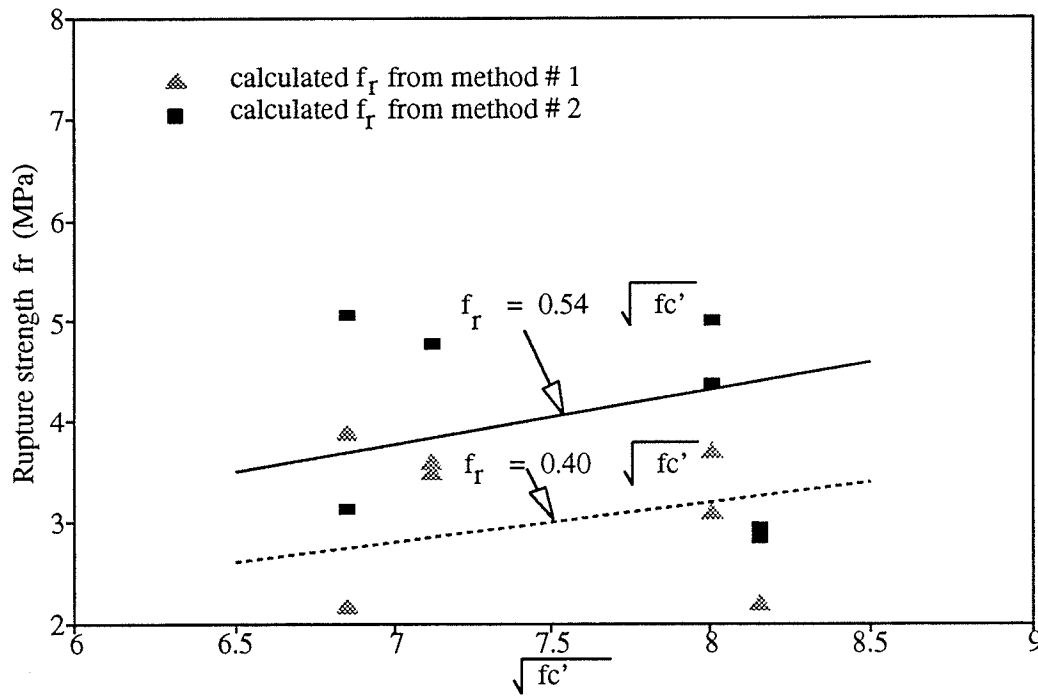


Fig.7-3 Calculated rupture strength of concrete

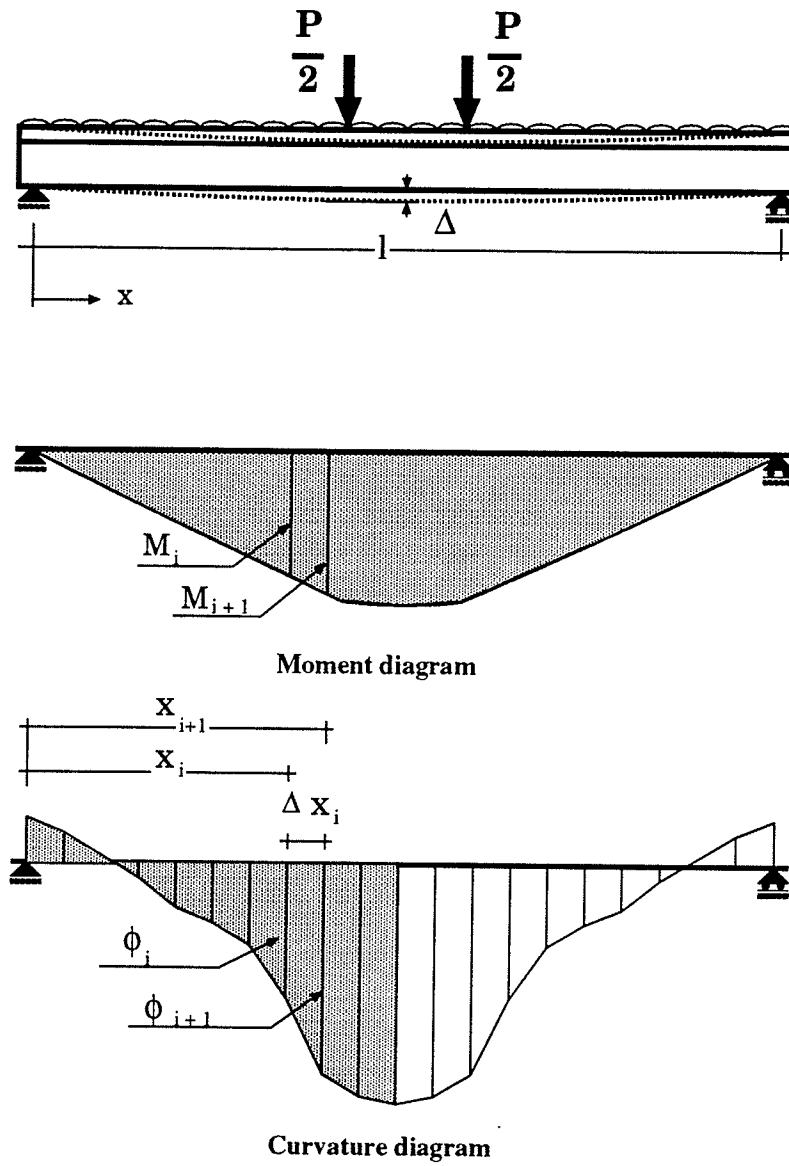


Fig.7-4 Numerical integration of the curvature for deflection calculation

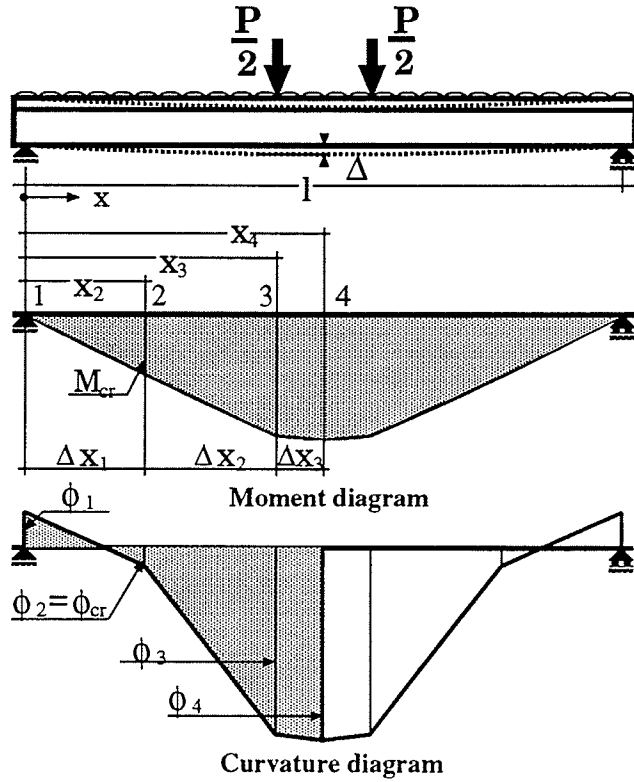


Fig.7-5 Integration of the curvature at key sections

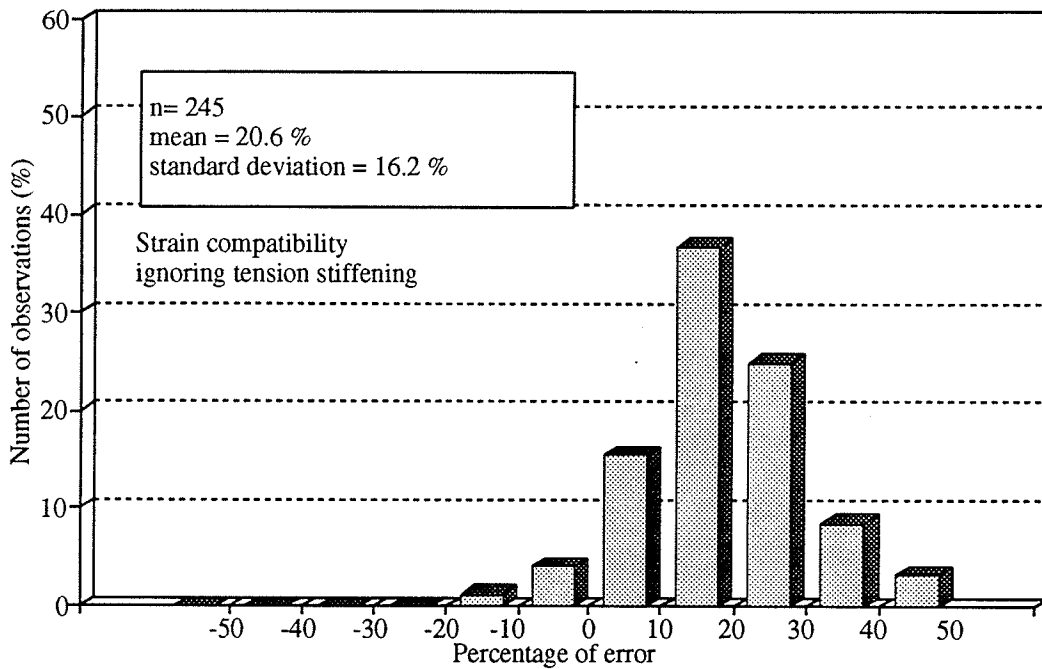


Fig.7-6 Error distribution of the predicted deflection ignoring tension stiffening

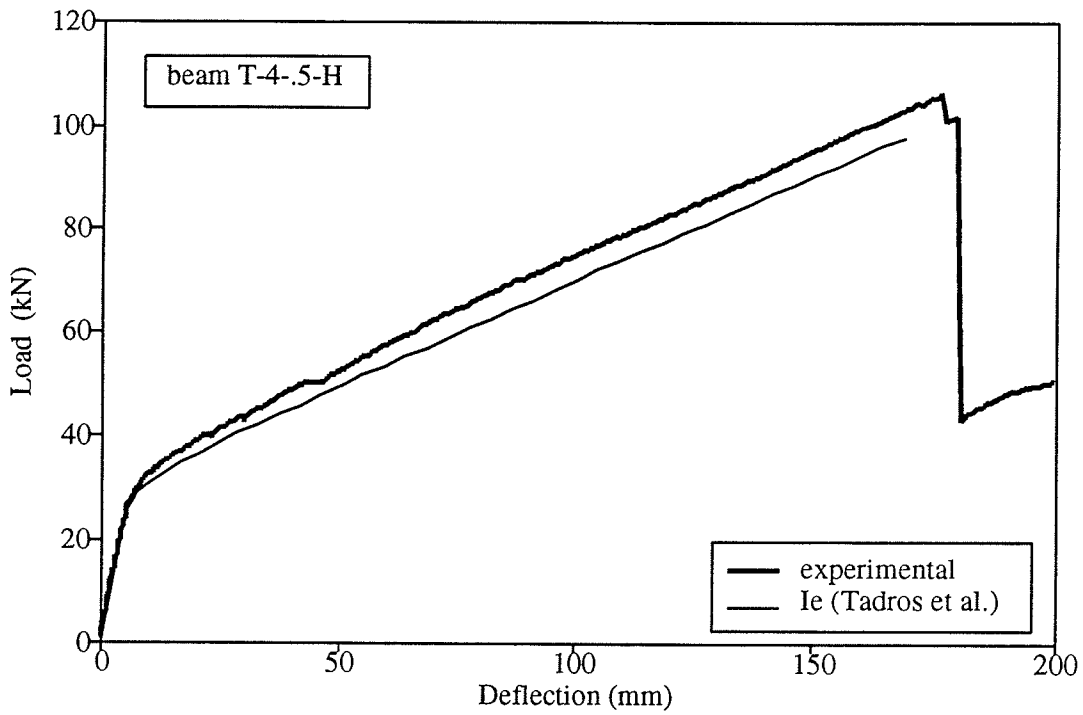


Fig.7-7 Load-deflection using I_e method (Tadros et al.)

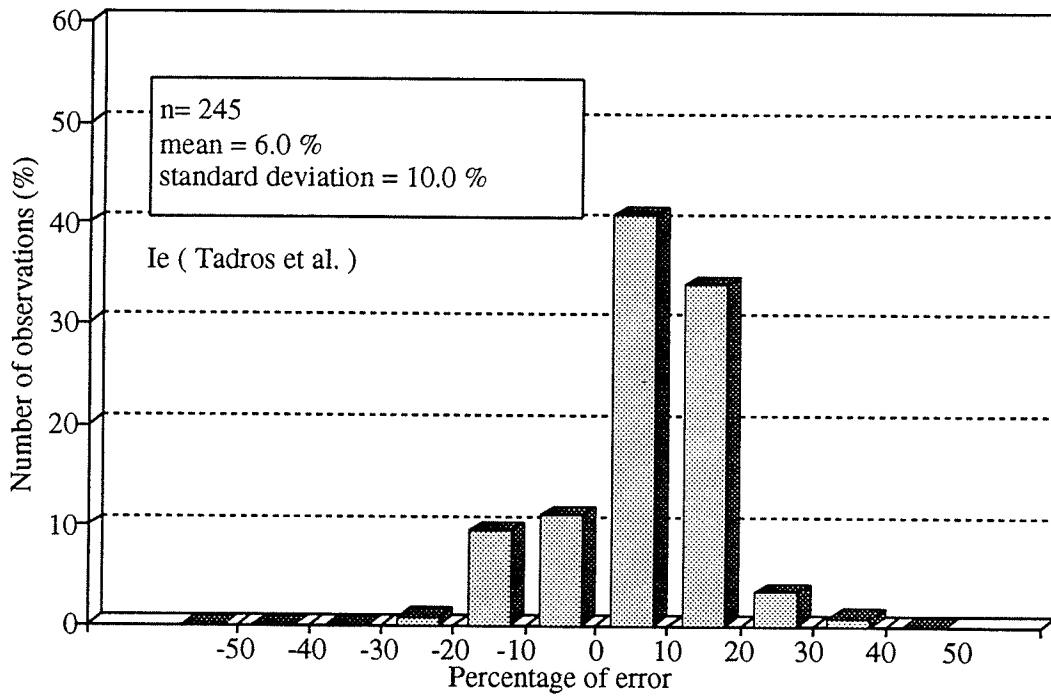


Fig.7-8 Error distribution of the predicted deflection using I_e method (Tadros et al.)

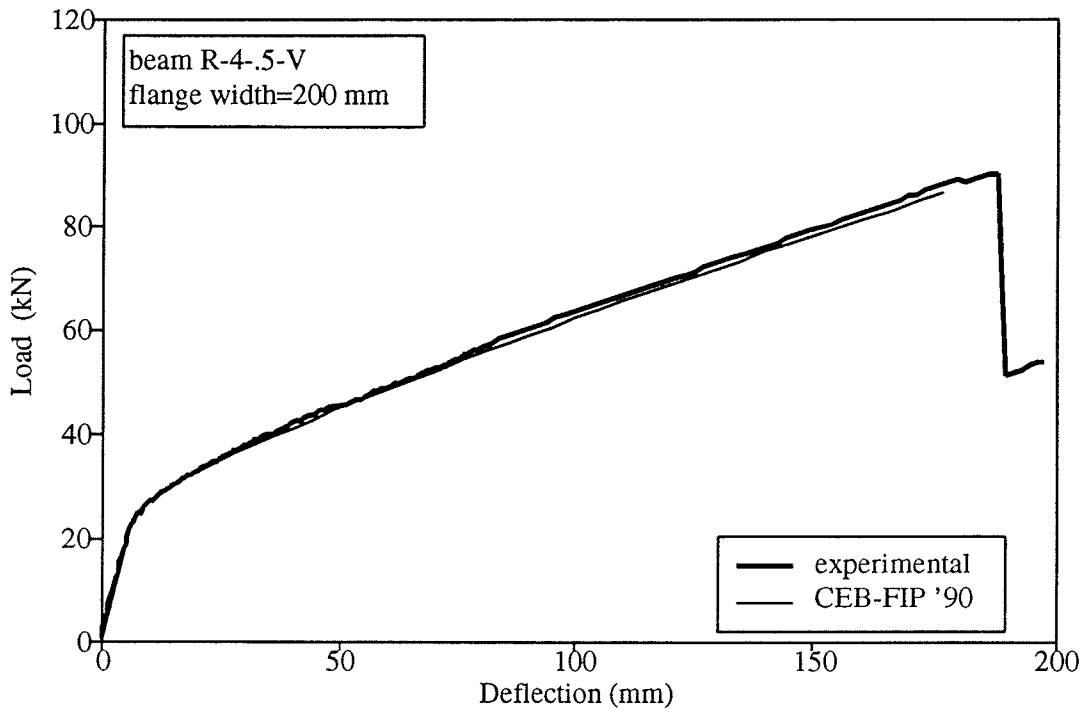


Fig.7-9 Predicted deflection using CEB-FIP Code for beam with small flange width

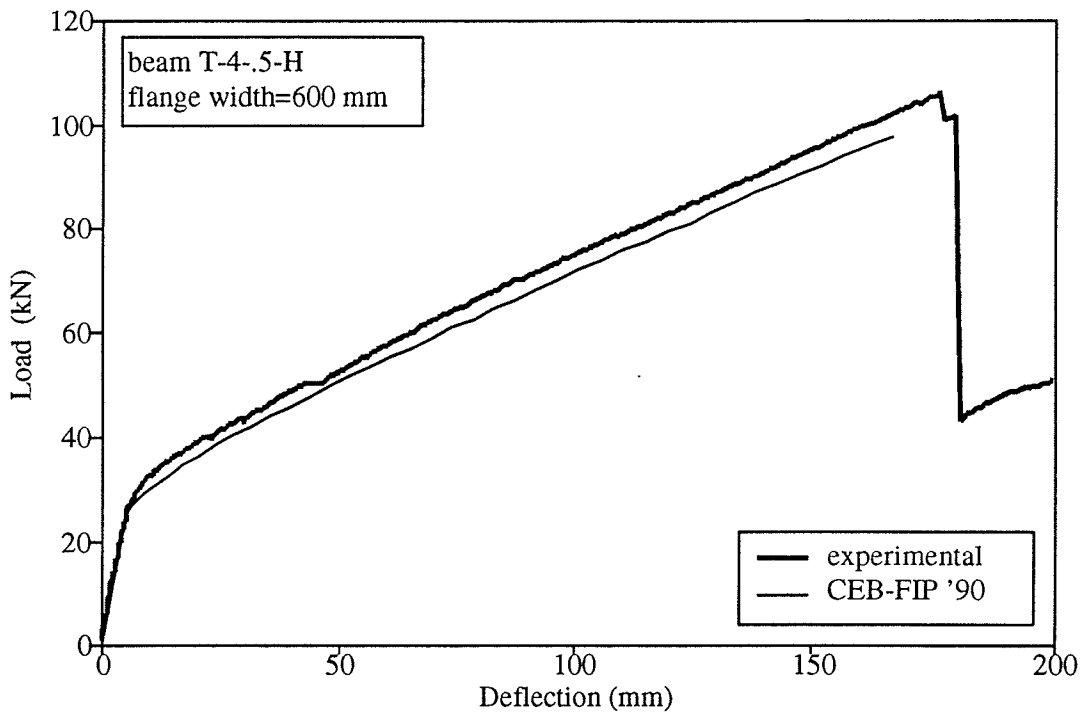


Fig.7-10 Predicted deflection using CEB-FIP Code for beam with large flange width

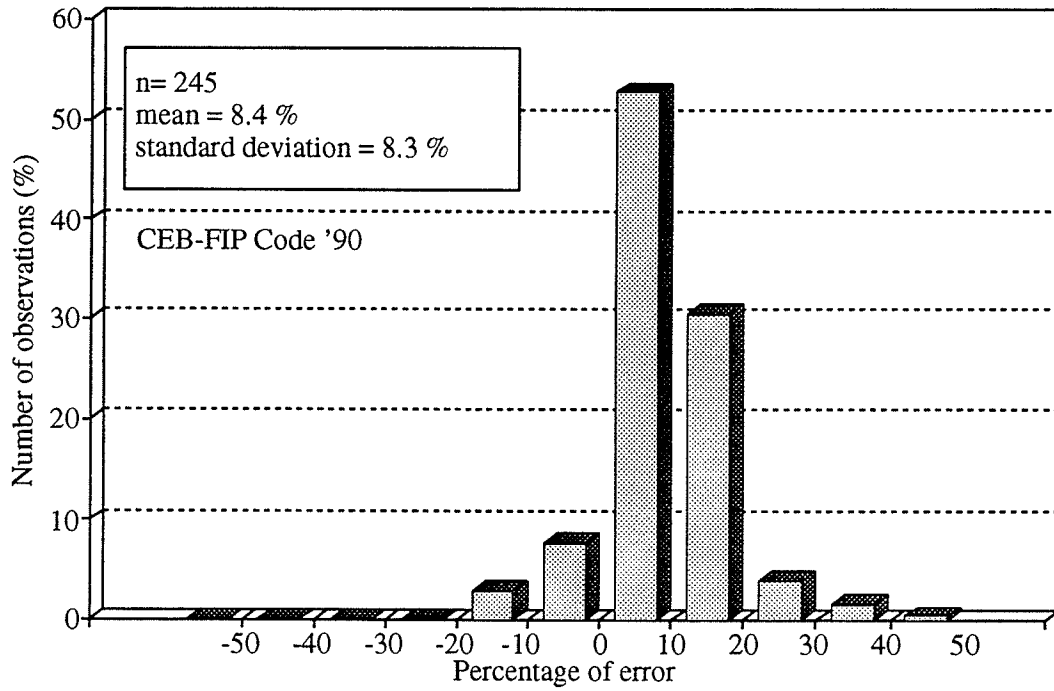


Fig.7-11 Error distribution of the predicted deflection using the CEB-FIP Code

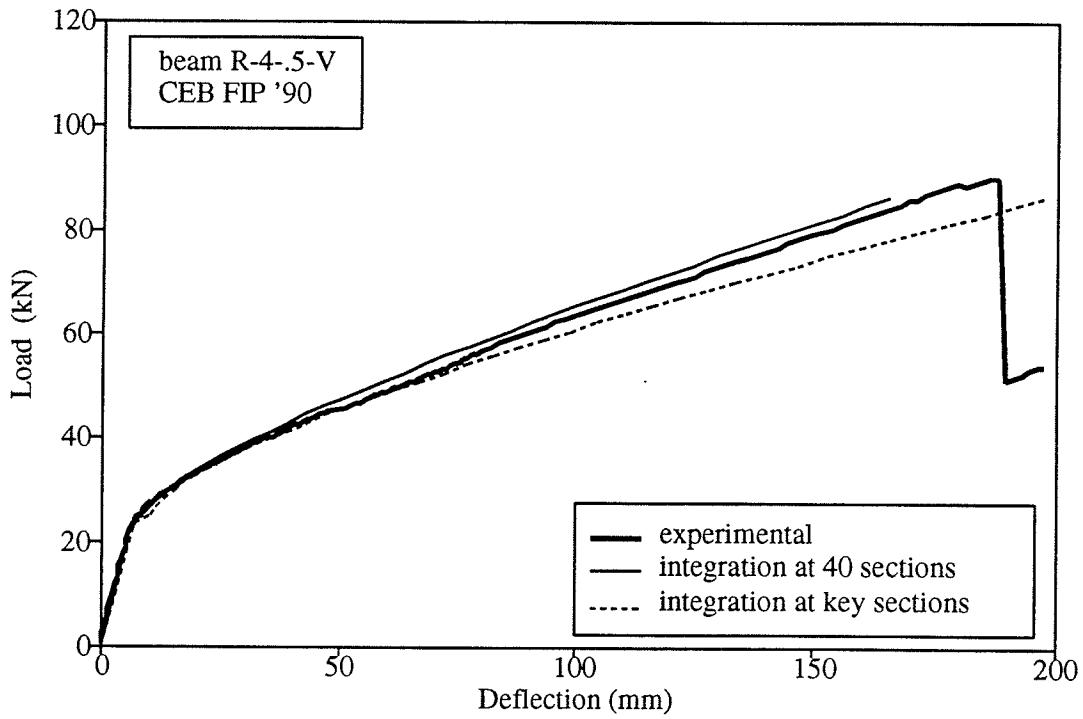


Fig.7-12 Predicted deflection using integration at key sections

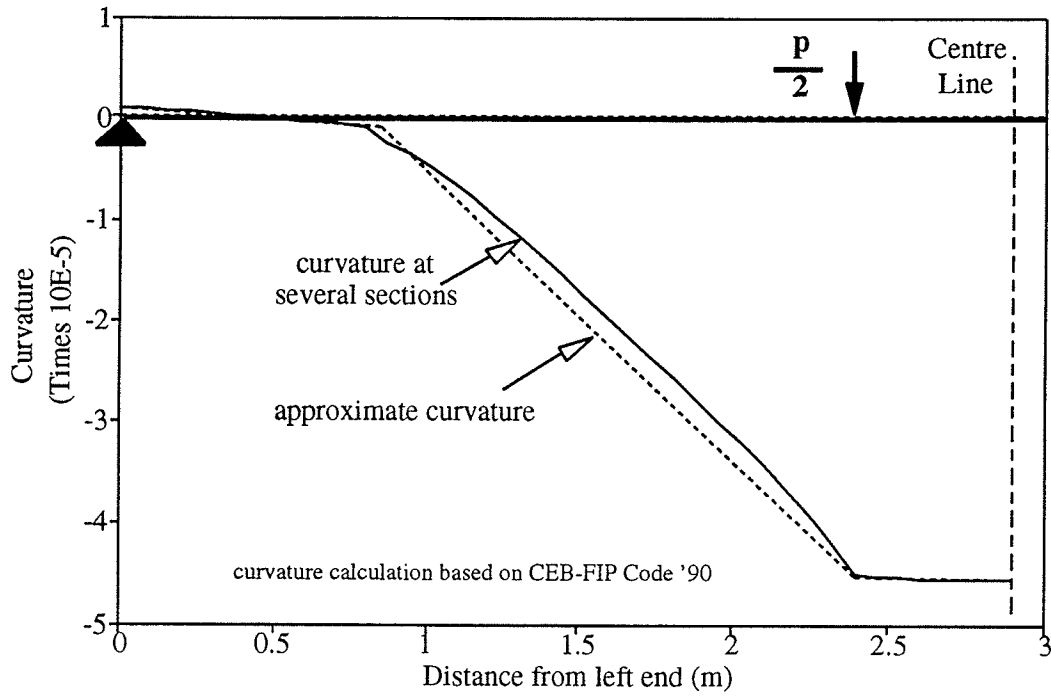


Fig.7-13 Curvature along the beam span using the CEB-FIP Code '90

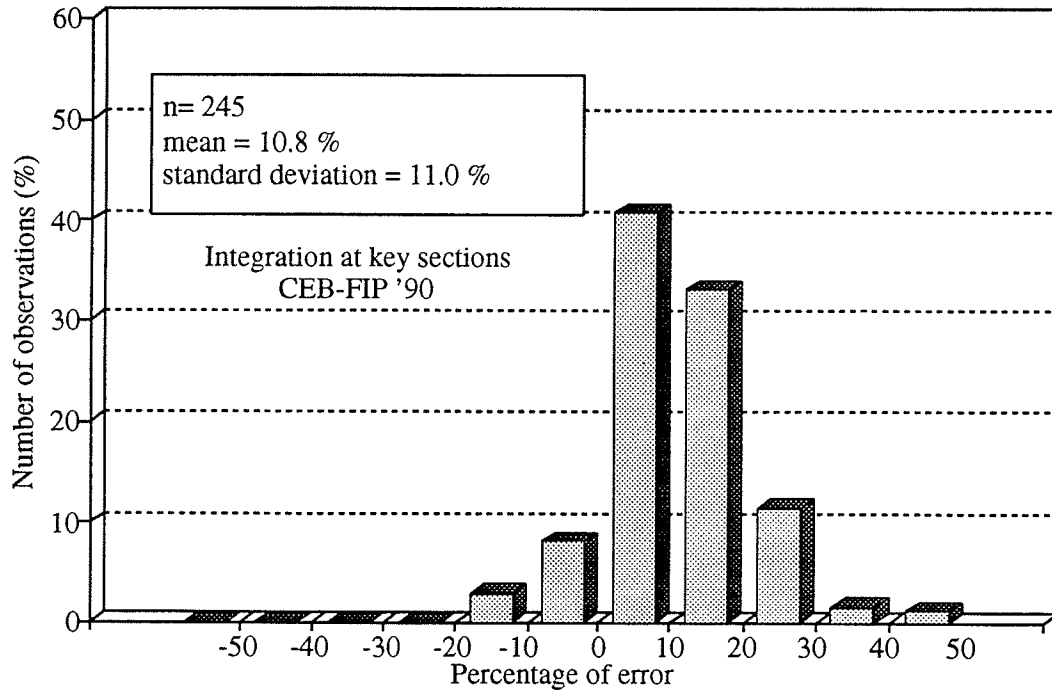


Fig.7-14 Error distribution of the predicted deflection using integration at key sections

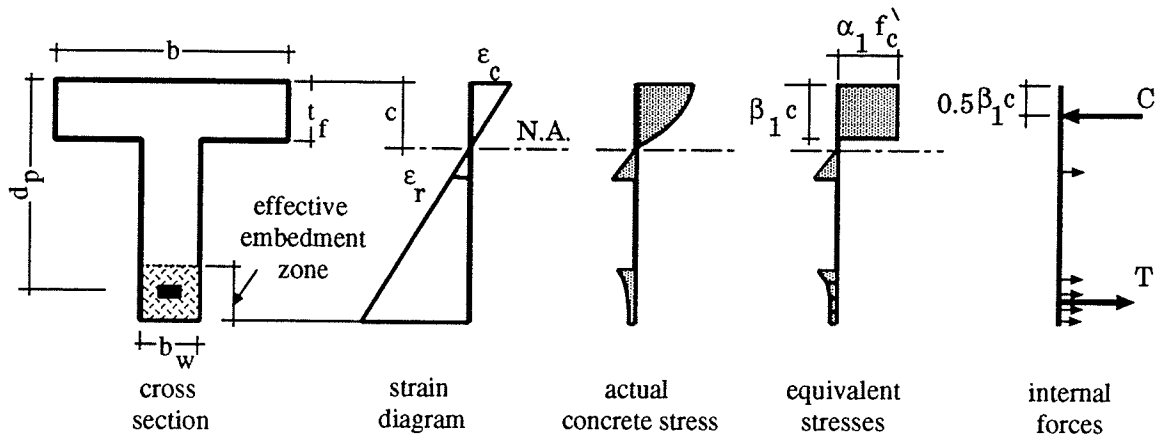


Fig.7-15 Strain compatibility of prestressed concrete section accounting for concrete in tension

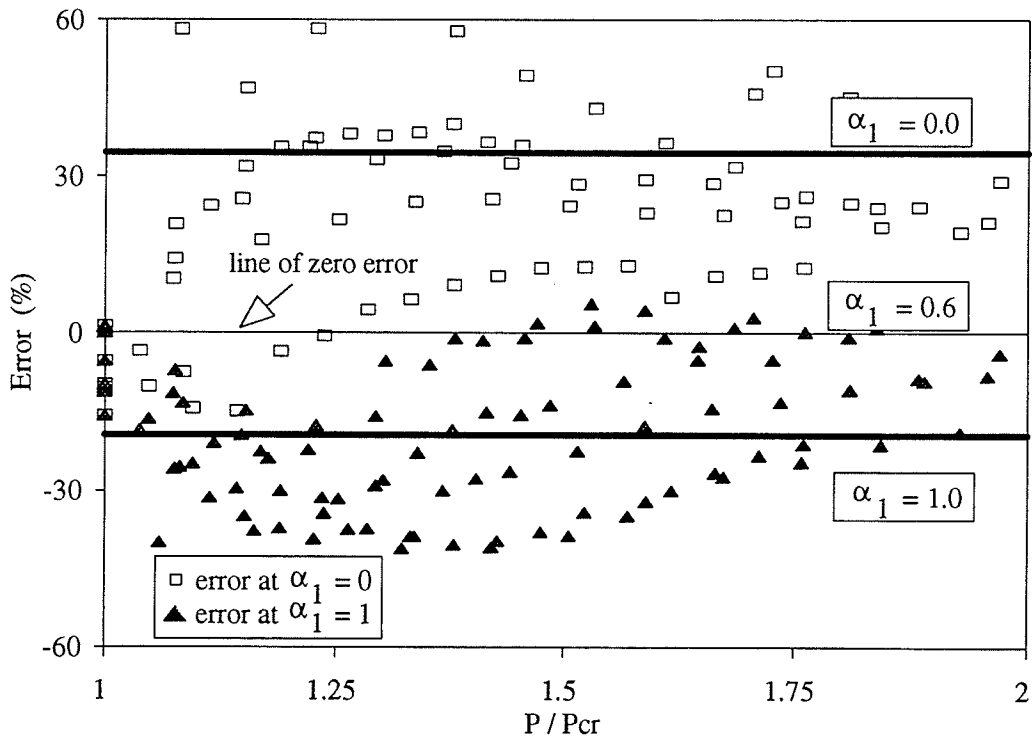


Fig.7-16 Prediction of α_1 for beams prestressed by Leadline

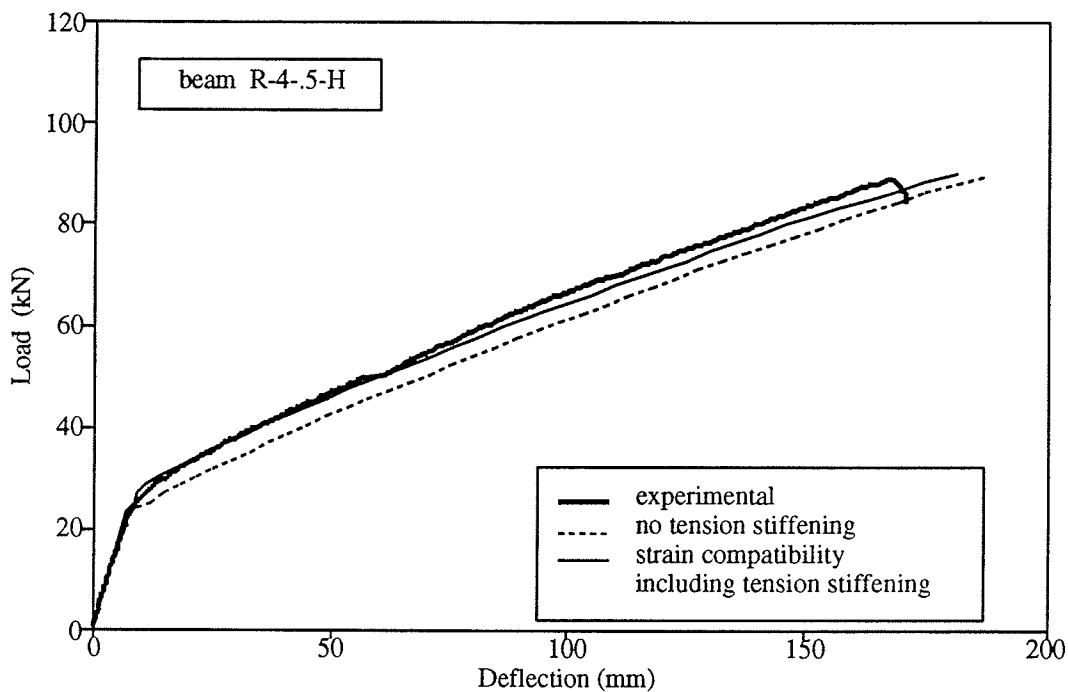


Fig.7-17 Predicted deflection using strain compatibility with and without accounting for tension stiffening

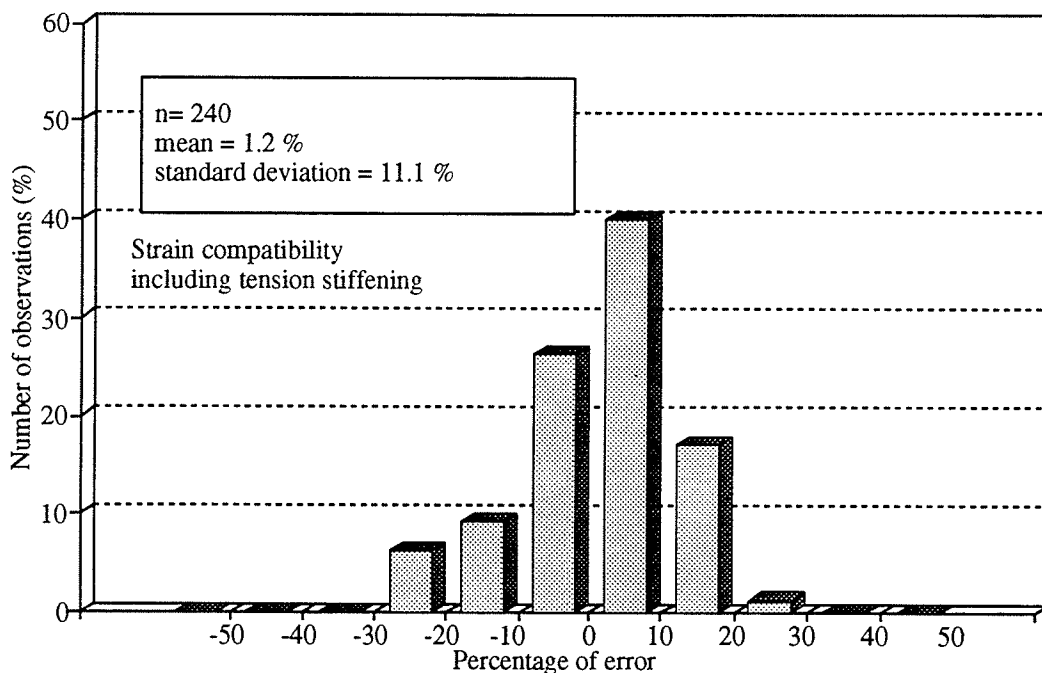


Fig.7-18 Error distribution of the predicted deflection using strain compatibility accounting for concrete in tension

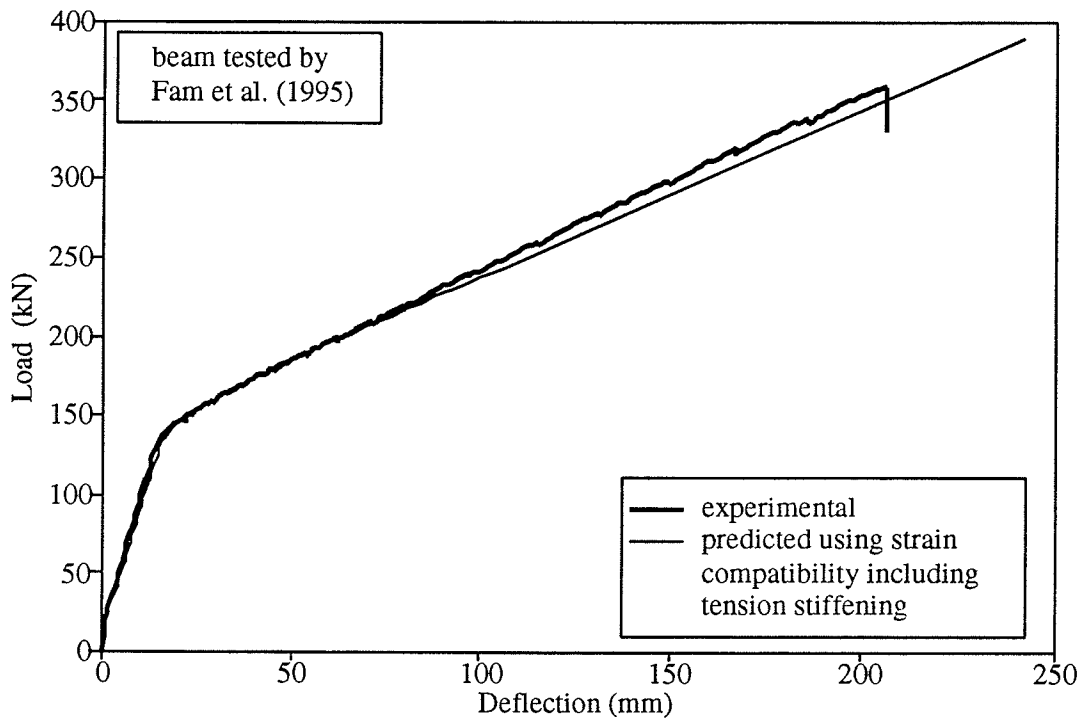


Fig.7-19 Predicted deflection using method 3 for a beam prestressed by Leadline tested by Fam and Rizkalla (1995)

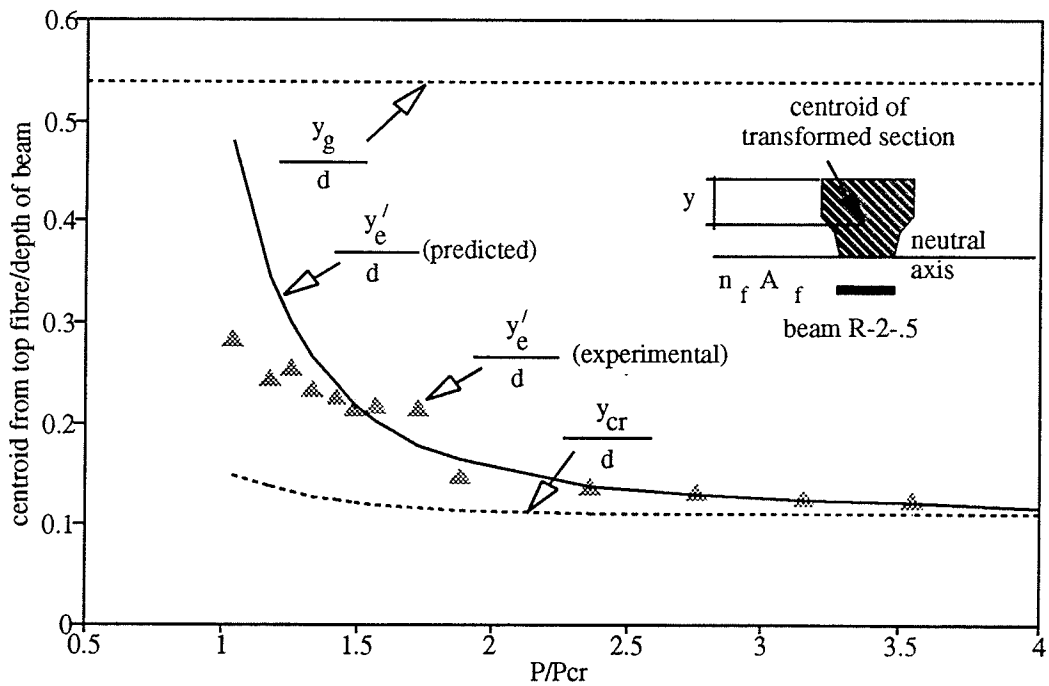


Fig.7-20 Predicted vs. measured effective centroidal distance, y'_e

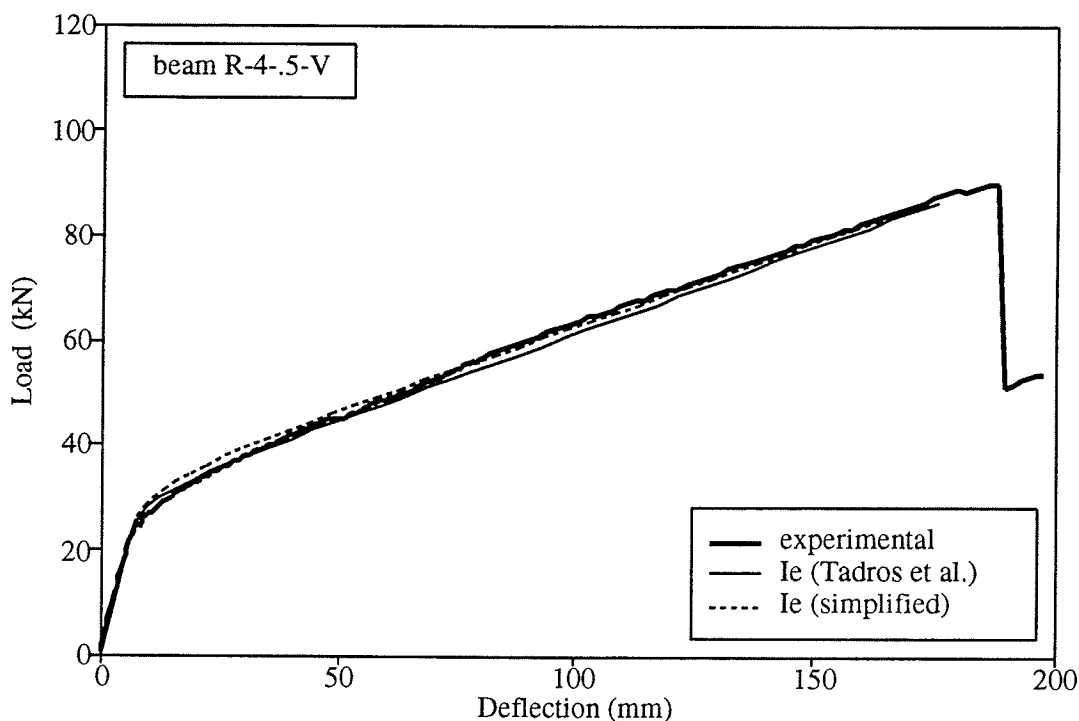


Fig.7-21 Predicted deflection using I_e methods (Tadros et al. 1985 and simplified method)

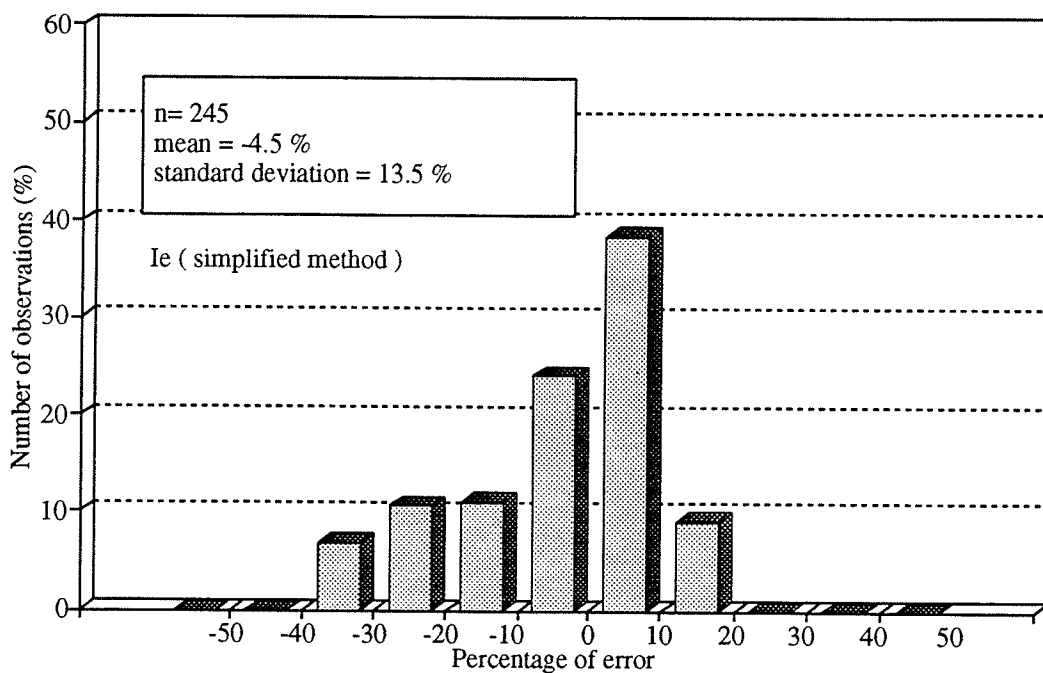


Fig.7-22 Error distribution of the predicted deflection using the simplified method

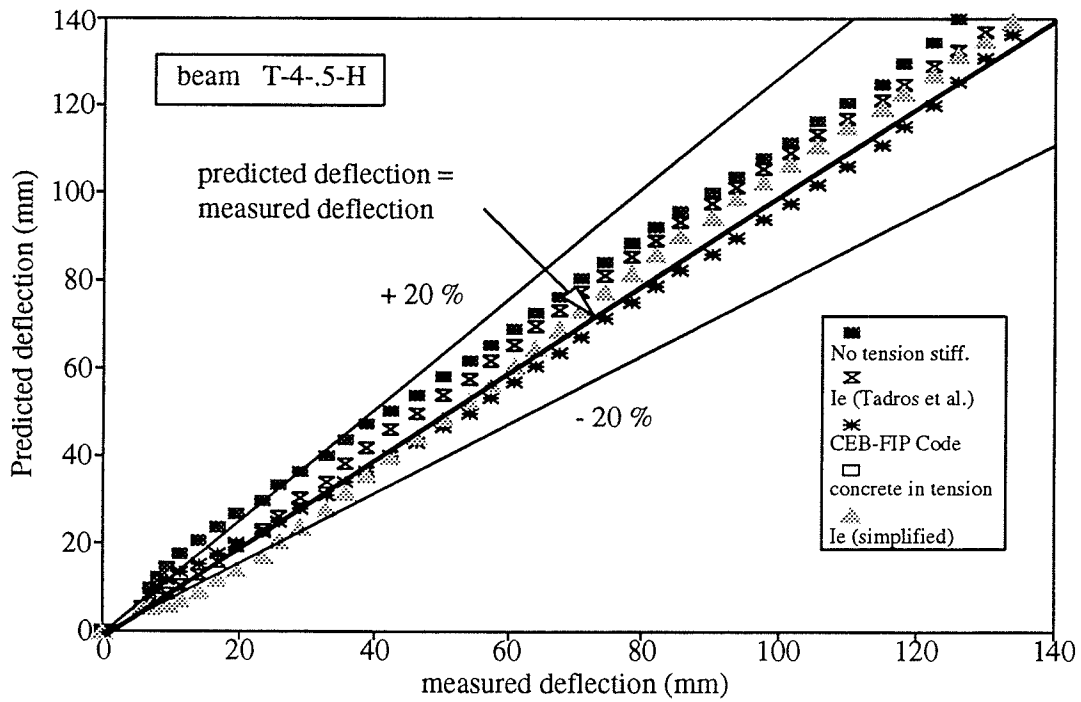


Fig.7-23 Predicted versus measured deflection for a typical beam

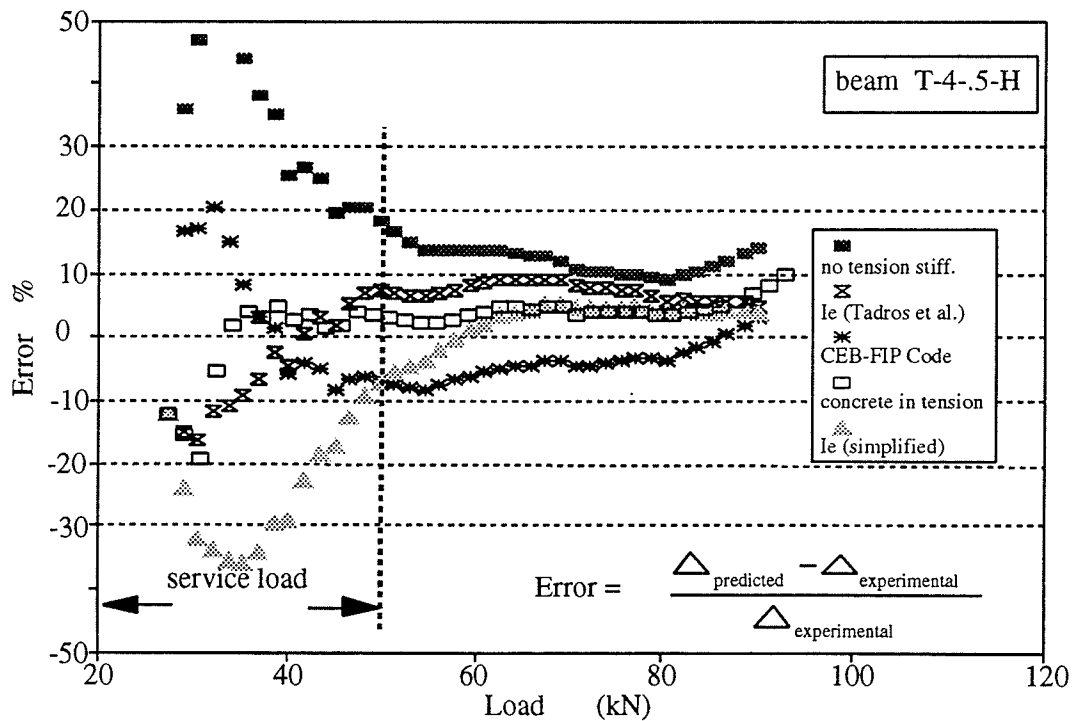


Fig.7-24 Error distribution of the predicted deflection for a typical beam

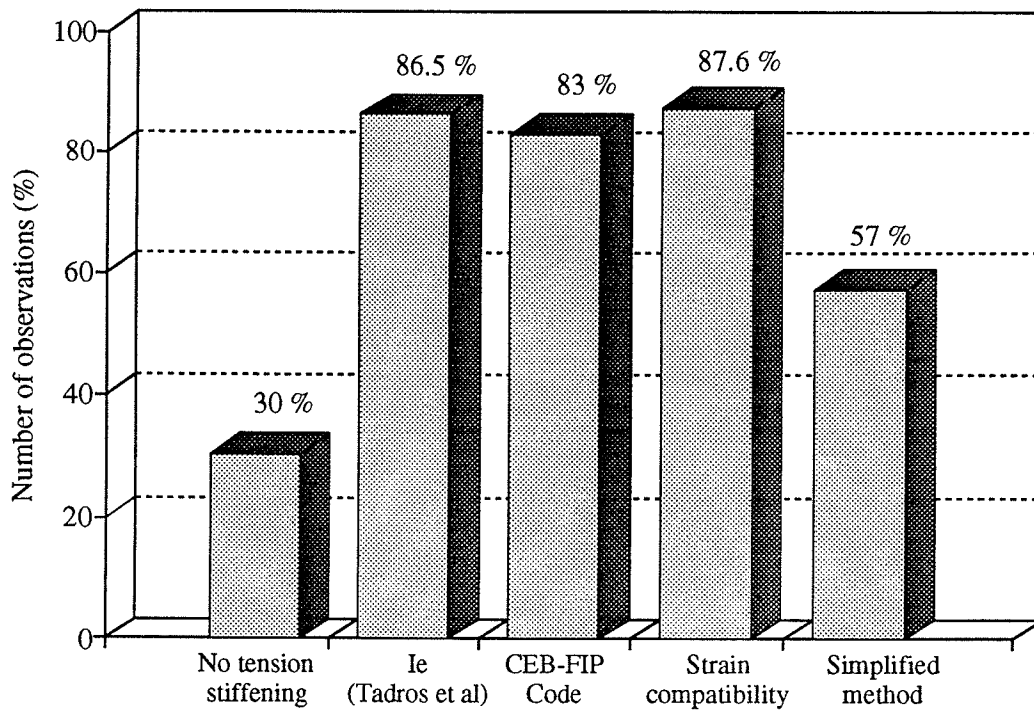


Fig.7-25 Accuracy of the deflection calculation within service load range

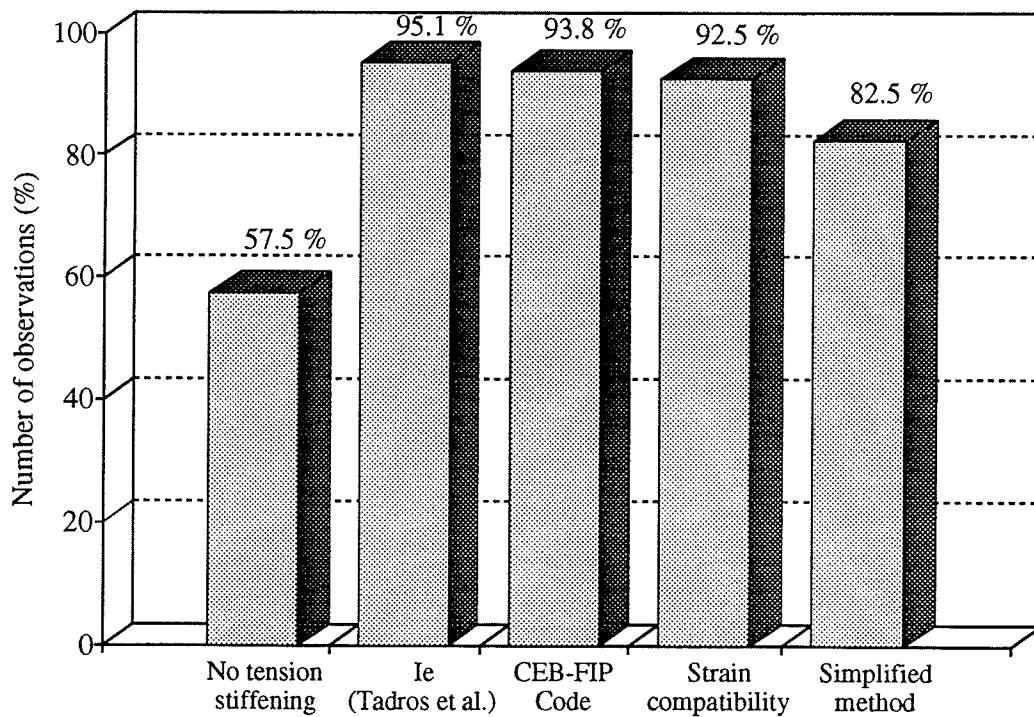


Fig.7-26 Accuracy of the deflection calculation up to the ultimate load

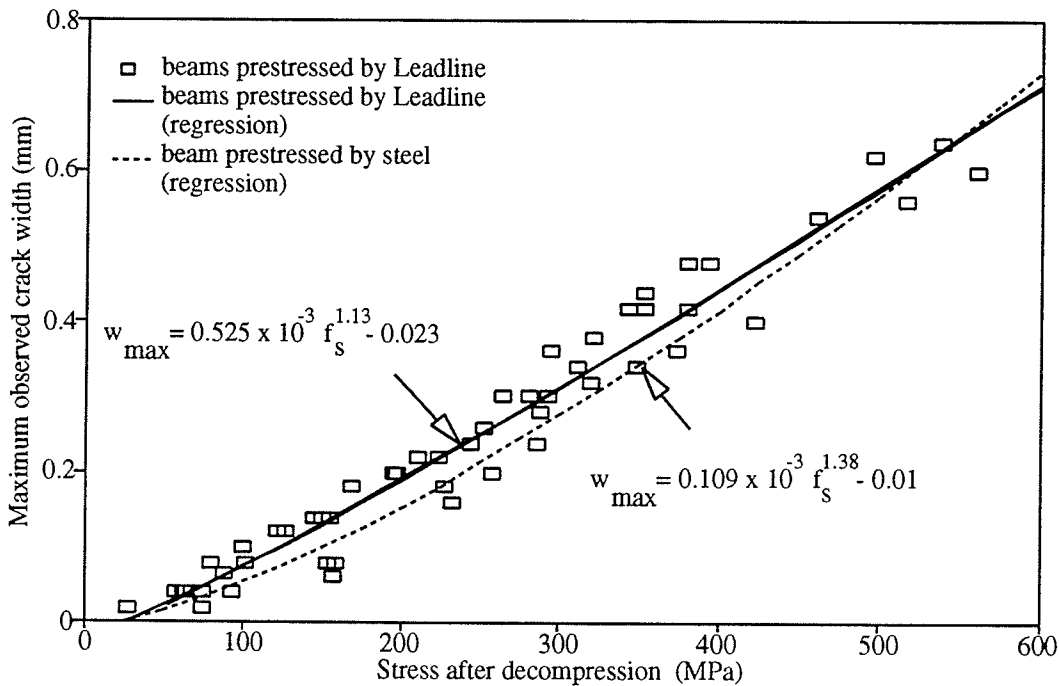


Fig.7-27 Non-linear regression of the stress of prestressing reinforcement after decompression versus crack width

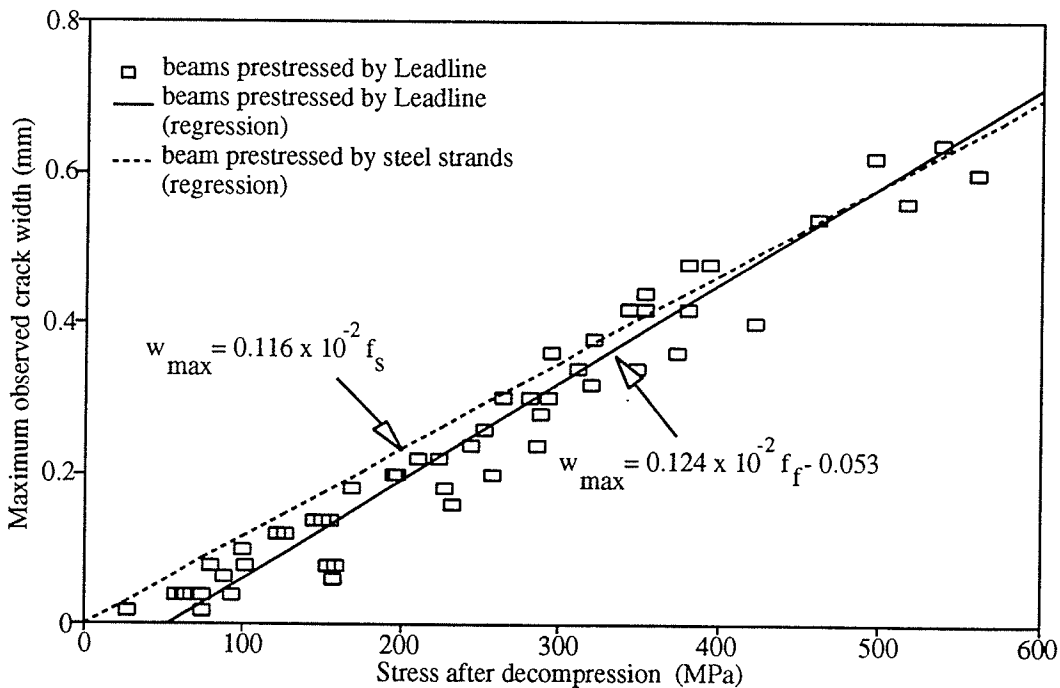


Fig.7-28 Linear regression of the stress of prestressing reinforcement after decompression versus crack width

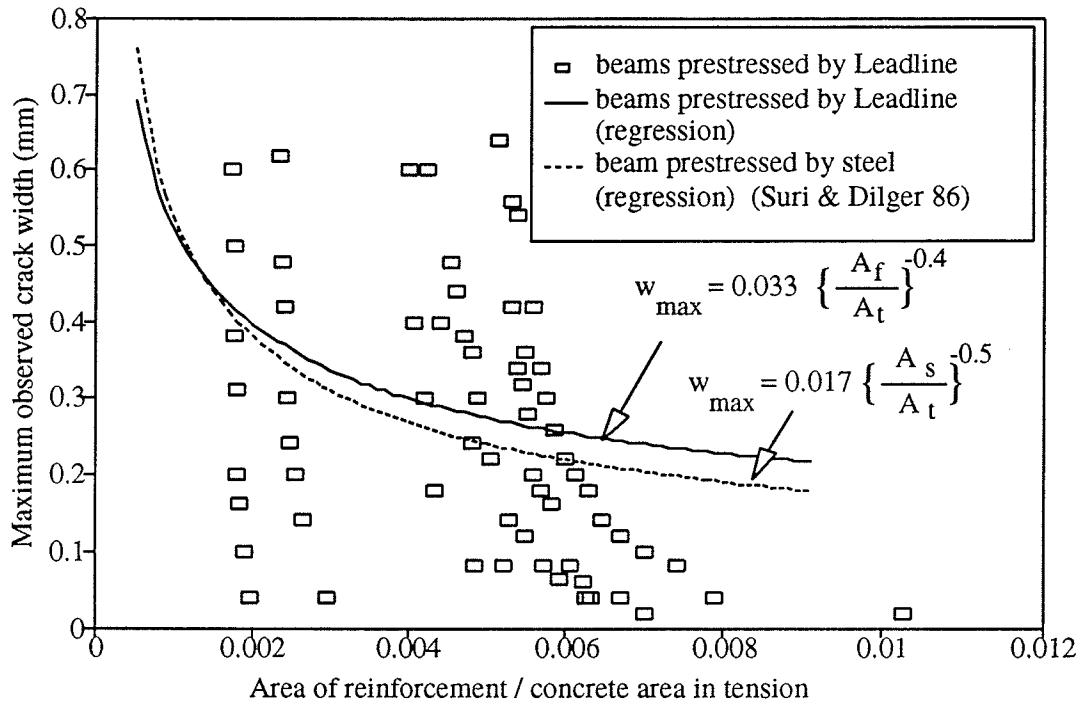


Fig.7-29 Correlation between concrete area in tension, A_t , and crack width

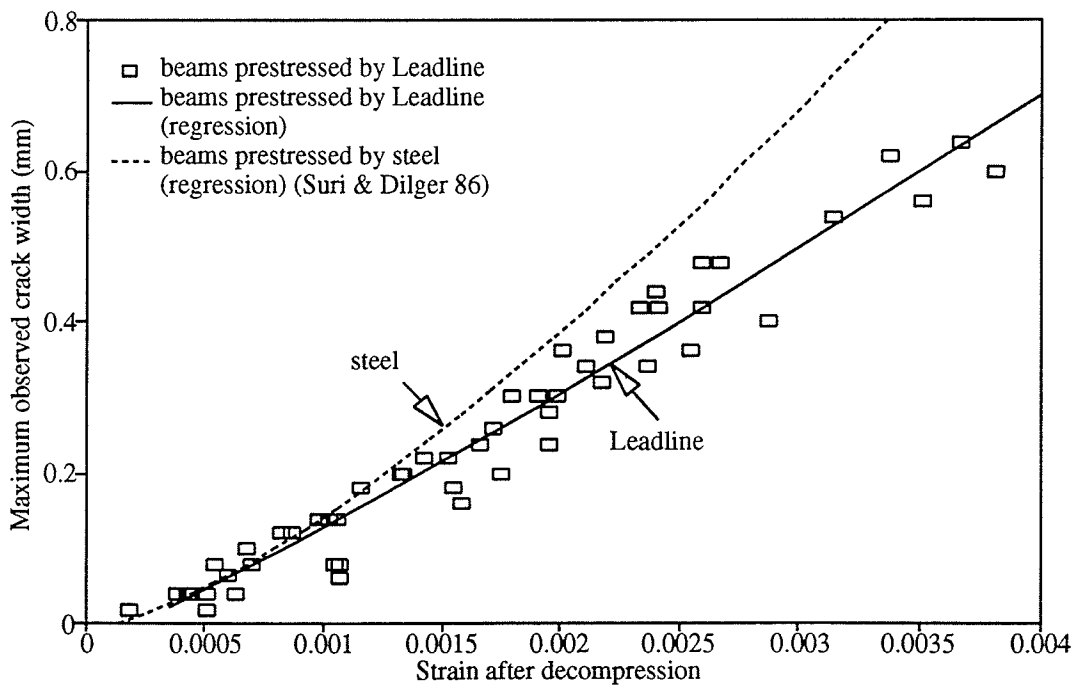


Fig.7-30 Strain versus maximum crack width for beams prestressed by Leadline and steel

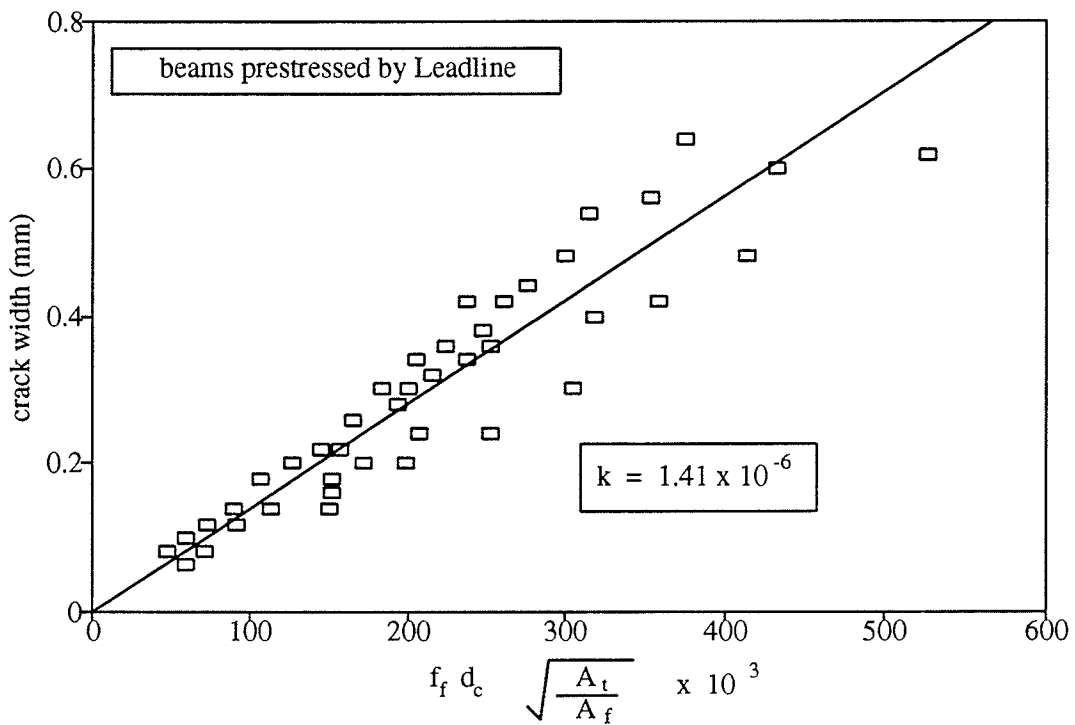


Fig.7-31 Calculation of bond factor, k, using Suri and Dilger method (1986)

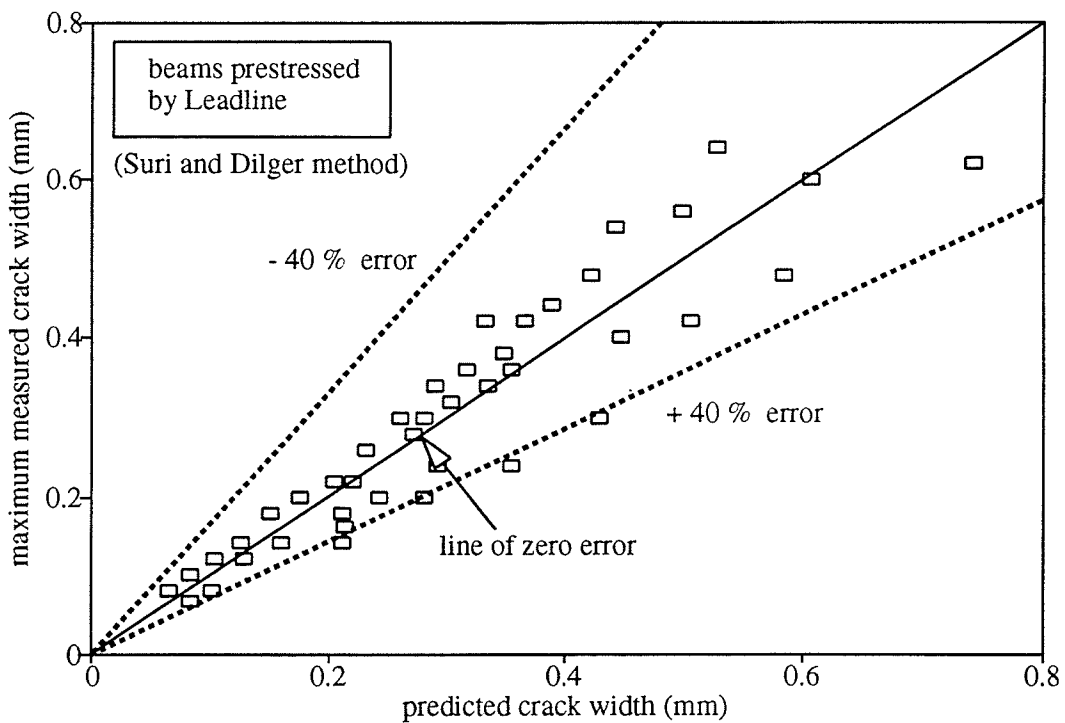


Fig.7-32 Crack width prediction using Suri and Dilger method (1986)

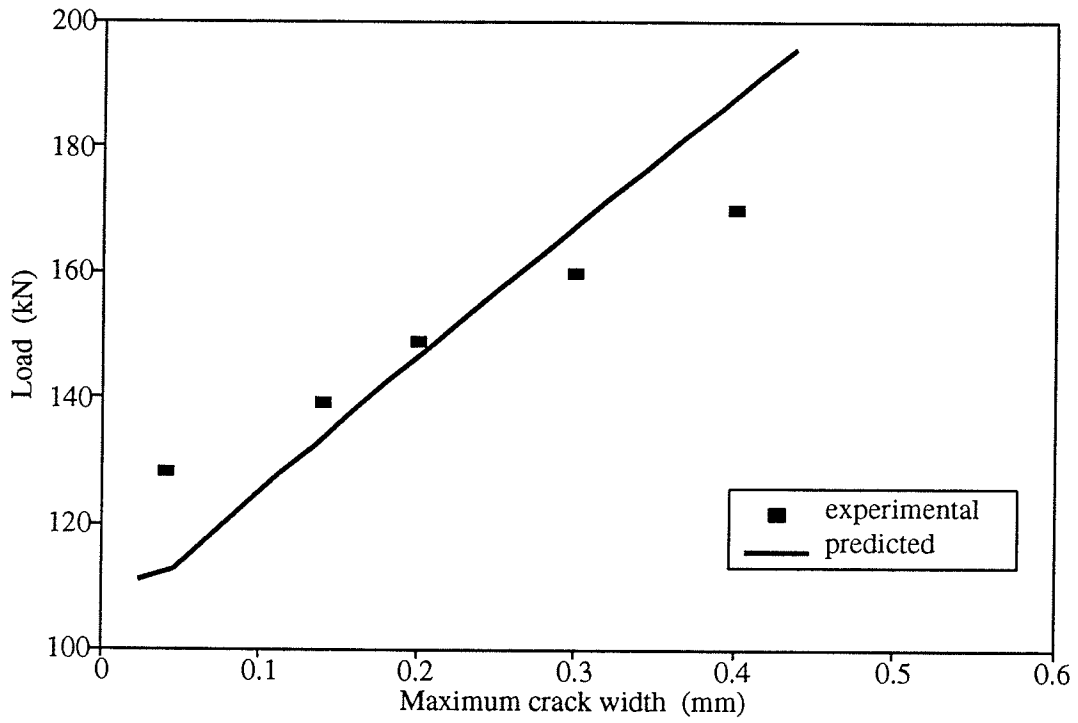


Fig.7-33 Predicted crack width using Suri and Dilger method for a beam tested by (Fam and Rizkalla 1995)

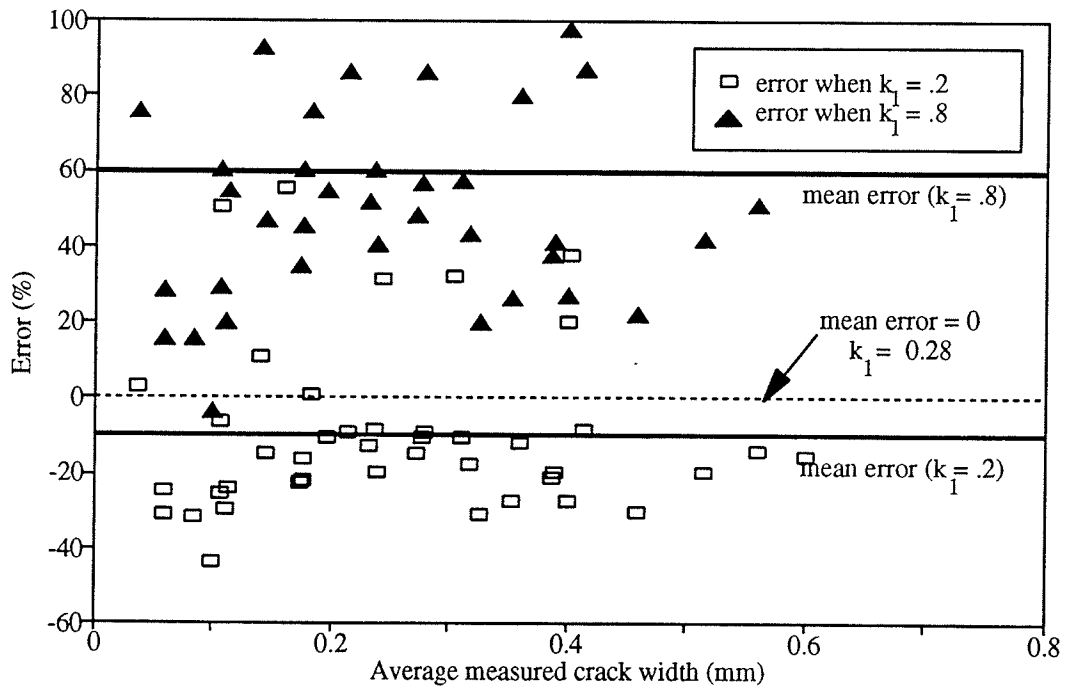


Fig.7-34 Calculation of bond factor, k_1 , using the CEB-FIP Code (1978)

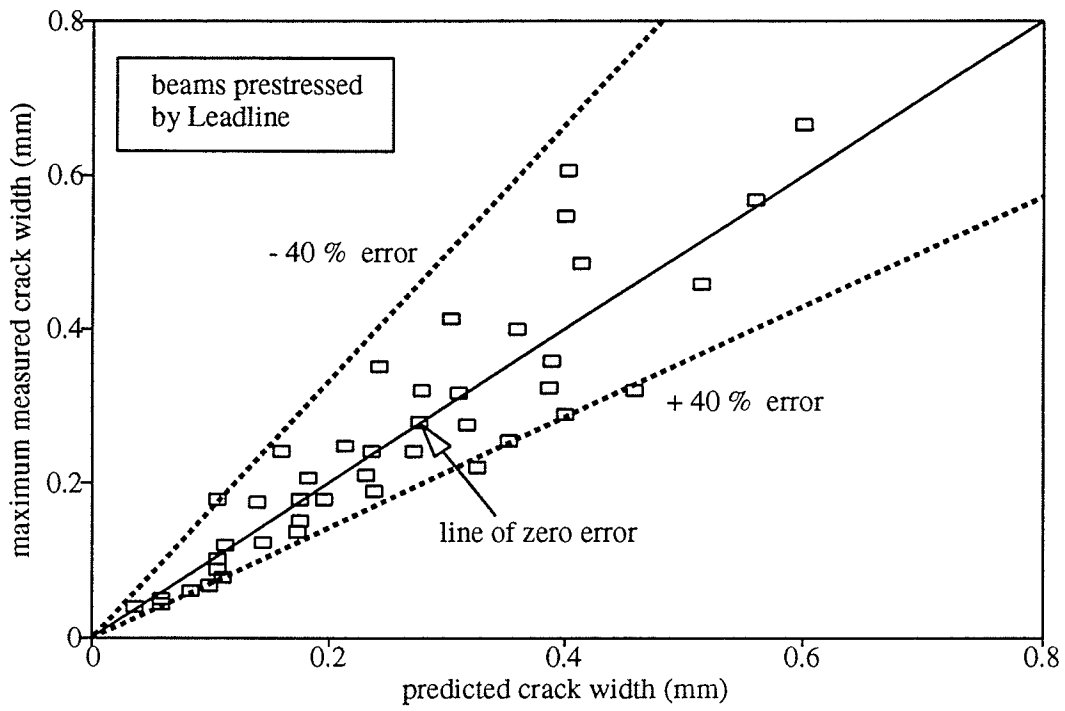


Fig.7-35 Crack width prediction using the CEB-FIP Code (1978)

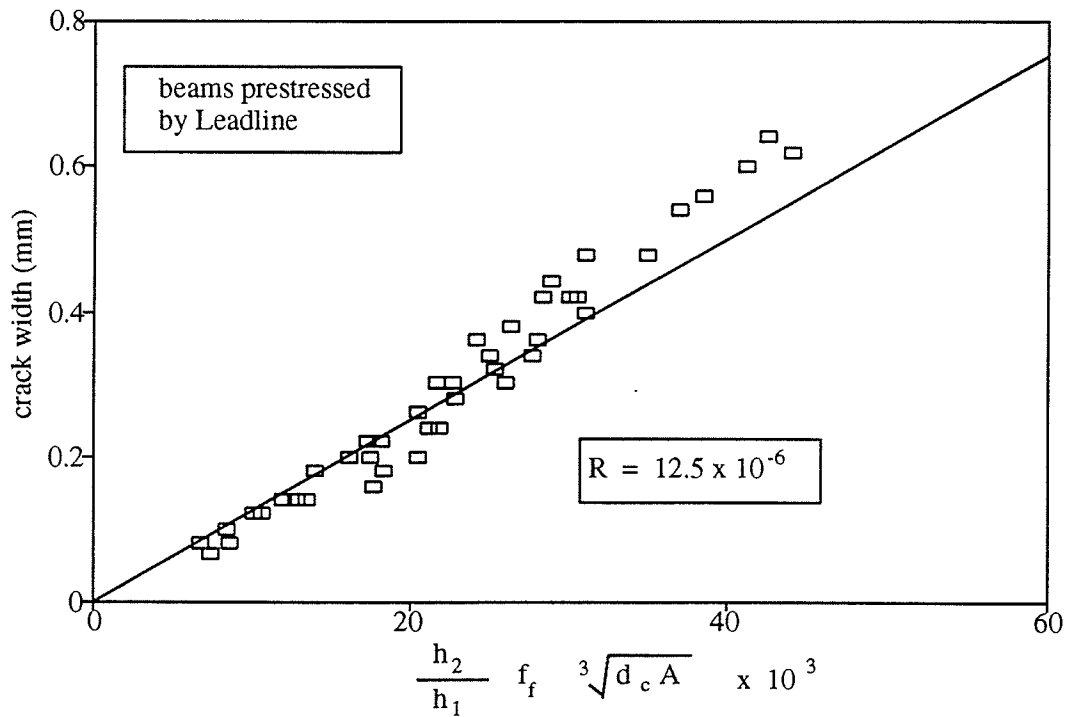


Fig.7-36 Calculation of bond factor, R, using Gergely and Lutz method (1966)

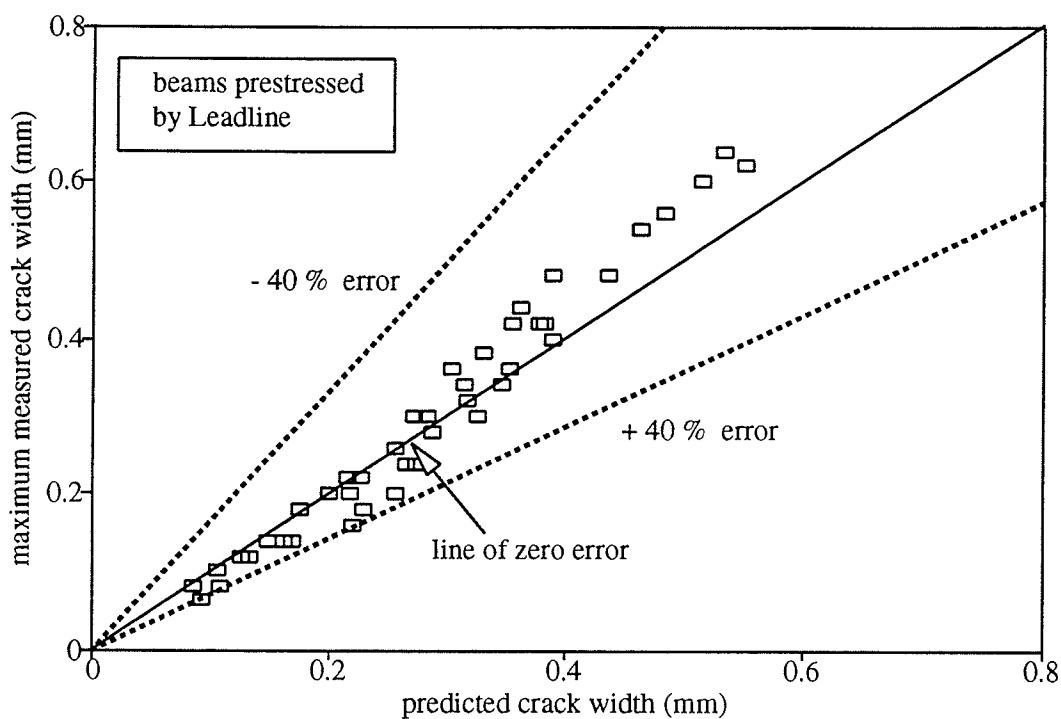


Fig.7-37 Crack width prediction using Gergely and Lutz method (1966)

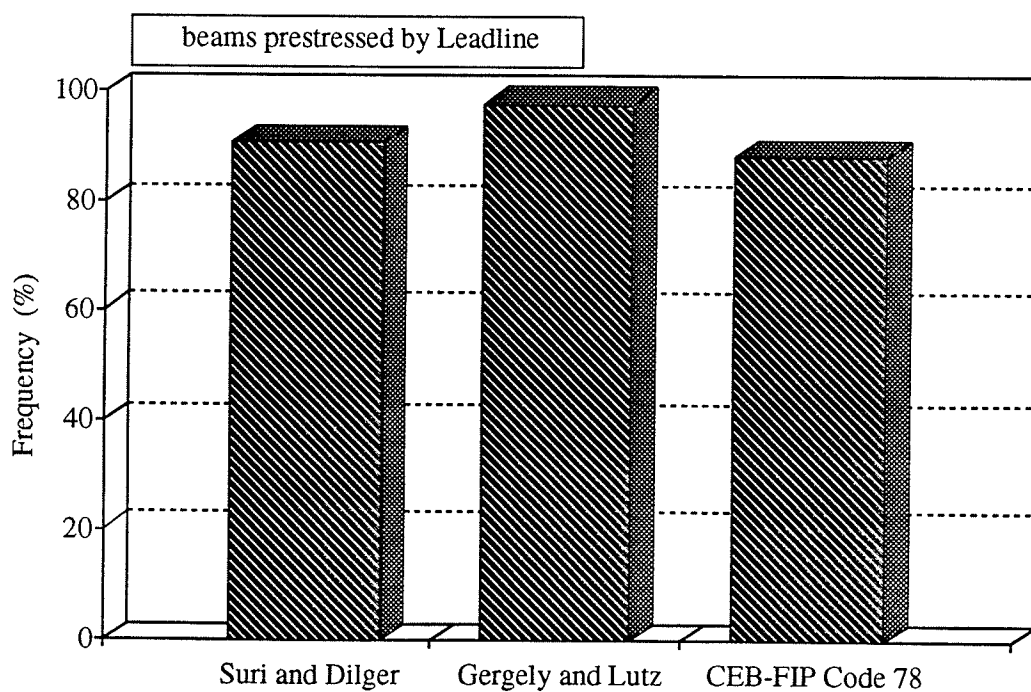


Fig.7-38 Accuracy of the three methods used for calculating the crack width

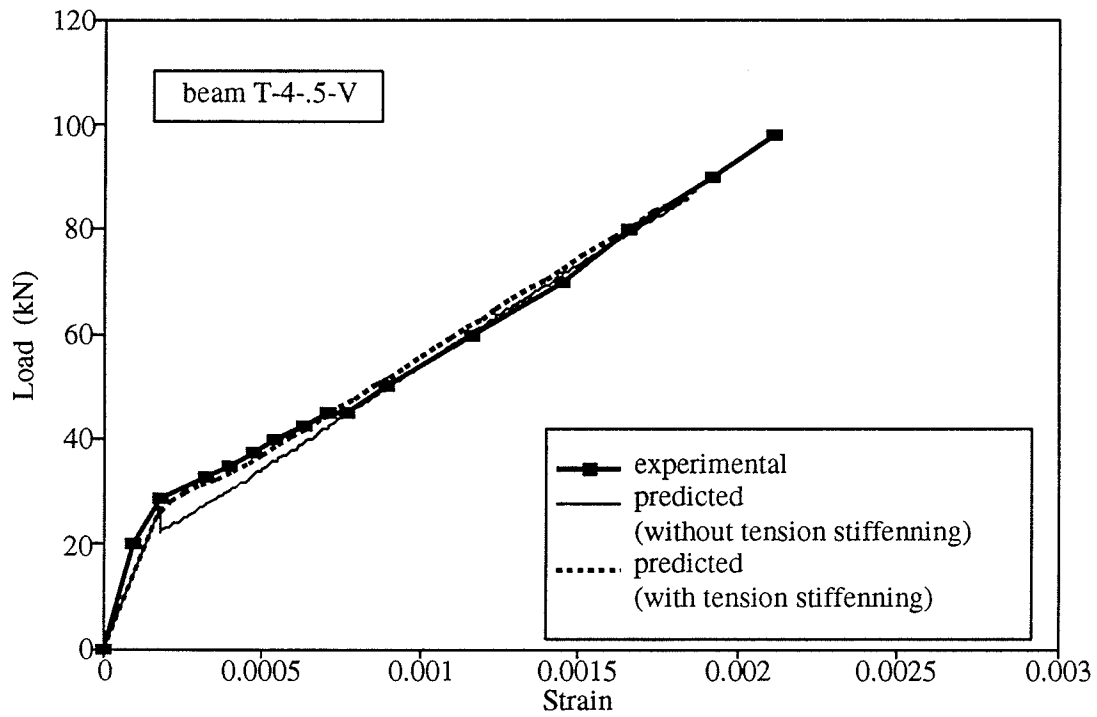


Fig.7-39 Predicted vs. measured strain at the extreme compression fibre

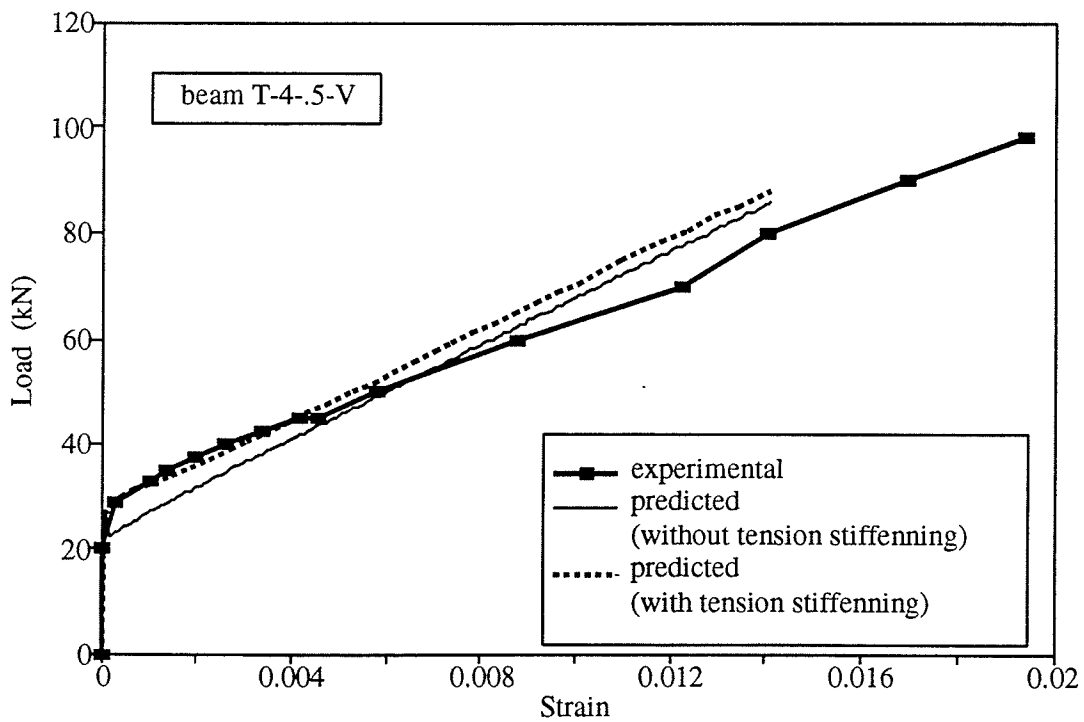


Fig.7-40 Predicted vs. measured strain at the level of the bottom CFRP bars

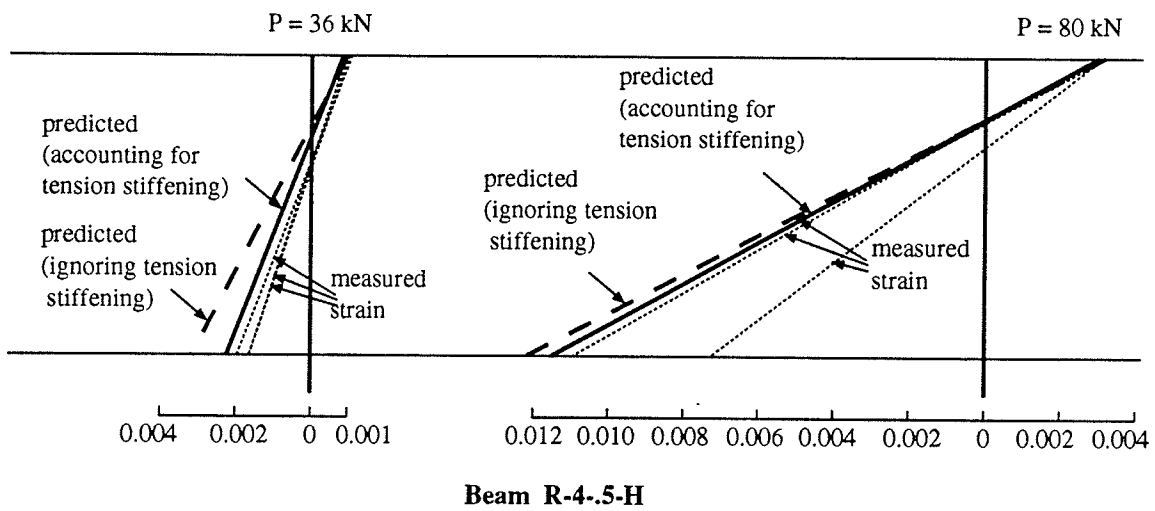
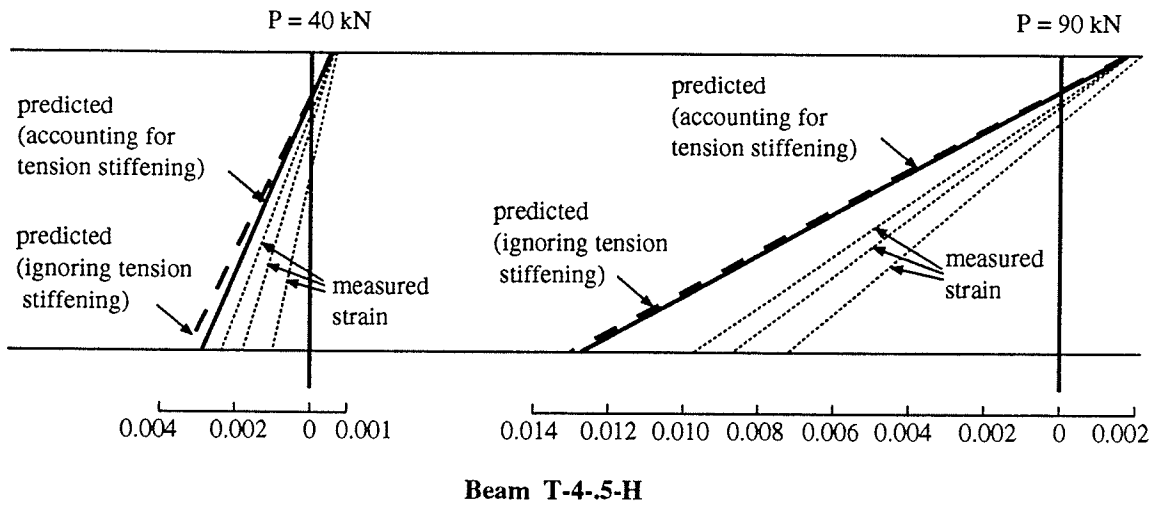
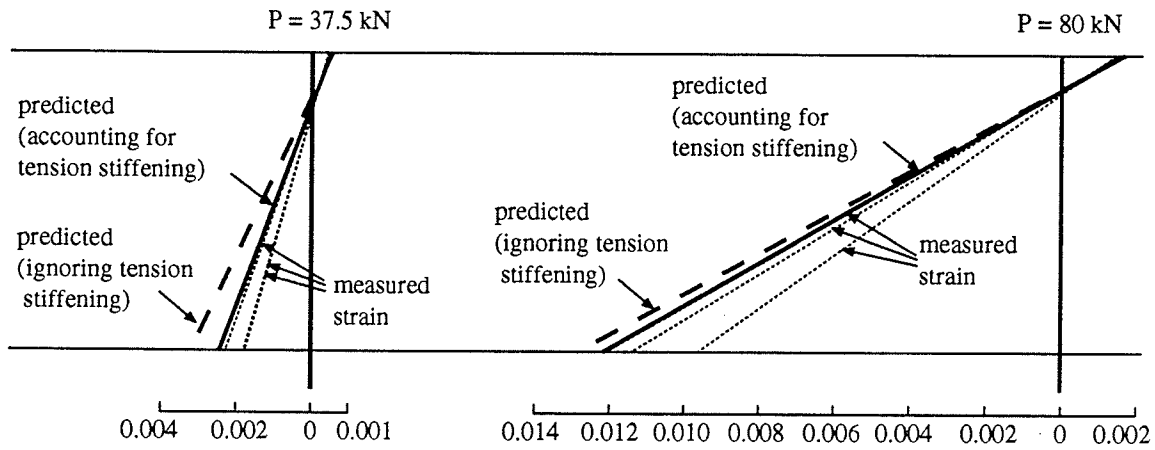
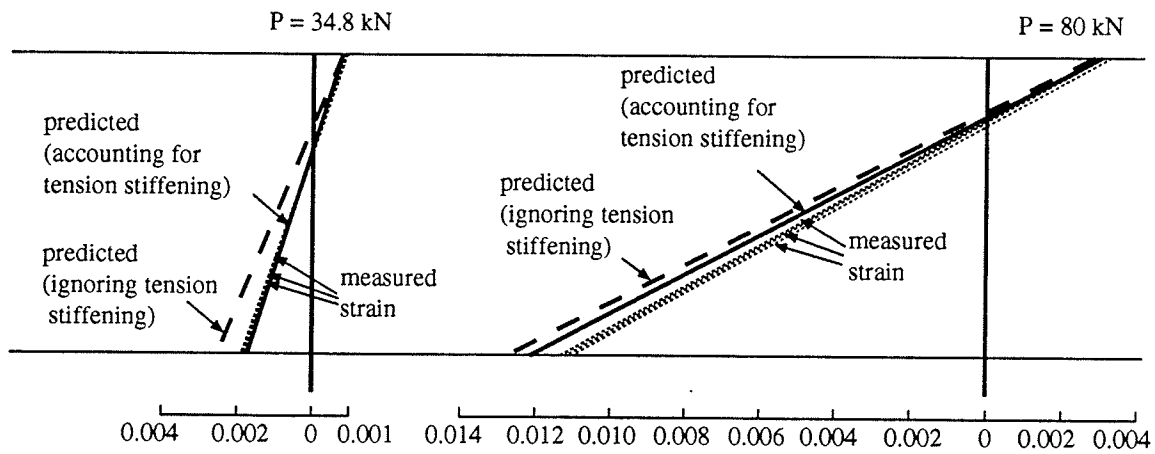


Fig.7-41 Predicted vs. measured strain profiles at service load and before failure



Beam T-4.5-V



Beam R-4.5-V

Fig.7-41 Predicted vs. measured strain profiles at service load and before failure (Cont'd)

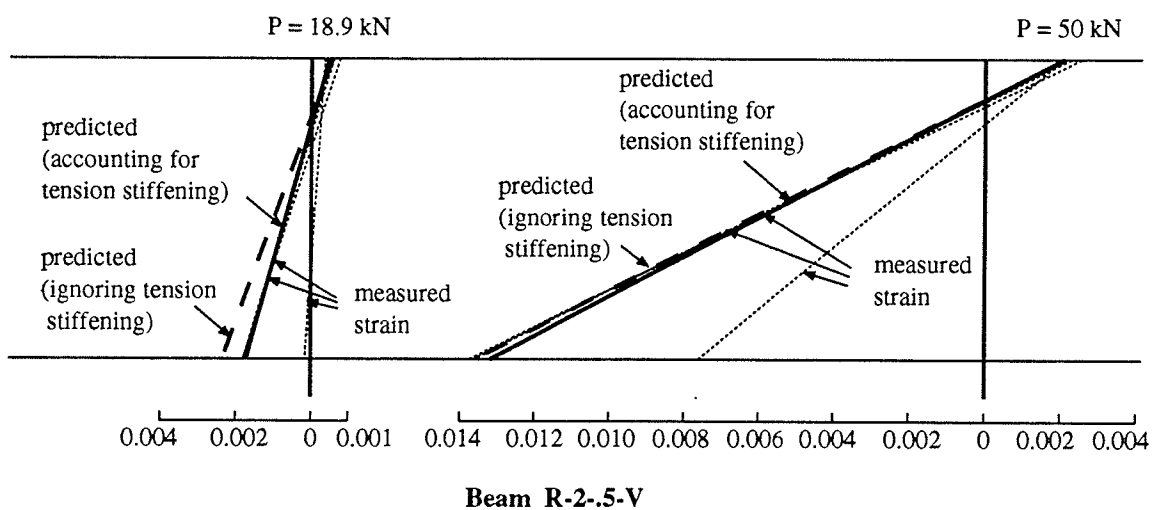
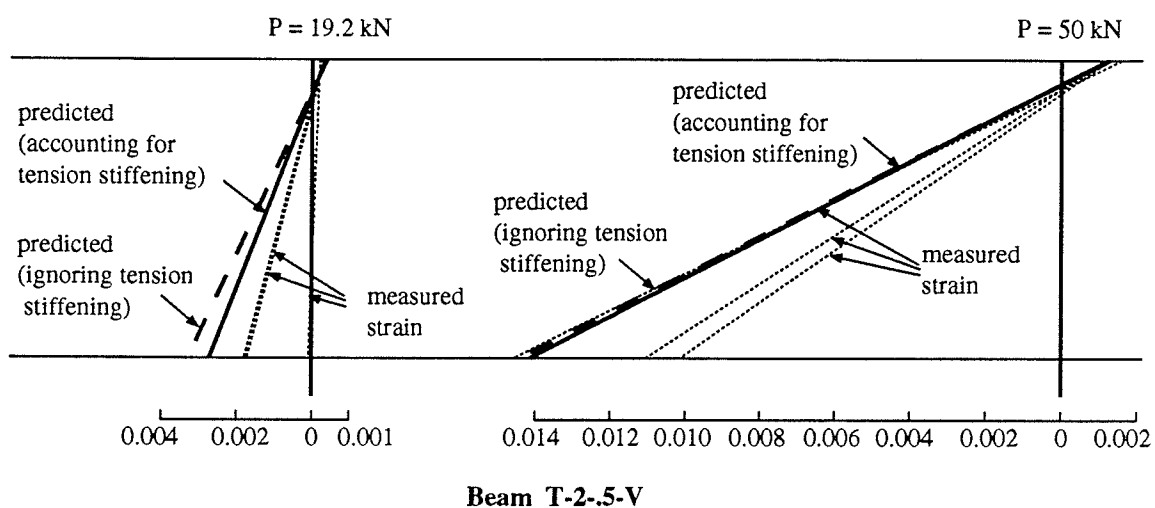


Fig.7-41 Predicted vs. measured strain profiles at service load and before failure (Cont'd)

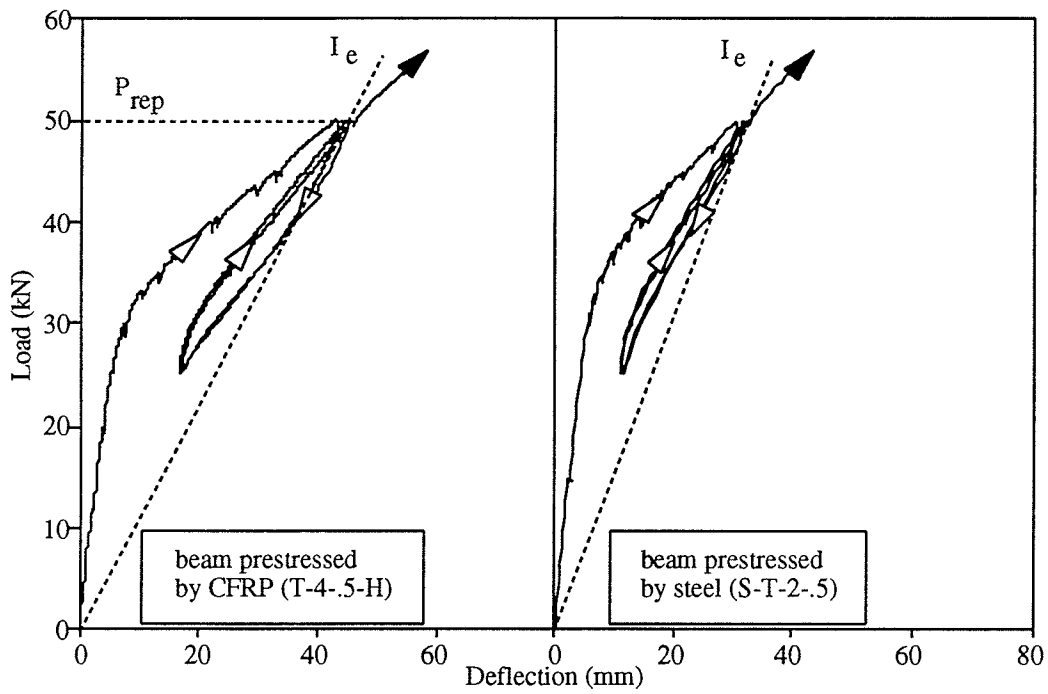


Fig.7-42 Load-deflection of beams prestressed by CFRP bars and steel under repeated load

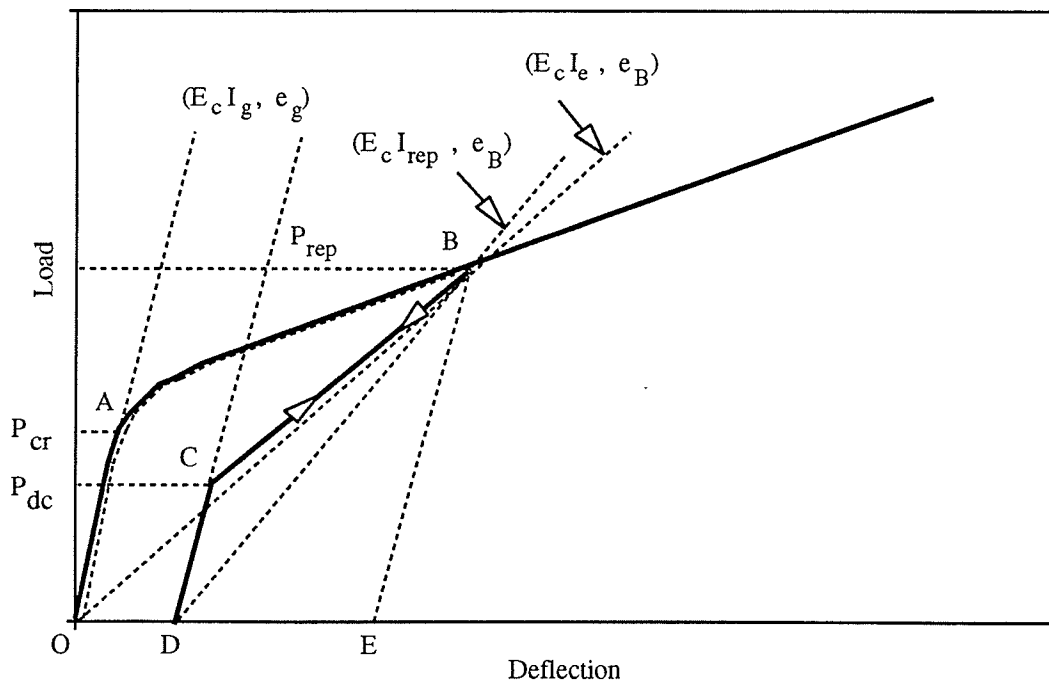


Fig.7-43 Proposed model to calculate the deflection of beams prestressed by CFRP bars under repeated load

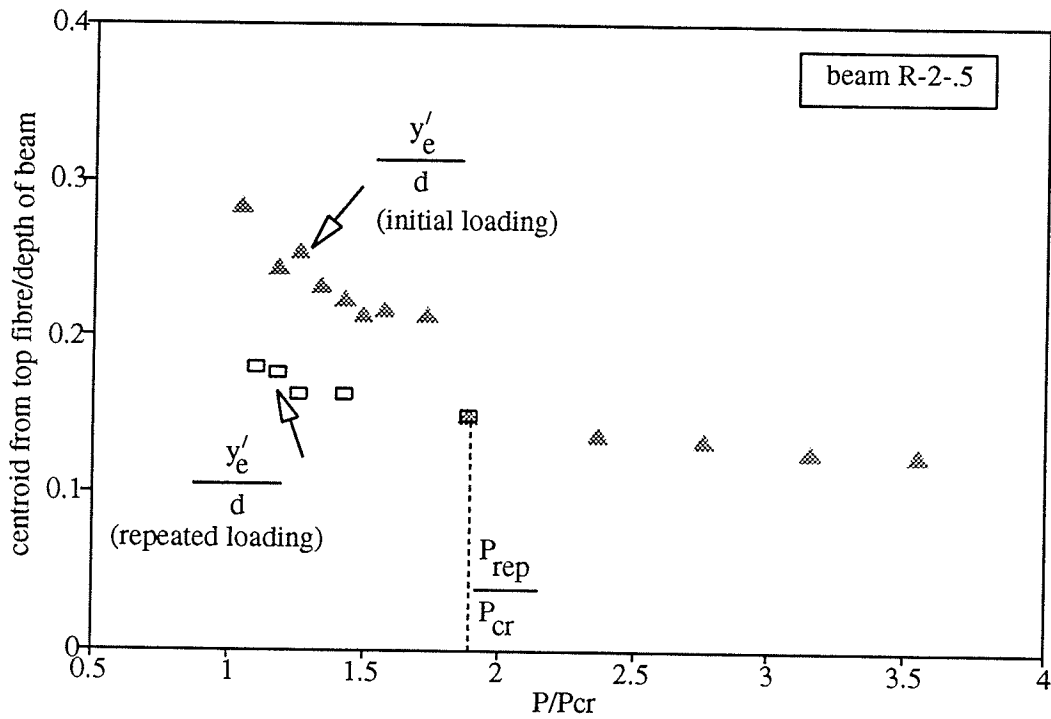


Fig.7-44 Comparison between centroidal distance at initial and repeated cycles

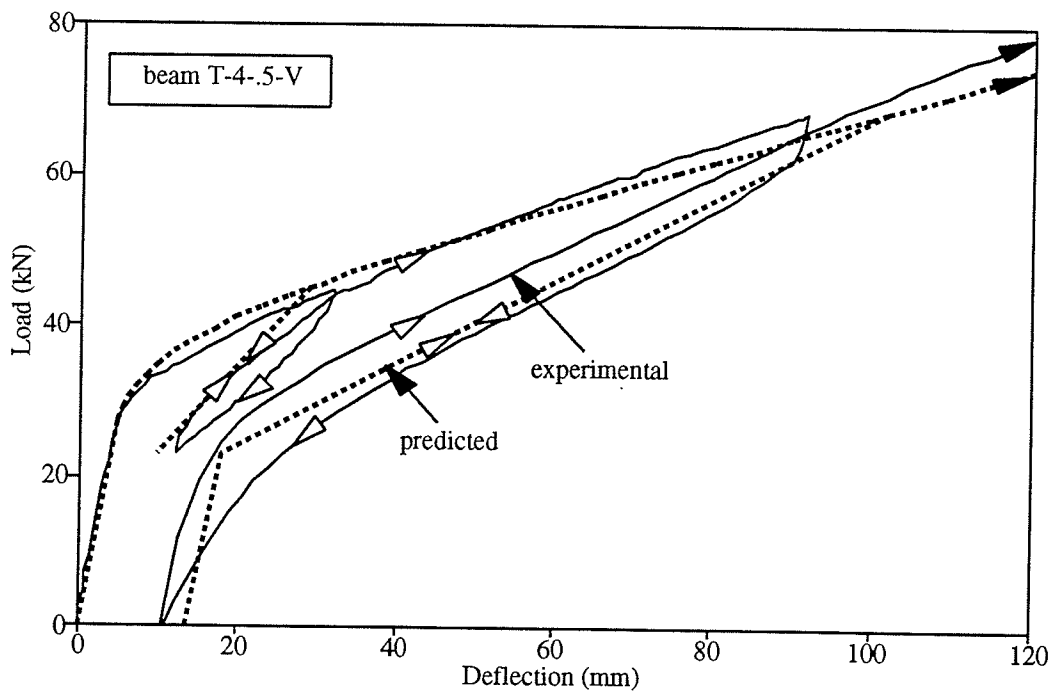


Fig.7-45 Predicted vs. measured deflection for a beam prestressed by CFRP bars under repeated loading

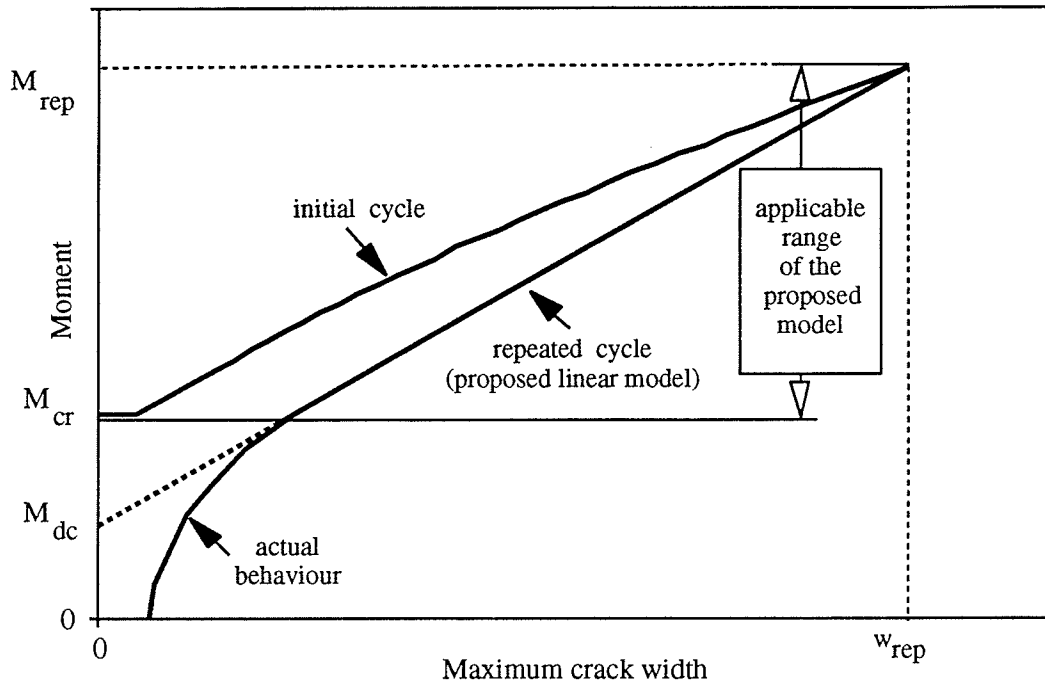


Fig.7-46 Proposed model to calculate the crack width of beams prestressed by CFRP bars under repeated load

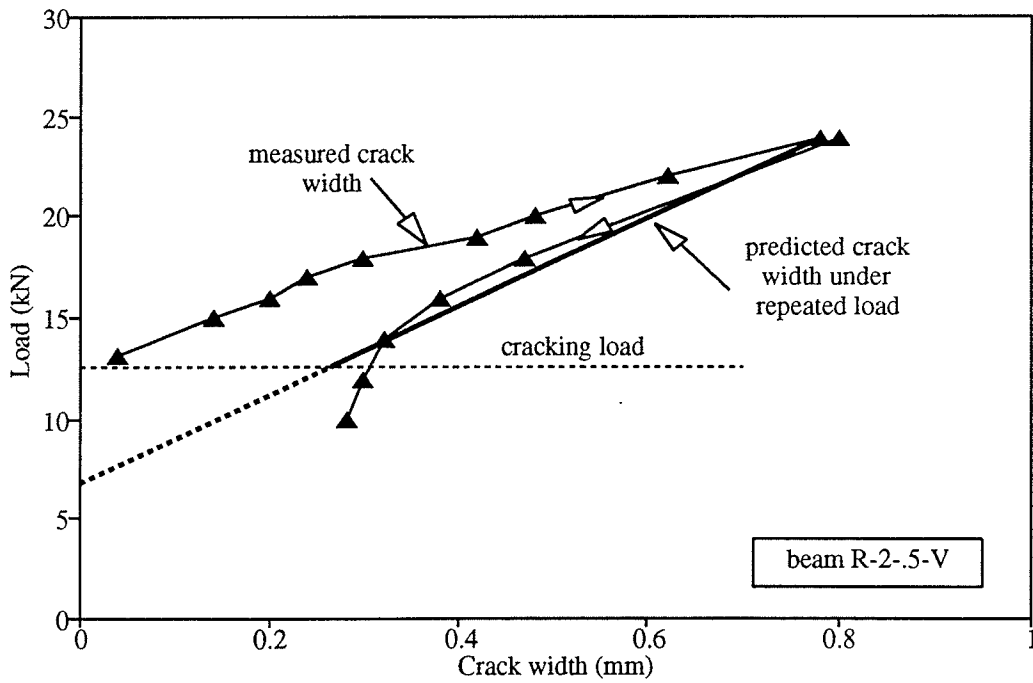


Fig.7-47 Predicted crack width for one of the tested beams under repeated loading

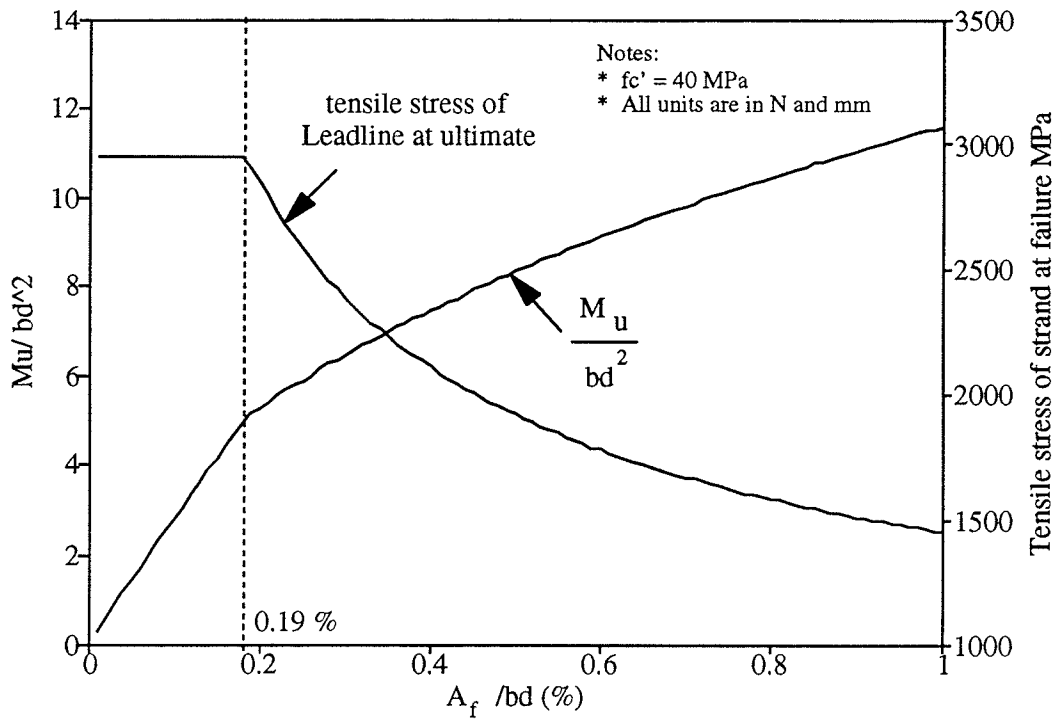


Fig.7-48 Predicted capacity and maximum tensile stress of reinforcement for beams prestressed by Leadline

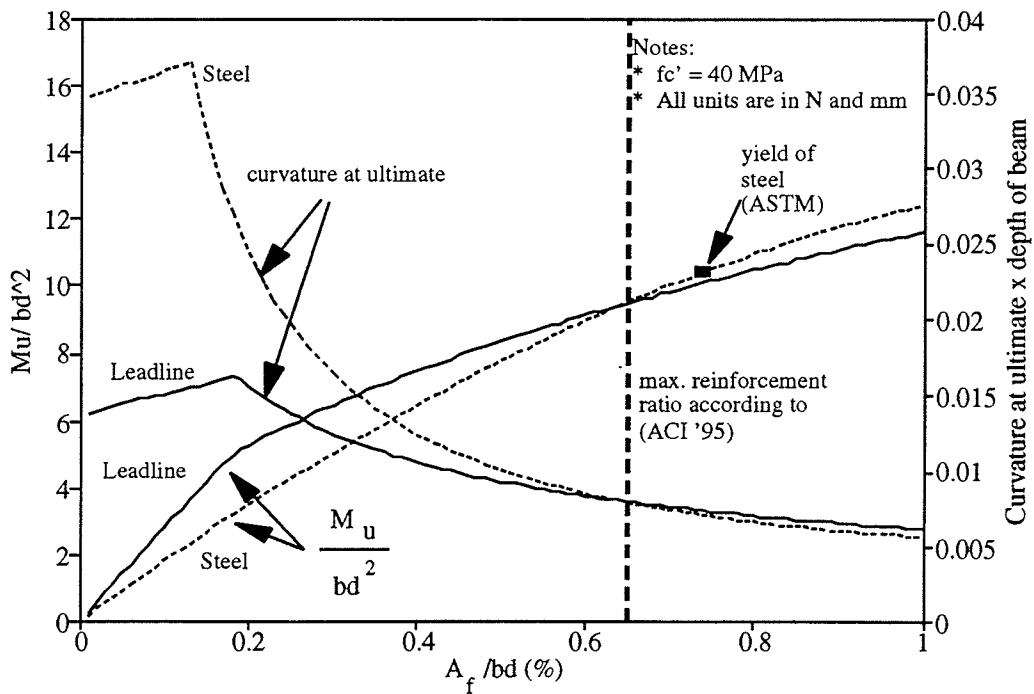


Fig.7-49 Capacity and deformability of beams prestressed by Leadline and steel

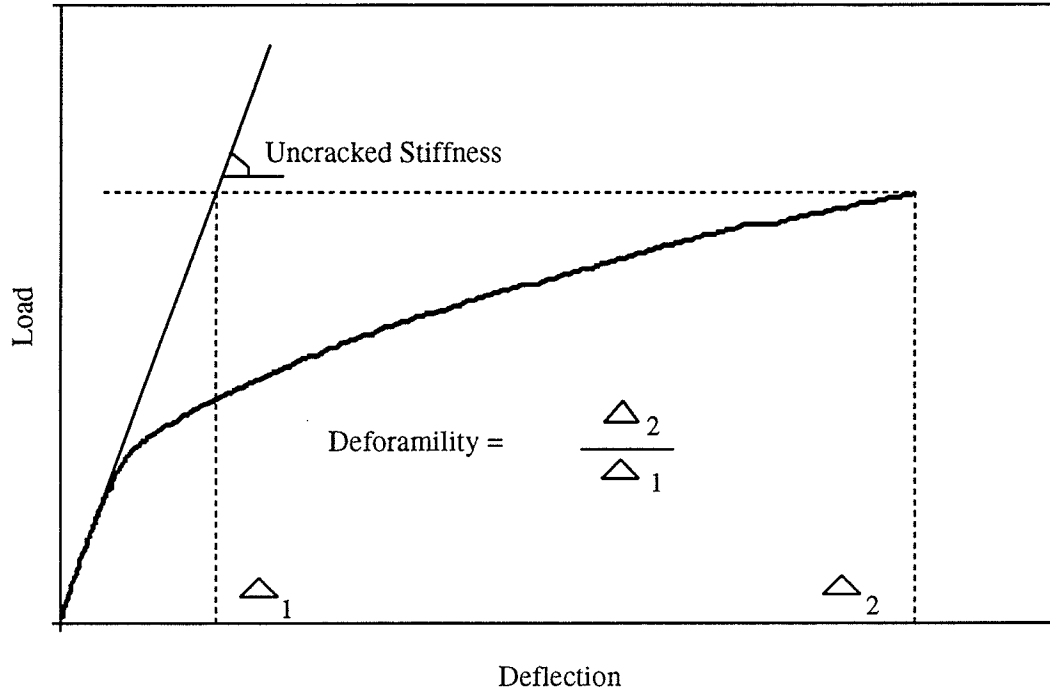


Fig.7-50 Proposed deformability of concrete beams prestressed by FRP

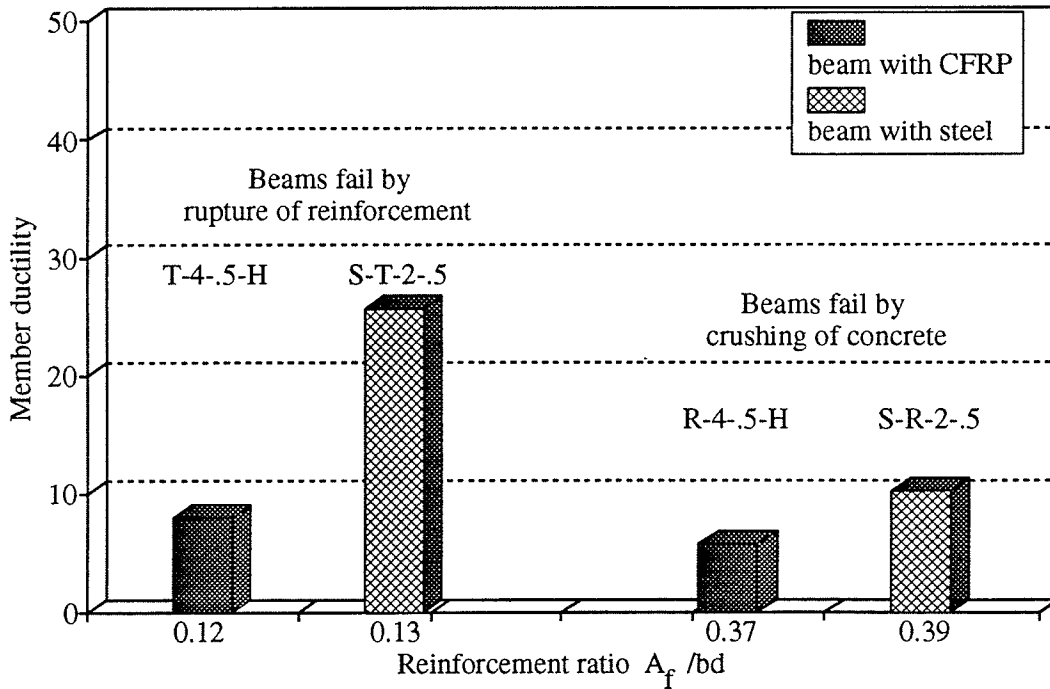


Fig.7-51 Deformability of beams prestressed by Leadline and steel

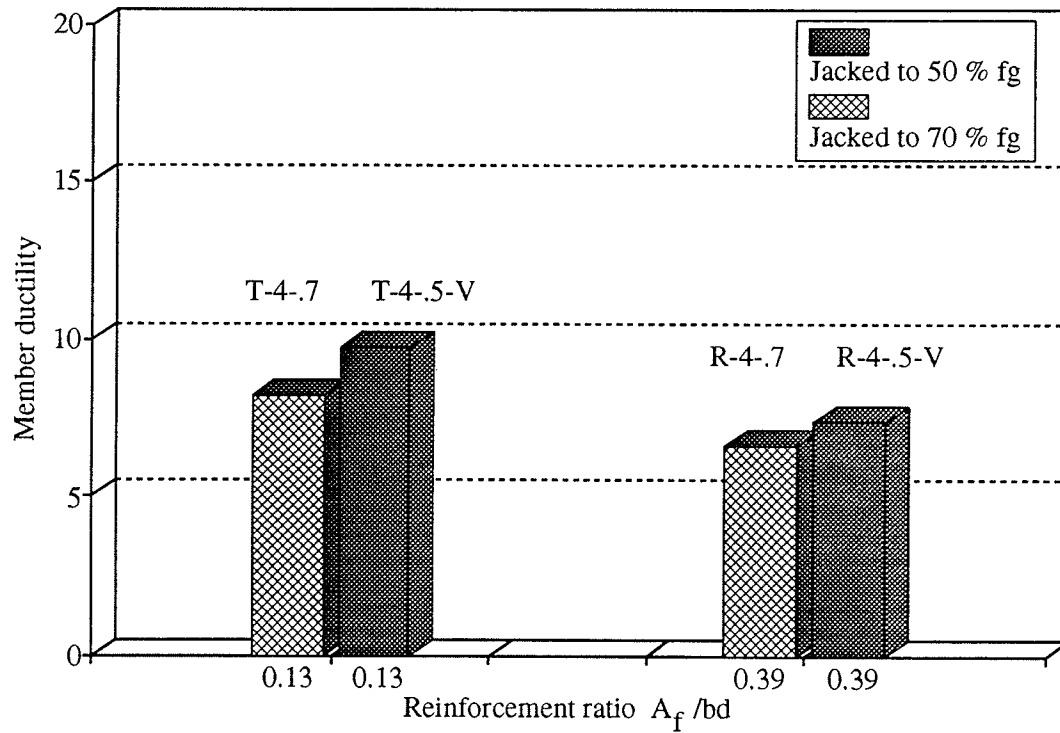


Fig.7-52 Deformability of beams prestressed by Leadline with different jacking stress

8. ————— SUMMARY AND CONCLUSIONS

8.1 SUMMARY

The program has investigated serviceability of concrete beams partially prestressed by carbon fibre reinforced plastic (*CFRP*) reinforcement. The main objective of the study was to examine the various flexural limit states behaviour in terms of deflection prior to and after cracking, cracking behaviour, and modes of failure. The program consisted of experimental and analytical phases. The experimental program includes testing of ten 6.2-m-long partially prestressed concrete beams, eight beams prestressed by *CFRP* Leadline bars and two beams prestressed by steel strands. The beams were tested under quasi-static load and cycled three times in the service load range. The variables in the experimental program were the reinforcement ratio, degree of prestressing, number of prestressing bars and distribution of the reinforcement in the tension zone. The analytical phase included a rational analysis using the strain compatibility approach to describe the behaviour of the beams in terms of strain distribution, cracking and ultimate carrying capacity of the beams as well as calculation of the deflection and the crack width of the beams. Based on this investigation, various models have been introduced including new

parameters that can be used to predict the deflection, before and after cracking, and the crack width, taking into account the bond characteristics of the *CFRP* prestressing reinforcements. Three detailed methods to calculate the deflection of beams prestressed by Leadline using integration of the curvature and including the tension stiffening have been examined. A simplified method to calculate the deflection of the beams has been proposed. An expression to calculate the effective centroidal distance of cracked section prestressed by Leadline bars has also been presented. Two models to calculate the deflection and the crack width of beams prestressed by Leadline under repeated loading have been introduced. The deformability of the beams has been compared to the deformability of beams prestressed by conventional steel strands. A new definition for the deformability of beams prestressed by fibre reinforced plastic, *FRP*, reinforcement has also been introduced and compared to the traditional ductility definition.

An extensive survey of the characteristics and the applications of *FRP* reinforcement in the field of civil engineering has been presented. In addition, a literature review of the behaviour of concrete beams prestressed by *FRP* reinforcement, in terms of flexure, bond, fatigue, long-term effect and serviceability has been presented.

8.2 CONCLUSIONS

The present study has shown that *CFRP* reinforcement can be successfully used for partial prestressing of concrete beams. The advantages of using this technique are to reduce the cost and to increase the deformability. The following summarizes the findings of this investigation:

1. The transfer length of the 8-mm indented Leadline bars is estimated to be 360 mm, or 46 times the bar diameter, when the stress of the Leadline after release is 950 MPa (50 percent of the guaranteed tensile strength) and 500 mm, or 64 times the bar diameter, when the Leadline stress after release is 1310 MPa (70 percent of the guaranteed tensile strength). It should be noted that the concrete compressive strength ranged between 37 and 50 MPa.
2. The transfer bond strength of the Leadline in the transfer zone was found to be comparable to that of the prestressing steel strands and higher than the transfer bond strength of prestressing steel wires, reported in the literature. However, the flexural bond strength of the Leadline bars is less than that of steel strands.
3. The measured strength of the 8-mm Leadline bars is much higher than the guaranteed strength which is reported to be 1970 MPa by the manufacturing company. The measured value is 2950 MPa, with 24.3-MPa standard deviation, based on tension test of Leadline bars using sufficient concrete embedment length,

while the calculated strength based on the ultimate carrying capacity of the tested beams is 3230 MPa with 100-MPa standard deviation.

4. The tensile stress-strain relationship of the Leadline is bilinear with an elastic modulus of 170 GPa up to the level of 1000 MPa and an elastic modulus of 190 GPa up to failure. The maximum measured strain of the Leadline bars is 1.85 percent, measured from beam tests. The average measured elastic modulus of the Leadline bars based on tension test was found to be in the range of 180 GPa compared to 147 GPa reported by the manufacturer. This can be attributed to the difference in the rate of loading used during the tension test.
5. Two modes of failure were observed for the tested beams, rupture of Leadline bars, which occurred when the furthest *CFRP* bar from the neutral axis reached its ultimate strain, and crushing of the concrete at the extreme compression fibres.
6. The behaviour of the tested beams was linearly elastic up to the cracking load and linear after cracking with a reduced stiffness.
7. The behaviour of the beam during the second and the third cycles within the service load range was identical. However, the deflection and the crack width in the second cycle were greater than those in the initial cycle.
8. The deflection of beams prestressed by Leadline is higher than that of beams prestressed by steel strands after cracking and equivalent to that of beams prestressed by steel before failure, provided that the failure is by crushing of the concrete. If the failure is governed by rupture of the Leadline bars, the deflection at failure is

considerably smaller for beams prestressed by Leadline.

9. Reducing the jacking stresses from 70 to 50 percent of the guaranteed strength of the Leadline resulted in an increase in the deflection at ultimate and a reduction of the ultimate load.
10. The number of cracks in beams prestressed by Leadline is smaller than that in comparable beams prestressed by steel strands due to the lower flexural bond strength of the Leadline bars. Consequently, the crack width and spacing are typically larger for a given load level. However, for a given strain level in the reinforcement, the crack width is the same for beams prestressed by Leadline or steel strands.
11. The stabilized crack pattern for beams prestressed by Leadline bars occurs at a much lower strain level than for beams prestressed by steel strands.
12. The crack width of the prestressed beam with four layers of Leadline bars is higher than the crack width of an identical beam with two layers of reinforcements in the service load range.
13. The analytical prediction of the cracking load, ultimate capacity and the strains of the tested beams using the strain compatibility approach are in good agreement with the measured values. However, the beams which failed by rupture of the Leadline bars had higher failure loads than the anticipated values. This is attributed to the underestimation of the ultimate tensile strength of the bars, which is normally controlled by the type of anchorage assembly. This result indicates that the

pretensioned system fully utilizes the actual strength of the *FRP* tendons, since no anchorage system is used. Anchorage of *FRP* could induce a state of stress concentration which could significantly affect the strength of *FRP* tendons.

14. Accurate prediction of the deflection of beams prestressed by Leadline should account for the tension stiffening of the concrete.
15. Calculation of the deflection using an integration of the curvature along the span using I_e method (Tadros et al.), the CEB-FIP Code, or strain compatibility accounting for concrete in tension gives an accurate prediction within 20 percent margin of error.
16. The simplified method using an equivalent moment of inertia I_e is a good preliminary design tool to predict the deflection of concrete beams partially prestressed by *CFRP* reinforcement as the margin of error was within 30 percent.
17. The effective centroidal distance of the cracked section prestressed by Leadline can be predicted with a reasonable accuracy using the proposed model.
18. Bond factors of the reinforcement used to calculate the deflection of prestressed beams should be corrected to the following:
 - a. A value of 1.0 should be used for Leadline bars for the factor β_f , introduced by the CEB-FIP Code 1990 for calculation of the deflection.
 - b. A value of 0.6 and 0.7 should be used for Leadline and steel strands, respectively, for the factor α_f , introduced by Collins and Mitchell to account for the tension in concrete.

19. Crack widths in beams partially prestressed by Leadline can be predicted using the Suri and Dilger method, the CEB-FIP Code, or the Gergely and Lutz method with 40 percent margin of error.
20. Bond factors of Leadline bars used to calculate the crack width of prestressed beams are as follows:
 - a. A value of 1.41×10^{-6} for the factor " k " introduced by the Suri and Dilger.
 - b. A value of 0.28 for the factor " k_1 " introduced in the crack width equation in the CEB-FIP Code 1978.
 - c. A value of 12.5×10^{-6} for the factor " R " introduced by Gergely and Lutz.
21. Deflection due to repeated loading can be predicted using the proposed model within a 20 percent margin of error.
22. Crack width due to repeated loading is linearly related to the applied load in the range between the maximum load at which the beam is unloaded and the cracking load.
23. The tested beams pretensioned by Leadline exhibited considerable warning before failure due to the presence of extensively distributed large cracks and large deflection before failure.
24. Beams prestressed by Leadline with a small reinforcement ratio have lower deformability than beams prestressed by steel and normally fail by rupture of the reinforcement. Increasing the reinforcement ratio results in a change in the mode of failure to crushing of the concrete and the difference in the deformability of

beams prestressed by Leadline and steel decreases.

25. The proposed deformability ratio provides an adequate model to measure the deformability of beams prestressed by *FRP* reinforcement.
26. Partial prestressing, which is achieved by reducing the jacking stresses of the prestressing reinforcement, increases the deformability of the beams.

REFERENCES

1. Abdelrahman, A.A., Tadros, G. and Rizkalla, S.H., 1995 "Test Model for the First Canadian Smart Highway Bridge", *ACI Structural Journal*, Vol.92, No.4, July-August, pp.451-458.
2. American Concrete Institute (ACI) 1990 "*Building Code Requirements For Reinforced Concrete (ACI 318M-89)*", Detroit, Michigan, 351p.
3. Bažant, Z. and Oh, B. 1984 "Deformation of progressively Cracking Reinforced Concrete Beams", *ACI Structural Journal*, V.81, No.3, May-June, pp.268-278.
4. Benmokrane, B., Masmoudi, R., and Chaallal, O. "Experimental and Analytical Study of the Flexural Behaviour of Concrete Beams Reinforced with *GFRP* Rebars", to be published.
5. Bennett, E. and Veerasubramanian, N. 1972 "Behaviour of Non-rectangular Beams with Limited Prestress after Flexural Cracking", *ACI Structural Journal*, V.69, No.9, September, pp.533-452.
6. Branson, D.E. 1977 "*Deformation of Concrete Structures*", McGraw Hill Inc., 546p.
7. Branson, D.E. and Trost, H. 1982 "Unified Procedures for Predicting the Deflection

-
- and Centroidal Axis Location of Partially Cracked Nonprestressed and Prestressed concrete Members", *ACI Structural Journal*, V.79, No.2, March-April, pp.119-130.
8. Burgoyne, C.J. 1992 "Tests on Beams Prestressed With Polyaramid Tendons", *Advanced Composite Materials in Bridges and Structures, Proceeding of the 1st International Conference*, Sherbrooke, pp. 231-239.
 9. Canadian Prestressed Concrete Institute CPCI 1989 "*Metric Design Manual, Precast and Prestressed Concrete*", Ottawa, Canada, Second Edition, Second Printing, 340p.
 10. Canadian Standards Association (CSA) 1985 "*Design of Concrete Structures for Buildings (CAN-A23.3-M84)*", Rexdale, Ontario, 485p.
 11. Chaallal, O., Benmokrane, B. and Masmoudi, R. 1992 "An Innovative Glass-Fibre Composite Rebar For Concrete Structures", *Advanced Composite Materials in Bridges and Structures, Proceeding of the 1st International Conference*, Sherbrooke, pp. 169-177.
 12. Collins, M. and Mitchell, D. 1991 "*Prestressed Concrete Structures*", Prentice Hall, Englewood Cliffs, New Jersey, 766p.
 13. Comité Euro-International Du Béton 1978 "*CEB-FIP Model Code for Concrete Structures*", 420p.
 14. Comité Euro-International du Béton 1985 "*CEB Manual: Cracking and Deformations*", EPFL, Lausanne, 230 p.
 15. Comité Euro-International Du Béton 1993 "*CEB-FIP Model Code 1990*", Design

Code, Thomas Telford, Great Britain, 416 p.

16. Currier, J., Dolan, C. and O'Neil, E. 1995 "Deflection Control of Fibre Reinforced Plastic Pretensioned Concrete Beams", Non-Metallic (*FRP*) Reinforcement for Concrete Structures, *Proceeding of the Second International RILEM Symposium (FRPRCS-2)*, Edited by L.Taerwe, E&FN Spon, Ghent, Belgium, 23-25 August, pp.413-420.
17. Daniali, S. 1992 "Development Length For Fibre Reinforced Plastic Bars", Advanced Composite Materials in Bridges and Structures, *Proceeding of the 1st International Conference*, Sherbrooke, pp 179-188.
18. Darwin, D., Manning, D., Hognestad, E., Beeby, A., Rice, P. and Ghowrwal, A. 1985 "Debate: Crack Width, Cover, and Corrosion", *ACI Concrete International*, Vol.7, No.5, May, pp.21-35.
19. Erki, M.-A. and Rizkalla, S.H. 1993 "*FRP* Reinforcement For Concrete Structures", *ACI Concrete International*, Vol.15, No.6, June, pp.48-53.
20. Erki, M.-A., and Rizkalla, S.H., 1993 "Anchorages for *FRP* Reinforcement", *ACI Concrete International*, Vol.15, No.6, June, pp.54-59.
21. Fam, A.Z., Rizkalla, S.H. and Saltzberg W. 1995 "Model Tests for Concrete Highway Bridges in Manitoba Fully Reinforced by *CFRP* Reinforcements", *Proceeding of the Annual Conference of the Canadian Society of Civil Engineering*, CSCE, Ottawa, June 1-3, pp. 595-604.
22. Hull, D., 1981 "*An Introduction to Composite Materials*", Cambridge Solid State

Science Series, Cambridge University Press, Great Britain.

23. Gangarao, V.S and Faza, S.S. 1991 "Bending and Bond Behaviour and Design of Concrete Beams Reinforced with Fibre Reinforced Plastic Rebars", *Technical Report*, Construction Facilities Center, West Virginia University, October, 120 p.
24. Gergely, P. and Lutz, L. 1966 "Maximum Crack Width in Reinforced Concrete Flexural Members", Causes, Mechanism, and Control of Cracking in Concrete, *ACI Publication SP-20*, pp.87-118.
25. Gerritse, A., and Werner, J., 1991 "Arapree, A Non-metallic Tendon - Performance and Design Requirements", Advanced Composite Materials in Civil Engineering Structures, *Proceeding of the Specialty Conference*, Las-Vegas, Nevada, Jan 31-Feb 1, ASCE, pp. 143-154.
26. Ghali, A. 1989 "Stress and Strain Analysis in Prestressed Concrete: A Critical Review", *PCI Journal*, November-December, pp.80-97.
27. Ghali, A. 1993 "Deflection of Reinforced Concrete Members", *ACI Structural Journal*, Vol.90, No.4, July-August, pp.364-373.
28. Ghali, A. and Favre, R. 1986 "*Concrete Structures: Stresses and Deformations*", Chapman and Hall, London, 352 p.
29. Hassoun, M. and Sahebjam, K. 1989 "Cracking of Partially Prestressed Concrete Beams", Cracking in Prestressed Concrete Structures, *ACI, SP-113*, pp.57-77.
30. Iyer, S.L. and Anigol, M. 1991 "Testing and evaluating Fibre Glass, Graphite and

-
- Steel Cables For Pretensioned Beams", *Advanced Composite Materials in Civil Engineering Structures, Proceeding of the Specialty Conference*, Las-Vegas, Nevada, Jan 31-Feb 1, ASCE, pp. 44-56.
31. Iyer, S.L., hubchandani, A.K. and Feng, J. 1991 "Fibre Glass and Graphite Cables For Bridge Decks", *Advanced Composite Materials in Civil Engineering Structures, Proceeding of the Specialty Conference*, Las-Vegas, Nevada, Jan 31-Feb 1, ASCE, pp. 371-382.
32. Japan Society of Civil Engineers, JSCE, 1992 "Design Concept for Concrete Members Using Continuous Fibre Reinforcing Materials", *Concrete Library International*, No.19, 1992.6, pp.91-105.
33. Jaeger, L.G. 1995 "Advanced Composite Materials in Bridges and Structures Think Tank", *Report of the Advanced Composite Materials Think Tank Held on November 24, 1994*, Toronto, April, 13p.
34. Jaeger, L.G., Tadros, G. and Mufti, A. 1995 "Balanced Section, Ductility and Deformability in Concrete with *FRP* Reinforcement", *Research Report No.2*, the Nova Scotia CAD/CAM Centre, Industry's Centre for Computer-Aided Engineering, Technical University of Nova Scotia, May, 30 p.
35. Kakihara, R., Kamiyoshi, M., Kumagai, S.-I., and Noritake, K., 1991 "A New Aramid Rod For The Reinforcement of Prestressing Concrete Structures", *Advanced Composite Materials in Civil Engineering Structures, Proceeding of The Specialty Conference*, Las-Vegas, Nevada, Jan 31-Feb 1, ASCE, pp. 132-142.
36. Kim, P., and Meier, U., 1991 "*CFRP* Cables For Large Structures", *Advanced*

-
- Composite Materials in Civil Engineering Structures, *Proceeding of The Specialty Conference*, Las-Vegas, Nevada, Jan 31-Feb 1, ASCE, pp. 233-244.
37. Kripanarayanan, K.M., and Branson, D.E. 1972 "Short-Time Deflections of Beams Under Single and Repeated Load Cycles" *ACI Structural Journal*, Vol. 69, No.2, February, pp.110-117.
 38. Krishna Mohan Rao, S.V. and Dilger, W.H. 1992 "Evaluation of Short-Term Deflections of Partially Prestressed Concrete Members", *ACI Structural Journal*, V.89, No.1, January-February, pp.71-78.
 39. Krishna Mohan Rao, S.V. and Dilger, W.H. 1992 "Control of Flexural Crack Width in Cracked Prestressed Concrete Members", *ACI Structural Journal*, Vol.89, No.2, March-April, pp.127-138.
 40. Leonhardt, F. 1977 "Crack control in concrete structures." *IABSE Surveys* No. S-4/77, Zürich, 26 p.
 41. Leonhardt, F. 1988 "Cracks and Crack Control in Concrete Structures", *PCI Journal*, Vol.33, No.4, July-August, pp.124-145.
 42. Maissen, A. and De Smet, C.A.M. 1995 "Comparison of Concrete Beams Prestressed with Carbon Fibre Reinforced Plastic and Steel Strands", Non-Metallic (FRP) Reinforcement for Concrete Structures, *Proceeding of the Second International RILEM Symposium (FRPRCS-2)*, Edited by L.Taerwe, E&FN Spon, Ghent, Belgium, 23-25 August, pp.430-439.
 43. Mallick, P.K., 1993 "*Fibre-Reinforced Composites, Manufacturing and Design*",

Second Edition, Library of Congress, USA, 566 p.

44. Mast, R.F. 1992 "Unified Design Provisions for Reinforced and Prestressed Concrete Flexural and Compression Members", *ACI Structural Journal*, V.89, No.2, pp.185-199.
45. Maunsell, International Consulting Engineers, 1989 "A 19 Tees Viaduct. Middlesbrough Bridge Enclosure", *Technical Report*, London.
46. McKay, K.S. and Erki, M.-A. 1992 "Aramid Tendons in Pretensioned Concrete Applications", *Advanced Composite Materials in Bridges and Structures, Proceeding of the 1st International Conference*, Sherbrooke, pp. 221-230.
47. Meier, U., 1988 "Proposal For Carbon Fibre Reinforced Composite Bridge Across The Strait of Gibraltar at Its Narrowest Site", *Les Matériaux Nouveaux pour la Précontrainte et la Renforcement d'ouvrages d'art*, Paris.
48. Meier, S.W. and Gergely, P. 1981 "Flexural Crack Width in Partially Prestressed Beams", *Journal of Structural Engineering, ASCE*, V.107, Feb., pp.429-433.
49. Meier, U., and Kaiser, H., 1991 "Strengthening of Structures with CFRP Laminates", *Advanced Composite Materials in Civil Engineering Structures, Proceeding of The Specialty Conference*, Las-Vegas, Nevada, Jan 31-Feb 1, ASCE, pp. 288-301.
50. Menn C. 1983 "Partial Prestressing from the Designer's Point of View", *ACI Concrete International*, Vol.5, No.3, March, pp.52-59.
51. Miesslerer, H., and Preis, L., 1989 "High Performance Glass Fibre Composite Bars

-
- as Reinforcement In Concrete and Foundation Structures", *Technical Report*, Strabag-Bau-AG, Germany.
52. Mikami, H., Kato, M., Tamura, T. and Ishibashi, K. 1990 "Fatigue Characteristics of Concrete Beams Reinforced With Braided *AFRP* Rods" *Transactions of the Japan Concrete Institute*, Vol.12, pp. 223-230.
53. Minosaku, K., 1992 "Using *FRP* Materials in Prestressed Concrete Structures", *ACI Concrete International*, Vol.14, No.8, pp 41-44.
54. Mitsubishi Kasei Corporation, 1992 "Leadline Carbon Fibre Tendons/Bars", *Product Manual*, December, 75p.
55. Mitsui Construction Co., Ltd., "FiBRA Technical Data", *Product Manual*, 13p.
56. Mufti, A.A., Erki, M.-A., and Jaeger, L.G., 1991 "Advanced Composite Materials With Application to Bridges", *State-of-the-Art Report*, Canadian Society of Civil Engineering, CSCE, 350 p.
57. Mufti, A.A., Erki, M.-A., and Jaeger, L.G., 1992 "Advanced Composite Materials in Bridges and Structures in Japan", *Task-Force Report*, Canadian Society of Civil Engineering, CSCE, 171 p.
58. Mutsuyoshi, H., Machida, A. and Sano, M. 1991 "Behaviour of Prestressed Concrete Beams Using *FRP* as External Cable", *Transactions of The Japan Concrete Institute*, Vol.13, pp 247-252.
59. Mutsuyoshi, H., Vehara, K. and Machida, A., 1990 "Mechanical Properties and

-
- Design Method of Concrete Beams Reinforced with Carbon Fibre Reinforced Plastics", *Transactions of the Japan Concrete Institute*, Vol.12, pp 231-238.
60. Naaman, A. 1982 "*Prestressed Concrete Analysis and Design Fundamentals*", McGraw Hill Book Company, 670p.
61. Naaman, A. 1985 "Partially Prestressed Concrete: Review and Recommendations", *PCI Journal*, Vol.30, No.6, November-December, pp.30-71.
62. Naaman, A. and Jeong, S. 1995 "Structural Ductility of Concrete Beams Prestressed with FRP Tendons", Non-Metallic (FRP) Reinforcement for Concrete Structures, *Proceeding of the Second International RILEM Symposium (FRPRCS-2)*, Edited by L.Taerwe, E&FN Spon, Ghent, Belgium, 23-25 August, pp.379-386.
63. Naaman, A. and Siriaksorn, A. 1979 "Serviceability Based Design of Partially Prestressed Beams", *PCI Journal*, Vol.24, No.2, March-April, pp.64-89 and Vol.24, No.3, May-June 1979, pp.40-60. See also Comments by T.Brøndum-Nielsen, A.Bruggeling, A.Hill, A.Prasada Rao, K.Rajagopalan, A.Tam and Authors, *PCI Journal*, Vol.25, No.1, January-February 1980, pp.146-158.
64. Nakai, H., Asai, H., Kumagai, S. and Okano, M. 1993 "Shearing Property of Prestressed Concrete Beams using Continuous Fibre Reinforcement Materials", *FIP Symposium (Modern Prestressing Techniques and Their Applications)*, Kyoto, Japan, 17-20 October, pp.789-796.
65. Nanni, A. and Tanigaki, M. 1992 "Pretensioned Prestressed Concrete Members With Bonded Fibre Reinforced Plastic Tendons: Development and Flexural Bond Lengths (Static)", *ACI Structural Journal*, Vol.89, No.4, July-August, pp. 433-441.

-
66. Nanni, A., Utsunomiya, T., Yonekura, H. and Tanigaki, M. 1992 "Transmission of Prestressing Force to Concrete by Bonded Fibre Reinforced Plastic Tendons", *ACI Structural Journal*, Vol.89, No.3, May-June, pp. 335-344.
 67. Nawy, E. 1989 "Flexural Cracking Behaviour of Partially Prestressed Pretensioned and Post-tensioned Beams - State-of-the-Art", *Cracking in Prestressed Concrete Structures*, *ACI, SP-113*, pp.1-28.
 68. Nawy, E. and Huang, P. 1977 "Crack and Deflection Control of Pretensioned Prestressed Beams", *PCI Journal*, Vol.22, No.3, May-June, pp.30-47.
 69. NEFMAC, 1987, "Technical Leaflet 2", New Fibre Composite Material For Reinforcing Shotcrete, *Technical Report*, NEFCOM Corporation, Japan, 15 p.
 70. Nilson, A. 1987 "*Design of Prestressed Concrete*", Second Edition, John Wiley & Sons, 592p.
 71. Noritake, K. and Kumagai, S-I. 1991 "Practical Use of Aramid *FRP* Rods For PC Structures", *The Third East Asia-Pacific Conference on Structural Engineering and Construction*, Shanghai, China.
 72. Padilla, J. and Robles, F. 1971 "Human Response to Cracking in Concrete Slabs, Cracking, Deflection, and Ultimate Load of Concrete Slab Systems", *ACI SP-30*, pp.43-54.
 73. Park, R. and Paulay, T. 1975 "*Reinforced Concrete Structures*", John Wiley & Sons, 769 p.

-
74. Pleimann, L.G. 1991 "Strength, Modulus of Elasticity and Bond of Deformed *FRP* Rods", Advanced Composite Materials in Civil Engineering Structures, *Proceeding of the Specialty Conference*, Las-Vegas, Nevada, Jan 31-Feb 1, ASCE, pp. 99-110.
 75. Rostásy, F.S., 1988 "Tendons of High-Strength Composites - Developments and Chances", *Les Matériaux Nouveaux pour la Précontrainte et la Renforcement d'ouvrages d'art*, Paris, 26 October, 15 p.
 76. Rostásy, F.S. and Budelmann, H. 1991 "*FRP*-Tendons For The Post-tensioning of Concrete Structures", Advanced Composite Materials in Civil Engineering Structures, *Proceeding of the Specialty Conference*, Las-Vegas, Nevada, Jan 31-Feb 1, ASCE, pp. 156-166.
 77. Scholz, H. 1991 "Simple Deflection and Cracking Rules for Partially Prestressed Members", *ACI Structural Journal*, V.88, No.2, March-April, pp.199-203.
 78. Sen, R., Issa, M., and Iyer, S., 1992 "Feasibility of Fibreglass Pretensioned Piles in a Marine Environment", *Final Draft Report*, University of South Florida, Tampa, January, 300 p.
 79. Sen, R., Iyer, S., Issa, M. and Shahawy, M. 1991 "Fibre Glass Pretensioned Piles For Marine Environment", *Proceeding of the Specialty Conference*, Las-Vegas, Nevada, Jan 31-Feb 1, ASCE, pp. 348-359.
 80. Suri, K.M. and Dilger, W.H. 1986 "Crack Width of Partially Concrete Members", *ACI Structural Journal*, Vol. 83, No.5, September-October, pp.784-797.
 81. Tadashi, O., Matsubara, S., Tanagaki, M. and Hasuo, K. 1993 "Long Term Loading

-
- Tests on PPC Beams using Braided FRP Rods", *FIP Symposium (Modern Prestressing Techniques and Their Applications)*, Kyoto, Japan, 17-20 October, pp.767-774.
82. Tadros, M. 1982 "Expedient Serviceability Analysis of Cracked Prestressed Concrete Beams", *PCI Journal*, Vol.27, No.6, November-December 1982, pp.86-111. See also Comments by Bachmann, H., Bennett, E., Branson, D., Brøndum-Nielsen, T., Bruggeling, A., Moustafa, S., Nilson, A., Prasada Rao, A. and Natarajan, S., Ramaswamy, G., Fattah Shaikh, A. and Author, *PCI Journal*, Vol.28, No.6, November-December, pp.137-158.
83. Tadros, M., Ghali, A. and Meyer, A. 1985 "Prestress Loss and Deflection of Precast Concrete Members", *PCI Journal*, Vol.30, No.1, January-February, pp.114-141. See also Comments by Nedelcu, L., Fitzpatrick, B. and Warwaruk, J., Weiss, D. and Authors, *PCI Journal*, Vol.31, No.3, May-June 1986, pp.144-156.
84. Taerwe, L. and Miessler, H.-J. 1992 "Structural Behaviour of Concrete Beams Prestressed With Glass Fibre Tendons", *Advanced Composite Materials in Bridges and Structures, Proceeding of the 1st International Conference*, Sherbrooke, pp. 211-220.
85. Tanigaki, M., Nomura, S., Okamoto, T. and Endo, K. 1989 "Flexural Behaviour of Partially Prestressed Concrete Beams Reinforced With Braided Aramid Fibre Rods", *Transactions of the Japan Concrete Institute*, Vol.11, pp. 215-222.
86. Tokyo Rope MFG.Co., Ltd., 1993 "Technical Data on CFCC", *Product Manual*, October, 65p.

87. Yonekura, A., Tazawa, E., Nakayama, H. and Nagata, K. 1991 "Flexural Characteristics of Prestressed Concrete Beams Using Fibre Reinforced Plastic Rods as Prestressing Tendons", *Transactions of the Japan Concrete Institute*, Vol.13, pp. 239-246.

NUMERICAL EXAMPLES

The following examples demonstrate the use of the simplified method and the proposed model for deflection calculation under repeated loading for one of the tested beams prestressed by *CFRP* bars . The calculated deflection is compared to the measured values.

Example 1

A simply supported beam with a span of 5.8 m and a cross-section shown in Fig. A-1, is subjected to its self weight and two symmetrical concentrated loads 1.0 meter apart. The beam is prestressed by four 8-mm diameter straight *CFRP* bars with an area of 47.3 mm^2 each, guaranteed strength of 1970 MPa and an elastic modulus of 147 GPa. The concrete has a compressive strength of 55 MPa after 28 days, rupture strength of 3.1 MPa and an elastic modulus of 29 GPa. The prestressing force after losses, P_e , is 155.6 kN. It is required to calculate the deflection at mid-span section due to a superimposed load, P , of 51 kN.

Cross section properties are as follows:

$$A_g = 67590 \quad \text{mm}^2$$

$$I_g = 6.905 \times 10^8 \quad \text{mm}^4$$

$$y_t = 112.9 \quad \text{mm}$$

$$y_b = 217.1 \quad \text{mm}$$

$$S_t = 6116120 \quad \text{mm}^3$$

$$S_b = 3180608 \quad \text{mm}^3$$

$$A_p = 189.2 \quad \text{mm}^2$$

$$d_p = 255 \quad \text{mm}$$

$$e_g = 142.1 \quad \text{mm}$$

$$M_d = 6.68 \quad \text{kN-m}$$

$$M_L = 61.2 \quad \text{kN-m (due to } P=51 \text{ kN)}$$

$$M_s = 67.88 \quad \text{kN-m (due to self weight and } P=51 \text{ kN)}$$

The cracking moment, M_{cr} could be calculated using the following equation to examine if the beam is cracked or not.

$$\begin{aligned} M_{cr} &= P_e e_g + \left(f_r + \frac{P_e}{A_g} \right) S_b \\ &= 39.3 \text{ kN-m} \end{aligned}$$

Since $M_s > M_{cr}$, section is cracked.

In order to calculate the neutral axis depth, the design charts in the CPCI metric design manual (1989) or in Tadros, Ghali and Meyer (1985) were used. The following parameters are needed to calculate the cracked inertia and cracked centroidal distance, I_{cr} and y_{cr} , respectively, assuming that the decompression force $P_{dc} \approx P_e$;

$$\frac{P_{dc} d}{M_s} = \frac{155.6 \times 10^3 \times 255}{67.88 \times 10^6} = 0.584$$

$$n \rho = \frac{147}{29} \times \frac{189.2}{600 \times 255} = 0.00627$$

$$\frac{b_w}{b} = \frac{127.5}{600} = 0.2125$$

$$\frac{h_f}{d} = \frac{54}{255} = 0.2118$$

Using the design charts in page 3-52 and page 3-53 in the CPCI metric design manual, the following factors can be obtained:

$$k_{pr} = 1.0$$

$$k_{cr} = 0.065$$

$$k_p = 1.0$$

$$k_c = 0.1$$

Consequently,

$$I_{cr} = k_{cr} k_{pr} \frac{b d^3}{12} = 0.065 \times 1.0 \times \frac{600 \times 255^3}{12} = 53889469 \text{ mm}^4$$

$$y_{cr} = k_c k_p d = 0.1 \times 1.0 \times 255 = 25.5 \text{ mm}$$

The decompression moment M_{dc} is calculated using the following equation;

$$\begin{aligned} M_{dc} &= P_e e_g + \frac{P_e S_b}{A_g} \\ &= 29.43 \text{ kN-m} \end{aligned}$$

Applying equations 4-13, 7-19 and 7-20, the following results are obtained;

$$\psi = \frac{39.3 - 29.4}{67.88 - 29.4} = 0.257$$

$$I_e = (0.257)^3 \times 6.905 \times 10^8 + \left(1 - (0.257)^3 \right) \times 53889469 = 64627789 \text{ mm}^4$$

$$y'_e = 25.5 + (0.257)^2 (112.9 - 25.5) = 31.27 \text{ mm}$$

The deflection due to $P = 51 \text{ kN}$ is calculated as the net difference between the deflection, Δ_1 , due to self weight, prestressing effect and the concentrated loads of 51 kN and the deflection, Δ_2 , due to self weight and the prestressing force. The deflection is calculated using the following equation;

$$\Delta = - \frac{P_e (d_p - y'_e) L^2}{8 E_c I_e} + \frac{5 M_d L^2}{48 E_c I_e} + \frac{M_L L^2}{10.36 E_c I_e}$$

$$\Delta_1 = - \frac{155.6 \times 10^3 (255 - 31.27) 5800^2}{8 \times 29000 \times 64627789} + \frac{5 \times 6.68 \times 10^6 \times 5800^2}{48 \times 29000 \times 64627789} + \frac{61.2 \times 10^6 \times 5800^2}{10.36 \times 29000 \times 64627789} = 40.41 \text{ mm}$$

$$\Delta_2 = - \frac{155.6 \times 10^3 (255 - 112.9) 5800^2}{8 \times 29000 \times 6.905 \times 10^8} + \frac{5 \times 6.68 \times 10^6 \times 5800^2}{48 \times 29000 \times 6.905 \times 10^8} = -3.47 \text{ mm}$$

$$\Delta = \Delta_1 - \Delta_2 = 40.41 - (-3.47) = 43.88 \text{ mm}$$

This deflection is compared to a measured value of 42.9 mm, which is within 2 percent error.

Example 2

For the same beam in the previous example, calculate the deflection due to unloading the beam at a load $P = 26$ kN, if the beam was subjected to a maximum load, P_{rep} , of 51 kN.

The moment corresponding to $P = 26$ kN, $M_s = 37.88$ kN-m $>$ $M_{dc} = 29.43$ kN-m. Therefore, the corresponding deflection will be calculated using an interpolation between the deflection at $P_{rep} = 51$ kN, $\Delta_{rep} = 43.88$ mm, as calculated in example 1), which is represented by point B in Fig.7-43, and the deflection at M_{dc} , Δ_{dc} , which is equivalent to a load of 18.96 kN and represented by point C in Fig.7-43.

1- Calculate the residual deflection due to complete unloading, Δ_0 , as the difference in the deflection at point B based on I_e and I_{rep} , using equations 7-18 and 7-29

$$\Delta_0 = \Delta_1 - \Delta_2$$

where

$$\Delta_1 = - \frac{P_e (d_p - y_e') L^2}{8 E_c I_e} + \frac{5 M_d L^2}{48 E_c I_e} + \frac{M_L L^2}{10.36 E_c I_e}$$

and

$$\Delta_2 = - \frac{P_e (d_p - y_e') L^2}{8 E_c I_{rep}} + \frac{5 M_d L^2}{48 E_c I_{rep}} + \frac{M_L L^2}{10.36 E_c I_{rep}}$$

From the previous example, $\Delta_1 = 40.41$ mm.

Applying equation 7-30 at $P = 51$ to calculate I_{rep} :

$$I_{rep} = 53889469 + (0.257)^{2.5} (6.905 \times 10^8 - 53889469) = 75093921 \text{ mm}^4$$

$$\begin{aligned} \Delta_2 = & - \frac{155.6 \times 10^3 (255 - 31.27) 5800^2}{8 \cdot 29000 \cdot 75093921} + \frac{5 \cdot 6.67 \times 10^6 \cdot 5800^2}{48 \cdot 29000 \cdot 75093921} \\ & + \frac{61.2 \times 10^6 \cdot 5800^2}{10.36 \cdot 29000 \cdot 75093921} = 34.8 \text{ mm} \end{aligned}$$

$$\therefore \Delta_0 = 40.41 - 34.8 = 5.61 \text{ mm}$$

2- Calculate the deflection at load equal to 18.96 kN which corresponds to M_{dc} as follows:

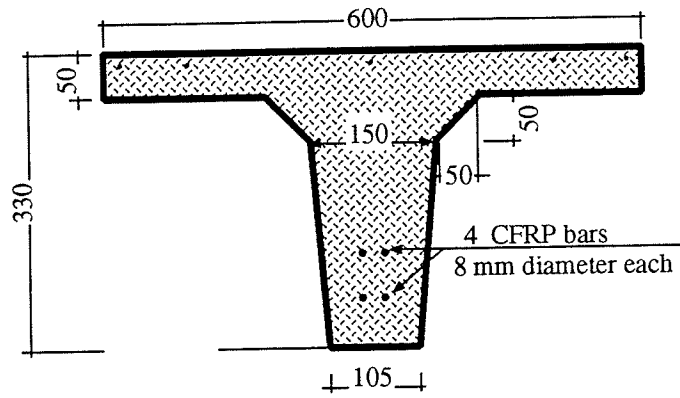
$$\begin{aligned} \Delta_{dc} &= \Delta_0 + \frac{M_{dc} L^2}{10.36 E_c I_g} \\ \therefore \Delta_{dc} &= 5.61 + \frac{29.43 \times 10^6 \cdot 5800^2}{10.36 \cdot 29000 \cdot 6.905 \cdot 10^8} = 10.38 \text{ mm} \end{aligned}$$

3- Using linear interpolation Δ at $M_s = 37.88$ kN-m can be estimated as follows:

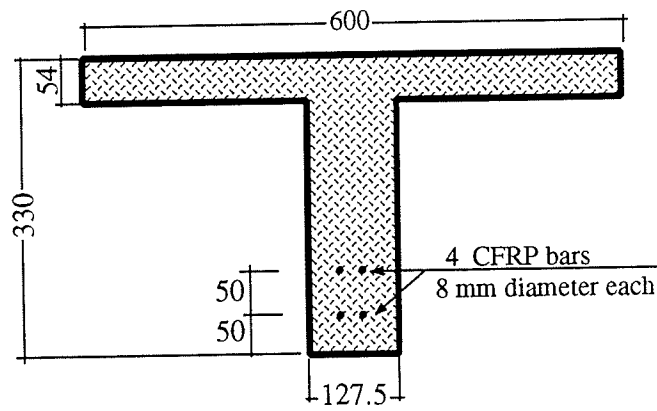
$$\Delta = \Delta_{dc} + \frac{M_s - M_{dc}}{M_{rep} - M_{dc}} \times (\Delta_{rep} - \Delta_{dc})$$

$$\Delta = 10.38 + \frac{37.88 - 29.43}{67.88 - 29.43} \times (43.88 - 10.38) = 17.74 \text{ mm}$$

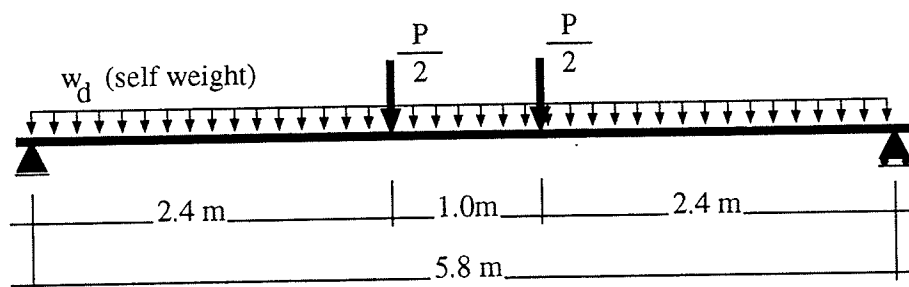
This deflection is compared to a measured value of 16.67 mm, which means that the error in the deflection calculation is 6.4%.



(a) Cross section



(b) Idealized cross section



(c) Schematic of load distribution

Fig. A-1 Details of one of the tested beams prestressed by CFRP bars